

Bat Skull Evolution: the Impact of Echolocation

Giada Giacomini

Thesis submitted in partial fulfilment of the requirements of Liverpool John
Moores University for the degree of Doctor of Philosophy

September 2019

Table of Contents

Table of Contents	2
Abstract	6
Declaration	8
Acknowledgements	8
CHAPTER ONE: General Introduction.....	11
Morphological adaptations to vocalization	12
Bat phylogeny, emission type and call design	14
Sound generation and call parameters.....	17
Bat head diversity: sensory specializations.....	19
Bat skull diversity: feeding specializations.....	21
Functional trade-offs	22
Geometric morphometric approach and 3D models	23
Thesis aims and outline.....	24
Statement on research contribution.....	26
References	27
CHAPTER TWO: General Methods.....	32
Data collection	32
Morphological data.....	32
Functional data	36
Ecological data	40
Statistical analyses	41
References	44
Appendix A	49
Appendix B	56
Appendix C	62

CHAPTER THREE: 3D Photogrammetry of Bat Skulls: Perspectives for Macroevolutionary Analyses	82
Statement on content presentation and publication.....	82
Abstract	83
Introduction	84
Methods.....	86
Sample	86
Data acquisition and model landmarking	86
Measurement error evaluation	88
Results	92
Mesh distances	92
Shape visualization.....	93
Error in geometric morphometrics	95
Error in evolutionary analyses.....	98
Discussion	102
Performance of the photogrammetry technique	102
Mixed data from different reconstruction techniques	103
Data accessibility	105
References	105
Supplementary Information	109
Supplementary Methods	109
Supplementary References	112
Supplementary Tables	113
Supplementary Figures.....	116
Appendix D	118
Appendix E	119
CHAPTER FOUR: Skull Shape of Insectivorous Bats: Evolutionary Trade-off between Feeding and Echolocation?	120
Statement on content presentation and publication.....	120

Abstract	121
Introduction	122
Methods.....	124
Sample	124
Functional, ecological and morphological data.....	124
Statistical analyses.....	126
Results	130
Phylogenetic signal and evolutionary allometry in bat skulls	130
Bat skull morphological variation by ecological groups	132
Drivers of skull evolution in echolocating bats	137
Functional trade-off in skull shape of insectivorous bats.....	139
Discussion	140
Skull morphology and bat ecological groups	140
Skull morphology and functional parameters in echolocating bats.....	142
Evolutionary trade-off in insectivorous bats	145
References	147
Supplementary Information	152
Supplementary Tables	152
Appendix F.....	157
CHAPTER FIVE: Skull Morphological Adaptations to Acoustic Emissions: Peak Frequency in Bats.....	164
Statement on content presentation and publication.....	164
Abstract	165
Introduction	166
Methods.....	168
Sample	168
Functional, ecological and morphological data.....	168
Statistical analyses.....	170
Results	172

Size and shape by ecological groups	172
Size and peak frequency	175
Shape and peak frequency	179
Discussion	184
Palate orientation and head position.....	184
Size and peak frequency	185
Shape and peak frequency	189
References	193
Supplementary Information	198
Supplementary Tables	198
Supplementary Figures	199
Appendix G	207
CHAPTER SIX: General Conclusion	222
Photogrammetry for small and complex skulls.....	222
Functional correlates of bat skull evolution	223
Skull shape adaptations to peak frequency	224
Thesis limitations and future directions	226
Photogrammetry of bat skulls.....	226
Functional correlates of bat skull evolution	227
Skull shape adaptation to peak frequency	228
References	230

Abstract

Morphological adaptations of the mammalian skull are influenced by a variety of functional, environmental and behavioural factors. Skulls of echolocating species, such as bats, also face the challenge of optimizing sound emission and propagation. A strong association between bat skull morphology and feeding behaviour has been suggested previously (in particular for the Phyllostomidae family). Morphological variation related to other drivers of adaptation (in particular echolocation) remains understudied. In this thesis, I investigated the relationship between bat skull morphology (*i.e.*, size and shape) and functional traits (*i.e.*, feeding and echolocation) with a focus on the echolocation adaptations. I applied geometric morphometrics on data acquired from 3D digital models of bat skulls reconstructed with photogrammetry and μ CT scan techniques. The power and limitations of photogrammetry have not been fully explored for studies of evolutionary processes of small animals. As such, I firstly demonstrated the reliability of photogrammetry for the reconstruction of 3D digital models of bat skulls by evaluating its potential for evolutionary morphology studies at the interspecific level. I found that the average distance between meshes reconstructed with different techniques (*i.e.*, photogrammetry, μ CT or laser scan) was 0.037 mm (0.25% of total skull length). Levels of random error (repeatability and Procrustes variance) were similar in all techniques and no systematic error was observed. Therefore, the same biological conclusions are obtained regardless of the reconstruction technique employed. I subsequently assessed variation in skull morphology, with respect to ecological group (*i.e.*, diet and emission type) and functional measures (*i.e.*, bite force, masticatory muscles and echolocation characteristics), using phylogenetic comparative methods. I found that skull diversification among bat families is mainly driven by sound emission type (*i.e.*, nasal and oral) and broad dietary preferences. Feeding parameters (*i.e.*, bite force and masticatory muscles) influence the shape and size of all families studied and not only in phyllostomids: bigger species

generate stronger bites and species with a short rostrum generate higher bite forces relative to their body size. Sensory parameters (*i.e.*, echolocation characteristics) scale with skull size and correlate with skull shape in insectivorous species. I estimated the relative effects of feeding and sensory functional demands on skull size and shape variation and found comparable effects within the insectivorous species. Echolocation and feeding functions appear to constrain the same skull shape characteristics (*i.e.*, rostrum length) in insect-eating species indicating a possible functional trade-off. These species possibly underwent strong selection on skull morphology due to the (almost) exclusive use of echolocation to pursue rapidly moving prey. Additionally, echolocation signals in bats vary in call design (*i.e.*, number of harmonics, constant frequency, quasi-constant frequency and frequency modulation components) and some have evolved multiple times in different lineages. Therefore, I tested the effect of emission type and call design on the relationship between peak frequency and skull morphology within a broad taxonomic context (219 species). Skull morphology (*i.e.*, size and shape) of constant frequency nasal emitting species is strongly associated with peak frequency to amplify the sound through resonance effect within the nasal chambers. Despite no resonance effect being known for oral emitting species, skull shape variation also correlates with peak frequency in these species. Spatial and mechanical demands of echolocating muscles might mould the skull shape during ontogenesis of oral emitting species: the correlation between peak frequency and shape may result from an indirect mechanical effect. Interestingly, the skull shape of some non-insectivorous species (*i.e.*, frugivorous phyllostomids) also shows an evolutionary correlation with peak frequency. This suggests that peak frequency is still constraining skull shape of phyllostomid bats or, as phyllostomids probably evolved from an insectivorous ancestor, the adaptations to echolocation are evolutionary conservative. This thesis advances our knowledge of bat skull adaptation to echolocation and encourages future evolutionary studies to focus more on under-studied echolocation parameters.

Declaration

I declare that no portion of the work referred to in this Thesis has been submitted in support of an application for another degree or qualification of this or any other university or other institute of learning.

Acknowledgements

This PhD research benefited from the help of various people, institutions and funding bodies and this acknowledgements section will not suffice to express all my gratitude.

The first thanks goes to Liverpool John Moores University (LJMU) for financially sponsoring me with a three year PhD Scholarship. I am extremely grateful for this opportunity as I would not have been able to conduct this research without LJMU's support. I also want to thank the European Community Research Infrastructure Action for granting me five SYNTHESYS 3 projects <http://synthesys3.myspecies.info/> (BE-TAF-6601, HU-TAF-6926, DK-TAF-6870, FR-TAF-6924, AT-TAF-6820). This gave me access to the following museums and facilities (CT and laser scans): Royal Belgian Institute of Natural Science (Brussels, [IRSNB]), Magyar Természettudományi Múzeum (Budapest, [MNSB]), Statens Naturhistoriske Museum (Copenhagen, [ZMUC]), Muséum National d'Histoire Naturelle (Paris, [MNHN]) and Naturhistorisches Museum (Vienna, [MNW]). I want to express my particular gratitude to the SYNTHESIS organisers and also to curators of the mammalian collections for providing access to the museums, always being willing to help during my data collection, and for making me feel at home. Thanks to Ms Carole Paleco and Dr Annalise Folie (IRSNB), Ms Bernadett Döme, Dr Görföl Tamás and Dr Csorba Gábor (MNSB), Ms Nana Manniche, Dr Eline Lorenzen and Dr Daniel Klingberg Johansson (ZMUC), Ms Maité Adam, Dr Virginie Bouetel and Dr Jean-Marc Pons (MNHN), Ms Astrid Hille, Mr Bibl Alexander and Dr Frank Zachos (MNW), Mr

Tony Parker (Liverpool World Museum) and Mr Roberto Portela-Miguez (London Natural History Museum).

A special thank you goes to my supervisory team, Dr Carlo Meloro and Professor Richard Brown, for providing scientific support during this 3 year journey. Both supervisors have always been willing to discuss any questions I had on data collection, data analyses and research in general. I am grateful to Dr Meloro for teaching me about geometric morphometrics and phylogenetic comparative methods. I would not have been able to navigate through such a massive amount of literature without his guidance. I also would like to express gratitude to Professor Brown for his help with MrBayes software used in *Chapter Three* and for providing much valuable advice on my (still very improvable) scientific writing.

Many people - researchers, colleagues and friends - helped me in different stages of this PhD. Dr Isabelle de Groote and Dr Peter Falkingham provided general guidelines for the application of photogrammetric methods at a very early stage of my PhD, and therefore, I am very grateful. Dr Alessio Veneziano provided the script for the mesh comparison used in *Chapter Three* and has encouraged me to develop my skills with R software ever since. A thank you goes to Professor Gareth Jones and Professor Rolf Müller for discussing with me bat bio-acoustics and providing useful related readings. My gratitude also goes to Dr Anthony Herrel and Dr Gloriana Chaverri for providing unpublished data on bat bite forces, masticatory muscles and echolocation parameters used in *Chapters Four* and *Five*. These data made possible to run some of the macroevolutionary analyses of *Chapter Four* and to enlarge the sample size of *Chapter Five*. My appreciation also goes to Dr Dino Scaravelli and Dr Danilo Russo for discussing matters of echolocation with me. A special thank you goes to Dr Chaverri for “distracting” me from my PhD with some field work on bat social behaviour in Costa Rica. It gave me the necessary strength to throw myself back into the office and finish writing this thesis. A huge thank you to my friends and colleagues

Deborah Vicari and Ashleigh Wiseman for the adventures outside the office and the Monday drinks, when the week seemed already too long. Thank you for sharing the good and the bad times of academic life, for fighting together Short Paper, and for always being there for an R or geometric morphometrics chat.

Maybe, the most difficult thank you to formulate. It does not matter how big it will be: it will never be adequate. Thank you to my family for understanding my black sheep nature. Thank you for supporting all of my decisions and being proud of me. A thank you to all my old friends for being always present despite thousands kilometres of distance. And thank you to my *Vulpes vulpes chocolates* (Chocolate Fox) for not giving up on me, for believing in my abilities when I was unable to see clearly and for supporting me during the hardest and darkest times at the end of this PhD.



CHAPTER ONE: General Introduction

Morphological adaptation to the environment is the most tangible cue of species evolution. How morphological variation links to ecological specializations and functional demands has been the focus of many scientific investigations across all living forms (Kulemeyer *et al.*, 2009; Meloro *et al.*, 2014; Klaczko *et al.*, 2016).

The morphology of the vertebrate skull is under multiple evolutionary pressures as it responds to different functional demands supporting the brain, the masticatory muscles and the organs responsible for different sensory systems (*i.e.*, vision, olfaction and taste) (e.g., Goswami *et al.*, 2011; van Valkenburgh *et al.*, 2014; Plotsky *et al.*, 2016). Brain and skull shape, for example, are strongly integrated as they persistently accommodate to one another during developmental stages (Richtsmeier & Flaherty, 2013).

Species using echolocation to navigate and pursue the prey also face physical acoustic demands on their skull morphology (e.g. toothed whales' mandibles: Au, 1993; rotation of bat heads: Pedersen, 2000). Despite many vertebrates using acoustic emissions to orientate (e.g. shrews, oilbirds and cave swiftlets), only odontocetes (*i.e.*, toothed whales and dolphins) and laryngeally echolocating Chiroptera (bats) use sounds as the main sensory system to pursue prey (Au, 1993). High frequency hearing in mammals is achieved through the motor protein Prestin whose genetic sequence found in bats and dolphins suggests convergent evolution in these taxa (Liu *et al.*, 2010). Therefore, different sound emission systems and morphological adaptations have arisen in these two lineages of the animal kingdom. Specifically, bats produce sounds by contraction of the laryngeal muscles (except *Rousettus* spp. that uses tongue clicks) and emit them through the nostrils and/or the mouth, while odontocetes force pressurised air through the nasal passages to generate and emit sounds (Au, 1993; Madsen *et al.*, 2002).

The order Chiroptera is the second most speciose order of mammals, and its skull diversity seems to be the result of both broad diet and emission type (*i.e.*, oral or nasal) specializations (Arbour *et al.*, 2019). These reasons make the Chiroptera skull an optimal study system to investigate the role of echolocation (described as emission type and sound parameters, see below) as a driver of cranial shape diversity of echolocating species. Furthermore, the adaptation of bat skulls to both diet and echolocation provides the chance to test for the presence of possible evolutionary trade-offs between echolocation and feeding functions.

Morphological adaptations to vocalization

The acoustic characteristic of vocalizations of birds and mammals are strongly associated to soft tissue specializations and spatial arrangements of the vocal tract (*i.e.*, laryngeal cavity, throat, oral and nasal cavity, lips and nostrils) (e.g. Harry, 1960; Riede *et al.*, 2013; Plotsky *et al.*, 2016). Specifically, the frequency of the sound is negatively correlated with the vocal fold length (Harry, 1960) and the magnitude of the resonance effect depends on the geometrical shape and length of the upper respiratory pathway (e.g. Riede *et al.*, 2013). The movement of muscles in the vocal tract and the size of the emitter aperture (*i.e.*, beak or mouth gape) influence the properties of the emitted sound (e.g. Westneat *et al.*, 1993; Riede *et al.*, 2013; Kounitsky *et al.*, 2015). This contributes to the acoustic flexibility observed within and between species.

Despite adaptations to sound emission seem to involve mainly soft tissues, the morphological variation of at least one bony structure (*i.e.*, hyoid apparatus) is associated with mammals vocalization ability (e.g. Weissengruber *et al.*, 2002; Veselka *et al.*, 2010; Frey *et al.*, 2012). For example, species producing roar-like sounds, such as pantherine felids and rutting cervids, present elongated hyoid bones (epihyoid and thyrohyoid, respectively) that support the larynx (Weissengruber *et al.*, 2002; Frey *et al.*, 2012). The

elongation of these structures, together with the elongation of the vocal tract itself, allows for the production of low frequency sounds. Moreover, only bats able to echolocate present an articulation between the stylohyoid bone (bone of the hyoid apparatus) and the tympanic bone (Veselka *et al.*, 2010). This adaptation presumably enables echolocating bats to extract information from the comparison between emitted sounds and returning echoes (Wittrock, 2010). Despite little is known on the relationship between cranial shape and vocalization characteristics, cranial morphological rearrangements can arise from extreme morphological adaptations of soft tissues to vocalization. Sexual selection in howler monkeys, for example, led to the enlargement of the male larynx remodelling the skull shape to allow for extension of the neck (Frey & Gebler, 2010; and references within). Larynx hypertrophy reaches its maximum in males of the hammer-headed fruit bat (*Hypsignathus monstrosus*; Yinpterochiroptera) where the larynx occupies the entire volume of the thoracic cavity displacing the lungs into the abdomen (Fitch, 2016; and references within). Males of this species have a peculiar skull shape with highly enlarged rostrum which seems unrelated to feeding strategy (Van Cakenberghe *et al.*, 2002). Whether the highly derived cranial shape of the hammer-headed fruit bat is related to larynx hypertrophy, or it plays a direct role in vocalization, is still unknown.

Mammals use sounds to establish dominance, defend territory, coordinate group behaviour, recognise offspring, and to attract mates (e.g. Darden & Dabelsteen, 2008; Neumann *et al.*, 2010; Townsend *et al.*, 2011; Knörnschild *et al.*, 2013). Species able to echolocate, such as bats, use sounds for all the above tasks and to navigate the environment and pursue prey (Au, 1993). This poses the question if the cranial shape of these species is more strongly influenced by sound emission compared to other mammals.

Bat phylogeny, emission type and call design

The order Chiroptera is divided in two suborders: Yinpterochiroptera and Yangochiroptera (Springer *et al.*, 2001). The former includes the Pteropodidae family, species incapable of echolocation, and five echolocating families (Craseonycteridae, Hipposideridae, Megadermatidae, Rhinolophidae and Rhinopomatidae). The Yangochiroptera suborder includes only echolocating species belonging to the remaining 14 families.

Different call designs (defined by bat ecologists as temporal and frequency structure of the sound, **Figure 1**) and emission types evolved multiple times within chiropterans, representing a case of convergent evolution (Jones & Holderied, 2007). Call design diversity is associated with specialization to different environments (*i.e.*, open, edge, cluttered habitats) and hunting strategies (Schnitzler & Kalko, 2001). For example, long narrowband calls provide higher spatial resolution, and as such, they are suited for hunting in open spaces. In contrast, short, broadband calls (which provide high temporal resolution) are used in cluttered habitats where the individual needs prompt information on the presence of obstacles. All the different combinations between emission type and call design have evolved in echolocating bats (**Figure 2** exemplifies such diversity within 219 echolocating bats- *i.e.*, species studied in *Chapter Five* of this thesis).

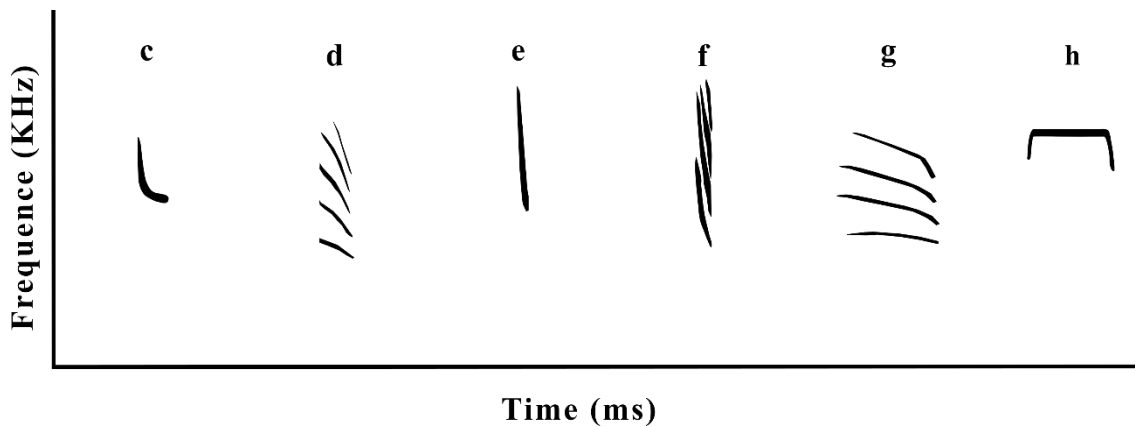


Figure 1. Call designs of laryngeally echolocating bats represented as spectrograms (*i.e.*, frequency vs time plots) [spectrograms not in scale]. The categorisation follows Jones and Teeling (2006). From left to right: narrowband and monoharmonic (c), narrowband and multiharmonic (d), short, broadband and monoharmonic (e), short, broadband and multiharmonic (f), long, narrowband and multiharmonic (g) and constant frequency (h). Non echolocating species (a) and species producing tongue clicks (b) were not included in this study.

Most of the echolocating families of the Yinpterochiroptera emit sounds from the nostrils (except for Rhinopomatidae and Craseonycteridae) but different call designs have evolved: hipposiderids and rhinolophids emit long constant frequency calls, craseonycterids and rhinopomatids produce narrowband multiharmonic calls while megadermatids emit short, broadband multiharmonic calls (Jones & Teeling, 2006). Most of the Yangochiroptera emit exclusively from the mouth with the exception of the Phyllostomidae and Nycteridae families (nasal emitters) and some other species that can shift between oral and nasal emission (including the vespertilionids *Plecotus* spp., *Barbastella* spp. and *Corynorhinus* spp; Pye, 1960). Recent studies have recorded some Phyllostomidae species also emit from the mouth, running counter to the idea of obligatory nasal emissions previously reported for this family (*e.g.* Surlykke *et al.*, 2013). Call design within the Yangochiroptera is more diverse with respect to Yinpterochiroptera: species present all the call designs listed above plus broadband calls dominated by fundamental harmonic; narrowband calls dominated by fundamental harmonic; and long, narrowband, multiharmonic calls (**Figure 2**).

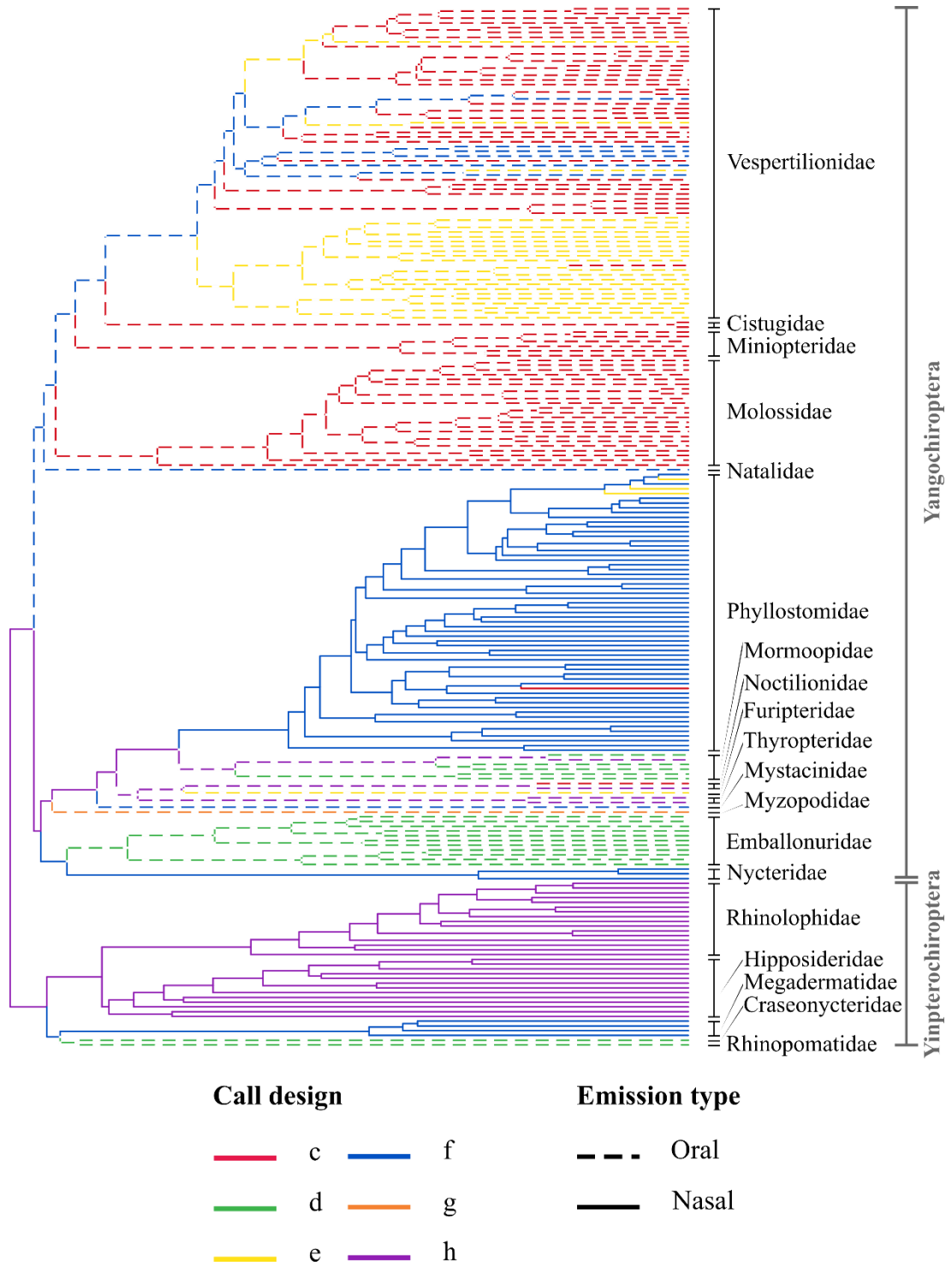


Figure 2. Call design and emission type of 219 species of echolocating bats included in this thesis. Colours represent the different call designs described in **Figure 1**, while line types represent different emission type.

Sound generation and call parameters

The air is forced through the vocal chords, causing them to vibrate. A series of waves of compressed air is sent out from the larynx generating the sound. The number of air compressions sent out over unit of time defines the frequency of the sound (measured in KHz). The generation of a specific frequency is achieved by adjusting the tension of the vocal folds by action of the larynx muscles (Harrison, 1995). Bats are able to emit ultrasounds (*i.e.*, frequency > 20 KHz), and their laryngeal muscles are particularly large with short contraction times in order to control tension and repetition of vocal chord oscillations (Elemans *et al.*, 2011). These ultrasounds are emitted in pulses and their “shape” can be broadly grouped by call design (**Figure 1**). To a finer scale, echolocation pulses can be described by quantifying frequency and time in a continuous manner (*i.e.*, echolocation call parameters; definition in **Table 1**). Call design and echolocation call parameters are closely related: call designs are classified using bandwidth, duration and number of harmonics of the call. For example, call design “e” is a monoharmonic call with a large bandwidth and short duration (**Figure 3**).

Table 1, Definition of commonly used echolocation parameters for species identification.

Parameter	Definition	Unit
Peak frequency	Frequency at maximum energy (dB) of the sound	KHz
Start frequency	Frequency at the beginning of the call	KHz
End frequency	Frequency at the end of the call	KHz
Bandwidth	Difference between start frequency and end frequency	KHz
Duration	Duration of the call	ms
Sweep rate	Ratio between bandwidth and duration	KHz/s

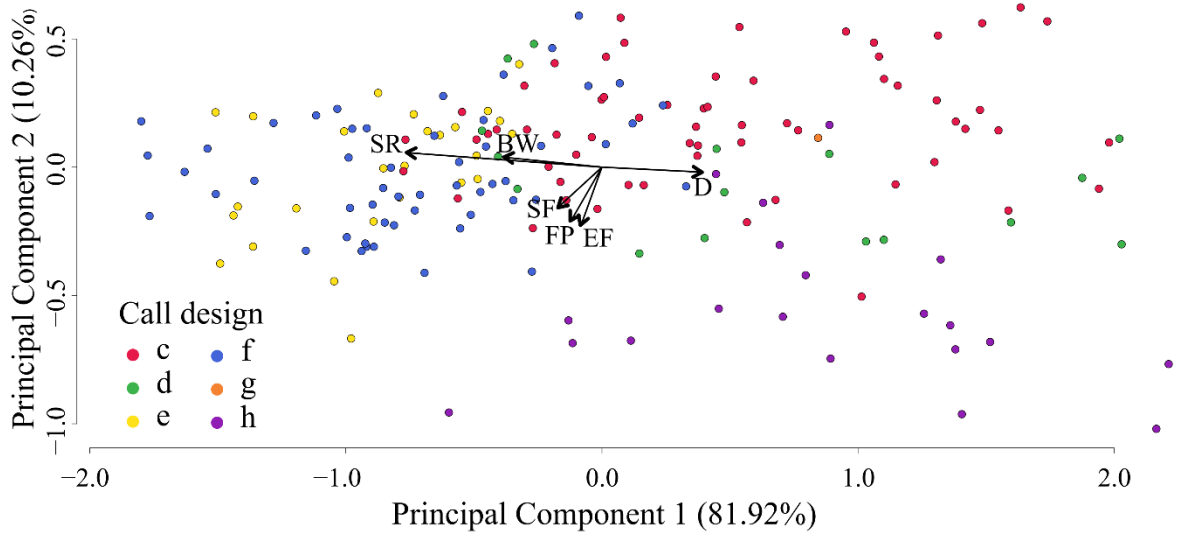


Figure 3. Principal component analysis of \log_{10} transformed echolocation parameters for 181 laryngeally echolocating species included in this thesis. Colours represent the call design and arrows define the direction of increments for six parameters (FP: peak frequency, SF: start frequency, EF: end frequency, BW: bandwidth, D: duration, SR: sweep rate).

Echolocation parameters (or characteristics) display a certain degree of within-species plasticity in relation to the task performed by the bat, habitat structure and presence of conspecifics (Kalko & Schnitzler, 1993; Siemers *et al.*, 2001; Ulanovsky *et al.*, 2004). Nonetheless, echolocation characteristics can be reliably used to identify individuals to the species or genus level (*e.g.* Bell & Fenton, 1981; López-Baucells *et al.*, 2019).

Echolocation parameters are part of a complex adaptive system in which echolocation sounds, hunting strategy and morphological features (*e.g.* wing shape) have co-adapted to increase hunting success (Norberg & Rayner, 1987; Siemers & Schnitzler, 2004). Among these echolocation parameters, peak frequency is most widely-used to separate species acoustically (except for some genera that use similar frequencies; *e.g.* *Myotis*, Parsons & Jones, 2000). Therefore, many morphological studies have used peak frequency to test the association between echolocation characteristics and morphological diversity such as the scaling of peak frequency on body size (Jones, 1999) (see next section).

Bat head diversity: sensory specializations

Head morphology in echolocating bats displays specialization to ultrasonic emission and reception at both soft and hard tissues level. Ears and noseleaves are extremely diverse across bats and vary in size, shape, symmetry, orientation and in presence/absence of anatomical features such as ridges or flaps (Bogdanowicz *et al.*, 1997; Müller, 2010; Ma & Müller, 2011). This diversity across species is not ornamental, and it has been correlated to the use of echolocation. Specifically, it has been shown that bats pinnae behave as beamforming baffles scattering the incoming ultrasonic sound in a frequency- and direction- dependent manner (Müller *et al.*, 2008). It has also been suggested that size and shape of the pinnae correlate with echolocation call parameters in some bat species (Gannon *et al.*, 2001; Wu *et al.*, 2015).

Similarly, the acoustic properties of a bat noseleaf (when present) determine the distribution of the sound energy in the three dimensional space during call emissions (Müller, 2010). In particular, the noseleaf contributes to increase beam directionality, which facilitates the spatial separation of echoes of interest from those of the environment/background (Surlykke *et al.*, 2009). The hypothesis of a correlation between echolocation parameters and noseleaf has been proposed (Jones, 1999), but no evidence has yet been obtained to confirm such a relationship (Goudy-Trainor & Freeman, 2002).

Adaptations to the use of echolocation as primary sensory system are evident also in gross skull rearrangement and morphological specialization of cranial structures (*e.g.* nasal chambers and inner ear). Regardless of the emission type evolved, bats need to optimise the sound emission and propagation once the call is generated in the larynx. Therefore, different arrangements in head rotation have evolved to straighten the sound pathway: the head of nasal emitting species is folded towards the chest so that the sound pathway travels perpendicularly to the nostril (and noseleaf) (**Figure 4**; Pedersen, 2000).

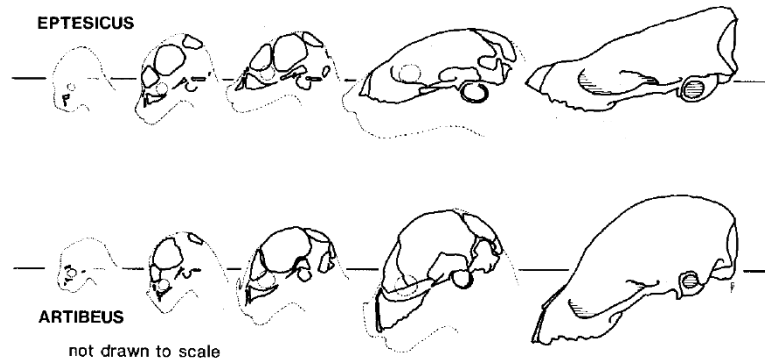


Figure 4. Head rotation during ontogenetic stages of an oral emitting bat (genus *Eptesicus*) and a nasal emitting bat (genus *Artibeus*) from Pedersen (2000).

Within the nasal emitting species, rhinolophids and hipposiderids have evolved a sophisticated resonator in their rostra: the nasal chambers. Conversely, other nasal emitting species (*i.e.*, Phyllostomidae, Megadermatidae and Nycteridae) are considered more rudimentary because their nasal passages are not dramatically enlarged. It has been shown that the size of nasal chambers is inversely correlated with peak frequency. This augments the energy of the frequency by resonating it (Armstrong & Coles, 2007; Jacobs *et al.*, 2014). All echolocating species present enlarged cochleae compared to other mammals and non-echolocating bats (Simmons *et al.*, 2008). Furthermore, the morphology of the inner ear is known to correlate with peak frequency that negatively correlates with basilar membrane length and positively with number of cochlea turns (Davies *et al.*, 2013).

Whether the skull as a whole is adapted to enable emission of specific frequencies remains to be investigated. Despite the well supported negative scaling between bat skull size and peak frequency no information is available on the relationship between skull shape and emitted frequencies (Jones, 1999; Thiagavel *et al.*, 2017; Jacobs & Bastian, 2018).

Bat skull diversity: feeding specializations

Bat feeding habits are very diverse, and species are known to feed on insects, fruits, nectar, vertebrates, fish or blood. Despite this diversity, most bat species (around 70%) are small-sized insectivores and use echolocation as the main sensory system to locate and catch their prey (Barclay & Brigham, 1991). Species that feed, exclusively or partially, on insects are present in all echolocating bat families and are distributed worldwide.

Laryngeally echolocating species feeding on blood, nectar and fruit have evolved exclusively in the Phyllostomidae family (Norberg & Rayner, 1987). Some phyllostomids, megadermatids, nycterids and vespertilionids are carnivorous, eating birds, reptiles, amphibians and other smaller bats. To varying extents, the two *Noctilio* species and two vespertilionids (*Myotis vivesi* and *M. capaccinii*) are able to catch fish but also feed on insects (Wilson & Reeder, 2005).

Given the diversity of feeding habits within the phyllostomids, many studies have focused on the association between dietary preferences (*i.e.*, diet type and food hardness) and morphological adaptations in this family (*e.g.* Freeman, 1998; Nogueira *et al.*, 2009; Santana *et al.*, 2010). Diet type and food hardness are believed to promote bat skull morphological diversification reflecting adaptations to bite force and masticatory muscles mass. Generally speaking, bite performance increases with increased masticatory muscle mass (the temporalis muscle in particular), greater skull size, shortening of the rostrum and increased skull height (*i.e.*, greater distance between the basicranium and the sagittal crest) (Nogueira *et al.*, 2009). For example, highly specialised frugivorous species (*e.g.* *Centurio senex*) present very short and broad skulls that provide a great area for the temporalis muscle attachment which, in turn, generates the high bite force necessary to process hard food items (Santana *et al.*, 2012). Conversely, carnivorous bats tend to present long rostra that allow capture of larger prey and enable fast jaw closure (Santana & Cheung, 2016). Nectarivorous species present particularly elongated and narrow rostra in order to reach the

nectar inside the flower but produce low bite forces (Nogueira *et al.*, 2009). Our knowledge of the relationship between diet and skull morphology in families other than Phyllostomidae remains limited (but see Hedrick & Dumont, 2018; Arbour *et al.*, 2019).

Functional trade-offs

Functional trade-offs appear when the adaptation of one trait to a function decreases adaptation (of the same trait) for another function (Garland, 2014). Complex adaptive systems and/or functional trade-offs can result from the simultaneous influence of multiple functional drivers on the same phenotypic trait (Majid & Kruspe, 2018; Wu *et al.*, 2018). Since bat skull morphology is under different evolutionary pressures linked to feeding and sensorial functions we might expect functional trade-offs to occur. Bite performance, diet type and diet hardness are known to play an important role in adaptation of bat skull shape, in particular within the super diverse Phyllostomidae family (*e.g.* Nogueira *et al.*, 2009; Santana *et al.*, 2010, 2012). It remains to be investigated how feeding adaptations are related to echolocation adaptations and whether a functional trade-off exists between the mechanical advantages and the sensorial specializations.

Some functional trade-offs between different sensory systems have been identified or hypothesized in bats. The loss of colour vision in Rhinolophidae and Hipposideridae has probably been driven by ecological specialization suggesting a possible functional trade-off between vision and echolocation in these species (Zhao *et al.*, 2009; Jones *et al.*, 2013). Through an adaptive radiation, phyllostomids evolved from an echolocating and insect-eating ancestor to species with highly specialised diets (*i.e.*, frugivorous, sanguivorous, nectarivorous and vertebrate eater) (Freeman, 2000). It has been suggested that non-insectivorous species might be less adapted to acoustic emission because echolocation traded-off with vision and olfaction – which are intensively used by these species to locate food (Pedersen & Müller, 2013). This is supported by the aforementioned lack of a

specialised nasal chamber in this family. Nevertheless, even if a possible trade-off between vision and echolocation has been identified in some non-insectivorous phyllostomids (Wu *et al.*, 2018), there is currently no evidence of nasal passage morphological adaptation to enhanced olfactory ability (Eiting *et al.*, 2014).

Geometric morphometric approach and 3D models

Multivariate statistical analyses of anatomical homologous points (*i.e.*, landmarks) has proved particularly useful for the study of morphological variation in relation to functional demands in many animal lineages (Kulemeyer *et al.*, 2009; Jacobs *et al.*, 2014; Dumont *et al.*, 2016). This approach, called the geometric morphometric method, quantifies the differences in forms of complex biological structures by approximating their geometry through Cartesian coordinates of anatomical landmarks and their mutual relationships (Zelditch *et al.*, 2012). Geometric morphometrics holds several advantages with respect to traditional morphometrics, and the possibility to investigate shape, separately from size, led to a large use of the technique since the early 1990's (Rohlf & Marcus, 1993). For example, shape changes can be graphically represented and clearly interpreted through deformation grids or 3D model warping methods with geometric morphometrics (Klingenberg, 2013). Furthermore, the quantification of 2D and 3D anatomical curves/surfaces (*i.e.*, semilandmarks) allows the analysis of morphological variation even when anatomical homologous points cannot be identified (Gunz & Mitteroecker, 2013).

Digital materials, such as digital pictures and three-dimensional (3D) models, have been largely employed in the geometric morphometric field, as they represent a reliable, transferable and reusable raw material (*e.g.* Cardini *et al.*, 2007). In the last decade, the use of 3D models in morphological studies has notably increased as different reconstruction techniques has become more accessible (*e.g.* 3D photogrammetry, Falkingham, 2012).

However, the accuracy of 3D model reconstruction using the photogrammetry technique is

potentially limited by the size and pattern complexity of the specimens and a full evaluation of such limitations has not been assessed yet.

The 3D approach offers additional information on morphological features compared to 2D images in particular when highly 3D objects with curved elements, such as skulls, are studied (marmots: Cardini, 2014; bats: Santana *et al.*, 2019). Compared to the 2D approach, the application of geometric morphometrics on 3D data has proved particularly useful for bat studies in differentiating cryptic species (*e.g.* Sztencel-Jabłonka *et al.*, 2009), describing morphological variation (*e.g.* Schmieder *et al.*, 2015) and studying bat evolution (*e.g.* Bogdanowicz *et al.*, 2005).

In this thesis, the photogrammetry performance on small skulls was assessed and 3D models were used to test the predictions of each chapter (see next section).

Thesis aims and outline

The aim of this thesis is to improve our understanding of the evolutionary drivers, in particular echolocation, responsible for bat crania morphological diversification at the macroevolutionary scale. Specifically, the evolutionary correlations between bat skull morphology and functional traits (*i.e.*, feeding behaviours and echolocation) are assessed under a phylogenetic comparative methods framework. This thesis carries three original pieces of research consisting of a methodological paper published in a peer-reviewed journal (*Chapter Three*) and two macroevolutionary studies in preparation for submission to peer-reviewed journals (*Chapters Four and Five*). The thesis' chapters are outlined as follows:

Chapter Two describes the general methods used to collect morphological, functional and ecological data in this thesis. This chapter also presents the phylogenetic framework

applied in the successive chapters. Details on specific analyses are provided within the methodological section of each data chapter (*i.e.*, *Chapters Three, Four and Five*).

Chapter Three investigates the reliability of the photogrammetry technique for the 3D reconstruction of small mammal skulls. Within this chapter, I compare the photogrammetric approach against two more expensive and widely used reconstruction techniques (*i.e.*, μ CT scan and laser scan) using bat skulls as a model system. I present results on 3D mesh comparison and assess the measurement error in geometric morphometric and macroevolutionary (between species) analyses for the three reconstruction techniques. The effects on result interpretation generated by phylogenetic uncertainty and combination of multiple-techniques datasets are presented. This chapter also aims to provide a photogrammetric protocol to reconstruct small and complex objects (*e.g.* bat skulls) in 3D with an affordable and accurate method.

Chapter Four examines the relative influence of feeding traits (*i.e.*, bite force and muscles) and echolocation parameters on skull morphological diversity of 10 bat families. This chapter tests the prediction that skull shape of insectivorous bats is evolutionarily associated with echolocation parameters as these species (almost) exclusively rely on echolocation strategies to pursue prey. I then investigate the correlation between skull morphology and feeding descriptors (*i.e.*, diet category, bite force and muscles mass) comparing these findings with those of previous studies. After assessing which shape features are associated with variation of echolocation parameters between insectivorous bats, I discuss the presence of a possible trade-off between feeding and sensorial function.

Chapter Five follows on from the results of *Chapter Four* by focusing on skull adaptations of all echolocating bat families (n =219 species) to peak frequency. Conversely to *Chapter Four*, here the sample size allowed me to test the prediction that skull morphology of non-insectivorous bats (specifically frugivorous phyllostomid) does not exhibit an evolutionary association with peak frequency. I then consider whether phylogenetic relatedness,

emission type (nasal or oral) and call design (*i.e.*, temporal and frequency structure of the sound), play a role in shaping the relationship between skull morphological adaptations and peak frequency in insectivorous bats. Therefore, I describe these association patterns between shape and peak frequency, and I present two non-mutually exclusive hypotheses to explain the evolutionary relationship between skull shape and peak frequency.

Chapter Six summarises the findings of the previous chapters, discusses the limitations of this study and suggests future research directions.

Chapters Three, Four and Five are structured as papers that have been published or are currently in preparation for submission to peer-reviewed journals. For such a reason, some duplication of their contents was unavoidable within the thesis particularly within the methodological sections where the geometric morphometric approach and the criterion of data collection are presented. For each chapter, I state whether parts of the results were presented to conferences, are in preparation for submission or are published.

Statement on research contribution

I carried out the study design, collection of morphological data, performed and interpreted the analyses and wrote this thesis. Nonetheless, this thesis uses unpublished data provided by Anthony Herrel (*i.e.*, bite force and muscles data) and Gloriana Chaverri (*i.e.*, echolocation call parameters of Central American species). These data were used in *Chapters Four and Five*, allowing me to conduct analyses on a taxonomically wider sample. Within *Chapter Three*, Antonio Veneziano provided the R coding for the mesh comparison used to assess the surface similarity between 3D models reconstructed with different techniques.

References

- Arbour, J.H., Curtis, A.A. & Santana, S.E. 2019. Signatures of echolocation and dietary ecology in the adaptive evolution of skull shape in bats. *Nat. Commun.* **10**: 2036.
- Armstrong, K.N. & Coles, R.B. 2007. Echolocation Call Frequency Differences Between Geographic Isolates of *Rhinonicteris Aurantia* (Chiroptera: Hipposideridae): Implications of Nasal Chamber Size. *J. Mammal.* **88**: 94–104.
- Au, W.W.L. 1993. *The Sonar of Dolphins*, 1st ed. Springer-Verlag New York, New York.
- Barclay, R.M.R. & Brigham, R.M. 1991. Prey detection, dietary niche breadth, and body size in bats: why are aerial insectivorous bats so small? *Am. Soc. Nat.* **137**: 693–703.
- Bell, G.P. & Fenton, M.B. 1981. Recognition of Species of Insectivorous Bats by Their Echolocation Calls. *J. Mammal.* **62**: 233–243.
- Bogdanowicz, W., Csada, R.D. & Fenton, M.B. 1997. Structure of Noseleaf, Echolocation, and Foraging Behavior in the Phyllostomidae (Chiroptera). *J. Mammal.* **78**: 942–953.
- Bogdanowicz, W., Juste, J., Owen, R.D. & Sztencel, A. 2005. Geometric morphometrics and cladistics: testing evolutionary relationships in mega- and microbats. *Acta Chiropterologica* **7**: 39–49.
- Cardini, A. 2014. Missing the third dimension in geometric morphometrics: how to assess if 2D images really are a good proxy for 3D structures? *Hystrix, Ital. J. Mammal.* **25**: 73–81.
- Cardini, A., Jansson, A.-U. & Elton, S. 2007. A geometric morphometric approach to the study of ecogeographical and clinal variation in vervet monkeys. *J. Biogeogr.* **34**: 1663–1678.
- Darden, S.K. & Dabelsteen, T. 2008. Acoustic territorial signalling in a small, socially monogamous canid. *Anim. Behav.* **75**: 905–912.
- Davies, K.T.J., Maryanto, I. & Rossiter, S.J. 2013. Evolutionary origins of ultrasonic hearing and laryngeal echolocation in bats inferred from morphological analyses of the inner ear. *Front. Zool.* **10**: 2.
- Dumont, M., Wall, C.E., Botton-Divet, L., Goswami, A., Peigné, S. & Fabre, A.-C. 2016. Do functional demands associated with locomotor habitat, diet, and activity pattern drive skull shape evolution in musteloid carnivorans? *Biol. J. Linn. Soc.* **117**: 858–878.
- Eiting, T.P., Perot, J.B. & Dumont, E.R. 2014. How much does nasal cavity morphology matter? Patterns and rates of olfactory airflow in phyllostomid bats. *Proc. R. Soc. B Biol. Sci.* **282**: 20142161–20142161.
- Elemans, C.P.H., Mead, A.F., Jakobsen, L. & Ratcliffe, J.M. 2011. Superfast Muscles Set Maximum Call Rate in Echolocating Bats. *Science* **333**: 1885–1888.
- Falkingham, P.L. 2012. Acquisition of high resolution three-dimensional models using free, open-source, photogrammetric software. *Palaeontol. Electron.* **15**: 1–15.
- Fitch, W.T. 2016. Vertebrate Bioacoustics: Prospects and Open Problems BT - Vertebrate Sound Production and Acoustic Communication. In: (R. A. Suthers, W. T. Fitch, R. R. Fay, & A. N. Popper, eds), pp. 297–328. Springer International Publishing, Cham.
- Freeman, P.W. 1998. Form, function, and evolution in skulls and teeth of bats. In: *Bat Biology and Conservation* (T. H. Kunz & P. A. Racey, eds), pp. 140–156. Smithsonian Institution Press, Washington.

- Freeman, P.W. 2000. Macroevolution in Microchiroptera : Recoupling morphology and ecology with phylogeny. *Evol. Ecol. Res.* **2**: 317–335.
- Frey, R. & Gebler, A. 2010. Chapter 10.3 - Mechanisms and evolution of roaring-like vocalization in mammals. In: *Handbook of Mammalian Vocalization* (S. M. B. T.-H. of B. N. Brudzynski, ed), pp. 439–450. Elsevier.
- Frey, R., Volodin, I., Volodina, E., Carranza, J. & Torres-Porras, J. 2012. Vocal anatomy, tongue protrusion behaviour and the acoustics of rutting roars in free-ranging Iberian red deer stags (*Cervus elaphus hispanicus*). *J. Anat.* **220**: 271–292. John Wiley & Sons, Ltd (10.1111).
- Gannon, W.L., Sherwin, R.E., DeCarvalho, T.N. & O’Farrell, M.J. 2001. Pinnae and echolocation call differences between *Myotis californicus* and *M. ciliolabrum* (Chiroptera: Vespertilionidae). *Acta Chiropterologica* **3**: 77–91.
- Garland Jr., T. 2014. Trade-offs. *Curr. Biol.* **24**: R60–R61.
- Goswami, A., Milne, N. & Wroe, S. 2011. Biting through constraints: cranial morphology, disparity and convergence across living and fossil carnivorous mammals. *Proc. R. Soc. B Biol. Sci.* **278**: 1831–1839. Royal Society.
- Goudy-Trainor, A. & Freeman, P.W. 2002. Call Parameters and Facial Features in Bats: A Surprising Failure of form Following Function. *Acta Chiropterologica* **4**: 1–16.
- Gunz, P. & Mitteroecker, P. 2013. Semilandmarks: a method for quantifying curves and surfaces. *Hystrix, Ital. J. Mammal.* **24**: 103–109.
- Harrison, D.F.N. 1995. *The Anatomy and Physiology of the Mammalian Larynx*. Cambridge University Press, Cambridge.
- Harry, H. 1960. Vocal Pitch Variation Related to Changes in Vocal Fold Length. *J. Speech Hear. Res.* **3**: 150–156. American Speech-Language-Hearing Association.
- Hedrick, B.P. & Dumont, E.R. 2018. Putting the leaf-nosed bats in context: a geometric morphometric analysis of three of the largest families of bats. *J. Mammal.* **99**: 1042–1054.
- Jacobs, D.S. & Bastian, A. 2018. High Duty Cycle Echolocation May Constrain the Evolution of Diversity within Horseshoe Bats (Family: Rhinolophidae). *Diversity* **10**: 85.
- Jacobs, D.S., Bastian, A. & Bam, L. 2014. The influence of feeding on the evolution of sensory signals: A comparative test of an evolutionary trade-off between masticatory and sensory functions of skulls in southern African Horseshoe bats (Rhinolophidae). *J. Evol. Biol.* **27**: 2829–2840.
- Jones, G. 1999. Scaling of echolocation call parameters in bats. *J. Exp. Biol.* **202**: 3359 – 3367.
- Jones, G. & Holderied, M.W. 2007. Bat echolocation calls: adaptation and convergent evolution. *Proc. R. Soc. B Biol. Sci.* **274**: 905–912.
- Jones, G. & Teeling, E. 2006. The evolution of echolocation in bats. *Trends Ecol. Evol.* **21**: 149–156.
- Jones, G., Teeling, E. & Rossiter, S. 2013. From the ultrasonic to the infrared: molecular evolution and the sensory biology of bats. *Frontiers in Physiology* **4**: 117.
- Kalko, E.K. V & Schnitzler, H.-U. 1993. Plasticity in echolocation signals of European pipistrelle bats in search flight: implications for habitat use and prey detection. *Behav. Ecol. Sociobiol.* **33**: 415–428.

- Klaczko, J., Sherratt, E. & Setz, E.Z.F. 2016. Are Diet Preferences Associated to Skulls Shape Diversification in Xenodontine Snakes? *PLoS One* **11**: e0148375.
- Klingenberg, C.P. 2013. Visualizations in geometric morphometrics: how to read and how to make graphs showing shape changes. *Hystrix, Ital. J. Mammal.* **24**: 15–24.
- Knörnschild, M., Feifel, M. & Kalko, E.K. V. 2013. Mother–offspring recognition in the bat *Carollia perspicillata*. *Anim. Behav.* **86**: 941–948.
- Kounitsky, P., Rydell, J., Amichai, E., Boonman, A., Eitan, O., Weiss, A.J., *et al.* 2015. Bats adjust their mouth gape to zoom their biosonar field of view. *Proc. Natl. Acad. Sci.* **112**: 6724 LP – 6729.
- Kulemeyer, C., Asbahr, K., Gunz, P., Frahnert, S. & Bairlein, F. 2009. Functional morphology and integration of corvid skulls – a 3D geometric morphometric approach. *Front. Zool.* **6**: 2.
- Liu, Y., Cotton, J.A., Shen, B., Han, X., Rossiter, S.J. & Zhang, S. 2010. Convergent sequence evolution between echolocating bats and dolphins. *Curr. Biol.* **20**: R53–R54.
- López-Baucells, A., Torrent, L., Rocha, R., E.D. Bobrowiec, P., M. Palmeirim, J. & F.J. Meyer, C. 2019. Stronger together: Combining automated classifiers with manual post-validation optimizes the workload vs reliability trade-off of species identification in bat acoustic surveys. *Ecol. Inform.* **49**: 45–53.
- Ma, J. & Müller, R. 2011. A method for characterizing the biodiversity in bat pinnae as a basis for engineering analysis. *Bioinspir. Biomim.* **6**: 026008.
- Madsen, P.T., Payne, R., Kristiansen, N.U., Wahlberg, M., Kerr, I. & Møhl, B. 2002. Sperm whale sound production studied with ultrasound time/depth-recording tags. *J. Exp. Biol.* **205**: 1899 – 1906.
- Majid, A. & Kruspe, N. 2018. Hunter-Gatherer Olfaction Is Special. *Curr. Biol.* **28**: 409-413.e2.
- Meloro, C., Cáceres, N., Carotenuto, F., Passaro, F., Sponchiado, J., Melo, G.L., *et al.* 2014. Ecogeographical variation in skull morphometry of howler monkeys (Primates: Atelidae). *Zool. Anzeiger* **253**: 345–359.
- Müller, R. 2010. Numerical analysis of biosonar beamforming mechanisms and strategies in bats. *J. Acoust. Soc. Am.* **128**: 1414–1425.
- Müller, R., Lu, H. & Buck, J.R. 2008. Sound-Diffracting Flap in the Ear of a Bat Generates Spatial Information. *Phys. Rev. Lett.* **100**: 108701.
- Neumann, C., Assahad, G., Hammerschmidt, K., Perwitasari-Farajallah, D. & Engelhardt, A. 2010. Loud calls in male crested macaques, *Macaca nigra*: a signal of dominance in a tolerant species. *Anim. Behav.* **79**: 187–193.
- Nogueira, M.R., Peracchi, A.L. & Monteiro, L.R. 2009. Morphological correlates of bite force and diet in the skull and mandible of phyllostomid bats. *Funct. Ecol.* **23**: 715–723.
- Norberg, U.M. & Rayner, J.M.V. 1987. Ecological Morphology and Flight in Bats (Mammalia; Chiroptera): Wing Adaptations , Flight Performance , Foraging Strategy and Echolocation. *Philos. Trans. R. Soc. Lond. B. Biol. Sci.* **316**: 335–427.
- Parsons, S. & Jones, G. 2000. Acoustic identification of twelve species of echolocating bat by discriminant function analysis and artificial neural networks. *J. Exp. Biol.* **203**: 2641 – 2656.

- Pedersen, S.C. 2000. Skull growth and the acoustical axis of the head in bats. In: Ontogeny, functional ecology, and evolution of bats (R. A. Adams & S. C. Pedersen, eds), p. 174:213. Cambridge University Press, New York.
- Pedersen, S.C. & Müller, R. 2013. Nasal-emission and nose leaves. In: Bat Evolution, Ecology, and Conservation. (R.A. Adams and S.C. Pedersen, ed), p. 71:91. Springer New York Heidelberg Dordrecht London.
- Plotsky, K., Rendall, D., Chase, K. & Riede, T. 2016. Cranio-facial remodeling in domestic dogs is associated with changes in larynx position. *J. Anat.* **228**: 975–983. John Wiley & Sons, Ltd (10.1111).
- Pye, J.D. 1960. A theory of echolocation by bats. *J. Laryngol. Otol.* **74**: 718–729.
- Richtsmeier, J.T. & Flaherty, K. 2013. Hand in glove: brain and skull in development and dysmorphogenesis. *Acta Neuropathol.* **125**: 469–489.
- Riede, T., Schilling, N. & Goller, F. 2013. The acoustic effect of vocal tract adjustments in zebra finches. *J. Comp. Physiol. A* **199**: 57–69.
- Rohlf, F.J. & Marcus, L.F. 1993. A revolution morphometrics. *Trends Ecol. Evol.* **8**: 129–132.
- Santana, S.E., Arbour, J.H., Curtis, A.A. & Stanchak, K.E. 2019. 3D Digitization in Functional Morphology: Where is the Point of Diminishing Returns? *Integr. Comp. Biol.*, doi: 10.1093/icb/icz101.
- Santana, S.E. & Cheung, E. 2016. Go big or go fish: morphological specializations in carnivorous bats. *Proc. R. Soc. B Biol. Sci.* **283**: 20160615.
- Santana, S.E., Dumont, E.R. & Davis, J.L. 2010. Mechanics of bite force production and its relationship to diet in bats. *Funct. Ecol.* **24**: 776–784.
- Santana, S.E., Grosse, I.R. & Dumont, E.R. 2012. Dietary Hardness , Loading Behavior , and the Evolution of Skull Form in Bats. *Evolution* **66**: 2587–2598.
- Schmieder, D.A., Benítez, H.A., Borissov, I.M. & Fruciano, C. 2015. Bat species comparisons based on external morphology: A test of traditional versus geometric morphometric approaches. *PLoS One* **10**: 8–13.
- Schnitzler, H.-U. & Kalko, E.K. V. 2001. Echolocation by Insect-Eating Bats. *Bioscience* **51**: 557–569.
- Siemers, B.M., Kalko, E.K. V & Schnitzler, H.U. 2001. Echolocation behavior and signal plasticity in the Neotropical bat *Myotis nigricans* (Schinz, 1821) (Vespertilionidae): A convergent case with European species of *Pipistrellus*? *Behav. Ecol. Sociobiol.* **50**: 317–328.
- Siemers, B.M. & Schnitzler, H.-U. 2004. Echolocation signals reflect niche differentiation in five sympatric congeneric bat species. *Nature* **429**: 657.
- Simmons, N.B., Seymour, K.L., Habersetzer, J. & Gunnell, G.F. 2008. Primitive Early Eocene bat from Wyoming and the evolution of flight and echolocation. *Nature* **451**: 818.
- Springer, M.S., Teeling, E.C., Madsen, O., Stanhope, M.J. & de Jong, W.W. 2001. Integrated fossil and molecular data reconstruct bat echolocation. *Proc. Natl. Acad. Sci.* **98**: 6241– 6246.
- Surlykke, A., Jakobsen, L., Kalko, E. & Page, R. 2013. Echolocation intensity and directionality of perching and flying fringe-lipped bats, *Trachops cirrhosus* (Phyllostomidae). *Frontiers in Physiology* **4**: 1-9.

- Surlykke, A., Pedersen, S.B. & Jakobsen, L. 2009. Echolocating bats emit a highly directional sonar sound beam in the field. *Proc. R. Soc. B Biol. Sci.* **276**: 853–860.
- Sztencel-Jabłonka, A., Jones, G. & Bogdanowicz, W. 2009. Skull morphology of two cryptic bat species: *Pipistrellus pipistrellus* and *P. pygmaeus* - a 3D geometric morphometrics approach with landmark reconstruction. *Acta Chiropterologica* **11**: 113–126.
- Thiagavel, J., Santana, S.E. & Ratcliffe, J.M. 2017. Body Size Predicts Echolocation Call Peak Frequency Better than Gape Height in Vespertilionid Bats. *Sci. Rep.* **7**: 828.
- Townsend, S.W., Zöttl, M. & Manser, M.B. 2011. All clear? Meerkats attend to contextual information in close calls to coordinate vigilance. *Behav. Ecol. Sociobiol.* **65**: 1927–1934.
- Ulanovsky, N., Fenton, M.B., Tsoar, A. & Korine, C. 2004. Dynamics of jamming avoidance in echolocating bats. *Proc. R. Soc. London. Ser. B Biol. Sci.* **271**: 1467–1475.
- Van Cakenberghe, V., Herrel, A. & Aguirre, L.F. 2002. Evolutionary Relationships between Cranial Shape and Diet in Bats (Mammalia: Chiroptera). In: *Topics in Functional and Ecological Vertebrate Morphology* (P. Aerts, K. D’Aout, A. Herrel, & R. Van Damme, eds), p. 372. Shaker Publishing B.V., Maastricht, Netherlands.
- Van Valkenburgh, B., Pang, B., Bird, D., Curtis, A., Yee, K., Wysocki, C., *et al.* 2014. Respiratory and Olfactory Turbinates in Feliform and Caniform Carnivores: The Influence of Snout Length. *Anat. Rec.* **297**: 2065–2079. John Wiley & Sons, Ltd.
- Veselka, N., McErlain, D.D., Holdsworth, D.W., Eger, J.L., Chhem, R.K., Mason, M.J., *et al.* 2010. A bony connection signals laryngeal echolocation in bats. *Nature* **463**: 939–942. Nature Publishing Group.
- Weissengruber, G.E., Forstenpointner, G., Peters, G., Kübber-Heiss, A. & Fitch, W.T. 2002. Hyoid apparatus and pharynx in the lion (*Panthera leo*), jaguar (*Panthera onca*), tiger (*Panthera tigris*), cheetah (*Acinonyx jubatus*) and domestic cat (*Felis silvestris f. catus*). *J. Anat.* **201**: 195–209. John Wiley & Sons, Ltd (10.1111).
- Westneat, M.W., Long, J.H., Hoese, W. & Nowicki, S. 1993. Kinematics of birdsong: functional correlation of cranial movements and acoustic features in sparrows. *J. Exp. Biol.* **182**: 147 LP – 171.
- Wilson, D.E. & Reeder, D.M. 2005. *Mammal Species of the World: A Taxonomic and Geographic Reference*, 3rd ed. (D. E. Wilson & D. M. Reeder, eds). The John Hopkins University Press, Baltimore.
- Wittrock, U. 2010. Laryngeally echolocating bats. *Nature* **466**: E6–E6.
- Wu, H., Jiang, T.-L., Müller, R. & Feng, J. 2015. The allometry of echolocation call frequencies in horseshoe bats: nasal capsule and pinna size are the better predictors than forearm length. *J. Zool.* **297**: 211–219.
- Wu, J., Jiao, H., Simmons, N.B., Lu, Q. & Zhao, H. 2018. Testing the sensory trade-off hypothesis in New World bats. *Proc. R. Soc. B Biol. Sci.* **285**: 20181523.
- Zelditch, M., Swiderski, D. & Sheets, H. 2012. *Geometric Morphometrics for Biologists. A Primer.*, 2nd editio. Cambridge. Academic Press. 488.
- Zhao, H., Rossiter, S.J., Teeling, E.C., Li, C., Cotton, J.A. & Zhang, S. 2009. The evolution of color vision in nocturnal mammals. *Proc. Natl. Acad. Sci.* **106**: 8980 – 8985.

CHAPTER TWO: General Methods

In order to test the predictions presented in *Chapter One*, I collected morphological (*i.e.*, skull shape and size), functional (*i.e.*, bite force, masticatory muscles mass, echolocation call parameters) and ecological data (*i.e.*, diet, emission type and call design). The same data collection approach was applied within each chapter unless otherwise stated.

Data collection

Morphological data

Size and shape of bat crania were extracted from 3D digital models of bat skulls. The 3D reconstruction of the models was achieved using three alternative techniques: photogrammetry, μ CT scan and laser scan. The chapter on the reconstruction technique comparison (*i.e.*, *Chapter Three*) reports the details on the equipment and workflow for all three reconstruction methods. Only photogrammetry and μ CT were used to reconstruct the samples used in the macroevolutionary analyses of *Chapters Four* and *Five*.

Skull size and shape of each specimen (*i.e.*, bat skull 3D model) were quantified through geometric morphometric methods. Compared to traditional linear measurements, geometric morphometrics provides a better framework for shape analyses, as the size variance is removed through Procrustes superimposition (Zelditch *et al.*, 2004). By means of Procrustes superimposition, each landmark configuration is translated and rotated to reduce the distances between homologous anatomical points and, therefore, these new coordinates are scaled to a unit centroid size (*i.e.*, the square root of the sum of square distances between a set of landmarks and their centroid) (Bookstein, 1991). The proxy for size is therefore called centroid size, while the shape is represented by the Procrustes coordinates, which are the new coordinates after Procrustes superimposition (Kendall, 1984; Rohlf &

Slice, 1990). Given that after superimposition the variation of each single landmark coordinate is distributed throughout the whole shape, Procrustes coordinates cannot be interpreted as singular traits but need to be analysed in a multivariate statistical framework (Zelditch *et al.*, 2004).

The following geometric morphometric routine was applied independently within each chapter. Bilateral asymmetry (*i.e.*, shape variation between the right and the left side of the cranium) does not account for a significant portion of shape variance when statistical analyses are performed at the interspecific level (Cardini, 2016). Therefore, landmarks were acquired unilaterally only. The open source software Landmark Editor (Wiley *et al.*, 2005) was used to place 24 or 29 unilateral anatomical landmarks on the dorsal, lateral and ventral side of the cranium (the 29 landmark configuration for *Chapters Four* and *Five* is presented in **Figure 1**; the 24 landmark configuration for *Chapter Three* is reported in the main text of the relative chapter). Landmark configurations were adapted from Bogdanowicz *et al.* (2005) and Sztencel-Jablonka *et al.* (2009). Homologous anatomical points were chosen to be easy to identify in all samples, reducing the degree of digitizing error (Bookstein, 1991). Landmarks were defined by 3D coordinates along arbitrary x, y and z axes. The 3D raw coordinates were imported in the open source programming language R for subsequent analyses (R Core Team, 2019). Estimation of missing landmarks can provide valuable information in representing the morphological variation of the specimens (Couette & White, 2010). Therefore, missing landmarks were mirrored on the sagittal plane or, if landmarks were missing on both sides, they were estimated with the thin-plate spline interpolation method (Dempster *et al.*, 1977; [TPS]). Using a single complete landmark configuration as reference, the TPS algorithm interpolates the missing information based on the subset of landmarks available for both the reference and incomplete specimen. The missing landmarks are estimated minimizing the deformation between the reference and the incomplete specimen (*i.e.*, minimum bending energy

principle). Reference specimens for the TPS interpolation were selected using the following approaches in order of preference: 1) individuals of the same species when available; 2) specimens of the same genus; or 3) individuals of the genetically closest species (Gunz *et al.*, 2009).

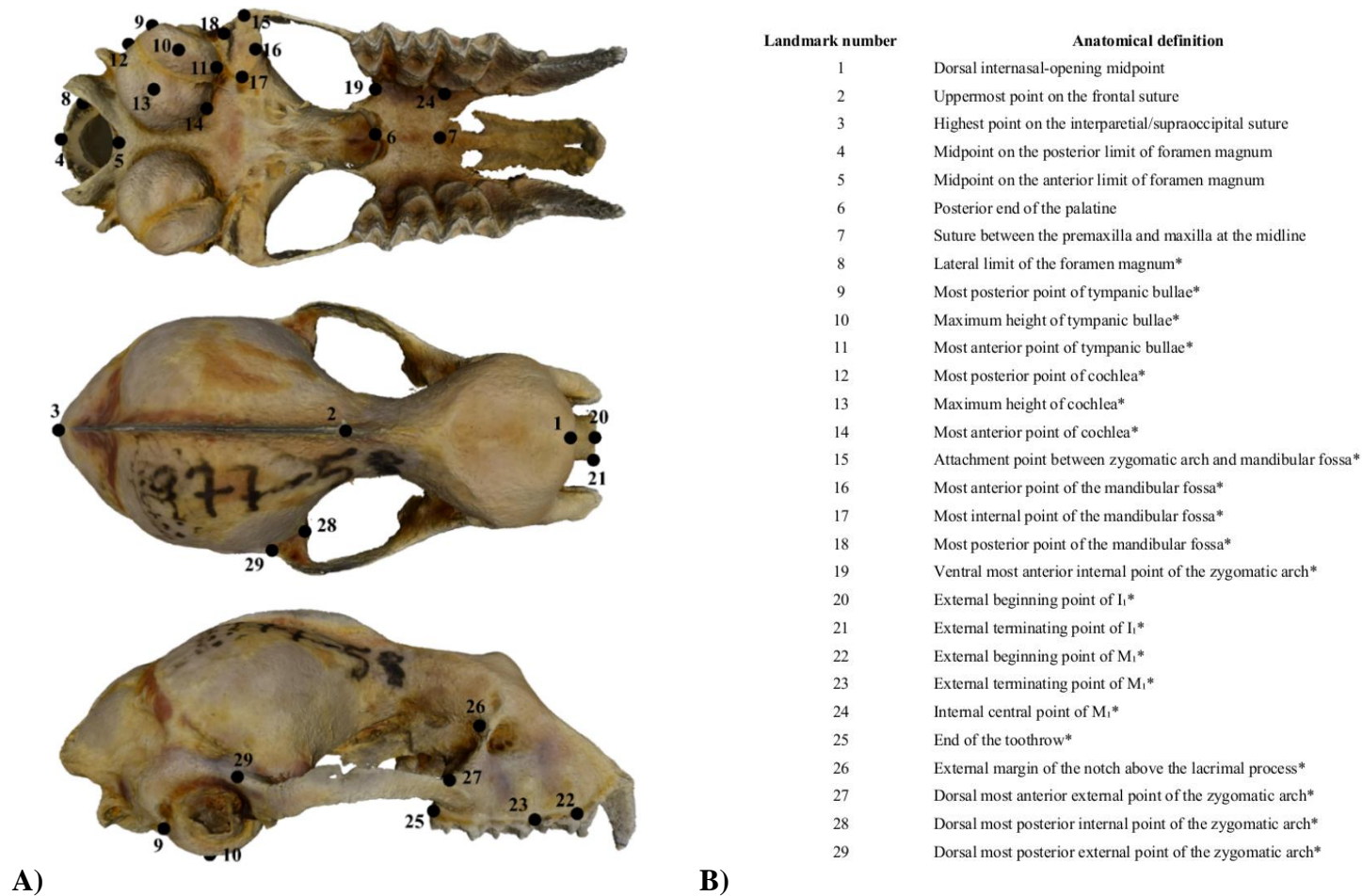


Figure 1. Landmark configuration used in *Chapters Four* and *Five* (29 landmarks). **A)** Representation on *Rhinolophus ferrumequinum*. **B)** Anatomical definitions. Landmarks with * are symmetric landmarks and were placed only on the right side of the skull.

For each specimen, skull size was quantified by the centroid size, and shape by Procrustes coordinates, which were obtained through Generalised Procrustes Analysis (or Procrustes superimposition). Species represented by multiple specimens were averaged in both centroid size and Procrustes coordinates, and these metrics were used for all subsequent statistical analyses in each dataset. When datasets were subsampled (*e.g.* by emission type), the same procedure was repeated separately on each subsample of data (*i.e.*, separate Procrustes superimposition on each dataset). The R packages “geomorph” (Adams & Otárola-Castillo, 2013), “Morpho” (Schlager, 2013) and “RRPP” (Collyer & Adams, 2018) were used in morphological data preparation.

Functional data

Functional data (*i.e.*, echolocation parameters, bite force and muscles mass) were acquired from the literature or collected in the field (data sources, reference literature and estimates are presented within the text for *Chapter Three*, in **Appendices A & B** for *Chapter Four*, and **Appendix C** for *Chapter Five*).

It is widely known that most bat species produce species-specific echolocation sounds (Bell & Fenton, 1981; Vaughan *et al.*, 1997; Ahlén & Baagøe, 1999; Jones & Siemers, 2011; López-Baucells *et al.*, 2019). However, sound estimates display some degree of plasticity due to intrinsic (*e.g.* sexual dimorphism) and extrinsic (*e.g.* degree of environmental clutter) factors. The main sources of variation were evaluated in order to standardise echolocation data used in the analyses (see **Table 1** for a summary).

Table 1. Main sources of variation of echolocation call parameters in bats that were controlled for within this thesis.

Source of variation	Controlled for
Age (<i>i.e.</i> , adult or juvenile)	yes
Jamming avoidance	yes
Habitat structure	yes
Recording condition	yes
Bat detector	yes
Geographical variation	no
Sexual dimorphism	no

Intraspecific differences in echolocation calls are linked to age (*e.g.* Jones & Ransome Roger, 1993) and presence of other conspecifics in the flying area (*i.e.*, jamming avoidance) (Jones *et al.*, 1994; Obrist, 1995). The impact of these sources of variation is relatively easy to control for as published studies usually record only adult bats (or they state otherwise) and control for presence of conspecifics in the recording area. Also, environmental cluttering and recording condition (*e.g.* hand-release or free flight) can play an important role in echolocation call parameters variation (Kalko & Schnitzler, 1993; Parsons, 1998; Kraker-Castañeda *et al.*, 2018). It has also been suggested that the recording device employed (*e.g.* real time or zero-crossing devices) may (Fenton, 2000) or may not (Corben & Fellers, 2001) introduce some error. However, a more recent study reported no differences in echolocation estimates recorded with different bat detectors (Adams *et al.*, 2012). Geographical variation and sexual dimorphism are other known causes of echolocation call variation in some bat species (Fu *et al.*, 2015; Jacobs *et al.*, 2017).

These sources of intraspecific variation are known to be generally smaller than interspecific variation for most of the species (Russo *et al.*, 2018). Other smaller sources of variation are factors related to physical properties of sound such as the Doppler effect (dependent on bat direction of flight) and atmospheric attenuation (dependent on humidity, temperature and distance: Chaverri & Quirós, 2017). These latter sources of variation tend to be negligible when comparing variation between species (Obrist, 1995; Murray *et al.*, 2001). Even if acoustic character displacement is described in some bat species, the current knowledge available does not allow us to control for it on a macroevolutionary scale (Russo *et al.*, 2007). See Russo *et al.* (2018) for an extensive literature review on the factors influencing inter- and intraspecific bat echolocation calls.

Based on these factors, the most recent and complete published data (*i.e.*, frequencies, duration and bandwidth) were selected from the literature available for each species. Data produced with real-time and time-expansion bat detectors were preferred over zero crossing detectors thus zero crossing references were included only when other sources were unavailable (< 10% of the species). Literature with sounds recorded in uncluttered space was selected to avoid variation in call structure due to environmental clutter. Free flight recordings should be preferred over other recording conditions, but most of the references from call libraries are produced following hand-release or roost emergence. Thus, I preferentially selected references recorded under free flight conditions, but hand-release, and, to a smaller extent, roost emergence conditions were included too. Some bat species produce multi-components echolocation calls where each component presents different signal design and frequency (e.g. Molossidæ family, Jung *et al.*, 2014). In order to standardise the data collection, I selected the component with lowest frequency and used its parameters in the analyses. Unpublished data included in this research were collected on adult bats released from the hand in open space conditions. These sounds were recorded with a CM16 microphone mounted on an UltraSoundGate 116 Hm (Avisoft Bioacoustics,

Germany) and the echolocation call parameters of each bat were automatically extracted with SASLab Pro (Avisoft Bioacoustics, Germany). By using R's built-in functions, outliers were excluded from the dataset before averaging each call parameter by species. Chosen references and echolocation matrices are reported in **Appendix A** and **C** for *Chapters Four* and *Five*, respectively.

A recent study suggested that bite force experimental heterogeneity does not affect biological interpretation in macroevolutionary analyses (Manhães *et al.*, 2017).

Nonetheless, bite force data collection was standardised by controlling for the equipment used and gape angle. Unpublished bite force data used in this research were collected by Dr. Anthony Herrel using the protocol described by Aguirre *et al.* (2002). *In vivo* bite forces from the literature were included in the study only when the equipment used was equivalent to that employed to collect the aforementioned unpublished data (details on equipment in Herrel *et al.*, 1999; Aguirre *et al.*, 2002). Gape angle for both the unpublished data and the selected literature was $\sim 25^\circ$, and maximum bite force was used for the analyses (*i.e.*, molar bite force).

Data on masticatory muscles mass (*i.e.*, temporalis, masseter, digastric and pterygoid muscles) from the literature and collected within this study were acquired through dissection of ethanol-preserved specimens. Cranial muscles were removed from both sides under a binocular microscope and measured to the nearest 0.001 g (details in Herrel *et al.*, 2008). The muscles weight was then used in the analyses. References chosen and raw data on both bite force and masticatory muscles are provided in **Appendix B** for *Chapter Four*.

All sensory (*i.e.*, echolocation call parameters) and feeding (*i.e.*, bite forces and muscles mass) estimates were \log_{10} transformed prior to the statistical analyses.

Ecological data

Categorical variables were used in *Chapters Four* and *Five* to assess the relationship between morphology and ecological specializations. In both chapters, species were categorised by broad diet specializations. Specifically, diet was categorised in traditional groups inferred from Wilson and Reeder (2005): insectivorous, frugivorous, hematophagous, predominately vertebrate eater, nectarivorous, omnivorous (*i.e.*, fruit, insect and nectar eater), frugi/insectivorous, nectar/frugivorous and, insect eater that occasionally eat vertebrate. Food hardness was not included as a categorical variable as a recent comparative research failed to find a correlation between hardness and skull shape in three of the largest bat families (Hedrick & Dumont, 2018).

In *Chapter Four*, species ($n = 67$) were additionally categorised as able and unable to laryngeally echolocate as in Thiagavel *et al.* (2018). In this chapter echolocating bats were further categorised according to emission mode in mouth emission, nasal emission and emission from both nose and mouth, following references in **Appendix A** and additional references (Pedersen, 1998; Goudy-Trainor & Freeman, 2002; Brinkløv *et al.*, 2009; Surlykke *et al.*, 2013; Seibert *et al.*, 2015; Jakobsen *et al.*, 2018).

Although the categorisation into oral, nasal and mixed emissions is biologically meaningful, relatively few studies have focused on the topic, preventing the use of the same categorisation for the highly diverse dataset of *Chapter Five* (219 species). Thus, in *Chapter Five*, emission type was categorised as oral emission or nasal emission, the latter subcategorised into New World (*i.e.*, Phyllostomidae species) and Old World species (references in **Appendix C**). Nasal emission implies considerable rearrangements of skull morphology (Pedersen, 2000), but different selective pressures might apply to these two groups as nasal chambers in some Old World nasal-emitters are known to behave as resonance structures (Armstrong & Coles, 2007; Jacobs *et al.*, 2014). Furthermore, in

Chapter Five, species were grouped by call designs following Jones & Teeling (2006). Specifically, this categorisation takes into consideration the number of harmonics, the magnitude of broadband portions in the call and the call duration (**Figure 1** in *Chapter One*).

Statistical analyses

Similarity of phenotypic traits between related taxa can be attributed to inheritance from a shared ancestor or to adaptation to similar environments (*i.e.*, independent evolution of the trait) (Edwards & Naeem, 1993). Therefore, shared phylogenetic history can be responsible for some variation in any morphological, sensory and feeding trait (Blomberg *et al.*, 2003). Evolutionary analyses have to take into account non-independence of species to avoid misleading results (Felsenstein, 1985; Freckleton *et al.*, 2002). In order to test if the morphological data (*i.e.*, skull size and shape) presented a significant phylogenetic signal (*i.e.*, phylogenetic non-independence), I used Blomberg *et al.*'s (2003) K statistic and its multivariate extension for shape (K_{multiv}) (Adams, 2014). The K statistic reflects the degree of congruence between phenotypic data and the phylogeny (Blomberg *et al.*, 2003). When a significant phylogenetic signal was present, phylogenetic comparative methods were applied within the statistical analyses. Phylogenetic relatedness was taken into account using the variance-covariance matrix of a phylogenetic tree computed under Brownian Motion model of evolution (Rohlf, 2006). I used a series of pruned trees, extracted from the Chiroptera phylogenetic tree published by Shi & Rabosky (2015), with the tips corresponding to the species of each chapter.

Statistical analyses were first performed under a classic approach (*i.e.*, ordinary least square regression [OLS] and partial least squares regression [PLS]) and repeated taking phylogenetic non-independence into account (*i.e.*, phylogenetic generalised least squares regression [PGLS] and phylogenetic PLS) (Rohlf, 2007; Adams & Felice, 2014). In OLS

and PGLS models, the morphological trait (*i.e.*, univariate skull size and multivariate shape) was input as the dependent variable and the functional/ecological trait as the independent (*e.g.* shape ~ peak frequency). Variables were input into PLS and phylogenetic PLS in blocks (*e.g.* block 1 = shape variables VS block 2 = echolocation parameters). The order of input does not change the results as PLS analysis does not assume any directionality (*i.e.*, does not assume a block as dependent variable). It identifies the vectors of each block that maximises blocks covariation (Rohlf & Corti, 2000). For this reason, PLS vectors are interpreted in pair and the strength of block covariation is quantified using the RV coefficient that ranges from 0 (no covariation) to 1 (perfect covariation, *i.e.*, identity) (Escoufier, 1973). The RV is broadly used to test hypotheses of functional integration and modularity of anatomical structures (*e.g.* rostrum vs braincase) (*e.g.* Santana & Lofgren, 2013). The RV estimation is dependent on sample size and number of variables (Fruciano *et al.*, 2013), therefore, I reported it only as an indicative metric of association between blocks of variables. The standardised test statistic (z-score) proposed by Adams and Collyer (2016) was employed to control for sample size and number of variables, obtaining comparable measures of associations between datasets. These allowed me to test the prediction of differences in the strength of associations between morphology and functional parameters in *Chapter Four* (*e.g.* association strength of shape block-echolocation block compared to shape block-feeding block).

Misleading interpretations on shape variance appear also when a significant allometric effect (*i.e.*, correlation between shape and size) co-occurs with significant correlation between size and the trait of interest (*e.g.* peak frequency) (Loy *et al.*, 1996). If the allometric effect is not taken into account, it can obscure the correlation pattern between shape and the trait. Therefore, I first examined allometry using Procrustes shape coordinates as dependent variables and size (as \log_{10} transformed centroid size) as the independent variable under both OLS and PGLS models (Cardini & Polly, 2013). When

evolutionary allometry was present, size was included in the OLS and PGLS models as a fixed effect and in interaction with the trait when testing for shape variance (*i.e.*, shape ~ size+trait+trait:size). In this way, shape variation due to size, trait and their interaction can be assessed (Freckleton, 2009; Adams & Collyer, 2018). As the PLS method does not assume any directionality, functional traits correlating with size were corrected for the centroid size (CS) before testing for covariation with shape in PLS analyses (in order to remove allometric effect). The Blomberg *et al.*'s (2003) approach was used to correct traits for size. First the phylogenetic standardised contrasts (PICs) were computed on the log₁₀ transformed CS and trait. Second, I computed an OLS regression (*lm*) through the origin and noted the slope *b* (allometric exponent):

$$lm(PICs(\log_{10}Trait) \sim PICs(\log_{10}CS) - 1)$$

Finally, the corrected trait (*corr.Trait*) was defined as follows:

$$corr.Trait = \frac{Trait}{CS^b}$$

This procedure was repeated for all sensory and feeding traits, and the log₁₀ size-corrected traits (log₁₀corr.Trait) were then input in the PLS and phylogenetic PLS as a block of variables in order to test their covariation with shape.

The shape variation of the sample was analysed through Principal Component Analysis (PCA). The variance-covariance matrix of the Procrustes coordinates was used to extract orthogonal vectors (PCs) that summarise variation within the sample. Variation of 3D features was visualised along PC axes applying the Thin-Plate-Spline algorithm (TPS) on the mean shape of the morphospace (Bookstein 1989). The bat skull with lowest deviation from the mean shape was chosen for the visualisation. This model was warped along the positive and the negative sides of PC axes to display the shape variation within the sample (Drake and Klingenberg 2010).

The relationship between shape (multivariate trait) and a continuous trait obtained under multivariate regression models (OLS or PGLS) can be plotted using the univariate descriptor of shape called regression score (Drake & Klingenberg, 2008). The regression score is the shape variable that shows maximal covariation with the trait. The trait was input in the plot as $\log_{10}\text{corr.Trait}$ in order to remove the shape variance explained by the allometric effect. By plotting the regression score versus the trait (as $\log_{10}\text{corr.Trait}$), both the predicted and residual components of shape variation are shown. 3D variation of shape was visualised along the regression vector to identify the features of shape that covary with the trait. Therefore, the same TPS approach described above was used to visualise shape deformations. In this case, the predicted values of the PGLS model ($\text{shape} \sim \log_{10}\text{corr.Trait}$) were used to warp the skull shapes associated with the minimum value for the trait (*e.g.* lowest peak frequency) and the maximum value for the same trait (*e.g.* maximum peak frequency). This approach was used in *Chapters Four and Five*.

All the analyses were performed in R software using “geomorph” (Adams & Otárola-Castillo, 2013), “Morpho” (Schlager, 2013), RRPP (Collyer & Adams, 2018), “phytools” (Revell, 2012), and “geiger” (Pennell *et al.*, 2014) packages. The specific statistical analyses performed to address the different evolutionary predictions are detailed in the methods section of each chapter.

References

- Adams, A.M., Jantzen, M.K., Hamilton, R.M. & Fenton, M.B. 2012. Do you hear what I hear? Implications of detector selection for acoustic monitoring of bats. *Methods Ecol. Evol.* **3**: 992–998.
- Adams, D.C. 2014. A Generalized K Statistic for Estimating Phylogenetic Signal from Shape and Other High-Dimensional Multivariate Data. *Syst. Biol.* **63**: 685–697.
- Adams, D.C. & Collyer, M.L. 2016. On the comparison of the strength of morphological integration across morphometric datasets. *Evolution (N. Y.)* **70**: 2623–2631.
- Adams, D.C. & Collyer, M.L. 2018. Phylogenetic ANOVA: Group-clade aggregation, biological challenges, and a refined permutation procedure. *Evolution (N. Y.)* **72**: 1204–1215.

- Adams, D.C. & Felice, R.N. 2014. Assessing Trait Covariation and Morphological Integration on Phylogenies Using Evolutionary Covariance Matrices. *PLoS One* **9**: e94335. Public Library of Science.
- Adams, D.C. & Otárola-Castillo, E. 2013. geomorph: an r package for the collection and analysis of geometric morphometric shape data. *Methods Ecol. Evol.* **4**: 393–399.
- Aguirre, L.F., Herrel, A., van Damme, R. & Matthysen, E. 2002. Ecomorphological analysis of trophic niche partitioning in a tropical savannah bat community. *Proc. R. Soc. London. Ser. B Biol. Sci.* **269**: 1271–1278.
- Ahlén, I. & Baagøe, J.H. 1999. Use of ultrasound detectors for bat studies in Europe: experiences from field identification, surveys, and monitoring. *Acta Chiropterologica* **1**: 137–150.
- Armstrong, K.N. & Coles, R.B. 2007. Echolocation Call Frequency Differences Between Geographic Isolates of *Rhinonictis Aurantia* (Chiroptera: Hipposideridae): Implications of Nasal Chamber Size. *J. Mammal.* **88**: 94–104.
- Bell, G.P. & Fenton, M.B. 1981. Recognition of Species of Insectivorous Bats by Their Echolocation Calls. *J. Mammal.* **62**: 233–243.
- Blomberg, S.P., Garland, T. & Ives, A.R. 2003. Testing for phylogenetic signal in comparative data: behavioral traits are more labile. *Evolution (N. Y.)* **57**: 717–745.
- Bogdanowicz, W., Juste, J., Owen, R.D. & Sztencel, A. 2005. Geometric morphometrics and cladistics: testing evolutionary relationships in mega- and microbats. *Acta Chiropterologica* **7**: 39–49.
- Bookstein, F.L. 1991. *Morphometric tools for landmark data: geometry and biology [Orange book]*. Cambridge University Press, Cambridge New York.
- Brinkløv, S., Kalko, E.K. V & Surlykke, A. 2009. Intense echolocation calls from two ‘whispering’ bats, *Artibeus jamaicensis* and *Macrophyllum macrophyllum* (Phyllostomidae). *J. Exp. Biol.* **212**: 11–20.
- Cardini, A. 2016. Lost in the Other Half: Improving Accuracy in Geometric Morphometric Analyses of One Side of Bilaterally Symmetric Structures. *Syst. Biol.* **65**: 1096–1106.
- Cardini, A. & Polly, P.D. 2013. Larger mammals have longer faces because of size-related constraints on skull form. *Nat. Commun.* **4**: 2458.
- Chaverri, G. & Quirós, O.E. 2017. Variation in echolocation call frequencies in two species of free-tailed bats according to temperature and humidity. *J. Acoust. Soc. Am.* **142**: 146–150.
- Collyer, M.L. & Adams, D.C. 2018. RRPP: An r package for fitting linear models to high-dimensional data using residual randomization. *Methods Ecol. Evol.* **9**: 1772–1779.
- Corben, C. & Fellers, G.M. 2001. Choosing the ‘correct’ bat detector – a reply. *Acta Chiropterologica* **3**: 245–345.
- Couette, S. & White, J. 2010. 3D geometric morphometrics and missing-data. Can extant taxa give clues for the analysis of fossil primates? *Comptes Rendus Palevol* **9**: 423–433.
- Dempster, A., Laird, N., & Rubin, D. 1977. Maximum likelihood from incomplete data via the EM algorithm. *Journal of the Royal Statistical Society. Series B*, **39**: 1–38.
- Drake, A.G. & Klingenberg, C.P. 2008. The pace of morphological change: historical transformation of skull shape in St Bernard dogs. *Proc. R. Soc. B Biol. Sci.* **275**: 71–76.

- Edwards, S. V & Naeem, S. 1993. The Phylogenetic Component of Cooperative Breeding in Perching Birds. *Am. Nat.* **141**: 754–789. The University of Chicago Press.
- Escoufier, Y. 1973. Le Traitement des Variables Vectorielles. *Biometrics* **29**: 751:760.
- Felsenstein, J. 1985. Phylogenies and the Comparative Method. *Am. Nat.* **125**: 1–15.
- Fenton, M.B. 2000. Choosing the ‘correct’ bat detector. *Acta Chiropterologica* **2**: 215–224.
- Freckleton, R.P. 2009. The seven deadly sins of comparative analysis. *J. Evol. Biol.* **22**: 1367–1375.
- Freckleton, R.P., Harvey, P.H. & Pagel, M. 2002. Phylogenetic Analysis and Comparative Data: A Test and Review of Evidence. *Am. Nat.* **160**: 712–726.
- Fruciano, C., Franchini, P. & Meyer, A. 2013. Resampling-Based Approaches to Study Variation in Morphological Modularity. *PLoS One* **8**: e69376.
- Fu, Z.-Y., Dai, X.-Y., Xu, N., Shi, Q., Li, G.-J., Li, B., *et al.* 2015. Sexual dimorphism in echolocation pulse parameters of the CF-FM bat, *Hipposideros pratti*. *Zool. Stud.* **54**: 44.
- Goudy-Trainor, A. & Freeman, P.W. 2002. Call Parameters and Facial Features in Bats: A Surprising Failure of form Following Function. *Acta Chiropterologica* **4**: 1–16.
- Gunz, P., Mitteroecker, P., Neubauer, S., Weber, G.W. & Bookstein, F.L. 2009. Principles for the virtual reconstruction of hominin crania. *J. Hum. Evol.* **57**: 48–62.
- Hedrick, B.P. & Dumont, E.R. 2018. Putting the leaf-nosed bats in context: a geometric morphometric analysis of three of the largest families of bats. *J. Mammal.* **99**: 1042–1054.
- Herrel, A., Spithoven, L., van Damme, R. & de Vree, F. 1999. Sexual dimorphism of head size in *Gallotia galloti*: testing the niche divergence hypothesis by functional analyses. *Funct. Ecol.* **13**: 289–297.
- Jacobs, D.S., Bastian, A. & Bam, L. 2014. The influence of feeding on the evolution of sensory signals: A comparative test of an evolutionary trade-off between masticatory and sensory functions of skulls in southern African Horseshoe bats (Rhinolophidae). *J. Evol. Biol.* **27**: 2829–2840.
- Jacobs, D.S., Catto, S., Mutumi, G.L., Finger, N. & Webala, P.W. 2017. Testing the Sensory Drive Hypothesis: Geographic variation in echolocation frequencies of Geoffroy’s horseshoe bat (Rhinolophidae: *Rhinolophus clivosus*). *PLoS One* **12**: e0187769.
- Jakobsen, L., Hallam, J., Moss, C.F. & Hedenström, A. 2018. Directionality of nose-emitted echolocation calls from bats without a nose leaf (*Plecotus auritus*). *J. Exp. Biol.* **221**.
- Jones, G. & Ransome Roger, D. 1993. Echolocation calls of bats are influenced by maternal effects and change over a lifetime. *Proc. R. Soc. London. Ser. B Biol. Sci.* **252**: 125–128.
- Jones, G. & Siemers, B.M. 2011. The communicative potential of bat echolocation pulses. *J. Comp. Physiol. A* **197**: 447–457.
- Jones, G., Sripathi, K., Waters, D.A. & Marimuthu, G. 1994. Individual variation in the echolocation calls of three sympatric Indian hipposiderid bats, and an experimental attempt to jam bat echolocation. *FOLIA Zool.* **43**: 347–361.
- Jones, G. & Teeling, E. 2006. The evolution of echolocation in bats. *Trends Ecol. Evol.* **21**: 149–156.

- Jung, K., Molinari, J. & Kalko, E.K. V. 2014. Driving Factors for the Evolution of Species-Specific Echolocation Call Design in New World Free-Tailed Bats (Molossidae). *PLoS One* **9**: 1–9.
- Kalko, E.K. V & Schnitzler, H.-U. 1993. Plasticity in echolocation signals of European pipistrelle bats in search flight: implications for habitat use and prey detection. *Behav. Ecol. Sociobiol.* **33**: 415–428.
- Kendall, D.G. 1984. Shape Manifolds, Procrustean Metrics, and Complex Projective Spaces. *Bull. London Math. Soc.* **16**: 81–121.
- Klingenberg, C.P. 2013. Visualizations in geometric morphometrics: how to read and how to make graphs showing shape changes. *Hystrix, Ital. J. Mammal.* **24**: 15–24.
- Kraker-Castañeda, C., Santos-Moreno, A., Lorenzo, C. & Mac Swiney González, M.C. 2018. Effect of intrinsic and extrinsic factors on the variability of echolocation pulses of *Myotis nigricans* (Schinz, 1821) (Chiroptera: Vespertilionidae). *Bioacoustics* **28**: 366–380
- López-Baucells, A., Torrent, L., Rocha, R., E.D. Bobrowiec, P., M. Palmeirim, J. & F.J. Meyer, C. 2019. Stronger together: Combining automated classifiers with manual post-validation optimizes the workload vs reliability trade-off of species identification in bat acoustic surveys. *Ecol. Inform.* **49**: 45–53.
- Loy, A., Cataudella, S. & Corti, M. 1996. Shape Changes during the Growth of the Sea Bass, *Dicentrarchus labrax* (Teleostea: Perciformes), in Relation to Different Rearing Conditions BT - Advances in Morphometrics. In: (L. F. Marcus, M. Corti, A. Loy, G. J. P. Naylor, & D. E. Slice, eds), pp. 399–405. Springer US, Boston, MA.
- Manhães, I.A., Nogueira, M.R. & Monteiro, L.R. 2017. Bite force and evolutionary studies in phyllostomid bats: a meta-analysis and validation. *J. Zool.* **302**: 288–297.
- Murray, K.L., Robbins, L.W. & Britzke, E.R. 2001. Variation in Search-Phase Calls of Bats. *J. Mammal.* **82**: 728–737.
- Obrist, M.K. 1995. Flexible bat echolocation: the influence of individual, habitat and conspecifics on sonar signal design. *Behav. Ecol. Sociobiol.* **36**: 207–219.
- Parsons, S. 1998. The effect of recording situation on the echolocation calls of the New Zealand lesser short-tailed bat (*Mystacina tuberculata* Gray). *New Zeal. J. Zool.* **25**: 147–156.
- Pedersen, S.C. 1998. Morphometric Analysis of the Chiropteran Skull with Regard to Mode of Echolocation. *J. Mammal.* **79**: 91–103.
- Pedersen, S.C. 2000. Skull growth and the acoustical axis of the head in bats. In: *Ontogeny, functional ecology, and evolution of bats* (R. A. Adams & S. C. Pedersen, eds), p. 174:213. Cambridge University Press, New York.
- Pennell, M.W., Eastman, J.M., Slater, G.J., Brown, J.W., Uyeda, J.C., FitzJohn, R.G., *et al.* 2014. geiger v2.0: an expanded suite of methods for fitting macroevolutionary models to phylogenetic trees. *Bioinformatics* **30**: 2216–2218.
- R Core Team 2019. R: A language and environment for statistical computing. R Foundation for Statistical Computing, Vienna, Austria. URL <https://www.R-project.org/>.
- Revell, L.J. 2012. phytools: an R package for phylogenetic comparative biology (and other things). *Methods Ecol. Evol.* **3**: 217–223.
- Rohlf, F.J. 2006. A Comment on Phylogenetic Correction. *Evolution (N. Y.)* **60**: 1509–1515.

- Rohlf, F.J. 2007. Comparative methods for the analysis of continuous variables: geometric interpretations. *Evolution (N. Y.)* **55**: 2143–2160.
- Rohlf, F.J. & Corti, M. 2000. Use of Two-Block Partial Least-Squares to Study Covariation in Shape. *Syst. Biol.* **49**: 740–753.
- Rohlf, F.J. & Slice, D. 1990. Extensions of the Procrustes Method for the Optimal Superimposition of Landmarks. *Syst. Zool.* **39**: 40–59.
- Russo, D., Ancillotto, L. & Jones, G. 2018. Bats are still not birds in the digital era: echolocation call variation and why it matters for bat species identification. *Can. J. Zool.* **96**: 63–78.
- Russo, D., Mucedda, M., Bello, M., Biscardi, S., Pidinchedda, E. & Jones, G. 2007. Divergent echolocation call frequencies in insular rhinolophids (Chiroptera): a case of character displacement? *J. Biogeogr.* **34**: 2129–2138.
- Santana, S.E. & Lofgren, S.E. 2013. Does nasal echolocation influence the modularity of the mammal skull? *J. Evol. Biol.* **26**: 2520–2526.
- Schlager, S. 2013. Morpho: Calculations and visualizations related to Geometric Morphometrics. R package version 0.17. <http://sourceforge.net/projects/morpho-rpackage/>.
- Seibert, A.-M., Koblitz, J.C., Denzinger, A. & Schnitzler, H.-U. 2015. Bidirectional Echolocation in the Bat *Barbastella barbastellus*: Different Signals of Low Source Level Are Emitted Upward through the Nose and Downward through the Mouth. *PLoS One* **10**: e0135590.
- Shi, J.J. & Rabosky, D.L. 2015. Speciation dynamics during the global radiation of extant bats. *Evolution (N. Y.)* **69**: 1528–1545.
- Surlykke, A., Jakobsen, L., Kalko, E. & Page, R. 2013. Echolocation intensity and directionality of perching and flying fringe-lipped bats, *Trachops cirrhosus* (Phyllostomidae). *Frontiers in Physiology* **4**: 1-9.
- Sztencel-Jabłonka, A., Jones, G. & Bogdanowicz, W. 2009. Skull morphology of two cryptic bat species: *Pipistrellus pipistrellus* and *P. pygmaeus* - a 3D geometric morphometrics approach with landmark reconstruction. *Acta Chiropterologica* **11**: 113–126.
- Thiagavel, J., Cechetto, C., Santana, S.E., Jakobsen, L., Warrant, E.J. & Ratcliffe, J.M. 2018. Auditory opportunity and visual constraint enabled the evolution of echolocation in bats. *Nat. Commun.* **9**: 98.
- Vaughan, N., Jones, G. & Harris, S. 1997. Identification of British bat species by multivariate analysis of echolocation call parameters. *Bioacoustics* **7**: 189–207.
- Wiley, D.F., Amenta, N., Alcantara, D.A., Ghosh, D., Kil, Y.J., Delson, E., *et al.* 2005. Evolutionary Morphing. In: *Proceedings of IEEE Visualization*, pp. 431–438.
- Zelditch, M.L., Swiderski, D.L., Sheets, H.D. & Fink, W.L. 2004. 4 - Theory of shape. In: (M. L. Zelditch, D. L. Swiderski, H. D. Sheets, & W. L. B. T.-G. M. for B. Fink, eds), pp. 73–104. Academic Press, San Diego.

Appendix A

Estimates for sensorial traits and categorical variables used in *Chapter Four*. Abbreviations stand for SF: start frequency (KHz), EF: end frequency (KHz), BW: bandwidth (KHz), FP: peak frequency (KHz), D: duration (ms), SR: sweep rate (KHz/ms), E: ability to echolocate (LE: echolocating species; NLE: non echolocating species), ET: emission type (M: oral; R: nasal; B: both oral and nasal). References: data sources.

Species	SF	EF	BW	FP	D	SR	E	ET	References
<i>Emballonura monticola</i>	53.55	38.98	64.18	51.24	5.42	11.84	LE	M	(Hughes <i>et al.</i> , 2010)
<i>Taphozous melanopogon</i>	36.60	22.58	55.78	29.71	6.02	9.27	LE	M	(Hughes <i>et al.</i> , 2010)
<i>Hipposideros cervinus</i>	131.27	111.46	19.86	130.37	4.48	4.43	LE	R	(Pavey & Burwell, 2008; Collen, 2012)
<i>Hipposideros diadema</i>	54.90	50.90	4.00	54.90	11.12	0.36	LE	R	(Fenton, 1982; Collen, 2012)
<i>Hipposideros larvatus</i>	91.50	81.50	10.80	92.30	6.60	1.64	LE	R	(Phauk <i>et al.</i> , 2013)
<i>Hipposideros ridleyi</i>	62.51	54.27	8.26	62.36	7.06	1.17	LE	R	(Kingston <i>et al.</i> , 2000; Collen, 2012)
<i>Miniopterus schreibersi</i>	85.20	52.10	33.10	54.20	5.80	5.71	LE	M	(Russo & Jones, 2002)
<i>Cheirosmeles torquatus</i>	32.00	18.70	13.30	24.10	21.10	0.63	LE	M	(Kingston <i>et al.</i> , 2003)
<i>Molossus molossus</i>	39.17	37.30	2.47	38.67	10.33	0.24	LE	M	(Jung & Kalko, 2011; Jung <i>et al.</i> , 2014)
<i>Molossus rufus</i>	31.75	30.05	1.70	31.45	13.30	0.13	LE	M	(MacSwiney G. <i>et al.</i> , 2008)

Species	SF	EF	BW	FP	D	SR	E	ET	References
<i>Nyctinomops laticaudatus</i>	29.70	25.10	4.60	26.40	12.50	0.37	LE	M	(MacSwiney G. <i>et al.</i> , 2008)
<i>Tadarida teniotis</i>	17.00	12.10	4.90	13.00	16.60	0.30	LE	M	(Russo & Jones, 2002)
<i>Pteronotus parnellii</i>	63.13	37.23	30.45	59.02	22.10	1.38	LE	M	(Pio <i>et al.</i> , 2010)
<i>Noctilio albiventris</i>	72.80	67.00	5.80	72.80	9.70	0.60	LE	M	(Kalko <i>et al.</i> , 1998)
<i>Noctilio leporinus</i>	57.00	31.10	25.90	57.00	12.80	2.02	LE	M	(Schnitzler <i>et al.</i> , 1994)
<i>Anoura geoffroyi</i>	105.87	66.30	39.57	83.08	2.08	19.02	LE	R	(Zamora-Gutierrez <i>et al.</i> , 2016)
<i>Artibeus jamaicensis</i>	90.40	66.00	24.40	78.80	0.90	27.11	LE	R	(Brinkløv <i>et al.</i> , 2009)
<i>Artibeus lituratus</i>	80.30	50.60	29.70	63.00	2.30	12.91	LE	R	(Pio <i>et al.</i> , 2010; Zamora-Gutierrez <i>et al.</i> , 2016)
<i>Carollia brevicauda</i>	60.20	43.23	21.00	49.84	0.77	27.27	LE	B	(Pinilla-Cortés & Rodríguez-Bolaños, 2017)
<i>Carollia castanea</i>	115.31	53.70	61.51	82.36	0.67	92.36	LE	B	Chaverri G. unpublished data
<i>Carollia perspicillata</i>	84.90	50.00	43.90	56.60	1.50	29.27	LE	B	(Thies <i>et al.</i> , 1998)
<i>Chiroderma villosum</i>	112.90	81.30	31.60	91.80	1.40	22.57	LE	R	(Pio <i>et al.</i> , 2010)
<i>Desmodus rotundus</i>	83.23	43.97	39.26	72.56	5.55	7.07	LE	B	(Rodríguez-San Pedro & Allendes, 2017)
<i>Glossophaga soricina</i>	136.95	56.99	77.59	87.88	1.10	70.54	LE	B	Chaverri G. unpublished data
<i>Lophostoma silvicolum</i>	104.27	46.12	60.67	69.95	0.75	80.89	LE	B	Chaverri G. unpublished data
<i>Micronycteris hirsuta</i>	97.90	69.10	28.80	80.80	1.40	20.57	LE	B	(Pio <i>et al.</i> , 2010)
<i>Micronycteris megalotis</i>	116.00	81.20	34.80	98.10	1.50	23.20	LE	B	(Pio <i>et al.</i> , 2010)

Species	SF	EF	BW	FP	D	SR	E	ET	References
<i>Micronycteris minuta</i>	82.00	48.00	34.00	61.20	1.60	21.25	LE	B	(Pio <i>et al.</i> , 2010)
<i>Mimon crenulatum</i>	83.00	58.00	25.00	66.10	1.50	16.67	LE	B	(Pio <i>et al.</i> , 2010)
<i>Phyllostomus discolor</i>	86.53	37.19	49.16	57.28	0.94	52.30	LE	R	Chaverri G. unpublished data
<i>Phyllostomus hastatus</i>	58.30	38.00	20.30	47.10	2.70	7.52	LE	R	(Pio <i>et al.</i> , 2010)
<i>Platyrrhinus helleri</i>	137.40	79.47	56.98	98.46	0.51	111.73	LE	R	Chaverri G. unpublished data
<i>Sturnira lilium</i>	121.48	45.54	78.09	84.02	0.64	122.02	LE	R	Chaverri G. unpublished data
<i>Trachops cirrhosus</i>	106.23	37.81	71.38	69.55	0.53	134.68	LE	B	Chaverri G. unpublished data
<i>Uroderma bilobatum</i>	89.10	62.10	27.00	74.70	1.60	16.88	LE	R	(Pio <i>et al.</i> , 2010)
<i>Cynopterus brachyotis</i>							NLE		(Jones & Teeling, 2006)
<i>Eidolon helvum</i>							NLE		(Jones & Teeling, 2006)
<i>Epomophorus wahlbergi</i>							NLE		(Jones & Teeling, 2006)
<i>Pteropus poliocephalus</i>							NLE		(Jones & Teeling, 2006)
<i>Pteropus vampyrus</i>							NLE		(Jones & Teeling, 2006)
<i>Rousettus aegyptiacus</i>							NLE		(Jones & Teeling, 2006)
<i>Rhinolophus affinis</i>	74.86	66.66	17.32	85.86	46.48	0.37	LE	R	(Jiang <i>et al.</i> , 2008; Son <i>et al.</i> , 2016)
<i>Rhinolophus blasii</i>	90.30	78.10	12.20	94.00	44.10	0.28	LE	R	(Siemers <i>et al.</i> , 2005)
<i>Rhinolophus ferrumequinum</i>	70.20	67.30	2.90	81.30	50.50	0.06	LE	R	(Russo & Jones, 2002)

Species	SF	EF	BW	FP	D	SR	E	ET	References
<i>Rhinolophus hipposideros</i>	99.00	96.60	2.40	111.10	43.60	0.06	LE	R	(Russo & Jones, 2002)
<i>Rhinolophus mehelyi</i>	69.82	86.50	20.30	106.80	19.56	1.04	LE	R	(Salsamendi <i>et al.</i> , 2005)
<i>Eptesicus furinalis</i>	40.40	36.40	4.00	37.60	7.10	0.56	LE	M	(MacSwiney G. <i>et al.</i> , 2008)
<i>Eptesicus serotinus</i>	50.40	27.10	23.30	29.90	7.30	3.19	LE	M	(Russo & Jones, 2002)
<i>Hypsugo savii</i>	47.30	32.80	14.50	34.60	8.10	1.79	LE	M	(Russo & Jones, 2002)
<i>Kerivoula papillosa</i>	191.96	67.53	115.94	114.29	2.36	49.13	LE	M	(Schmieder <i>et al.</i> , 2012)
<i>Murina cyclotis</i>	121.38	57.35	69.27	93.81	1.78	38.92	LE	M	(Hughes <i>et al.</i> , 2011)
<i>Myotis albescens</i>	103.50	43.30	29.00	56.20	5.50	5.27	LE	M	Giacomini G. unpublished data
<i>Myotis bechsteinii</i>	111.00	33.80	77.20	51.00	2.54	30.39	LE	M	(Vaughan <i>et al.</i> , 1997)
<i>Myotis blythii</i>	74.40	30.40	44.00	41.40	4.30	10.23	LE	M	(Russo & Jones, 2002)
<i>Myotis brandtii</i>	85.50	33.70	51.80	47.90	3.06	16.93	LE	M	(Vaughan <i>et al.</i> , 1997)
<i>Myotis capaccinii</i>	83.60	39.70	43.90	50.40	3.80	11.55	LE	M	(Russo & Jones, 2002)
<i>Myotis dasycneme</i>	73.20	29.40	43.70	40.20	1.70	25.71	LE	M	(Siemers & Schnitzler, 2004)
<i>Myotis daubentoni</i>	77.00	32.20	44.80	47.00	3.20	14.00	LE	M	(Russo & Jones, 2002)
<i>Myotis emarginatus</i>	109.00	41.20	67.80	58.00	3.60	18.83	LE	M	(Russo & Jones, 2002)
<i>Myotis myotis</i>	79.60	27.90	51.70	39.10	4.60	11.24	LE	M	(Russo & Jones, 2002)
<i>Myotis mystacinus</i>	96.40	32.40	64.00	47.50	4.20	15.24	LE	M	(Russo & Jones, 2002)

Species	SF	EF	BW	FP	D	SR	E	ET	References
<i>Myotis nattereri</i>	111.80	24.40	87.40	46.90	4.70	18.60	LE	M	(Russo & Jones, 2002)
<i>Myotis nigricans</i>	62.00	51.00	11.00	54.00	7.20	1.53	LE	M	(Siemers <i>et al.</i> , 2001)
<i>Nyctalus noctula</i>	30.55	21.90	8.65	22.60	18.40	0.47	LE	M	(Russo & Jones, 2002)
<i>Pipistrellus pipistrellus</i>	68.80	46.60	22.20	46.90	5.90	3.76	LE	M	(Russo & Jones, 2002)
<i>Plecotus austriacus</i>	41.40	23.60	17.80	32.60	3.80	4.68	LE	B	(Russo & Jones, 2002)
<i>Scotophilus kuhlii</i>	84.90	36.60	48.30	43.30	4.10	11.78	LE	M	(Pottie <i>et al.</i> , 2005)

References Appendix A

- Brinkløv, S., Kalko, E.K. V & Surlykke, A. 2009. Intense echolocation calls from two 'whispering' bats, *Artibeus jamaicensis* and *Macrophyllum macrophyllum* (Phyllostomidae). *J. Exp. Biol.* **212**: 11–20.
- Collen, A. 2012. The evolution of echolocation in bats: a comparative approach. University College London.
- Fenton, M.B. 1982. Echolocation Calls and Patterns of Hunting and Habitat Use of Bats (Microchiroptera) from Chillagoe, North Queensland. *Aust. J. Zool.* **30**: 417–425.
- Hughes, A.C., Satasook, C., Bates, P.J.J., Soisook, P., Sritongchuay, T., Jones, G., *et al.* 2010. Echolocation Call Analysis and Presence-Only Modelling as Conservation Monitoring Tools for Rhinolophoid Bats in Thailand. *Acta Chiropterologica* **12**: 311–327.
- Hughes, A.C., Satasook, C., Bates, P.J.J., Soisook, P., Sritongchuay, T., Jones, G., *et al.* 2011. Using Echolocation Calls to Identify Thai Bat Species: Vespertilionidae, Emballonuridae, Nycteridae and Megadermatidae. *Acta Chiropterologica* **13**: 447–455.
- Jiang, T., Feng, J., Sun, K. & Wang, J. 2008. Coexistence of two sympatric and morphologically similar bat species *Rhinolophus affinis* and *Rhinolophus pearsoni*. *Prog. Nat. Sci.* **18**: 523–532.
- Jones, G. & Teeling, E. 2006. The evolution of echolocation in bats. *Trends Ecol. Evol.* **21**: 149–156.
- Jung, K. & Kalko, E.K. V. 2011. Adaptability and vulnerability of high flying Neotropical aerial insectivorous bats to urbanization. *Divers. Distrib.* **17**: 262–274.
- Jung, K., Molinari, J. & Kalko, E.K. V. 2014. Driving Factors for the Evolution of Species-Specific Echolocation Call Design in New World Free-Tailed Bats (Molossidae). *PLoS One* **9**: 1–9.
- Kalko, E.K. V, Schnitzler, H., Kaipf, I. & Grinnell, A.D. 1998. Echolocation and Foraging Behavior of the Lesser Bulldog Bat, *Noctilio albiventris*: Preadaptations for Piscivory? *Behav. Ecol. Sociobiol.* **42**: 305–319.
- Kingston, T., Jones, G., Akbar, Z. & Kunz, T.H. 2003. Alternation of Echolocation Calls in 5 Species of Aerial-Feeding Insectivorous Bats from Malaysia. *J. Mammal.* **84**: 205–215.
- Kingston, T., Jones, G., Zubaid, A. & Kunz, T.H. 2000. Resource Partitioning in Rhinolophoid Bats Revisited. *Oecologia* **124**: 332–342. Springer.
- MacSwiney G., M.C., Clarke, F.M. & Racey, P.A. 2008. What you see is not what you get: the role of ultrasonic detectors in increasing inventory completeness in Neotropical bat assemblages. *J. Appl. Ecol.* **45**: 1364–1371.
- Pavey, C.R. & Burwell, C.J. 2008. Fawn Leafnosed Bat *Hipposideros cervinus*. In: *The Mammals of Australia* (S. Van Dyck & R. Strahan, eds), pp. 459–461. New Holland Books, Chatswood, NSW.
- Phauk, S., Phen, S. & Furey, N.M. 2013. Cambodian bat echolocation: a first description of assemblage call parameters and assessment of their utility for species identification. *Cambodian J. Nat. Hist.* **1**: 16:26.
- Pinilla-Cortés, P.C. & Rodríguez-Bolaños, A. 2017. Bioacoustical characterization of Phyllostomidae bats in Colombian low montane rain forest. *Rev. Biodivers. Neotrop.*

7: 119–133.

- Pio, D.V. ., Clarke, F.M., MacKie, I. & Racey, P.A. 2010. Echolocation Calls of the Bats of Trinidad, West Indies: Is Guild Membership Reflected in Echolocation Signal Design? *Acta Chiropterologica* **12**: 217–229.
- Pottie, S.A., Lane, D.J.W., Kingston, T. & Lee, B.P.Y.-H. 2005. The microchiropteran bat fauna of Singapore. *Acta Chiropterologica* **7**: 237–247.
- Rodríguez-San Pedro, A. & Allendes, J.L. 2017. Echolocation calls of free-flying common vampire bats *Desmodus rotundus* (Chiroptera: Phyllostomidae) in Chile. *Bioacoustics* **26**: 153–160.
- Russo, D. & Jones, G. 2002. Identification of twenty-two bat species (Mammalia: Chiroptera) from Italy by analysis of time-expanded recordings of echolocation calls. *J. Zool.* **258**: S0952836902001231.
- Salsamendi, E., Aihartza, J., Goiti, U., Almenar, D. & Garin, I. 2005. Echolocation calls and morphology in the Mehelyi's (*Rhinolophus mehelyi*) and mediterranean (*R. euryale*) horseshoe bats: implications for resource partitioning. *Hystrix, Ital. J. Mammal.* **16**.
- Schmieder, D.A., Kingston, T., Hashim, R. & Siemers, B.M. 2012. Sensory constraints on prey detection performance in an ensemble of vespertilionid understorey rain forest bats. *Funct. Ecol.* **26**: 1043–1053.
- Schnitzler, H.-U., Kalko, E.K. V, Kaipf, I. & Grinnell, A.D. 1994. Fishing and echolocation behavior of the greater bulldog bat, *Noctilio leporinus*, in the field. *Behav. Ecol. Sociobiol.* **35**: 327–345.
- Siemers, B.M., Beedholm, K., Dietz, C., Dietz, I. & Ivanova, T. 2005. Is species identity, sex, age or individual quality conveyed by echolocation call frequency in European horseshoe bats? *Acta Chiropterologica* **7**: 259–274.
- Siemers, B.M., Kalko, E.K. V & Schnitzler, H.U. 2001. Echolocation behavior and signal plasticity in the Neotropical bat *Myotis nigricans* (Schinz, 1821) (Vespertilionidae): A convergent case with European species of *Pipistrellus*? *Behav. Ecol. Sociobiol.* **50**: 317–328.
- Siemers, B.M. & Schnitzler, H.-U. 2004. Echolocation signals reflect niche differentiation in five sympatric congeneric bat species. *Nature* **429**: 657. Macmillan Magazines Ltd.
- Son, N., O'shea, T., Gore, J., Csorba, G., Tu, V., Oshida, T., *et al.* 2016. Bats (Mammalia: Chiroptera) of the southeastern Truong Son Mountains, Quang Ngai Province, Vietnam. *J. Threat. Taxa* **8**.
- Thies, W., Kalko, E.K. V. & Schnitzler, H.-U. 1998. The roles of echolocation and olfaction in two Neotropical fruit-eating bats, *Carollia perspicillata* and *C. castanea*, feeding on *Piper*. *Behav. Ecol. Sociobiol.* **42**: 397–409.
- Vaughan, N., Jones, G. & Harris, S. 1997. Identification of British bat species by multivariate analysis of echolocation call parameters. *Bioacoustics* **7**: 189–207.
- Zamora-Gutierrez, V., Lopez-Gonzalez, C., MacSwiney Gonzalez, M.C., Fenton, B., Jones, G., Kalko, E.K. V, *et al.* 2016. Acoustic identification of Mexican bats based on taxonomic and ecological constraints on call design. *Methods Ecol. Evol.* **7**: 1082–1091.

Appendix B

Estimates for feeding traits and categorical variables used in *Chapter Four*. ^{a)} references for bite force (BF); ^{b)} references for muscles, DIG: digastric, MAS: masseter, TEM: temporalis, PTE: pterygoid muscle. References for diet were reported in the main text of *Chapter Two*.

Species	BF (N)	DIG (g)	MAS (g)	TEM (g)	PTE (g)	Diet	References
<i>Emballonura monticola</i>	1.06					I	^a (Senawi <i>et al.</i> , 2015)
<i>Taphozous melanopogon</i>	7.78					I	^a (Senawi <i>et al.</i> , 2015)
<i>Hipposideros cervinus</i>	4.30					I	^a (Senawi <i>et al.</i> , 2015)
<i>Hipposideros diadema</i>	24.81					I	^a (Senawi <i>et al.</i> , 2015)
<i>Hipposideros larvatus</i>	9.40					I	^a (Senawi <i>et al.</i> , 2015)
<i>Hipposideros ridleyi</i>	3.74					I	^a (Senawi <i>et al.</i> , 2015)
<i>Miniopterus schreibersi</i>	2.76					I	^a Herrel A. unpublished data
<i>Cheiromeles torquatus</i>	16.41					I	^a (Senawi <i>et al.</i> , 2015)
<i>Molossus molossus</i>	8.34	11.97	29.78	142.73	10.95	I	^a (Aguirre <i>et al.</i> , 2002), ^b (Herrel <i>et al.</i> , 2008)
<i>Molossus rufus</i>	8.40	2.01	21.72	97.20	7.65	I	^a (Aguirre <i>et al.</i> , 2002), ^b (Herrel <i>et al.</i> , 2008)
<i>Nyctinomops laticaudatus</i>	0.99					I	^a Herrel A. unpublished data

Species	BF (N)	DIG (g)	MAS (g)	TEM (g)	PTE (g)	Diet	References
<i>Tadarida teniotis</i>	6.21					I	^a Herrel A. unpublished data
<i>Pteronotus parnellii</i>	2.09					I	^a Herrel A. unpublished data
<i>Noctilio albiventris</i>	11.91	32.78	31.71	393.00	30.83	I,V	^a (Aguirre <i>et al.</i> , 2002), ^b (Herrel <i>et al.</i> , 2008)
<i>Noctilio leporinus</i>	19.90	56.44	78.99	699.92	57.18	V	^a (Aguirre <i>et al.</i> , 2002), ^b (Herrel <i>et al.</i> , 2008)
<i>Anoura geoffroyi</i>	1.48	9.20	9.00	67.15	8.40	N	^{a,b} (Santana <i>et al.</i> , 2010)
<i>Artibeus jamaicensis</i>	24.96	33.66	57.66	382.59	47.99	N,F	^a (Aguirre <i>et al.</i> , 2002), ^b (Herrel <i>et al.</i> , 2008)
<i>Artibeus lituratus</i>	27.34					F	^a Herrel A. unpublished data
<i>Carollia brevicauda</i>	8.53	14.50	31.00	184.00	16.07	F,I	^{a,b} (Santana <i>et al.</i> , 2010; Curtis & Santana, 2018)
<i>Carollia castanea</i>	4.03					F,I	^a (Santana, 2016)
<i>Carollia perspicillata</i>	6.65	12.73	25.58	134.98	15.90	F,I	^a (Aguirre <i>et al.</i> , 2002), ^b (Santana <i>et al.</i> , 2010)
<i>Chiroderma villosum</i>	10.64					F	^a (Santana, 2016)
<i>Desmodus rotundus</i>	8.60	19.32	20.08	192.22	17.81	H	^a (Aguirre <i>et al.</i> , 2002), ^b (Herrel <i>et al.</i> , 2008)
<i>Glossophaga soricina</i>	2.25	5.28	9.12	49.93	4.63	O	^a (Aguirre <i>et al.</i> , 2002), ^b (Herrel <i>et al.</i> , 2008)
<i>Lophostoma silvicolum</i>	21.63					I	^a (Aguirre <i>et al.</i> , 2002)
<i>Micronycteris hirsuta</i>	12.48	19.30	28.95	207.27	12.85	I	^{a,b} (Santana <i>et al.</i> , 2010)
<i>Micronycteris megalotis</i>	2.31	5.13	7.85	53.03	4.30	I	^{a,b} (Santana <i>et al.</i> , 2010)
<i>Micronycteris minuta</i>	2.18	5.75	7.45	52.20	5.30	I	^a (Aguirre <i>et al.</i> , 2002), ^b (Santana <i>et al.</i> , 2010)

Species	BF (N)	DIG (g)	MAS (g)	TEM (g)	PTE (g)	Diet	References
<i>Mimon crenulatum</i>	6.96	14.98	19.90	174.48	12.23	I	^a (Aguirre <i>et al.</i> , 2002), ^b (Santana <i>et al.</i> , 2010)
<i>Phyllostomus discolor</i>	21.61	38.64	69.56	456.41	36.71	O	^a (Aguirre <i>et al.</i> , 2002), ^b (Herrel <i>et al.</i> , 2008)
<i>Phyllostomus hastatus</i>	68.00	76.25	146.76	809.92	25.07	O	^a (Aguirre <i>et al.</i> , 2002), ^b (Herrel <i>et al.</i> , 2008)
<i>Platyrrhinus helleri</i>	11.50					F	^a (Santana, 2016)
<i>Sturnira lilium</i>	15.74	17.91	41.68	216.06	21.83	F	^a (Aguirre <i>et al.</i> , 2002), ^b Herrel A. unpublished data
<i>Trachops cirrhosus</i>	12.92	36.69	40.49	362.90	28.77	V	^a (Santana, 2016), ^b (Santana <i>et al.</i> , 2010)
<i>Uroderma bilobatum</i>	12.27	11.98	15.53	140.05	12.68	F	^a (Aguirre <i>et al.</i> , 2002), ^b (Santana <i>et al.</i> , 2010)
<i>Cynopterus brachyotis</i>	14.46					F	^a (Dumont & Herrel, 2003)
<i>Eidolon helvum</i>	93.24	154.43	283.22	664.26	125.41	F	^a (Dumont & Herrel, 2003), ^b (Herrel <i>et al.</i> , 2008)
<i>Epomophorus wahlbergi</i>	29.67					F	^a Herrel A. unpublished data
<i>Pteropus poliocephalus</i>	120.33					F	^a (Dumont & Herrel, 2003)
<i>Pteropus vampyrus</i>	162.89					F	^a (Dumont & Herrel, 2003)
<i>Rousettus aegyptiacus</i>	35.57					F	^a (Dumont & Herrel, 2003)
<i>Rhinolophus affinis</i>	4.35					I	^a (Senawi <i>et al.</i> , 2015)
<i>Rhinolophus blasii</i>	3.40	9.43	16.53	68.40	9.70	I	^{a,b} Herrel A. unpublished data
<i>Rhinolophus ferrumequinum</i>	7.55	16.90	54.70	188.00	22.73	I	^{a,b} Herrel A. unpublished data
<i>Rhinolophus hipposideros</i>	1.19	3.17	6.63	25.70	6.60	I	^{a,b} Herrel A. unpublished data

Species	BF (N)	DIG (g)	MAS (g)	TEM (g)	PTE (g)	Diet	References
<i>Rhinolophus mehelyi</i>	3.73	9.33	20.43	66.93	9.00	I	^{a,b} Herrel A. unpublished data
<i>Eptesicus furinalis</i>	9.35					I	^a (Aguirre <i>et al.</i> , 2002)
<i>Eptesicus serotinus</i>	13.04	32.90	64.30	314.65	32.55	I	^{a,b} Herrel A. unpublished data
<i>Hypsugo savii</i>	2.20	6.53	12.00	56.97	7.73	I	^{a,b} Herrel A. unpublished data
<i>Kerivoula papillosa</i>	7.38					I	^a (Senawi <i>et al.</i> , 2015)
<i>Murina cyclotis</i>	11.90					I	^a (Senawi <i>et al.</i> , 2015)
<i>Myotis albescens</i>	2.18					I	^a (Aguirre <i>et al.</i> , 2002)
<i>Myotis bechsteinii</i>	2.37					I	^a Herrel A. unpublished data
<i>Myotis blythii</i>	10.34	20.27	48.67	208.77	22.87	I	^{a,b} Herrel A. unpublished data
<i>Myotis brandtii</i>	0.57					I	^a Herrel A. unpublished data
<i>Myotis capaccinii</i>	2.13	5.13	10.77	39.37	5.40	I,V	^{a,b} Herrel A. unpublished data
<i>Myotis dasycneme</i>	2.25					I	^a Herrel A. unpublished data
<i>Myotis daubentoni</i>	1.68	5.60	9.55	40.40	6.00	I	^{a,b} Herrel A. unpublished data
<i>Myotis emarginatus</i>	3.18	6.98	14.03	67.98	7.75	I	^{a,b} Herrel A. unpublished data
<i>Myotis myotis</i>	12.08	28.93	70.20	348.17	33.30	I	^{a,b} Herrel A. unpublished data
<i>Myotis mystacinus</i>	0.51					I	^a Herrel A. unpublished data
<i>Myotis nattereri</i>	1.28					I	^a Herrel A. unpublished data

Species	BF (N)	DIG (g)	MAS (g)	TEM (g)	PTE (g)	Diet	References
<i>Myotis nigricans</i>	1.27	7.32	16.11	74.17	5.66	I	^a (Aguirre <i>et al.</i> , 2002), ^b (Herrel <i>et al.</i> , 2008)
<i>Nyctalus noctula</i>	8.78	29.70	38.53	216.50	26.33	I	^{a,b} Herrel A. unpublished data
<i>Pipistrellus pipistrellus</i>	1.19	3.30	6.10	27.05	4.00	I	^{a,b} Herrel A. unpublished data
<i>Plecotus austriacus</i>	3.34					I	^a Herrel A. unpublished data
<i>Scotophilus kuhlii</i>	9.18					I	^a (Senawi <i>et al.</i> , 2015)

References Appendix B

- Aguirre, L.F., Herrel, A., van Damme, R. & Matthysen, E. 2002. Ecomorphological analysis of trophic niche partitioning in a tropical savannah bat community. *Proc. R. Soc. London. Ser. B Biol. Sci.* **269**: 1271–1278.
- Curtis, A.A. & Santana, S.E. 2018. Jaw-Dropping: Functional Variation in the Digastric Muscle in Bats. *Anat. Rec.* **301**: 279–290.
- Dumont, E.R. & Herrel, A. 2003. The effects of gape angle and bite point on bite force in bats. *J. Exp. Biol.* **206**: 2117–2123.
- Herrel, A., De Smet, A., Aguirre, L.F. & Aerts, P. 2008. Morphological and mechanical determinants of bite force in bats: do muscles matter? *J. Exp. Biol.* **211**: 86–91.
- Santana, S.E. 2016. Quantifying the effect of gape and morphology on bite force: biomechanical modelling and in vivo measurements in bats. *Funct. Ecol.* **30**: 557–565.
- Santana, S.E., Dumont, E.R. & Davis, J.L. 2010. Mechanics of bite force production and its relationship to diet in bats. *Funct. Ecol.* **24**: 776–784.
- Senawi, J., Schmieder, D., Siemers, B. & Kingston, T. 2015. Beyond size – morphological predictors of bite force in a diverse insectivorous bat assemblage from Malaysia. *Funct. Ecol.* **29**: 1411–1420.

Appendix C

Estimates for sensorial traits and categorical variables used in *Chapter Five*. Abbreviations stand for ET: emission type, CC: call category, FP: peak frequency (KHz). References: data sources for ET, CC and FP. References for diet were reported in the main text of *Chapter Two*

Family	Species	Diet	ET	CC	FP	References
Cistugidae	<i>Cistugo lesueuri</i>	I	M	c	46.50	(Schoeman & Jacobs, 2008)
Cistugidae	<i>Cistugo seabrae</i>	I	M	c	45.80	(Schoeman & Jacobs, 2008)
Craseonycteridae	<i>Craseonycteris thonglongyai</i>	I	M	d	81.78	(Pereira <i>et al.</i> , 2006)
Emballonuridae	<i>Balantiopteryx plicata</i>	I	M	d	41.20	(Ibáñez <i>et al.</i> , 2002)
Emballonuridae	<i>Diclidurus virgo</i>	I	M	d	24.27	(Jung <i>et al.</i> , 2007)
Emballonuridae	<i>Emballonura diana</i>	I	M	d	35.35	(Pennay & Lavery, 2017)
Emballonuridae	<i>Emballonura monticola</i>	I	M	d	51.24	(Hughes <i>et al.</i> , 2010)
Emballonuridae	<i>Peropteryx macrotis</i>	I	M	d	39.60	(MacSwiney G. <i>et al.</i> , 2008)
Emballonuridae	<i>Rhynchonycteris naso</i>	I	M	d	51.30	(Pio <i>et al.</i> , 2010)
Emballonuridae	<i>Saccolaimus saccolaimus</i>	I	M	d	32.03	(Hughes <i>et al.</i> , 2011)
Emballonuridae	<i>Saccopterix bilineata</i>	I	M	d	42.00	(Pio <i>et al.</i> , 2010)
Emballonuridae	<i>Taphozous longimanus</i>	I	M	d	30.83	(Hughes <i>et al.</i> , 2011)

Family	Species	Diet	ET	CC	FP	References
Emballonuridae	<i>Taphozous melanopogon</i>	I	M	d	29.71	(Hughes <i>et al.</i> , 2011)
Emballonuridae	<i>Taphozous nudiventris</i>	I	M	d	23.38	(Hackett <i>et al.</i> , 2017)
Furipteridae	<i>Furipterus horrens</i>	I	M	e	158.97	(Falcão <i>et al.</i> , 2015)
Hipposideridae	<i>Asellia tridens</i>	I	R	h	121.30	(Benda <i>et al.</i> , 2008)
Hipposideridae	<i>Aselliscus stoliczkanus</i>	I	R	h	120.30	(Li <i>et al.</i> , 2007)
Hipposideridae	<i>Cloeotis percivali</i>	I	R	h	212.00	(Bell & Fenton, 1981)
Hipposideridae	<i>Hipposideros bicolor</i>	I	R	h	131.00	(Kingston <i>et al.</i> , 2001)
Hipposideridae	<i>Hipposideros calcaratus</i>	I	R	h	117.20	(Pennay & Lavery, 2017)
Hipposideridae	<i>Hipposideros cervinus</i>	I	R	h	130.37	(Collen, 2012)
Hipposideridae	<i>Hipposideros cyclops</i>	I	R	h	59.70	(Decher & Fahr, 2005)
Hipposideridae	<i>Hipposideros diadema</i>	I	R	h	54.90	(Fenton, 1982)
Hipposideridae	<i>Hipposideros fulvus</i>	I	R	h	151.10	(Jones <i>et al.</i> , 1994)
Hipposideridae	<i>Hipposideros larvatus</i>	I	R	h	92.30	(Phauk <i>et al.</i> , 2013)
Hipposideridae	<i>Hipposideros ridleyi</i>	I	R	h	62.36	(Collen, 2012)
Hipposideridae	<i>Rhinonictoris aurantia</i>	I	R	h	116.75	(Armstrong & Coles, 2007)
Hipposideridae	<i>Triaenops persicus</i>	I	R	h	83.00	(Taylor <i>et al.</i> , 2005)
Megadermatidae	<i>Cardioderma cor</i>	I,V	R	f	49.13	(Smarsh & Smotherman, 2015)

Family	Species	Diet	ET	CC	FP	References
Megadermatidae	<i>Macroderma gigas</i>	I,V	R	f	50.50	(Hourigan, 2011)
Megadermatidae	<i>Megaderma lyra</i>	I,V	R	f	62.10	(Hughes <i>et al.</i> , 2011)
Megadermatidae	<i>Megaderma spasma</i>	I	R	f	72.99	(Hughes <i>et al.</i> , 2011)
Miniopteridae	<i>Miniopterus australis</i>	I	M	c	61.46	(Hughes <i>et al.</i> , 2011)
Miniopteridae	<i>Miniopterus inflatus</i>	I	M	c	47.40	(Monadjem <i>et al.</i> , 2010)
Miniopteridae	<i>Miniopterus magnater</i>	I	M	c	47.36	(Hughes <i>et al.</i> , 2011)
Miniopteridae	<i>Miniopterus pusillus</i>	I	M	c	62.85	(Hughes <i>et al.</i> , 2011)
Miniopteridae	<i>Miniopterus schreibersi</i>	I	M	c	54.20	(Russo & Jones, 2002)
Miniopteridae	<i>Miniopterus tristis</i>	I	M	c	36.16	(Pennay & Lavery, 2017)
Molossidae	<i>Chaerephon ansorgei</i>	I	M	c	17.80	(Bell & Fenton, 1981)
Molossidae	<i>Chaerephon nigeriae</i>	I	M	c	17.00	(Bell & Fenton, 1981)
Molossidae	<i>Chaerephon plicatus</i>	I	M	c	26.22	(Kusuminda & Yapa, 2017)
Molossidae	<i>Chaerephon pumilus</i>	I	M	c	25.60	(Taylor <i>et al.</i> , 2005)
Molossidae	<i>Cheiromeles torquatus</i>	I	M	c	24.10	(Kingston <i>et al.</i> , 2003)
Molossidae	<i>Eumops auripendulus</i>	I	M	c	23.30	(Barataud <i>et al.</i> , 2013)
Molossidae	<i>Eumops bonariensis</i>	I	M	c	19.50	Giacomini G. unpublished data
Molossidae	<i>Eumops perotis</i>	I	M	c	13.20	(León-Tapia & Hortelano-Moncada, 2016)

Family	Species	Diet	ET	CC	FP	References
Molossidae	<i>Eumops underwoodi</i>	I	M	c	15.90	(Orozco-Lugo <i>et al.</i> , 2013)
Molossidae	<i>Molossops temminckii</i>	I	M	c	50.40	(Guillén-Servent & Ibáñez, 2007)
Molossidae	<i>Molossus molossus</i>	I	M	c	38.67	(Jung & Kalko, 2011)
Molossidae	<i>Molossus rufus</i>	I	M	c	31.45	(MacSwiney G. <i>et al.</i> , 2008)
Molossidae	<i>Mops condylurus</i>	I	M	c	24.70	(Taylor, 1999)
Molossidae	<i>Mormopterus jugularis</i>	I	M	c	24.00	(Russ <i>et al.</i> , 2001)
Molossidae	<i>Mormopterus planiceps</i>	I	M	c	39.20	(Fullard <i>et al.</i> , 1991)
Molossidae	<i>Nyctinomops laticaudatus</i>	I	M	c	26.40	(MacSwiney G. <i>et al.</i> , 2008)
Molossidae	<i>Otomops martiensseni</i>	I	M	c	12.00	(Taylor <i>et al.</i> , 2005)
Molossidae	<i>Otomops wroughtoni</i>	I	M	c	15.12	(Deshpande & Kelkar, 2015)
Molossidae	<i>Promops centralis</i>	I	M	c	24.70	(Gonzalez-Terrazas <i>et al.</i> , 2016)
Molossidae	<i>Sauromys petrophilus</i>	I	M	c	32.75	(Jacobs & Fenton, 2002)
Molossidae	<i>Tadarida aegyptiaca</i>	I	M	c	20.12	(Deshpande & Kelkar, 2015)
Molossidae	<i>Tadarida brasiliensis</i>	I	M	c	24.31	(Rodríguez-San Pedro & Simonetti, 2013)
Molossidae	<i>Tadarida teniotis</i>	I	M	c	13.00	(Russo & Jones, 2002)
Mormoopidae	<i>Mormoops blainvillei</i>	I	M	d	54.25	(Jennings <i>et al.</i> , 2004)
Mormoopidae	<i>Mormoops megalophylla</i>	I	M	d	51.60	(MacSwiney G. <i>et al.</i> , 2008)

Family	Species	Diet	ET	CC	FP	References
Mormoopidae	<i>Pteronotus davyi</i>	I	M	d	58.00	(Ibáñez <i>et al.</i> , 1999)
Mormoopidae	<i>Pteronotus parnellii</i>	I	M	h	59.02	(Pio <i>et al.</i> , 2010)
Mormoopidae	<i>Pteronotus personatus</i>	I	M	d	70.00	(Smotherman & Guillén-Servent, 2008)
Mormoopidae	<i>Pteronotus rubiginosus</i>	I	M	d	59.64	(López-Baucells <i>et al.</i> , 2018)
Mystacinidae	<i>Mystacina tuberculata</i>	I	M	f	48.52	(Parsons, 1997)
Myzopodidae	<i>Myzopoda aurita</i>	I	M	g	41.00	(Göpfert & Wasserthal, 1995)
Natalidae	<i>Natalus tumidirostris</i>	I	M	f	120.20	(Barataud <i>et al.</i> , 2013)
Noctilionidae	<i>Noctilio albiventris</i>	I,V	M	c	72.80	(Farias, 2012)
Noctilionidae	<i>Noctilio leporinus</i>	V	M	h	57.00	(Schnitzler <i>et al.</i> , 1994)
Nycteridae	<i>Nycteris grandis</i>	V	R	f	20.00	(Fenton <i>et al.</i> , 1983)
Nycteridae	<i>Nycteris hispida</i>	I	R	f	80.80	(Monadjem <i>et al.</i> , 2010)
Nycteridae	<i>Nycteris thebaica</i>	I,V	R	f	70.18	(Hackett <i>et al.</i> , 2017)
Phyllostomidae	<i>Ametrida centurio</i>	F	N	e	80.00	(Barataud <i>et al.</i> , 2013)
Phyllostomidae	<i>Anoura caudifer</i>	N	N	f	87.50	(Barataud <i>et al.</i> , 2013)
Phyllostomidae	<i>Anoura geoffroyi</i>	N	N	f	83.08	(Zamora-Gutierrez <i>et al.</i> , 2016)
Phyllostomidae	<i>Ariteus flavescens</i>	F	N	e	78.17	Brinkløv S. unpublished data
Phyllostomidae	<i>Artibeus fuliginosus</i>	F	N	f	75.35	(Rivera <i>et al.</i> , 2015a)

Family	Species	Diet	ET	CC	FP	References
Phyllostomidae	<i>Artibeus jamaicensis</i>	N,F	N	f	78.80	(Brinkløv <i>et al.</i> , 2009)
Phyllostomidae	<i>Artibeus lituratus</i>	F	N	f	63.00	(Zamora-Gutierrez <i>et al.</i> , 2016)
Phyllostomidae	<i>Artibeus planirostris</i>	F,I	N	f	88.19	(Rivera <i>et al.</i> , 2015b)
Phyllostomidae	<i>Brachyphylla cavernarum</i>	O	N	f	51.40	(Jennings <i>et al.</i> , 2004)
Phyllostomidae	<i>Carollia brevicauda</i>	F,I	N	f	49.84	(Pinilla-Cortés & Rodríguez-Bolaños, 2017)
Phyllostomidae	<i>Carollia castanea</i>	F,I	N	f	82.36	Chaverri G. unpublished data
Phyllostomidae	<i>Carollia perspicillata</i>	F,I	N	f	56.60	(Thies <i>et al.</i> , 1998)
Phyllostomidae	<i>Centurio senex</i>	F	N	e	94.66	Chaverri G. unpublished data
Phyllostomidae	<i>Chiroderma trinitatum</i>	F	N	f	96.90	(Pio <i>et al.</i> , 2010)
Phyllostomidae	<i>Chiroderma villosum</i>	F	N	f	91.80	(Pio <i>et al.</i> , 2010)
Phyllostomidae	<i>Choeronycteris mexicana</i>	N	N	f	34.92	(Zamora-Gutierrez <i>et al.</i> , 2016)
Phyllostomidae	<i>Chrotopterus auritus</i>	V	N	f	90.40	Chaverri G. unpublished data
Phyllostomidae	<i>Dermanura phaeotis</i>	F	N	f	65.81	(Collen, 2012)
Phyllostomidae	<i>Desmodus rotundus</i>	H	N	f	72.56	(Rodríguez-San Pedro & Allendes, 2017)
Phyllostomidae	<i>Diaemus youngi</i>	H	N	f	52.00	(Barataud <i>et al.</i> , 2013)
Phyllostomidae	<i>Diphylla eucaudata</i>	H	N	f	40.82	Chaverri G. unpublished data
Phyllostomidae	<i>Erophylla sezekorni</i>	O	N	f	45.10	(Murray <i>et al.</i> , 2001)

Family	Species	Diet	ET	CC	FP	References
Phyllostomidae	<i>Glossophaga longirostris</i>	O	N	f	90.80	(Jennings <i>et al.</i> , 2004)
Phyllostomidae	<i>Glossophaga soricina</i>	O	N	f	87.88	Chaverri G. unpublished data
Phyllostomidae	<i>Lionycteris spurrelli</i>	N	N	f	111.00	(Barataud <i>et al.</i> , 2013)
Phyllostomidae	<i>Lonchorhina aurita</i>	F,I	N	f	47.50	(Arias-Aguilar <i>et al.</i> , 2018)
Phyllostomidae	<i>Lophostoma silvicolum</i>	I	N	f	69.95	Chaverri G. unpublished data
Phyllostomidae	<i>Macrophyllum macrophyllum</i>	I	N	f	56.60	(Brinkløv <i>et al.</i> , 2009)
Phyllostomidae	<i>Macrotus californicus</i>	I	N	f	60.39	(Zamora-Gutierrez <i>et al.</i> , 2016)
Phyllostomidae	<i>Macrotus waterhousii</i>	I	N	f	69.20	(Murray <i>et al.</i> , 2001)
Phyllostomidae	<i>Mesophylla macconnelli</i>	F	N	f	99.87	(Rivera <i>et al.</i> , 2015c)
Phyllostomidae	<i>Micronycteris hirsuta</i>	I	N	f	80.80	(Pio <i>et al.</i> , 2010)
Phyllostomidae	<i>Micronycteris megalotis</i>	I	N	f	98.10	(Pio <i>et al.</i> , 2010)
Phyllostomidae	<i>Micronycteris microtis</i>	I,V	N	f	101.39	Chaverri G. unpublished data
Phyllostomidae	<i>Micronycteris minuta</i>	I	N	f	61.20	(Pio <i>et al.</i> , 2010)
Phyllostomidae	<i>Mimon bennetti</i>	I	N	f	56.84	(Macaulay Library, 2019)
Phyllostomidae	<i>Mimon crenulatum</i>	I	N	f	66.10	(Pio <i>et al.</i> , 2010)
Phyllostomidae	<i>Monophyllus luciae</i>	N	N	f	42.10	(Jennings <i>et al.</i> , 2004)
Phyllostomidae	<i>Monophyllus redmani</i>	N	N	f	99.53	Brinkløv S. unpublished data

Family	Species	Diet	ET	CC	FP	References
Phyllostomidae	<i>Phylloderma stenops</i>	O	N	f	59.50	(Barataud <i>et al.</i> , 2013)
Phyllostomidae	<i>Phyllonycteris poeyi</i>	N	N	c	38.74	(Mora & Macías, 2007)
Phyllostomidae	<i>Phyllostomus discolor</i>	O	N	f	57.28	Chaverri G. unpublished data
Phyllostomidae	<i>Phyllostomus elongatus</i>	O	N	f	62.93	(Rivera <i>et al.</i> , 2015d)
Phyllostomidae	<i>Phyllostomus hastatus</i>	O	N	f	47.10	(Pio <i>et al.</i> , 2010)
Phyllostomidae	<i>Phyllostomus latifolius</i>	O	N	f	61.40	(Barataud <i>et al.</i> , 2013)
Phyllostomidae	<i>Platyrrhinus brachycephalus</i>	F	N	f	92.00	(Barataud <i>et al.</i> , 2013)
Phyllostomidae	<i>Platyrrhinus helleri</i>	F	N	f	98.46	Chaverri G. unpublished data
Phyllostomidae	<i>Platyrrhinus lineatus</i>	F	N	f	64.33	(Collen, 2012)
Phyllostomidae	<i>Pygoderma bilabiatum</i>	F	N	f	62.68	(Collen, 2012)
Phyllostomidae	<i>Rhinophylla pumilio</i>	F	N	f	60.00	(Barataud <i>et al.</i> , 2013)
Phyllostomidae	<i>Sphaeronycteris toxophyllum</i>	F	N	f	67.02	(Collen, 2012)
Phyllostomidae	<i>Sturnira lilium</i>	F	N	f	84.02	Chaverri G. unpublished data
Phyllostomidae	<i>Sturnira ludovici</i>	F	N	f	68.65	(Zamora-Gutierrez <i>et al.</i> , 2016)
Phyllostomidae	<i>Sturnira tilda</i>	F	N	f	70.80	(Pio <i>et al.</i> , 2010)
Phyllostomidae	<i>Trachops cirrhosus</i>	V	N	f	69.55	Chaverri G. unpublished data
Phyllostomidae	<i>Uroderma bilobatum</i>	F	N	f	74.70	(Pio <i>et al.</i> , 2010)

Family	Species	Diet	ET	CC	FP	References
Phyllostomidae	<i>Vampyriscus brocki</i>	F	N	f	73.00	(Barataud <i>et al.</i> , 2013)
Phyllostomidae	<i>Vampyrodes caraccioli</i>	F	N	f	73.15	Chaverri G. unpublished data
Phyllostomidae	<i>Vampyrum spectrum</i>	V	N	f	79.40	(Pio <i>et al.</i> , 2010)
Rhinolophidae	<i>Rhinolophus affinis</i>	I	R	h	85.86	(Jiang <i>et al.</i> , 2008)
Rhinolophidae	<i>Rhinolophus alcyone</i>	I	R	h	87.00	(Monadjem <i>et al.</i> , 2010)
Rhinolophidae	<i>Rhinolophus blasii</i>	I	R	h	95.15	(Siemers <i>et al.</i> , 2005)
Rhinolophidae	<i>Rhinolophus capensis</i>	I	R	h	84.20	(Fawcett <i>et al.</i> , 2015)
Rhinolophidae	<i>Rhinolophus clivosus</i>	I	R	h	87.30	(Benda <i>et al.</i> , 2008)
Rhinolophidae	<i>Rhinolophus darlingi</i>	I	R	h	87.10	(Schoeman & Jacobs, 2008)
Rhinolophidae	<i>Rhinolophus ferrumequinum</i>	I	R	h	81.30	(Russo & Jones, 2002)
Rhinolophidae	<i>Rhinolophus fumigatus</i>	I	R	h	53.60	(Stoffberg <i>et al.</i> , 2011)
Rhinolophidae	<i>Rhinolophus hildebrandtii</i>	I	R	h	41.50	(Bell & Fenton, 1981)
Rhinolophidae	<i>Rhinolophus hipposideros</i>	I	R	h	111.10	(Russo & Jones, 2002)
Rhinolophidae	<i>Rhinolophus landeri</i>	I	R	h	107.30	(Schoeman & Jacobs, 2008)
Rhinolophidae	<i>Rhinolophus megaphyllus</i>	I	R	h	68.60	(Fullard <i>et al.</i> , 2008)
Rhinolophidae	<i>Rhinolophus mehelyi</i>	I	R	h	106.80	(Salsamendi <i>et al.</i> , 2005)
Rhinolophidae	<i>Rhinolophus pusillus</i>	I	R	h	112.20	(Phauk <i>et al.</i> , 2013)

Family	Species	Diet	ET	CC	FP	References
Rhinolophidae	<i>Rhinolophus simulator</i>	I	R	h	78.00	(Bell & Fenton, 1981)
Rhinolophidae	<i>Rhinolophus swinnyi</i>	I	R	h	106.10	(Schoeman & Jacobs, 2008)
Rhinopomatidae	<i>Rhinopoma microphyllum</i>	I	M	d	29.42	(Hackett <i>et al.</i> , 2017)
Thyropteridae	<i>Thyroptera discifera</i>	I	M	d	112.50	(Barataud <i>et al.</i> , 2013)
Thyropteridae	<i>Thyroptera tricolor</i>	I	M	d	58.21	Chaverri G. unpublished data
Vespertilionidae	<i>Antrozous pallidus</i>	I,V	M	c	30.00	(Thomas <i>et al.</i> , 1987)
Vespertilionidae	<i>Barbastella barbastellus</i>	I	M	f	33.20	(Russo & Jones, 2002)
Vespertilionidae	<i>Chalinolobus gouldii</i>	I	M	c	33.70	(McKenzie <i>et al.</i> , 2002)
Vespertilionidae	<i>Eptesicus brasiliensis</i>	I	M	c	41.10	(Pio <i>et al.</i> , 2010)
Vespertilionidae	<i>Eptesicus furinalis</i>	I	M	c	37.60	(MacSwiney G. <i>et al.</i> , 2008)
Vespertilionidae	<i>Eptesicus fuscus</i>	I	M	c	31.00	(Briones-Salas <i>et al.</i> , 2013)
Vespertilionidae	<i>Eptesicus hottentotus</i>	I	M	c	30.60	(Schoeman & Jacobs, 2008)
Vespertilionidae	<i>Eptesicus nilssonii</i>	I	M	c	30.50	(Fukui <i>et al.</i> , 2004)
Vespertilionidae	<i>Eptesicus serotinus</i>	I	M	c	29.90	(Russo & Jones, 2002)
Vespertilionidae	<i>Glauconycteris argentata</i>	I	M	c	40.38	(López-Baucells <i>et al.</i> , 2017)
Vespertilionidae	<i>Glischropus tylopus</i>	I	M	c	47.00	(Heller, 1989)
Vespertilionidae	<i>Harpiocephalus harpia</i>	I	M	e	57.00	(Raghuram <i>et al.</i> , 2014)

Family	Species	Diet	ET	CC	FP	References
Vespertilionidae	<i>Hesperoptenus tickelli</i>	I	M	c	28.32	(Wordley <i>et al.</i> , 2014)
Vespertilionidae	<i>Histiotus montanus</i>	I	M	f	35.36	(Rodríguez-San Pedro & Simonetti, 2013)
Vespertilionidae	<i>Hypsugo savii</i>	I	M	c	34.60	(Russo & Jones, 2002)
Vespertilionidae	<i>Ia io</i>	I	M	c	27.60	(Thabah <i>et al.</i> , 2007)
Vespertilionidae	<i>Kerivoula hardwickei</i>	I	M	e	118.25	(Hughes <i>et al.</i> , 2011)
Vespertilionidae	<i>Kerivoula papillosa</i>	I	M	e	114.29	(Schmieder <i>et al.</i> , 2012)
Vespertilionidae	<i>Kerivoula picta</i>	I	M	e	115.81	(Sripathi <i>et al.</i> , 2006)
Vespertilionidae	<i>Laephotis wintoni</i>	I	M	c	22.10	(Jacobs <i>et al.</i> , 2005)
Vespertilionidae	<i>Lasionycteris noctivagans</i>	I	M	c	30.04	(Zamora-Gutierrez <i>et al.</i> , 2016)
Vespertilionidae	<i>Lasiurus borealis</i>	I	M	c	31.65	(Balcombe & Fenton, 1988)
Vespertilionidae	<i>Lasiurus cinereus</i>	I	M	c	28.80	(Belwood & Fullard, 1984)
Vespertilionidae	<i>Lasiurus ega</i>	I	M	c	32.20	(MacSwiney G. <i>et al.</i> , 2008)
Vespertilionidae	<i>Murina cyclotis</i>	I	M	e	93.81	(Hughes <i>et al.</i> , 2011)
Vespertilionidae	<i>Murina tubinaris</i>	I	M	e	88.70	(Hughes <i>et al.</i> , 2011)
Vespertilionidae	<i>Myotis albescens</i>	I	M	e	56.20	Giacomini G. unpublished data
Vespertilionidae	<i>Myotis bechsteinii</i>	I	M	e	51.00	(Vaughan <i>et al.</i> , 1997)
Vespertilionidae	<i>Myotis blythii</i>	I	M	e	41.40	(Russo & Jones, 2002)

Family	Species	Diet	ET	CC	FP	References
Vespertilionidae	<i>Myotis bocagii</i>	I	M	e	44.60	(Schoeman & Jacobs, 2008)
Vespertilionidae	<i>Myotis brandtii</i>	I	M	e	47.90	(Vaughan <i>et al.</i> , 1997)
Vespertilionidae	<i>Myotis capaccinii</i>	I,V	M	e	50.40	(Russo & Jones, 2002)
Vespertilionidae	<i>Myotis dasycneme</i>	I	M	e	40.20	(Siemers & Schnitzler, 2004)
Vespertilionidae	<i>Myotis daubentonii</i>	I	M	e	47.00	(Russo & Jones, 2002)
Vespertilionidae	<i>Myotis emarginatus</i>	I	M	e	58.00	(Russo & Jones, 2002)
Vespertilionidae	<i>Myotis keenii</i>	I	M	e	97.41	(Faure <i>et al.</i> , 1993)
Vespertilionidae	<i>Myotis myotis</i>	I	M	e	39.10	(Russo & Jones, 2002)
Vespertilionidae	<i>Myotis mystacinus</i>	I	M	e	47.50	(Russo & Jones, 2002)
Vespertilionidae	<i>Myotis nattereri</i>	I	M	e	46.90	(Russo & Jones, 2002)
Vespertilionidae	<i>Myotis nigricans</i>	I	M	c	54.00	(Siemers <i>et al.</i> , 2001)
Vespertilionidae	<i>Myotis simus</i>	I	M	e	57.74	(Collen, 2012)
Vespertilionidae	<i>Myotis welwitschii</i>	I	M	e	34.00	(Schoeman & Jacobs, 2008)
Vespertilionidae	<i>Neoromicia capensis</i>	I	M	c	39.80	(Mutavhatsindi, 2017)
Vespertilionidae	<i>Neoromicia nana</i>	I	M	c	70.00	(Bell & Fenton, 1981)
Vespertilionidae	<i>Nyctalus lasiopterus</i>	I,V	M	c	12.80	(Presetnik & Knapič, 2015)
Vespertilionidae	<i>Nyctalus leisleri</i>	I	M	c	30.70	(Russo & Jones, 2002)

Family	Species	Diet	ET	CC	FP	References
Vespertilionidae	<i>Nyctalus noctula</i>	I	M	c	22.60	(Russo & Jones, 2002)
Vespertilionidae	<i>Nycticeinops schlieffeni</i>	I	M	c	42.00	(Taylor, 1999)
Vespertilionidae	<i>Nyctophilus geoffroyi</i>	I	M	c	48.50	(McKenzie <i>et al.</i> , 2002)
Vespertilionidae	<i>Otonycteris hemprechi</i>	I	M	c	22.20	(Benda <i>et al.</i> , 2008)
Vespertilionidae	<i>Pipistrellus kuhlii</i>	I	M	c	41.40	(Russo & Jones, 2002)
Vespertilionidae	<i>Pipistrellus nathusii</i>	I	M	c	39.30	(Russ, 2012)
Vespertilionidae	<i>Pipistrellus pipistrellus</i>	I	M	c	46.90	(Russo & Jones, 2002)
Vespertilionidae	<i>Pipistrellus pygmaeus</i>	I	M	c	55.10	(Russ, 2012)
Vespertilionidae	<i>Plecotus auritus</i>	I	M	f	33.10	(Russ, 2012)
Vespertilionidae	<i>Plecotus austriacus</i>	I	M	f	32.60	(Russo & Jones, 2002)
Vespertilionidae	<i>Plecotus macrobullaris</i>	I	M	f	28.53	(Dietrich <i>et al.</i> , 2006)
Vespertilionidae	<i>Rhogeessa tumida</i>	I	M	f	48.65	(Collen, 2012)
Vespertilionidae	<i>Rhogeessa parvula</i>	I	M	e	54.20	(Orozco-Lugo <i>et al.</i> , 2013)
Vespertilionidae	<i>Scotomanes ornatus</i>	I	M	e	31.70	(Furey <i>et al.</i> , 2009)
Vespertilionidae	<i>Scotophilus kuhlii</i>	I	M	c	43.30	(Pottie <i>et al.</i> , 2005)
Vespertilionidae	<i>Scotophilus leucogaster</i>	I	M	c	50.70	(Bakwo Fils <i>et al.</i> , 2018)
Vespertilionidae	<i>Scotophilus nigrita</i>	I	M	c	30.00	(Bell & Fenton, 1981)

Family	Species	Diet	ET	CC	FP	References
Vespertilionidae	<i>Scotophilus nux</i>	I	M	c	44.54	(Peereboom & van Leishout, 2015)
Vespertilionidae	<i>Tylonycteris pachypus</i>	I	M	e	50.46	(Hughes <i>et al.</i> , 2011)
Vespertilionidae	<i>Vespertilio murinus</i>	I	M	c	35.80	(Obriest <i>et al.</i> , 2004)

References Appendix C

- Arias-Aguilar, A., Hintze, F., Aguiar, L.M.S., Rufay, V., Bernard, E. & Pereira, M.J.R. 2018. Who's calling? Acoustic identification of Brazilian bats. *Mammal Res.* **63**: 231–253.
- Armstrong, K.N. & Coles, R.B. 2007. Echolocation Call Frequency Differences Between Geographic Isolates of *Rhinonicteris Aurantia* (Chiroptera: Hipposideridae): Implications of Nasal Chamber Size. *J. Mammal.* **88**: 94–104.
- Bakwo Fils, E.M., Manga Mongombe, A., Tsala, D.E. & Tamesse, J.L. 2018. Acoustic identification of five insectivorous bats by their echolocation calls in the Sahelian zone of Far North Cameroon. *J. Basic Appl. Zool.* **79**: 28.
- Balcombe, J.P. & Fenton, M.B. 1988. Eavesdropping by Bats: The Influence of Echolocation Call Design and Foraging Strategy. *Ethology* **79**: 158–166.
- Barataud, M., Giosa, S., Leblanc, F., Rufay, V., Disca, T., Tillon, L., *et al.* 2013. Identification et écologie acoustique des chiroptères de Guyane française. *Le Rhinolophe* **19**: 103–145.
- Bell, G.P. & Fenton, M.B. 1981. Recognition of Species of Insectivorous Bats by Their Echolocation Calls. *J. Mammal.* **62**: 233–243.
- Belwood, J.J. & Fullard, J.H. 1984. Echolocation and foraging behaviour in the Hawaiian hoary bat, *Lasiurus cinereus semotus*. *Can. J. Zool.* **62**: 2113–2120.
- Benda, P., Dietz, C., Andreas, M., Hotoýy, J., Lučan, R., Maltby, A., *et al.* 2008. Bats (Mammalia: Chiroptera) of the Eastern Mediterranean and Middle East. Part 6. Bats of Sinai (Egypt) with some taxonomic, ecological and echolocation data on that fauna. *Acta Soc. Zool. Bohem.* **72**: 1–103.
- Brinkløv, S., Kalko, E.K. V & Surlykke, A. 2009. Intense echolocation calls from two 'whispering' bats, *Artibeus jamaicensis* and *Macrophyllum macrophyllum* (Phyllostomidae). *J. Exp. Biol.* **212**: 11–20.
- Briones-Salas, M., Peralta-Pérez, M. & García-Luis, M. 2013. Acoustic characterization of new species of bats for the State of Oaxaca, Mexico. *THERYA* **4**: 15–32.
- Collen, A. 2012. The evolution of echolocation in bats: a comparative approach. University College London.
- Decher, J. & Fahr, J. 2005. *Hipposideros cyclops*. *Mamm. Species* 1–7.
- Deshpande, K. & Kelkar, N. 2015. Acoustic Identification of *Otomops wroughtoni* and other Free-Tailed Bat Species (Chiroptera: Molossidae) from India. *Acta Chiropterologica* **17**: 419–428.
- Dietrich, S., Szameitat, D.P., Kiefer, A., Schnitzler, H.-U. & Denzinger, A. 2006. Echolocation signals of the plecotine bat, *Plecotus macrobullaris* Kuzyakin, 1965. *Acta Chiropterologica* **8**: 465–475.
- Falcão, F., Ugarte-Núñez, J.A., Faria, D. & Caselli, C.B. 2015. Unravelling the calls of discrete hunters: acoustic structure of echolocation calls of furipterid bats (Chiroptera, Furipteridae). *Bioacoustics* **24**: 175–183.
- Farias, H.M. 2012. Monitoramento e identificação acústica de espécies de morcegos da Mata Atlântica por sinais de ecolocalização : contribuições ecológicas e potencial para conservação. Universidade Estadual de Santa Cruz.
- Faure, P.A., Fullard, J.H. & Dawson, J.W. 1993. The gleaning attacks of the northern long-

- eared bat, *Myotis septentrionalis*, are relatively inaudible to moths. *J. Exp. Biol.* **178**: 173 LP – 189.
- Fawcett, K., Jacobs, D.S., Surlykke, A. & Ratcliffe, J.M. 2015. Echolocation in the bat, *Rhinolophus capensis*: the influence of clutter, conspecifics and prey on call design and intensity. *Biol. Open* **4**: 693–701.
- Fenton, M.B. 1982. Echolocation Calls and Patterns of Hunting and Habitat Use of Bats (Microchiroptera) from Chillagoe, North Queensland. *Aust. J. Zool.* **30**: 417–425.
- Fenton, M.B., Gaudet, C.L. & Leonard, M.L. 1983. Feeding behaviour of the bats *Nycteris grandis* and *Nycteris thebaica* (Nycteridae) in captivity. *J. Zool. Lond.* **200**: 347–354.
- Fukui, D., Agetsuma, N. & Hill, D.A. 2004. Acoustic Identification of Eight Species of Bat (Mammalia: Chiroptera) Inhabiting Forests of Southern Hokkaido, Japan: Potential for Conservation Monitoring. *Zoolog. Sci.* **21**: 947–955.
- Fullard, J.H., Jackson, M.E., Jacobs, D.S., Pavey, C.R. & Burwell, C.J. 2008. Surviving cave bats: auditory and behavioural defences in the Australian noctuid moth, *Speiredonia spectans*. *J. Exp. Biol.* **211**: 3808 LP – 3815.
- Fullard, J.H., Koehler, C., Surlykke, A. & McKenzie, N.L. 1991. Echolocation Ecology and Flight Morphology of Insectivorous Bats (Chiroptera) in South-Western Australia. *Aust. J. Zool.* **39**: 427–438.
- Furey, N.M., MacKie, I.J. & Racey, P.A. 2009. The role of ultrasonic bat detectors in improving inventory and monitoring surveys in Vietnamese karst bat assemblages. *Curr. Zool.* **55**: 327–341.
- Gonzalez-Terrazas, T.P., Martel, C., Milet-Pinheiro, P., Ayasse, M., Kalko, E.K. V & Tschapka, M. 2016. Finding flowers in the dark: nectar-feeding bats integrate olfaction and echolocation while foraging for nectar. *R. Soc. Open Sci.* **3**: 160199.
- Göpfert, M.C. & Wasserthal, L.T. 1995. Notes on echolocation calls, food and roosting behaviour of the Old World Sucker-footed bat *Myzopoda aurita* (Chiroptera, Myzopodidae). *Z. Säugetierkd.* **60**: 1–8.
- Guillén-Servent, A. & Ibáñez, C. 2007. Unusual echolocation behavior in a small molossid bat, *Molossops temminckii*, that forages near background clutter. *Behav. Ecol. Sociobiol.* **61**: 1599.
- Hackett, T.D., Holderied, M.W. & Korine, C. 2017. Echolocation call description of 15 species of Middle-Eastern desert dwelling insectivorous bats. *Bioacoustics* **26**: 217–235.
- Heller, K.G. 1989. Echolocation calls of Malaysian bats. *Z. Säugetierkd.* 1–8.
- Hourigan, C. 2011. *Ghost bat, Macroderma gigas. Targeted species survey guidelines. Queensland Herbarium, Department of Environment and Science, Brisbane.*
- Hughes, A.C., Satasook, C., Bates, P.J.J., Soisook, P., Sritongchuay, T., Jones, G., *et al.* 2010. Echolocation Call Analysis and Presence-Only Modelling as Conservation Monitoring Tools for Rhinolophoid Bats in Thailand. *Acta Chiropterologica* **12**: 311–327.
- Hughes, A.C., Satasook, C., Bates, P.J.J., Soisook, P., Sritongchuay, T., Jones, G., *et al.* 2011. Using Echolocation Calls to Identify Thai Bat Species: Vespertilionidae, Emballonuridae, Nycteridae and Megadermatidae. *Acta Chiropterologica* **13**: 447–455.
- Ibáñez, C., Guillén, A., Javier, J.B. & Pérez-Jordá, J.L. 1999. Echolocation Calls of *Pteronotus davyi* (Chiroptera: Mormoopidae) from Panama. *J. Mammal.* **80**: 924–928.

- Ibáñez, C., Juste, J., López-Wilchis, R., Albuja V., L. & Núñez-Garduño, A. 2002. Echolocation of three Species of Sac-Winged Bats (Balantiopteryx). *J. Mammal.* **83**: 1049–1057.
- Jacobs, D.S., Barclay, R.M.R. & Schoeman, M.C. 2005. Foraging and roosting ecology of a rare insectivorous bat species, *Laephotis wintoni* (Thomas, 1901), Vespertilionidae. *Acta Chiropterologica* **7**: 101–109.
- Jacobs, D.S. & Fenton, M.B. 2002. *Mormopterus petrophilus*. *Mamm. Species* 1–3.
- Jennings, N.V., Parsons, S., Barlow, K.E. & Gannon, M.R. 2004. Echolocation Calls and Wing Morphology of Bats from the West Indies. *Acta Chiropterologica* **6**: 75–90.
- Jiang, T., Feng, J., Sun, K. & Wang, J. 2008. Coexistence of two sympatric and morphologically similar bat species *Rhinolophus affinis* and *Rhinolophus pearsoni*. *Prog. Nat. Sci.* **18**: 523–532.
- Jones, G., Sripathi, K., Waters, D.A. & Marimuthu, G. 1994. Individual variation in the echolocation calls of three sympatric Indian hipposiderid bats, and an experimental attempt to jam bat echolocation. *FOLIA Zool.* **43**: 347–361.
- Jung, K. & Kalko, E.K. V. 2011. Adaptability and vulnerability of high flying Neotropical aerial insectivorous bats to urbanization. *Divers. Distrib.* **17**: 262–274.
- Jung, K., Kalko, E.K. V & Von Helversen, O. 2007. Echolocation calls in Central American emballonurid bats: signal design and call frequency alternation. *J. Zool.* **272**: 125–137.
- Kingston, T., Jones, G., Akbar, Z. & Kunz, T.H. 2003. Alternation of Echolocation Calls in 5 Species of Aerial-Feeding Insectivorous Bats from Malaysia. *J. Mammal.* **84**: 205–215.
- Kingston, T., Lara, M.C., Jones, G., Akbar, Z., Kunz, T.H. & Schneider, C.J. 2001. Acoustic divergence in two cryptic *Hipposideros* species: a role for social selection? *Proc. R. Soc. London. Ser. B Biol. Sci.* **268**: 1381–1386.
- Kusuminda, T. & Yapa, W. 2017. First record of a Wrinkle-lipped Free-tailed Bat *Chaerephon plicatus* Buchannan, 1800 (Mammalia: Chiroptera: Molossidae) colony in Sri Lanka, with notes on echolocation calls and taxonomy. *J. Threat. Taxa* **9**.
- León-Tapia, M.Á. & Hortelano-Moncada, Y. 2016. Richness of insectivorous bats in a chaparral area in the municipality of Tecate, Baja California, Mexico. *Rev. Mex. Biodivers.* **87**: 1055–1061.
- Li, G., Liang, B., Wang, Y., Zhao, H., Helgen, K.M., Lin, L., *et al.* 2007. Echolocation Calls, Diet, and Phylogenetic Relationships of Stoliczka's Trident Bat, *Aselliscus stoliczkanus* (Hipposideridae). *J. Mammal.* **88**: 736–744.
- López-Baucells, A., Rocha, R., Webala, P.W., Nair, A., Uusitalo, R., Sironen, T., *et al.* 2017. Rapid assessment of bat diversity in the Taita Hills Afromontane cloud forests, southeastern Kenya. *Barbastella* **9**: 10.14709/BarbJ.9.1.2016.04.
- López-Baucells, A., Torrent, L., Rocha, R., Pavan, A.C., Bobrowiec, P.E.D. & Meyer, C.F.J. 2018. Geographical variation in the high-duty cycle echolocation of the cryptic common mustached bat *Pteronotus cf. rubiginosus* (Mormoopidae). *Bioacoustics* **27**: 341–357.
- Macaulay Library. 2019. *Mimon bennetti*. ML 104097; ML 104096; ML 104095; ML 104094. Cornell Lab of Ornithology. Author: Voigt C., 2000. <https://search.macaulaylibrary.org/catalog?taxonCode=t-11075788&view=List&q=golden%20bat%20-%20Mimon%20bennettii>.

- MacSwiney G., M.C., Clarke, F.M. & Racey, P.A. 2008. What you see is not what you get: the role of ultrasonic detectors in increasing inventory completeness in Neotropical bat assemblages. *J. Appl. Ecol.* **45**: 1364–1371.
- McKenzie, N.L., Start, A.N. & Bullen, R.D. 2002. Foraging ecology and organisation of a desert bat fauna. *Aust. J. Zool.* **50**: 529–548.
- Monadjem, A., Taylor, P.J., Cotterill, F.P.D. & Schoeman, M.C. 2010. *Bats of southern and central Africa A Biogeographic and Taxonomic Synthesis*. Wits University Press.
- Mora, E.C. & Macías, S. 2007. Echolocation calls of Poey's flower bat (*Phyllonycteris poeyi*) unlike those of other phyllostomids. *Naturwissenschaften* **94**: 380–383.
- Murray, K.L., Robbins, L.W. & Britzke, E.R. 2001. Variation in Search-Phase Calls of Bats. *J. Mammal.* **82**: 728–737.
- Mutavhatsindi, I. V. 2017. The influence of foraging habitat on acoustic signal source levels in two bat species, *Neoromicia capensis* (Vespertilionidae) and *Tadarida aegyptiaca* (Molossidae). University of Cape Town.
- Obrist, M.K., Boesch, R. & Flückiger, P.F. 2004. Variability in echolocation call design of 26 Swiss bat species: consequences, limits and options for automated field identification with a synergetic pattern recognition approach. *Mamm. mamm* **68**: 307.
- Orozco-Lugo, L., Guillén-Servent, Antonio Valenzuela-Galván, D. & Héctor, T.A. 2013. Descripción de los pulsos de ecolocalización de once especies de murciélagos insectívoros aéreos de una selva baja caducifolia en Morelos, México. *THERYA* **4**: 33–46.
- Parsons, S. 1997. Search-phase echolocation calls of the New Zealand lesser short-tailed bat (*Mystacina tuberculata*) and long-tailed bat (*Chalinolobus tuberculatus*). *Can. J. Zool.* **75**: 1487–1494.
- Peereboom, D. & van Leishout, S. 2015. Possible first record and echolocation call of *Scotophilus cf. nux* Thomas, 1904 from Gabon. *African Bat Conserv. News* **37**: 5–8.
- Pennay, M. & Lavery, T.H. 2017. Identification guide to bat echolocation calls of Solomon Islands & Bougainville. Available at: <http://ausbats.org.au/bat-calls-of-solomon-islands/4593992119>.
- Pereira, M.J.R., Rebelo, H., Teeling, E.C., O'Brien, S.J., Mackie, I., Bu, S.S.H., *et al.* 2006. Status of the world's smallest mammal, the bumble-bee bat *Craseonycteris thonglongyai*, in Myanmar. *Oryx* **40**: 456–463. Cambridge University Press.
- Phauk, S., Phen, S. & Furey, N.M. 2013. Cambodian bat echolocation: a first description of assemblage call parameters and assessment of their utility for species identification. *Cambodian J. Nat. Hist.* **1**: 16:26.
- Pinilla-Cortés, P.C. & Rodríguez-Bolaños, A. 2017. Bioacoustical characterization of Phyllostomidae bats in Colombian low montane rain forest. *Rev. Biodivers. Neotrop.* **7**: 119–133.
- Pio, D.V., Clarke, F.M., MacKie, I. & Racey, P.A. 2010. Echolocation Calls of the Bats of Trinidad, West Indies: Is Guild Membership Reflected in Echolocation Signal Design? *Acta Chiropterologica* **12**: 217–229.
- Pottie, S.A., Lane, D.J.W., Kingston, T. & Lee, B.P.Y.-H. 2005. The microchiropteran bat fauna of Singapore. *Acta Chiropterologica* **7**: 237–247.
- Presetnik, P. & Knapič, T. 2015. First confirmations of the greater noctule bat *Nyctalus lasiopterus* (Schreber, 1780) presence in Slovenia after more than 85 years. *Nat. Slov.* **17**: 41–46

- Raghuram, H., Jain, M. & Balakrishnan, R. 2014. Species and acoustic diversity of bats in a palaeotropical wet evergreen forest in southern India. *Curr. Sci.* **107**: 631–641.
- Rivera, M.D., Vallejo, A.F. & Burneo, S.F. 2015a. *Artibeus lituratus*, llamada de ecolocación. Brito, J., Camacho, M. A., Romero, V. (eds). Mamíferos de Ecuador. Version 2017.0. Museo de Zoología, Pontificia Universidad Católica del Ecuador. <https://bioweb.bio/faunaweb/mammaliaweb/Canto/Especie/Artibeus>.
- Rivera, M.D., Vallejo, A.F. & Burneo, S.F. 2015b. *Artibeus planirostris*, llamada de ecolocación. En: Brito, J., Camacho, M. A., Romero, V. (eds). Mamíferos de Ecuador. Version 2017.0. Museo de Zoología, Pontificia Universidad Católica del Ecuador. <https://bioweb.bio/faunaweb/mammaliaweb/Canto/Especie/A>.
- Rivera, M.D., Vallejo, A.F. & Burneo, S.F. 2015c. *Mesophylla macconnelli*, llamada de ecolocación. Brito, J., Camacho, M. A., Romero, V. (eds). Mamíferos de Ecuador. Version 2017.0. Museo de Zoología, Pontificia Universidad Católica del Ecuador. <https://bioweb.bio/faunaweb/mammaliaweb/Canto/Especie/Me>.
- Rivera, M.D., Vallejo, A.F. & Burneo, S.F. 2015d. *Phyllostomus elongatus*, llamada de ecolocación. En: Brito, J., Camacho, M. A., Romero, V. (eds). Mamíferos de Ecuador. Version 2017.0. Museo de Zoología, Pontificia Universidad Católica del Ecuador. <https://bioweb.bio/faunaweb/mammaliaweb/Canto/Especie/>.
- Rodríguez-San Pedro, A. & Allendes, J.L. 2017. Echolocation calls of free-flying common vampire bats *Desmodus rotundus* (Chiroptera: Phyllostomidae) in Chile. *Bioacoustics* **26**: 153–160.
- Rodríguez-San Pedro, A. & Simonetti, J.A. 2013. Acoustic identification of four species of bats (Order Chiroptera) in central Chile. *Bioacoustics* **22**: 165–172.
- Russ, J. 2012. *British Bat Calls: A Guide to Species Identification*. Pelagic Publishing, Exeter.
- Russ, J., Bennett, D., Ross, K. & Kofoky, A. 2001. *The Bats of Madagascar: A Field Guide with Descriptions of Echolocation Calls*. VIPER PRESS.
- Russo, D. & Jones, G. 2002. Identification of twenty-two bat species (Mammalia: Chiroptera) from Italy by analysis of time-expanded recordings of echolocation calls. *J. Zool.* **258**: S0952836902001231.
- Salsamendi, E., Aihartza, J., Goiti, U., Almenar, D. & Garin, I. 2005. Echolocation calls and morphology in the Mehelyi's (*Rhinolophus mehelyi*) and mediterranean (*R. euryale*) horseshoe bats: implications for resource partitioning. *Hystrix, Ital. J. Mammal.* **16**.
- Schmieder, D.A., Kingston, T., Hashim, R. & Siemers, B.M. 2012. Sensory constraints on prey detection performance in an ensemble of vespertilionid understory rain forest bats. *Funct. Ecol.* **26**: 1043–1053.
- Schnitzler, H.-U., Kalko, E.K. V, Kaipf, I. & Grinnell, A.D. 1994. Fishing and echolocation behavior of the greater bulldog bat, *Noctilio leporinus*, in the field. *Behav. Ecol. Sociobiol.* **35**: 327–345.
- Schoeman, M.C. & Jacobs, D.S. 2008. The Relative Influence of Competition and Prey Defenses on the Phenotypic Structure of Insectivorous Bat Ensembles in Southern Africa. *PLoS One* **3**: e3715.
- Siemers, B.M., Beedholm, K., Dietz, C., Dietz, I. & Ivanova, T. 2005. Is species identity, sex, age or individual quality conveyed by echolocation call frequency in European horseshoe bats? *Acta Chiropterologica* **7**: 259–274.

- Siemers, B.M., Kalko, E.K. V & Schnitzler, H.U. 2001. Echolocation behavior and signal plasticity in the Neotropical bat *Myotis nigricans* (Schinz, 1821) (Vespertilionidae): A convergent case with European species of *Pipistrellus*? *Behav. Ecol. Sociobiol.* **50**: 317–328.
- Siemers, B.M. & Schnitzler, H.-U. 2004. Echolocation signals reflect niche differentiation in five sympatric congeneric bat species. *Lett. to Nat.* **429**: 657–661.
- Smarsh, G.C. & Smotherman, M. 2015. Intra- and Interspecific Variability of Echolocation Pulse Acoustics in the African Megadermatid Bats. *Acta Chiropterologica* **17**: 429–443.
- Smotherman, M. & Guillén-Servent, A. 2008. Doppler-shift compensation behavior by Wagner's mustached bat, *Pteronotus personatus*. *J. Acoust. Soc. Am.* **123**: 4331–4339.
- Sripathi, K., Raghuram, H. & Nathan, P.T. 2006. Echolocation sounds of the painted bat *Kerivoula picta* (Vespertilionidae). *Curr. Sci.* **91**: 1145–1147.
- Stoffberg, S., Jacobs, D.S. & Matthee, C.A. 2011. The Divergence of Echolocation Frequency in Horseshoe Bats: Moth Hearing, Body Size or Habitat? *J. Mamm. Evol.* **18**: 117–129.
- Taylor, P.J. 1999. Echolocation calls of twenty southern African bat species. *South African J. Zool.* **34**: 114–124.
- Taylor, P.J., Geiselman, C., Kabochi, P., Agwanda, B. & Turner, S. 2005. Intraspecific variation in the calls of some African bats (Order Chiroptera). *Durban Museum Novit.* **30**: 24–37.
- Thabah, A., Li, G., Wang, Y., Liang, B., Hu, K., Zhang, S., *et al.* 2007. Diet, Echolocation Calls, and Phylogenetic Affinities of the Great Evening Bat (*Ia io*; Vespertilionidae): Another Carnivorous Bat. *J. Mammal.* **88**: 728–735.
- Thies, W., Kalko, E.K. V. & Schnitzler, H.-U. 1998. The roles of echolocation and olfaction in two Neotropical fruit-eating bats, *Carollia perspicillata* and *C. castanea*, feeding on *Piper*. *Behav. Ecol. Sociobiol.* **42**: 397–409.
- Thomas, D.W., Bell, G.P. & Fenton, M.B. 1987. Variation in Echolocation Call Frequencies Recorded from North American Vespertilionid Bats: A Cautionary Note. *J. Mammal.* **68**: 842–847.
- Vaughan, N., Jones, G. & Harris, S. 1997. Identification of British bat species by multivariate analysis of echolocation call parameters. *Bioacoustics* **7**: 189–207.
- Wordley, C.F.R., Foui, E.K., Mudappa, D., Sankaran, M. & Altringham, J.D. 2014. Acoustic Identification of Bats in the Southern Western Ghats, India. *Acta Chiropterologica* **16**: 213–222.
- Zamora-Gutierrez, V., Lopez-Gonzalez, C., MacSwiney Gonzalez, M.C., Fenton, B., Jones, G., Kalko, E.K. V, *et al.* 2016. Acoustic identification of Mexican bats based on taxonomic and ecological constraints on call design. *Methods Ecol. Evol.* **7**: 1082–1091.

CHAPTER THREE: 3D Photogrammetry of Bat Skulls: Perspectives for Macroevolutionary Analyses

Statement on content presentation and publication

This chapter constituted the basis of a paper published in the journal *Evolutionary Biology* (Appendix D).

Abstract

Photogrammetry is relatively cheap, easy to use, flexible and portable but its power and limitations have not been fully explored for studies of small animals.

Here I assessed the accuracy of photogrammetry for the reconstruction of 3D digital models of bat skulls by evaluating its potential for evolutionary morphology studies at the interspecific (19 species) level. Its reliability was assessed against the performance of μ CT scan and laser scan techniques. I used 3D geometric morphometrics and comparative methods to quantify the amount of size and shape variation due to the scanning technique and assess the strength of the biological signal in relation to both the technique error and phylogenetic uncertainty.

I found only minor variation among techniques. Levels of random error (repeatability and Procrustes variance) were similar in all techniques and no systematic error was observed (as evidenced from Principal Component Analysis). Similar levels of phylogenetic signal, allometries and correlations with ecological variables (*i.e.*, frequency of maximum energy and bite force) were detected among techniques. Phylogenetic uncertainty interacted with technique error but without affecting the biological conclusions driven by the evolutionary analyses.

My study confirms the accuracy of photogrammetry for the reconstruction of challenging specimens. These results encourage the use of photogrammetry as a reliable and highly accessible tool for the study of macro evolutionary processes of small mammals.

Introduction

The use of digital 3D models in morphological studies is increasing in many scientific disciplines, including palaeontology and evolutionary biology. The digitalization of an object not only facilitates detailed analysis of the size and shape of fragile specimens but also helps investigation of diverse evolutionary questions (*e.g.* Cornette *et al.*, 2013; Cardini *et al.*, 2015).

The use of close-range photogrammetry has grown in many fields because it is economical, portable, easy to apply and accurately reproduces the geometry and colour pattern of real and complex objects (Falkingham, 2012). For this reason, it has become widely employed in a variety of disciplines such as biology (Evin *et al.*, 2016), palaeontology (Bates *et al.*, 2010), anthropology (Katz & Friess, 2014) and medicine (Ege *et al.*, 2004), among others.

In the analyses of shape and size of objects (as in biological studies), the 3D models are often integrated with geometric morphometric methods. This approach has proved particularly useful in bats, where, for example, geometric morphometric has provided additional information on divergence of cryptic species (Sztencel-Jabłonka *et al.*, 2009). Nevertheless, acquiring landmarks on bone sutures of bat skulls, particularly for *Microchiroptera sensu* Simmons and Geisler (1998), is quite difficult due to early suture ossification and their small size. This challenge often forces researchers to employ extremely precise equipment at considerable cost. However, no studies have addressed the utility of photogrammetry for this group and other similar sized mammals.

Katz and Friess (2014) and Evin *et al.* (2016) demonstrated the accuracy of close-range photogrammetry for large skulls (humans and wolves, respectively) relative to laser scan models. Fahlke and Autenrieth (2016) compared photogrammetry performance relative to μ CT scan models for a vertebrate fossil skull (condyle-basal length = 37.5 cm) and similarly found high similarity. Very few studies have attempted to apply it to smaller

specimens although Muñoz-Muñoz *et al.* (2016) assessed the repeatability of photogrammetry for mice skulls (length = 45 mm) and suggested it might be appropriate for small mammals. Durão *et al.* (2018) suggested a protocol for 3D reconstruction of vole humeri by means of photogrammetry. Nevertheless, no tests were conducted to assess its performance against more established 3D reconstruction techniques (*e.g.* μ CT scan). High measurement error (random error, in particular) is well-known in small specimens and largely arises due to difficulties in landmark identification (Badawi-Fayad & Cabanis, 2007; Cramon-Taubadel *et al.*, 2007; Fourie *et al.*, 2011; Muñoz-Muñoz *et al.*, 2016; Marcy *et al.*, 2018). The extent of biological variation is of paramount importance when considering the impact of technique-based error on the results (Marcy *et al.*, 2018).

An additional incentive for analysing differences between techniques is that it may lead to an understanding of when it is feasible to combine data acquired using different techniques. The introduction of random and systematic errors intrinsic to each technique is known to create unreal patterns and/or obscure biological variation (Fruciano *et al.*, 2017; Robinson & Terhune, 2017; Marcy *et al.*, 2018).

This study was motivated by the need to assess photogrammetry as a tool for reliable analysis of bat skull morphology and assess its performance relative to μ CT scan and surface laser scan. I used geometric morphometrics to assess the relative accuracy of photogrammetry models for quantifying size and shape via anatomical landmarks.

Phylogenetic comparative methods (Cornwell & Nakagawa, 2017) were used to assess the strength of the biological signal against the technique error and the phylogenetic uncertainty. My aims were to quantify the extent of measurement error introduced by the photogrammetry/geometric morphometrics approach and assess the reliability of combining data extracted from different reconstruction techniques (photogrammetry, μ CT, laser scan).

Methods

Sample

Geometric morphometrics and phylogenetic comparative methods were used to examine the reliability of photogrammetry for the digital reconstruction of bat skulls and assess its performance in interspecific (19 species) statistical analyses.

Crania from nineteen different bat species from the Natural History Museum of Paris were reconstructed in 3D using three different techniques: photogrammetry, laser scan and μ CT scanning. The specimens were selected to represent bat species of small and medium size, with an average skull length of 15.62 mm (see **Appendix E**).

Data acquisition and model landmarking

The 3D models were reconstructed with three different techniques (photogrammetry, laser scan, μ CT).

The photogrammetry 3D models were obtained employing a digital SLR Nikon D5300 camera (24.2 megapixel) attached to a Nikkor 60 mm macro lens. The general camera lighting settings and positioning, specimen arrangement and number of pictures per specimen were adapted from Falkingham (2012) and Mallison and Wings (2014). Average mesh size was ~3,000,000 triangles.

For the laser scan models, I employed a Breuckmann Laser Scan, model SmartSCAN R5/C5 5.0 MegaPixel housed at the Natural History Museum of Paris. I used the field of view S-030 which is optimal for very small objects (240 mm length) and can achieve a maximum resolution of 10 μ m.

To obtain the CT models I used a phoenix v|tome|x s housed at the Natural History Museum of Paris. Scans resolution ranged between 18-28 μm (average 23 μm) in voxel size.

Detailed information on devices and workflow are available in the Supplementary Information.

The open source software Landmark Editor (Wiley *et al.*, 2005) was used to place 24 unilateral landmarks on the dorsal, lateral and ventral side of the cranium (**Figure 1A** and **Table S1**). See *Chapter Two* for details on landmark acquisition and coordinates transformation procedure (Procrustes Shape Coordinates). I assessed the landmarking error by recording coordinates three times on a subsample of nine species (*Carollia perspicillata*, *Desmodus rotundus*, *Glossophaga soricina*, *Myotis emarginatus*, *Myotis capaccinii*, *Nyctalus noctula*, *Rhinolophus hipposideros*, *Rhinolophus ferrumequinum* and *Tadarida teniotis*), selected to represent the morphological variation within the sample for each technique (laser scan, photogrammetry, μCT). Some species were morphologically very divergent, as assessed from principal component scores (see later)(*e.g. D. rotundus* and *G. soricina*), while others were very similar (*e.g. R. hipposideros* and *R. ferrumequinum*).

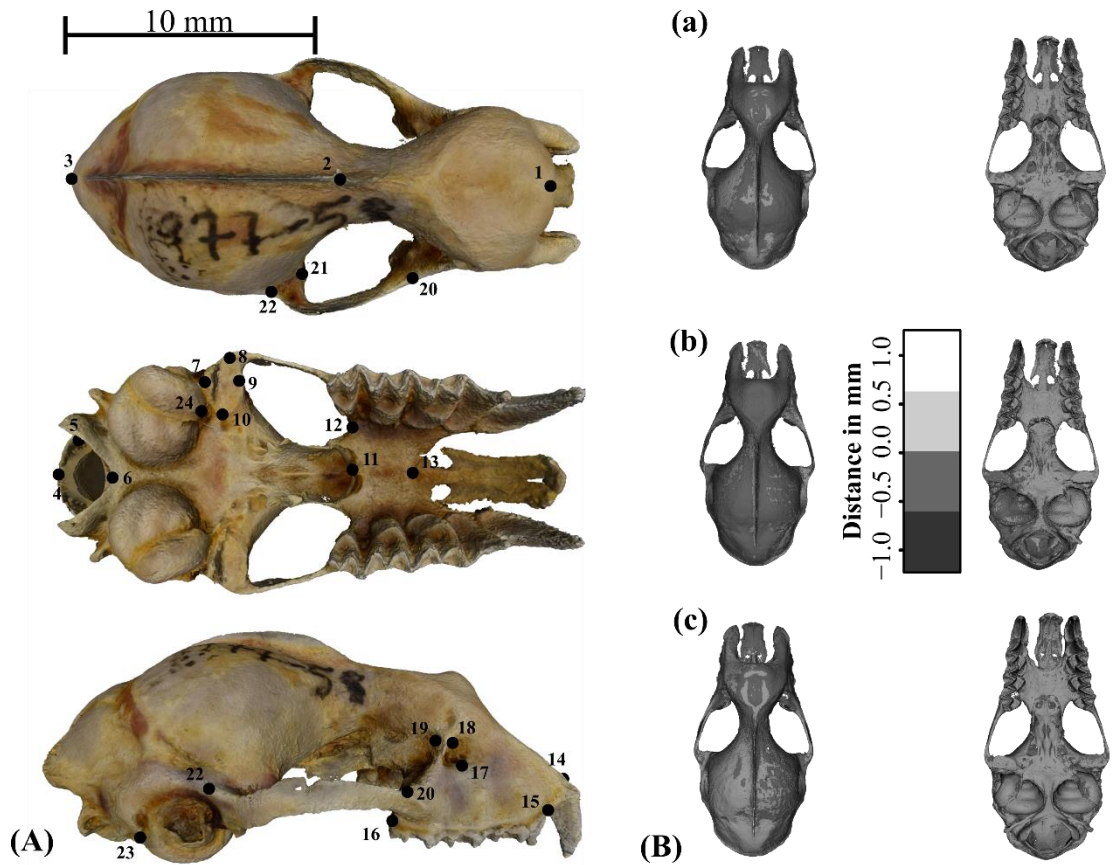


Figure 1. A) Landmark configuration used in the study. Species: *R. ferrumequinum*. Anatomical definition in **Table S1**. B) Visualization of mesh distances on dorsal and ventral views between a) photogrammetry and μ CT; b) photogrammetry and laser scan; c) μ CT and laser scan. The colour represents the distances in mm. Species: *R. ferrumequinum* (skull length: 18.78 mm).

Measurement error evaluation

Mesh distances. The average distances between the 19 paired models were calculated in R software (R Core Team 2019) using the meshDist function in the “Morpho” package (Schlager, 2013). This distance is defined as an average of the shortest distances between every triangle of a mesh and the closest triangle of the other (Bærentzen & Henrik, 2002). It returns the average distance and a coloured scale model that visually represents the differences between each pair of meshes.

Shape visualization. The preliminary visual analysis of the shape differences between the specimens was achieved using a Principal Component Analysis (PCA) for the interspecific dataset. I used the variance-covariance matrix of the Procrustes coordinates to extract orthogonal vectors (PCs) that summarise variation within the sample. Shape changes in 3D skulls were visualised by warping the 3D coordinates along the PC axes. This was achieved by applying a Thin-Plate-Spline (Bookstein, 1989) algorithm on the mean shape of the morphospace. The 3D bat skull with lowest deviation from the mean shape was chosen for the visualisation. This model was warped along the positive and the negative sides of PC axes to display the shape variation in the sample (Drake & Klingenberg, 2010).

Error in geometric morphometrics. Pearson and Mantel tests were employed to assess the similarity between the centroid size vectors produced by each technique, and their shape coordinates matrices, respectively (Cardini, 2014). Procrustes and standard ANOVAs (Ordinary Least Squares, [OLS]) were used to quantify the variance explained by the different techniques for shape and size, respectively. Nested ANOVAs were used to analyse replicate measurements to assess the landmarking error in a subsample of the data (nine species, see above), with repeatability computed using the intraclass correlation coefficient, *i.e.*, among individual-variance divided by within-individual variance components (see Fruciano, 2016). The variability of Procrustes variance, computed for each triplet of replicates, was used as a further indicator of random measurement error within each technique (Marcy *et al.*, 2018). The Procrustes variance, also known as morphological disparity, measures the magnitude of morphological variation for each triplet by technique (Zelditch *et al.*, 2012). Kruskal-Wallis tests were used to compare median Procrustes variances between techniques (greater variation suggests lower precision in landmark identification). Pearson correlation tests between Procrustes variance and centroid size assessed whether errors in landmark identification were greater for smaller specimens.

Error in evolutionary analyses. Additional analyses were performed to assess the use of photogrammetry-generated data in evolutionary studies. Phylogenetic trees for the nineteen selected species were inferred by Bayesian inference, as implemented in MrBayes version 3.2 (Huelsenbeck & Ronquist, 2001). Input data consisted of an alignment of 20364 base pairs of nuclear and mitochondrial DNA from Shi and Rabosky (2015). The alignment was divided into 29 partitions (for details see Shi & Rabosky, 2015) to allow for evolutionary differences between partitions. The GTR+G model was applied to each partition. A MCMC chain was run for 5 million generations, with trees saved every 500 generations and the first 5×10^3 trees discarded as burn-in. The remaining posterior sample of 1000 trees and the 50% majority rule consensus tree was used for subsequent analyses.

The R packages “ape” (Paradis *et al.*, 2004) and “geomorph” (Adams & Otárola-Castillo, 2013) were used to test for the presence of evolutionary allometry (Cardini & Polly, 2013) in the three datasets using the \log_{10} transformed centroid size as the independent variable and Procrustes shape coordinates (multivariate) as the dependent variable. Phylogenetic Generalised Least Squares (PGLS) analyses with 999 permutations were employed on the three datasets separately to test for the presence of evolutionary allometry after taking the phylogenetic variance-covariance matrix into account, with the phylogeny represented by the Bayesian consensus tree (Rohlf, 2007; Adams & Collyer 2015).

The presence of a phylogenetic signal (quantified by the K statistic, Blomberg *et al.*, 2003) in the three datasets and the degree of congruence for size and shape (Adams, 2014) were also assessed using the consensus tree. The K statistic reflects the degree of congruence between phenotypic data and the phylogeny (Blomberg *et al.*, 2003). Statistical significance of K and its multivariate extension K_{multiv} was assessed using randomization (Adams, 2014).

To examine whether the same evolutionary conclusions were obtained using different techniques, I computed a series of ANOVAs with morphological data (*i.e.*, \log_{10}

transformed centroid size and shape coordinates) as the dependent variable and ecological data (*i.e.*, \log_{10} transformed peak frequency, and \log_{10} transformed bite force) as the independent variables for all species in the study except *Pipistrellus nathusii* (no data on bite force were available for the species). Peak frequency data were extracted from the literature (Kalko *et al.*, 1998; Siemers *et al.*, 2001; Russo and Jones 2002; Siemers & Schnitzler, 2004; Rodríguez-San Pedro and Allendes 2017; Brinkløv *et al.*, 2011). I obtained unpublished (collected by Anthony Herrel) and published bite force data (Aguirre *et al.*, 2002) for these analyses. The same analyses were repeated under a phylogenetic comparative approach using PGLS.

To assess whether the same results were obtained from mixed datasets acquired from the three different 3D reconstruction techniques, I built 1000 morphological datasets. In each dataset, data for the nineteen species were randomly selected from one of the three techniques (photogrammetry, μ CT, laser scan). Allometry, phylogenetic signal and correlation with bite force and peak frequency (assessed as previously described) were analysed for each dataset using standard and phylogenetic comparative approaches (*i.e.*, OLS and PGLS models, respectively). The mean, standard deviation, minimum and maximum of the parameter distributions were used as statistical descriptors of the variable distributions and were compared to the original results obtained with singular-technique datasets (photogrammetry, μ CT, laser scan).

Fruciano *et al.*'s (2017) approach was used to assess the error due to phylogenetic uncertainty in the evolutionary analyses. The 1000 posterior trees represented the phylogenetic uncertainty in these analyses. Three common evolutionary analyses were performed: quantification of allometric effect, assessment of phylogenetic signal and relation between morphological data and functional data (*i.e.*, bite force and peak frequency). For each technique-tree combination, I performed the three analyses for both size and shape, obtaining a distribution of 1000 estimates for each analysis. ANOVAs were

performed on each distribution to assess the variance explained by both the phylogenetic uncertainty and reconstruction technique.

Results

The nineteen models were reconstructed in 3D with the three different techniques and the photogrammetric 3D model of *Rhinolophus ferrumequinum* (MNHN-ZM-MO-1977-58) can be downloaded as an example from Morphosource (model ID = M30222; <https://www.morphosource.org>).

Mesh distances

Visual examination of the meshes revealed strong general similarity between the three data sets, except in certain specific areas (**Figure S1**). There were small distances between the surfaces of the models as shown for *Rhinolophus ferrumequinum* (**Figure 1B**). The average distance between photogrammetry and laser scan models was 0.041 mm, in agreement with that found by Evin *et al.* (2016) for five wolf skulls (0.088 mm) (**Table 1**). The average distance between the photogrammetry and μ CT models was 0.054 mm. Finally, the μ CT and laser scan models were extremely similar with an average distance of 0.015 mm (**Table 1** and **Table S2** for percentage distances relative to total skull length).

Table 1. Average distances (mm) between the surfaces of the models. PH = Photogrammetry, LS = Laser scan, μ CT = μ CT scan.

Specimen	PH-LS	μ CT-PH	LS- μ CT
<i>Carollia perspicillata</i>	0.070	0.090	0.001
<i>Desmodus rotundus</i>	0.007	0.013	0.012
<i>Eptesicus serotinus</i>	0.028	0.035	0.020

<i>Glossophaga soricina</i>	0.051	0.071	0.023
<i>Hypsugo savii</i>	0.032	0.034	0.004
<i>Myotis daubentonii</i>	0.058	0.092	0.016
<i>Miniopterus schreibersii</i>	0.040	0.039	0.002
<i>Myotis capaccinii</i>	0.173	0.188	0.012
<i>Myotis emarginatus</i>	0.069	0.065	0.000
<i>Myotis nigricans</i>	0.040	0.083	0.029
<i>Myotis dasycneme</i>	0.026	0.046	0.060
<i>Noctilio albiventris</i>	0.001	0.002	0.003
<i>Nyctalus noctula</i>	0.004	0.058	0.043
<i>Pipistrellus pipistrellus</i>	0.027	0.037	0.016
<i>Pipistrellus nathusii</i>	0.036	0.042	0.012
<i>Plecotus austriacus</i>	0.075	0.076	0.002
<i>Rhinolophus ferrumequinum</i>	0.001	0.007	0.004
<i>Rhinolophus hipposideros</i>	0.030	0.021	0.011
<i>Tadarida teniotis</i>	0.016	0.033	0.015
MEAN	0.041	0.054	0.015
ST.DEV.	0.039	0.042	0.015

Shape visualization

The morphospace of the 111 specimens (*i.e.*, 57 models plus 54 replicates) displayed the shape variability in the sample (**Figure 2**). The first principal component (PC1) explained 40.26% of the total variance, while PC2 explained 20.26%. PC1 showed shape variation mainly related to the relative length of the supra-occipital bone, while PC2 represented variation in relative palate length (warped skulls in **Figure 2**).

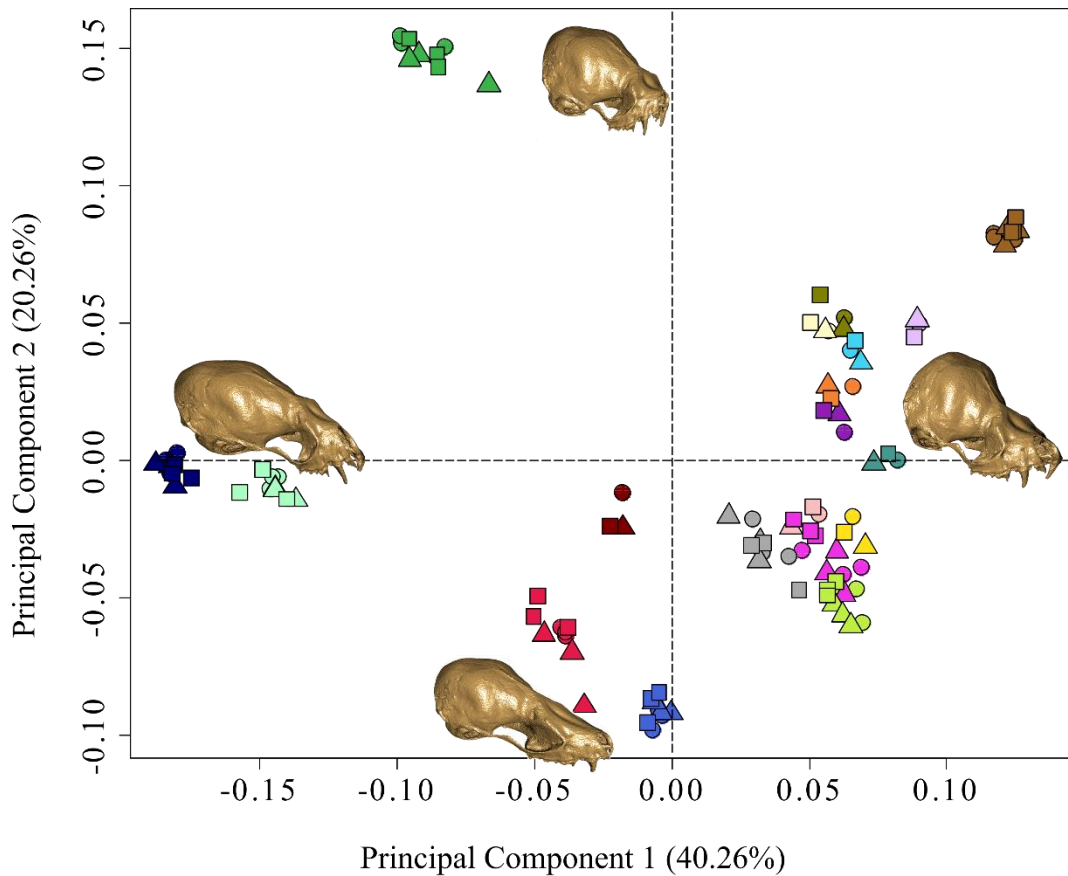


Figure 2. PCA of 57 models (19 specimens x 3 techniques) and 54 replicates (9 specimens x 2 replicates x 3 techniques). Each skull was reconstructed with three different techniques (● laser scan, ■ photogrammetry and ▲ μ CT). For nine specimens (*Carollia perspicillata*, *Desmodus rotundus*, *Glossophaga soricina*, *Myotis emarginatus*, *Myotis capaccinii*, *Nyctalus noctula*, *Rhinolophus hipposideros*, *Rhinolophus ferrumequinum* and *Tadarida teniotis*), I recorded the landmarks three times. The four skull images on the two axes represent the extreme shapes of the morphospace for PC1 and PC2 (species used as reference model for the warping: *Plecotus austriacus*).

Samples clearly clustered according to the species/individuals and not to the technique employed. Replicates were also tightly clustered, except for *M. capaccinii* (which had

some cartilage tissue still attached to the bone, making landmark identification difficult), *C. perspicillata* and *D. rotundus*. Specifically, one μ CT replicate for both *C. perspicillata* and *D. rotundus* did not cluster with the other replicates; this was probably due to the operator error during landmarking. Overall, replicate clusters indicated no evidence of explicit random or systematic (*i.e.*, bias) errors: none of the techniques showed greater variability relative to the others nor was there evidence of differences in mean positioning due to replicate/technique.

Error in geometric morphometrics

Correlations between centroid size vectors obtained from the different models provided coefficients greater than 0.99 for all combinations (photogrammetry-laser scan: $R = 0.997$, $p < 0.001$; μ CT-photogrammetry: $R = 0.996$, $p < 0.001$; laser scan- μ CT: $R = 0.998$, $p < 0.001$). Similarly, high associations were obtained from Mantel matrix correlations on the Procrustes distances between individual specimens across the techniques (photogrammetry-laser scan: $R = 0.988$, $p < 0.001$; μ CT-photogrammetry: $R = 0.988$, $p < 0.001$; laser scan- μ CT: $R = 0.992$, $p < 0.001$). Furthermore, the ANOVA test on size showed that 99.67% ($p = 0.001$) of the variance is explained by biological differences between specimens, with only 0.14% attributable to the technique ($p = 0.001$) (**Table 2**). In terms of shape, 94.52% ($p < 0.001$) of the shape variance was explained by specimen differences while only 0.26% was represented by the different techniques ($p = 0.001$).

Table 2 A) ANOVA on size and **B)** Procrustes ANOVA on shape for 57 models (19 specimens x 3 techniques) and 54 replicas (9 specimens x 2 replicas x 3 techniques).

A)	Df	SS	MS	R²	F	Z	Pr(>F)
Species	18	4016.129	223.118	0.997	2632.394	17.688	0.001
Technique	2	5.744	2.872	0.001	33.887	7.539	0.001
Residuals	90	7.628	0.085	0.002			
Total	110	4029.502					

B)	Df	SS	MS	Rsq	F	Z	Pr(>F)
Species	18	2.117	0.118	0.945	90.535	20.517	0.001
Technique	2	0.006	0.003	0.003	2.274	13.769	0.001
Residuals	90	0.117	0.001	0.052			
Total	110	2.240					

The landmarking error represented a small portion of the variance in both size (between-replicate variance: 0.02%, $p = 0.999$) and shape (between-replicate variance: 2.03%, $p = 0.001$). The repeatability was 0.99 for size and 0.97 for shape (**Table 3 A-B**).

The mean Procrustes variance was not statistically different between techniques ($p = 0.979$) suggesting that difficulty in landmark identification is similar between the techniques (**Figure 3**). Correlations between Procrustes variances (for each technique) and centroid size showed no significant associations (photogrammetry: $R = 0.16$, $p = 0.683$; CT: $R = 0.48$, $p = 0.187$; laser scan: $R = 0.052$, $p = 0.894$).

Table 3. Landmarking error and repeatability for replicas only. **A)** ANOVA on size and **B)** Procrustes

ANOVA on shape for 81 models (9 specimens x 3 replicas x 3 techniques).

A)	Df	SS	MS	R²	F	Z	Pr(>F)
Species	8	2645.123	330.640	0.939	12842.461	10.497	0.001
Species:Replicas	18	0.463	0.026	0.000	0.008	-6.129	0.999
Residuals	54	170.862	3.164	0.061			
Total	80	2816.449					

Repeatability: 0.99

B)	Df	SS	MS	R²	F	Z	Pr(>F)
Species	8	1.688	0.211	0.941	104.374	7.384	0.001
Species:Replicas	18	0.036	0.002	0.020	1.553	23.080	0.001
Residuals	54	0.070	0.001	0.039			
Total	80	1.795					

Repeatability: 0.97

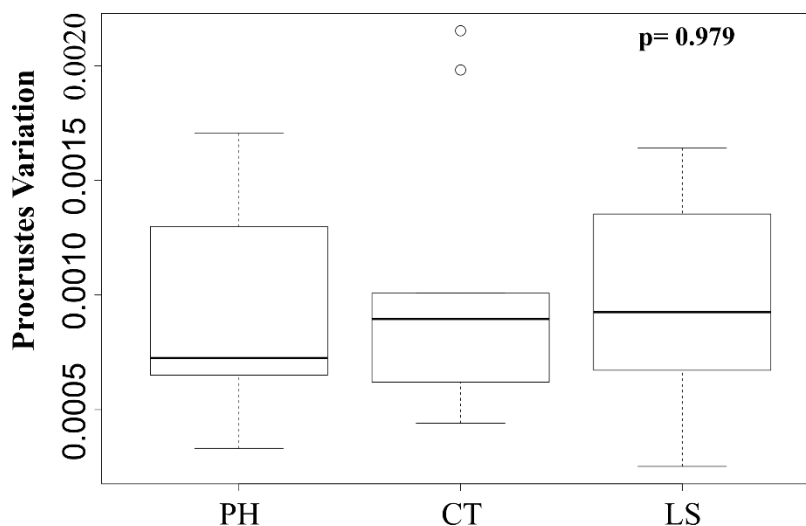


Figure 3. Procrustes variation (i.e., morphological disparity) of replicates for each technique and p value for Kruskal-Wallis test between techniques. The Procrustes variation was computed separately for each species (i.e., triplet of replicates) and the results were displayed and analysed by technique.

Error in evolutionary analyses

Comparisons between the three different scanning techniques for all nineteen species identified consistent (although non-significant) evolutionary allometry patterns (**Table 4**). These were validated by PGLS analyses (**Table 4**). When testing for phylogenetic signal across the three datasets using the consensus tree, I obtained K_{multiv} values that were highly significant and close to one (**Table 4**). The signal was less strong for size but equally significant regardless of the technique (**Table 4**). The results for the association between morphological data and ecological data (*i.e.*, bite force and peak frequency) are reported in **Table 4** for each technique, with and without phylogenetic correction, and show a high degree of concordance between techniques.

Table 4. Results of K_{multiv} phylogenetic signal and R^2 for allometry and correlation with ecological variables. Results are computed by technique (PH = photogrammetry; μ CT; LS = laser scan) with (PGLS) and without (OLS) phylogenetic correction. PS = phylogenetic signal; BF = \log_{10} (bite force); FP = \log_{10} (peak frequency).

	Allometry				Phylogenetic Signal			
	OLS		PGLS		PS Size		PS Shape	
	R^2	p	R^2	p	K	p	K_{multiv}	p
PH	0.062	0.297	0.098	0.160	0.818	0.027	0.919	0.001
μ CT	0.068	0.226	0.105	0.124	0.857	0.019	0.938	0.001
LS	0.072	0.196	0.099	0.145	0.868	0.018	0.972	0.001
mean	0.067	0.240	0.101	0.143	0.848	0.021	0.943	0.001
st.dev.	0.004	0.042	0.003	0.015	0.021	0.004	0.022	0.000

	Size~BF				Shape~BF			
	OLS		PGLS		OLS		PGLS	
	R^2	p	R^2	p	R^2	p	R^2	p
PH	0.780	0.001	0.846	0.001	0.080	0.196	0.037	0.724
μ CT	0.771	0.001	0.826	0.001	0.082	0.18	0.039	0.801
LS	0.774	0.001	0.835	0.001	0.097	0.103	0.051	0.577
mean	0.775	0.001	0.836	0.001	0.087	0.160	0.042	0.701
st.dev.	0.004	0.000	0.008	0.000	0.008	0.041	0.006	0.093

	Size~FP				Shape~FP			
	OLS		PGLS		OLS		PGLS	
	R^2	p	R^2	p	R^2	p	R^2	p
PH	0.012	0.680	0.316	0.004	0.152	0.013	0.093	0.051
μ CT	0.013	0.672	0.331	0.001	0.156	0.014	0.093	0.052
LS	0.012	0.681	0.329	0.002	0.158	0.013	0.092	0.056
mean	0.012	0.678	0.325	0.002	0.155	0.013	0.092	0.053
st.dev.	0.000	0.004	0.007	0.001	0.002	0.000	0.001	0.002

Comparisons of parameter values obtained with the single-techniques (photogrammetry, μ CT, laser scan), against the 1000 mixed datasets, revealed similar means and standard deviations. Nevertheless, in most of the cases, standard deviations were slightly greater for multi-technique datasets (**Table S3**).

When testing for variation due to the phylogenetic uncertainty and technique error the distributions of parameters estimates displayed similar shapes between techniques but in some cases the technique caused a shift in their location (see **Figure S2** for allometry, phylogenetic signal for shape and correlation between shape and bite force). In particular, means of R^2 distributions for allometry differed between each technique (photogrammetry = 0.098; μ CT = 0.105; laser scan = 0.099) but standard deviations did not (photogrammetry = μ CT = laser scan = 0.004). A similar pattern was observed for the K_{multiv} of shape (mean: photogrammetry = 0.916, μ CT = 0.936, laser scan = 0.969; standard deviation: photogrammetry = 0.024, μ CT = 0.026, laser scan = 0.025) and R^2 for correlations between shape and bite force (mean: photogrammetry = 0.100, μ CT = 0.105, laser scan = 0.107; standard deviation: photogrammetry = μ CT = laser scan = 0.004). Nevertheless, the p-values for K_{multiv} of shape were smaller than 0.001 for all combinations of trees/techniques. P-values for allometry and shape correlation with bite force equally resulted in coherent non-significant patterns ($p > 0.15$ in all cases).

The ANOVA on the allometry estimates revealed that 36.35% ($p < 0.001$) of the variance in allometry was explained by the technique employed, while 62.54% ($p < 0.001$) by the phylogenetic uncertainty. The ANOVA on the phylogenetic signal for size demonstrated that the majority of the variance was due to the phylogenetic uncertainty in the dataset (**Table 5**). The phylogenetic signal variance for shape was mainly represented by the phylogenetic uncertainty (55.75%, $p < 0.001$), but a significant portion of the variance was due to the different technique employed (43.75%, $p < 0.001$). When the correlation between morphological data and peak frequency was computed, the variance due to the

technique error was significant but small (size: 1.15%, $p < 0.001$; shape: 2.04%, $p < 0.001$). Similar results were obtained for the correlation between bite force and size (0.35%, $p < 0.001$). Nevertheless, 37.00% of the correlation between bite force and shape was explained by the technique ($p < 0.001$) and 61.65% was explained by phylogenetic uncertainty ($p < 0.001$) (**Table 5**).

Table 5. ANOVAs on parameter estimates of allometry (R^2); phylogenetic signal (K_{multiv}) for size (PS Size) and shape (PS shape); and correlation (R^2) with ecological variables (bite force, [BF] and peak frequency, [FP]) computed by technique and using 1000 trees from the posterior distribution.

		Df	SS	MS	R²	F value	Pr(>F)
PS Size	Technique	2	1.133	0.567	0.068	34190.410	< 0.001
	Tree	999	15.588	0.016	0.930	941.694	< 0.001
	Residuals	1998	0.033	0.000	0.002		
Size~BF	Technique	2	0.004	0.002	0.003	11421.015	< 0.001
	Tree	999	1.052	0.001	0.996	6568.066	< 0.001
	Residuals	1998	0.000	0.000	0.000		
Size~FP	Technique	2	0.004	0.002	0.011	16665.770	< 0.001
	Tree	999	0.325	0.000	0.988	2876.151	< 0.001
	Residuals	1998	0.000	0.000	0.001		
Allometry	Technique	2	0.028	0.014	0.363	32714.085	< 0.001
	Tree	999	0.049	0.000	0.625	112.698	< 0.001
	Residuals	1998	0.001	0.000	0.011		
PS Shape	Technique	2	1.447	0.724	0.438	90648.232	< 0.001
	Tree	999	1.844	0.002	0.558	231.240	< 0.001
	Residuals	1998	0.016	0.000	0.005		
Shape~BF	Technique	2	0.028	0.014	0.370	27415.477	< 0.001
	Tree	999	0.046	0.000	0.616	91.444	< 0.001
	Residuals	1998	0.001	0.000	0.013		
Shape~FP	Technique	2	0.002	0.001	0.020	4069.128	< 0.001
	Tree	999	0.078	0.000	0.975	388.964	< 0.001
	Residuals	1998	0.000	0.000	0.005		

Discussion

Performance of the photogrammetry technique

Analyses of mesh distances, shape visualisation (*i.e.*, PCA graphs) and geometric morphometric error demonstrated that photogrammetry, μ CT and laser scan provide comparable raw material (*i.e.*, centroid size and Procrustes coordinates) for geometric morphometrics analyses. This was supported by high correlation coefficients for centroid size and Procrustes coordinates between the techniques, and low proportion of variance explained by the techniques for both size and shape. This was in accordance with previous studies of much larger skulls, for example humans (Katz & Friess, 2014) and wolves (Evin *et al.*, 2016).

High intraclass correlation coefficients indicated high repeatability and reflected low random measurement error, which suggested that landmarking error was not important for this interspecific dataset. These coefficients (0.97-0.99) were similar to values previously obtained for human skulls (0.99; Badawi-Fayad & Cabanis, 2007), kangaroo-size skulls (0.95; Fruciano *et al.*, 2017), and was higher than small rodent skulls (0.75; Marcy *et al.*, 2018). No technique-related differences in landmarking difficulties were found, based on Procrustes variance, which contrasts with Marcy *et al.*'s (2018) finding of systematically better μ CT relative to laser scans. This difference might be due to their use of a fast data collection scheme (10 minutes/sample) without employing additional measures to ensure quality of the models. Alternatively, it could be linked to intrinsic differences in the laser scan and photogrammetry devices that were employed.

Experience plays an important role in identification and placement of landmarks (Sholts *et al.*, 2011; Osis *et al.*, 2015) and different approaches can induce different levels of systematic error (Marcy *et al.*, 2018). In the current study, I did not specifically test for

operator bias as previous studies reported inter-operator error being similar across different techniques (Robinson & Terhune, 2017).

I also showed that centroid size and Procrustes coordinates extracted from photogrammetry models are suitable for subsequent macroevolutionary analyses such as size-shape correlations (*i.e.*, allometry), calculation of phylogenetic signal and correlation between morphological (*i.e.*, size and shape) and functional (*i.e.*, peak frequency and bite force) data. Parameters estimates were similar among techniques even when accounting for the phylogenetic relatedness. All methods led to the same biological interpretation, further confirming that photogrammetry provides suitable raw data for evolutionary analysis.

Photogrammetry has several advantages in addition to being affordable and easy to use. It is particularly suitable when access to more expensive equipment is limited, where specimens cannot easily be transported, and/or where data collection has to take place in a remote location. Nevertheless, a significant down-side is the lack of detail achieved for teeth reconstruction and difficulties in reproducing thin structures (such as the zygomatic arch). Future studies may explore the use of focused stacking techniques in order to achieve a greater level of detail (Brecko *et al.*, 2014; Nguyen *et al.*, 2014; Santella & Milner 2017).

Mixed data from different reconstruction techniques

This examination of multi-technique datasets revealed increases in standard deviations for allometry, phylogenetic signal and correlation with ecological variables compared with single-technique datasets. However, this had no impact on the biological interpretation of the results. This suggests that multi-technique datasets could potentially be used (with caution and following exploratory studies), at least for interspecific analysis, as long as the use of different techniques is relatively balanced across different groups (such as species, populations or sex). Mixing data from different devices is not recommended when

researchers suspect a relatively small portion of biological variance in the sample (*e.g.* in population studies).

When the same analyses were performed using the set of posterior trees, the interaction between phylogenetic uncertainty and technique became significant. However, the amount of parameter variation was relatively small and mainly due to the phylogenetic variation rather than technique error. Also, the general biological conclusions are essentially the same for almost all analyses (*i.e.*, degrees of allometry and phylogenetic signal for size and variance explained by functional variables). For instance, under the different techniques, bite force predicts between 8.85 and 11.94% of the skull shape variance, supporting the inference that bite force moderately influences the evolution of skull shape in bats.

Fruciano *et al.* (2017) have pointed out that the phylogenetic signal in shape (as reflected by K statistics) is strongly influenced by both phylogenetic uncertainty and technique. In my sample, K_{multiv} varies from 0.85 to 1.05 between techniques which would lead to different evolutionary conclusions (Adams 2014; Blomberg *et al.*, 2003), but the significance of K is unaffected. Revell *et al.* (2008) noted that K is indicative of statistical dependence between traits and phylogenetic relatedness, but no inference on evolutionary rate and mode of evolution should be drawn from its value alone. Therefore, while I suggest that researchers should be cautious about inferring biological meaning from the magnitude of K for shape on mixed technique datasets, its significance can provide a reliable indicator of the presence of a phylogenetic signal.

In conclusion, combining data acquired from models reconstructed with different techniques inevitably introduces an additional source of error. Its impact needs to be assessed according to whether it has an effect on the biological conclusions. Phylogenetic uncertainty can interact with other sources of error (*e.g.* technique employed) suggesting preliminary tests on phylogenetic comparative analyses are essential to identify possible non-negligible sources of error.

Data accessibility

3D model available from the Morphosource repository:

https://www.morphosource.org/Detail/MediaDetail/Show/media_id/30222.

References

- Adams, D.C. 2014. A Generalized K Statistic for Estimating Phylogenetic Signal from Shape and Other High-Dimensional Multivariate Data. *Syst. Biol.* **63**: 685–697.
- Adams, D.C. & Collyer, M.L. 2015. Permutation tests for phylogenetic comparative analyses of high-dimensional shape data: What you shuffle matters. *Evolution (N. Y.)* **69**: 823–829.
- Adams, D.C. & Otárola-Castillo, E. 2013. geomorph: an r package for the collection and analysis of geometric morphometric shape data. *Methods Ecol. Evol.* **4**: 393–399.
- Aguirre, L.F., Herrel, A., van Damme, R. & Matthysen, E. 2002. Ecomorphological analysis of trophic niche partitioning in a tropical savannah bat community. *Proc. R. Soc. London. Ser. B Biol. Sci.* **269**: 1271–1278.
- Badawi-Fayad, J. & Cabanis, E.A. 2007. Three-dimensional procrustes analysis of modern human craniofacial form. *Anat. Rec.* **290**: 268–276.
- Bærentzen, J.A. & Henrik, A. 2002. Generating Signed Distance Fields From Triangle Meshes. Informatics and Mathematical Modelling. Imm-Techni Report 2002-21.
- Bates, K., Falkingham, P. & Rarity, F. 2010. Application of high-resolution laser scanning and photogrammetric techniques to data acquisition, analysis and interpretation in palaeontology. *Int. Arch. Photogramm. Remote Sens. Spat. Inf. Sci.* **38**: 68–73.
- Blomberg, S.P., Garland, T. & Ives, A.R. 2003. Testing for phylogenetic signal in comparative data: behavioral traits are more labile. *Evolution (N. Y.)* **57**: 717–745.
- Bookstein, F.L. 1989. “Size and Shape”: A Comment on Semantics. *Syst. Zool.* **38**: 173–180.
- Brecko, J., Mathys, A., Dekoninck, W., Leponce, M., VandenSpiegel, D. & Semal, P. 2014. Focus stacking: Comparing commercial top-end set-ups with a semi-automatic low budget approach. A possible solution for mass digitization of type specimens. *Zookeys* **464**: 1–23.
- Brinkløv, S., Jakobsen, L., Ratcliffe, J.M., Kalko, E.K. V & Surlykke, A. 2011. Echolocation call intensity and directionality in flying short-tailed fruit bats, *Carollia perspicillata* (Phyllostomidae). *J. Acoust. Soc. Am.* **129**: 427–435.
- Cardini, A. 2014. Missing the third dimension in geometric morphometrics: how to assess if 2D images really are a good proxy for 3D structures? *Hystrix, Ital. J. Mammal.* **25**: 73–81.
- Cardini, A., Polly, D., Dawson, R. & Milne, N. 2015. Why the Long Face? Kangaroos and Wallabies Follow the Same ‘Rule’ of Cranial Evolutionary Allometry (CREA) as Placentals. *Evol. Biol.* **42**: 169–176.

- Cardini, A. & Polly, P.D. 2013. Larger mammals have longer faces because of size-related constraints on skull form. *Nat. Commun.* **4**: 2458.
- Cornette, R., Baylac, M., Souter, T. & Herrel, A. 2013. Does shape co-variation between the skull and the mandible have functional consequences? A 3D approach for a 3D problem. *J. Anat.* **223**: 329–336.
- Cornwell, W. & Nakagawa, S. 2017. Phylogenetic comparative methods. *Curr. Biol.* **27**: R333–R336.
- Cramon-Taubadel, N. Von, Frazier, B.C. & Mirazo, M. 2007. The Problem of Assessing Landmark Error in Geometric Morphometrics : Theory, Methods, and Modifications. *Am. J. Phys. Anthropol.* **134**: 24–35.
- Drake, A.G. & Klingenberg, C.P. 2010. Large-Scale Diversification of Skull Shape in Domestic Dogs: Disparity and Modularity. *Am. Nat.* **175**: 289–301.
- Durão, A.F., Muñoz-Muñoz, F., Martínez-Vargas, J. & Ventura, J. 2018. Obtaining three-dimensional models of limb long bones from small mammals: A photogrammetric approach. In: MONOGRAFIES 14. Geometric Morphometrics. Trends in Biology, Paleobiology and Archaeology (C. Rissech, L. Lloveras, J. Nadal, & J. M. Fullola, eds). Seminari d'Estudis i Recerques Prehistòriques, Barcelona.
- Ege, A., Seker, D.Z., Tuncay, I. & Duran, Z. 2004. Photogrammetric Analysis of the Articular Surface of the Distal Radius. *J. Int. Med. Res.* **32**: 406–410.
- Evin, A., Souter, T., Hulme-Beaman, A., Ameen, C., Allen, R., Viacava, P., *et al.* 2016. The use of close-range photogrammetry in zooarchaeology: Creating accurate 3D models of wolf crania to study dog domestication. *J. Archaeol. Sci. Reports* **9**: 87–93.
- Fahlke, J. & Autenrieth, M. 2016. Photogrammetry VS. Micro-CT scanning for 3D surface generation of typical vertebrate fossil – a case study. *J. Paleontol. Tech.* **14**: 1–18.
- Falkingham, P.L. 2012. Acquisition of high resolution three-dimensional models using free, open-source, photogrammetric software. *Palaeontol. Electron.* **15**: 1–15.
- Fourie, Z., Damstra, J., Gerrits, P.O. & Ren, Y. 2011. Evaluation of anthropometric accuracy and reliability using different three-dimensional scanning systems. *Forensic Sci. Int.* **207**: 127–134.
- Fruciano, C. 2016. Measurement error in geometric morphometrics. *Dev. Genes Evol.* **226**: 139–158. Development Genes and Evolution.
- Fruciano, C., Celik, M.A., Butler, K., Dooley, T., Weisbecker, V. & Phillips, M.J. 2017. Sharing is caring? Measurement error and the issues arising from combining 3D morphometric datasets. *Ecol. Evol.* **7**: 7034–7046.
- Huelsenbeck, J.P. & Ronquist, F. 2001. MRBAYES: Bayesian inference of phylogenetic trees. *Bioinformatics* **17**: 754–755.
- Kalko, E.K. V, Schnitzler, H., Kaipf, I. & Grinnell, A.D. 1998. Echolocation and Foraging Behavior of the Lesser Bulldog Bat, *Noctilio albiventris* : Preadaptations for Piscivory? *Behav. Ecol. Sociobiol.* **42**: 305–319.
- Katz, D. & Friess, M. 2014. Technical Note: 3D From Standard Digital Photography of Human Crania - A Preliminary Assessment. *Am. J. Phys. Anthropol.* **154**: 152–158.
- Mallison, H. & Wings, O. 2014. Photogrammetry in paleontology- A practical guide. *J. Paleontol. Tech.* **12**: 1–31.

- Marcy, A.E., Fruciano, C., Phillips, M.J., Mardon, K. & Weisbecker, V. 2018. Low resolution scans can provide a sufficiently accurate, cost- and time-effective alternative to high resolution scans for 3D shape analyses. *PeerJ* **6**: e5032.
- Muñoz-Muñoz, F., Quinto-Sánchez, M. & González-José, R. 2016. Photogrammetry: A useful tool for three-dimensional morphometric analysis of small mammals. *J. Zool. Syst. Evol. Res.* **54**: 318–325.
- Nguyen, C. V, Lovell, D.R., Adcock, M. & La Salle, J. 2014. Capturing Natural-Colour 3D Models of Insects for Species Discovery and Diagnostics. *PLoS One* **9**: e94346.
- Osis, S.T., Hettinga, B.A., Macdonald, S.L. & Ferber, R. 2015. A novel method to evaluate error in anatomical marker placement using a modified generalized Procrustes analysis. *Comput. Methods Biomech. Biomed. Engin.* **18**: 1108–1116.
- Paradis, E., Claude, J. & Strimmer, K. 2004. APE: Analyses of Phylogenetics and Evolution in R language. *Bioinformatics* **20**: 289–290.
- R Core Team. 2019. R: A language and environment for statistical computing. R Found. Stat. Comput. Vienna, Austria. URL <https://www.R-project.org/>.
- Revell, L.J., Harmon, L.J. & Collar, D.C. 2008. Phylogenetic Signal, Evolutionary Process, and Rate. *Syst. Biol.* **57**: 591–601.
- Robinson, C. & Terhune, C.E. 2017. Error in geometric morphometric data collection: Combining data from multiple sources. *Am. J. Phys. Anthropol.* **164**: 62–75.
- Rodríguez-San Pedro, A. & Allendes, J.L. 2017. Echolocation calls of free-flying common vampire bats *Desmodus rotundus* (Chiroptera: Phyllostomidae) in Chile. *Bioacoustics* **26**: 153–160.
- Rohlf, F.J. 2007. Comparative methods for the analysis of continuous variables: geometric interpretations. *Evolution (N. Y.)* **55**: 2143–2160.
- Russo, D. & Jones, G. 2002. Identification of twenty-two bat species (Mammalia: Chiroptera) from Italy by analysis of time-expanded recordings of echolocation calls. *J. Zool.* **258**: S0952836902001231.
- Santella, M. & Milner, A.R.. 2017. Coupling focus stacking with photogrammetry to illustrate small fossil teeth. *J. Paleontol. Tech.* **18**: 1–17.
- Schlager, S. 2013. Morpho: Calculations and visualizations related to Geometric Morphometrics. R package version 0.17. <http://sourceforge.net/projects/morpho-rpackage/>.
- Shi, J.J. & Rabosky, D.L. 2015. Speciation dynamics during the global radiation of extant bats. *Evolution (N. Y.)* **69**: 1528–1545.
- Sholts, S.B., Flores, L., Walker, P.L. & Wärmländer, S.K.T.S. 2011. Comparison of coordinate measurement precision of different landmark types on human crania using a 3D laser scanner and a 3D digitiser: Implications for applications of digital morphometrics. *Int. J. Osteoarchaeol.* **21**: 535–543.
- Siemers, B.M., Kalko, E.K. V & Schnitzler, H.U. 2001. Echolocation behavior and signal plasticity in the Neotropical bat *Myotis nigricans* (Schinz, 1821) (Vespertilionidae): A convergent case with European species of *Pipistrellus*? *Behav. Ecol. Sociobiol.* **50**: 317–328.
- Siemers, B.M. & Schnitzler, H.-U. 2004. Echolocation signals reflect niche differentiation in five sympatric congeneric bat species. *Nature* **429**: 657.

- Simmons, N.B. & Geisler, J.H. 1998. Phylogenetic relationships of Icaronycteris, Archaeonycteris, Hassianycteris, and Palaeochiropteryx to extant bat lineages, with comments on the evolution of echolocation and foraging strategies in Microchiroptera. *Bull. Am. Museum Nat. Hist.* **235**: 1–182.
- Sztencel-Jabłonka, A., Jones, G. & Bogdanowicz, W. 2009. Skull morphology of two cryptic bat species: *Pipistrellus pipistrellus* and *P. pygmaeus* - a 3D geometric morphometrics approach with landmark reconstruction. *Acta Chiropterologica* **11**: 113–126.
- Wiley, D.F., Amenta, N., Alcantara, D.A., Ghosh, D., Kil, Y.J., Delson, E., *et al.* 2005. Evolutionary Morphing. In: Proceedings of IEEE Visualization, pp. 431–438.
- Zelditch, M., Swiderski, D. & Sheets, H. 2012. Geometric Morphometrics for Biologists. A Primer., 2nd editio. Cambridge. Academic Press. 488.

Supplementary Information

Supplementary Methods

Photogrammetry. Photogrammetry is widely used in palaeontological and zoological studies to extract reliable measurements from 2D images or 3D models. Although it is more intensively applied to scan live animals (Ratnaswamy & Winn, 1993; Postma *et al.*, 2015; Marchal *et al.*, 2016), studies of museum specimens have recently increased (Evin *et al.*, 2016; Moshobane *et al.*, 2016; Muñoz-Muñoz *et al.*, 2016). Precautions are required to obtain successful mesh reconstructions in 3D models of small and complex objects (Mallison & Wings, 2014), such as bat skulls. Photogrammetry 3D models were obtained by employing a 24 mega-pixel digital SLR Nikon D5300 camera (Nikon Corporation, Japan) attached to a Nikkor 60 mm macro lens (Nikon Corporation, Japan) and mounted on a tripod. The general camera lighting settings and positioning, specimen arrangement and number of pictures per specimen were adapted from Falkingham (2012) and Mallison and Wings (2014). A turning platform (~10 cm diameter), covered by black velvet, was placed inside a white photography tent and surrounded by three natural white lights to provide a constant and homogeneous illumination (enhancing the contrast between the skull components and avoiding excessive shadows and non-natural colouration). I positioned the specimen on the centre of the platform to ensure standardised data acquisition across all samples. The camera was positioned at approximately 10-15 cm from the skull at an angle of ca 30-40° relative to the platform plane.

Pictures were taken so that approximately 2/3 of the frame was occupied by the image of the cranium, thus optimizing the number of informative pixels in the frame. I took pictures at successive rotation intervals of 8-9 degrees, obtaining a total of 40-45 high quality image acquisitions for each complete platform rotation (= chunk), which was enough to ensure a sufficient frame overlap. A total of 120-135 pictures were acquired for each

specimen from three complete rotations of the skull: one rotation on the transverse axis (*i.e.*, laying on the basicranium: horizontal chunk) and a double rotation on the longitudinal axis (*i.e.*, standing on the occipital bone: vertical chunks).

The aperture of the camera lens was set at f32 to increase the depth of field (guaranteeing that most of the cranium was in focus) while the exposure time (usually between 0.33-0.63 secs) was dependent on light condition (exposure meter between 0 and -1). The data acquisition time with this protocol ranged between 20-30 minutes per sample.

Agisoft PhotoScan Professional v. 1.3.4 software (Agisoft LLC, Russia) was used to obtain 3D spatial data from the images and reconstruct the model. The same workflow was adopted for each chunk: 1) mask application to all pictures, 2) picture alignment with subsequent sparse cloud generation, 3) dense cloud production (~16,000,000 points), 4) dense cloud cleaning, 5) chunk alignment, 6) mesh creation (~3,000,000 faces) and saving of the 3D model in .ply format (for a review of photogrammetry workflows see Falkingham, 2012; Mallison & Wings 2014). Most of these steps can be performed efficiently in a semi-automatic manner (*i.e.*, batch process mode) and multiple projects can be processed at a time. The resulting .ply file was scaled in MeshLab 2016.12 software using a scale factor that was obtained from three skull measurements (*i.e.*, dorsal length, ventral length and width). These measurements were taken (to the nearest 0.01 mm) with a digital calliper (*Senator* 6, Senator Quality Tooling).

The average time required to perform all the steps listed above was around 150 minutes per model. To potentially reduce the reconstruction time, only one rotation on the longitudinal axis can be used and the second one kept as backup in case of failure of the first. This would reduce the reconstruction time to around 120 minutes without compromising the mesh reconstruction success. To further reduce the reconstruction time the pictures can be subsampled to reduce the number per chunk to around 36 here. Nevertheless, this tended to

lead to a failing of the dense cloud production step, preventing the mesh reconstruction in approximately one third of the samples.

Surface laser scan. Many fundamental and processing steps for laser scan are shared with photogrammetry. Breuckmann technology is widely used for morphometric analyses in biology and anthropology (Katz & Friess, 2014; Evin *et al.*, 2016 among others). I employed a Breuckmann Laser Scan, model SmartSCAN R5/C5 5.0 MegaPixel (AICON 3D systems, Braunschweig, Germany). It is equipped with two digital cameras (30° of triangulation angle) either side of a white light projector unit. An automatic turning platform is located at a distance of 37 cm from the cameras. The specimen was placed at the centre of the platform. This system requires stable lighting and a dark environment: any additional light acts as noise and can compromise the reconstruction process. I employed the field of view S-030 which is optimal for very small objects (240 mm length) and can achieve a maximum resolution of 10 µm. After calibrating the cameras, 12 pairs of pictures were taken for each complete rotation. The operator changed the specimen orientation at the end of each chunk and, depending on the size of the specimen, collected 3-4 chunks for each skull. Chunks were processed with OptoCat software (AICON 3D systems, Braunschweig, Germany). The software computes a primary mesh for each chunk that automatically aligns with the previous chunk. If unsuccessful, the operator can select three points that the software will use as a reference. When all chunks have been merged, the 3D model is saved in .ply format. This technique is the least time-consuming of the three with a total processing time of around 40 minutes (including image collection and 3D model generation).

Micro CT scan. The µCT scans of the 19 bat specimens were performed at the MNHN of Paris using a phoenix v|tome|x s (GE Sensing & Inspection Technologies, Germany) with a voxel size range of 18-28 µm (average 23 µm). The remaining specimens from the RBINS were scanned with a XRE UniTom µCT (XRE nv, Belgium) and the scans achieved a

voxel size ranging from 12 to 20 μm (average 15 μm). All crania were located inside a plastic tube separated from one another by a low-density material. The computed tomography technique uses x-rays to acquire cross sectional images on three dimensions, all at a specific distance from each other. I processed these virtual slices with the software Avizo (FEI Visualization, Hillsboro, USA) to reconstruct the 3D volume of the scanned object. The 3D models were obtained through a segmentation routine, by selecting the regions of interest in the 2D radiography images. Lastly, the model was saved as .ply file.

Supplementary References

- Bogdanowicz, W., Juste, J., Owen, R.D. & Sztencel, A. 2005. Geometric morphometrics and cladistics: testing evolutionary relationships in mega- and microbats. *Acta Chiropterologica* **7**: 39–49.
- Evin, A., Souter, T., Hulme-Beaman, A., Ameen, C., Allen, R., Viacava, P., *et al.* 2016. The use of close-range photogrammetry in zooarchaeology: Creating accurate 3D models of wolf crania to study dog domestication. *J. Archaeol. Sci. Reports* **9**: 87–93.
- Falkingham, P.L. 2012. Acquisition of high resolution three-dimensional models using free, open-source, photogrammetric software. *Palaeontol. Electron.* **15**: 1–15.
- Katz, D. & Friess, M. 2014. Technical Note: 3D From Standard Digital Photography of Human Crania - A Preliminary Assessment. *Am. J. Phys. Anthropol.* **154**: 152–158.
- Mallison, H. & Wings, O. 2014. Photogrammetry in paleontology- A practical guide. *J. Paleontol. Tech.* **12**: 1–31.
- Marchal, A.F.J., Lejeune, P. & Bruyn, P.J.N. 2016. Virtual plaster cast: digital 3D modelling of lion paws and tracks using close-range photogrammetry. *J. Zool.* **300**: 111–119.
- Moshobane, M.C., de Bruyn, P.J.N. & Bester, M. 2016. Assessing 3D photogrammetry techniques in craniometrics. In: The International Archive of Photogrammetry, Remote Sensing and Spatial Information Sciences. Vol. XLI-B6. XXIII ISPRS Congress, 12-19 July 2016, Prague, Czech Republic.
- Muñoz-Muñoz, F., Quinto-Sánchez, M. & González-José, R. 2016. Photogrammetry: A useful tool for three-dimensional morphometric analysis of small mammals. *J. Zool. Syst. Evol. Res.* **54**: 318–325.
- Postma, M., Tordiffe, A.S.W., Hofmeyr, M.S., Reisinger, R.R., Bester, L.C., Buss, P.E., *et al.* 2015. Terrestrial mammal three-dimensional photogrammetry: multispecies mass estimation. *Ecosphere* **6**: 1–16.
- Ratnaswamy, M.J. & Winn, H.E. 1993. Photogrammetric Estimates of Allometry and Calf Production in Fin Whales, *Balaenoptera physalus*. *J. Mammal.* **74**: 323–330.
- Sztencel-Jabłonka, A., Jones, G. & Bogdanowicz, W. 2009. Skull morphology of two cryptic bat species: *Pipistrellus pipistrellus* and *P. pygmaeus* - a 3D geometric

Supplementary Tables

Table S1. Anatomical definitions of 24 unilateral landmarks. Landmarks with * are symmetric landmarks and are only placed on the right side of the skull.

Landmark number	Anatomical definition
1	Dorsal internasal-opening midpoint
2	Uppermost point on the frontal suture
3	Highest point on the interparietal/supraoccipital suture
4	Midpoint on the posterior limit of foramen magnum
5	Lateral limit of the foramen magnum*
6	Midpoint on the anterior limit of foramen magnum
7	Most posterior point of the mandibular fossa*
8	Attachment point between zygomatic arch and mandibular fossa*
9	Most anterior point of the mandibular fossa*
10	Most internal point of the mandibular fossa*
11	Posterior end of the palatine
12	Ventral most anterior internal point of the zygomatic arch*
13	Ventral internasal-opening midpoint
14	External anterior base of C*
15	External posterior base of C*
16	End of the tooththrow*
17	Midpoint of the lower margin of the infraorbital foramen*
18	Midpoint of the higher margin of the infraorbital foramen*
19	External margin of the notch above the lacrimal process*
20	Dorsal most anterior external point of the zygomatic arch*
21	Dorsal most posterior internal point of the zygomatic arch*
22	Dorsal most posterior external point of the zygomatic arch*
23	Most posterior point of tympanic bullae*
24	Most anterior point of tympanic bullae*

Table S2. Percentage distances (relative to total skull length) between the surfaces of the models. PH = Photogrammetry, LS = Laser scan, μ CT = μ CT scan.

Specimen	PH-LS	μCT-PH	LS-μCT
<i>Carollia perspicillata</i>	0.342	0.440	0.005
<i>Desmodus rotundus</i>	0.031	0.058	0.053
<i>Eptesicus serotinus</i>	0.165	0.206	0.118
<i>Glossophaga soricina</i>	0.277	0.385	0.125
<i>Hypsugo savii</i>	0.274	0.291	0.034
<i>Myotis daubentonii</i>	0.426	0.676	0.118
<i>Miniopterus schreibersii</i>	0.303	0.295	0.015
<i>Myotis capaccinii</i>	1.142	1.241	0.079
<i>Myotis emarginatus</i>	0.503	0.473	0.000
<i>Myotis nigricans</i>	0.345	0.715	0.250
<i>Myotis dasycneme</i>	0.170	0.301	0.392
<i>Noctilio albiventris</i>	0.005	0.010	0.015
<i>Nyctalus noctula</i>	0.027	0.399	0.296
<i>Pipistrellus pipistrellus</i>	0.259	0.355	0.154
<i>Pipistrellus nathusii</i>	0.307	0.358	0.102
<i>Plecotus austriacus</i>	0.492	0.499	0.013
<i>Rhinolophus ferrumequinum</i>	0.005	0.037	0.021
<i>Rhinolophus hipposideros</i>	0.228	0.159	0.084
<i>Tadarida teniotis</i>	0.081	0.166	0.076
MEAN	0.283	0.372	0.103
ST.DEV.	0.253	0.278	0.104

Table S3. Results of K_{multiv} for phylogenetic signal **A)** and R^2 for allometry and correlation with ecological variables **B)** for the multi-and singular-technique datasets. Results are computed by technique with (PGLS) and without (OLS) phylogenetic correction. PS = phylogenetic signal; BF = bite force; FP = peak frequency

A)		Min	Mean	Max	SD				
PS Size	multi-technique	0.800	0.846	0.889	0.018				
	singular-technique	0.818	0.848	0.868	0.021				
PS Shape	multi-technique	0.899	0.940	0.984	0.016				
	singular-technique	0.919	0.943	0.972	0.022				

B)		OLS				PGLS			
		Min	Mean	Max	SD	Min	Mean	Max	SD
Allometry	multi-technique	0.058	0.066	0.076	0.003	0.083	0.096	0.110	0.004
	singular-technique	0.062	0.067	0.072	0.004	0.098	0.101	0.105	0.003
Size~BF	multi-technique	0.752	0.774	0.796	0.007	0.811	0.835	0.857	0.008
	singular-technique	0.771	0.775	0.780	0.004	0.826	0.836	0.846	0.008
Shape~BF	multi-technique	0.069	0.086	0.106	0.007	0.030	0.042	0.058	0.005
	singular-technique	0.080	0.087	0.097	0.008	0.037	0.042	0.051	0.006
Size~FP	multi-technique	0.007	0.011	0.017	0.002	0.304	0.324	0.339	0.008
	singular-technique	0.012	0.012	0.013	0.000	0.316	0.325	0.331	0.007
Shape~FP	multi-technique	0.145	0.155	0.168	0.004	0.084	0.092	0.102	0.002
	singular-technique	0.152	0.155	0.158	0.002	0.092	0.092	0.093	0.001

Supplementary Figures



Figure S1. Example of dorsal view for models built with photogrammetry, laser scan and μ CT scan (respectively from left to right).

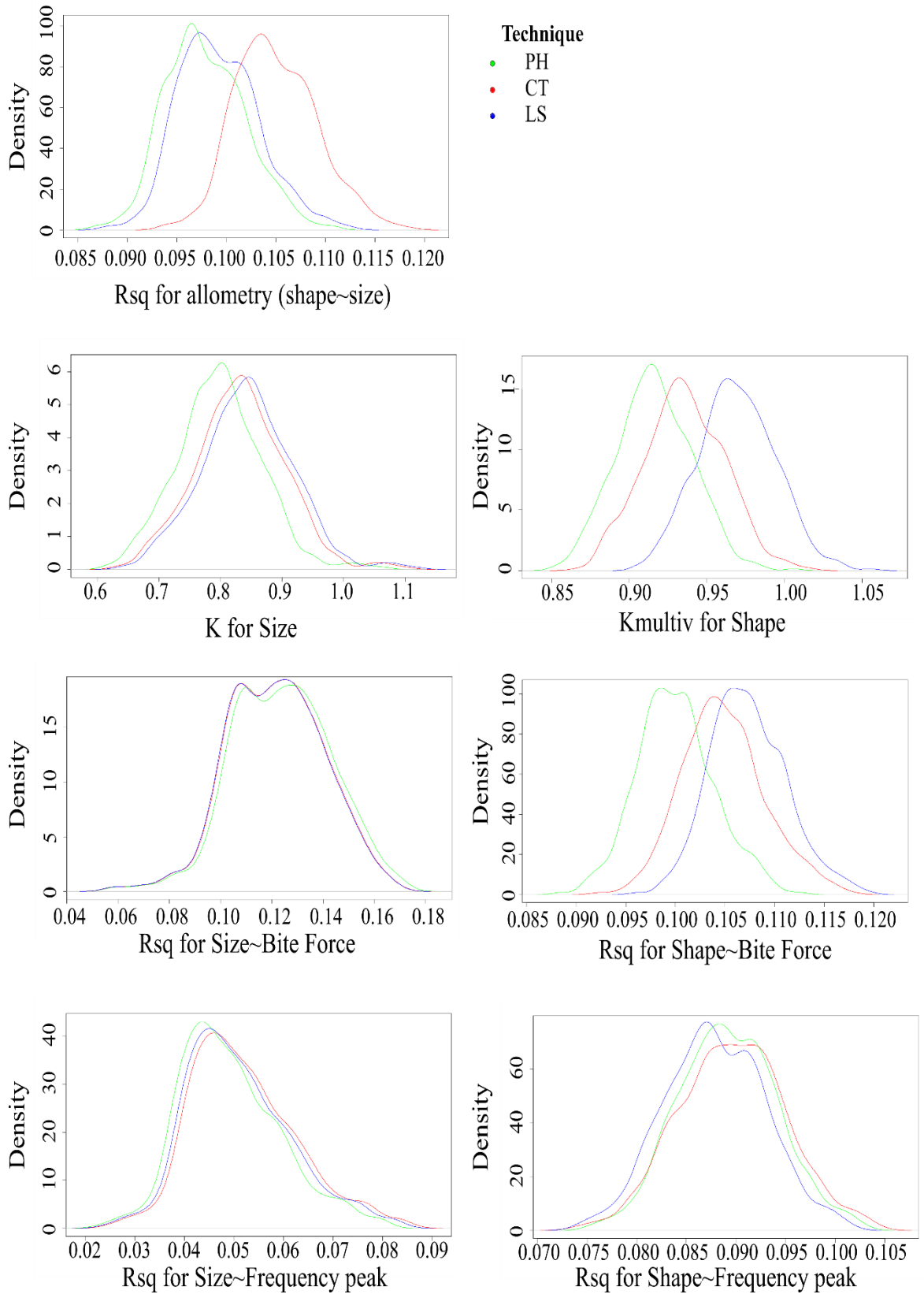


Figure S2. Parameters distribution of allometry, phylogenetic signal (for size and shape), correlation with bite force and with peak frequency computed under phylogenetic comparative approach using 1000 trees sampled from the posterior distribution.

Appendix D

First page of the published paper resulted from *Chapter Three* in *Evolutionary Biology*.

Evolutionary Biology
https://doi.org/10.1007/s11692-019-09478-6

TOOLS AND TECHNIQUES



3D Photogrammetry of Bat Skulls: Perspectives for Macro-evolutionary Analyses

Giada Giacomini¹ · Dino Scaravelli² · Anthony Herrel³ · Alessio Veneziano¹ · Danilo Russo^{4,5} · Richard P. Brown¹ · Carlo Meloro¹

Received: 7 February 2019 / Accepted: 4 May 2019
© The Author(s) 2019

Abstract

Photogrammetry (PH) is relatively cheap, easy to use, flexible and portable but its power and limitations have not been fully explored for studies of small animals. Here we assessed the accuracy of PH for the reconstruction of 3D digital models of bat skulls by evaluating its potential for evolutionary morphology studies at interspecific (19 species) level. Its reliability was assessed against the performance of micro CT scan (μ CT) and laser scan techniques (LS). We used 3D geometric morphometrics and comparative methods to quantify the amount of size and shape variation due to the scanning technique and assess the strength of the biological signal in relation to both the technique error and phylogenetic uncertainty. We found only minor variation among techniques. Levels of random error (repeatability and procrustes variance) were similar in all techniques and no systematic error was observed (as evidenced from principal component analysis). Similar levels of phylogenetic signal, allometries and correlations with ecological variables (frequency of maximum energy and bite force) were detected among techniques. Phylogenetic uncertainty interacted with technique error but without affecting the biological conclusions driven by the evolutionary analyses. Our study confirms the accuracy of PH for the reconstruction of challenging specimens. These results encourage the use of PH as a reliable and highly accessible tool for the study of macro evolutionary processes of small mammals.

Keywords 3D reconstruction · Geometric morphometrics · Measurement error · Technique comparison

Electronic supplementary material The online version of this article (<https://doi.org/10.1007/s11692-019-09478-6>) contains supplementary material, which is available to authorized users.

✉ Giada Giacomini
g.giacomini@2016.ljmu.ac.uk
Dino Scaravelli
dino.scaravelli@gmail.com
Anthony Herrel
anthony.herrel@mnhn.fr
Alessio Veneziano
veneziano.alessio@gmail.com
Danilo Russo
danrusso@unina.it
Richard P. Brown
r.p.brown@ljmu.ac.uk
Carlo Meloro
c.meloro@ljmu.ac.uk

Introduction

The use of digital 3D models in morphological studies is increasing in many scientific disciplines, including palaeontology and evolutionary biology. The digitalization of

- ¹ Research Centre in Evolutionary Anthropology and Paleocology, School of Natural Sciences and Psychology, Liverpool John Moores University, Byrom Street, Liverpool L3 3AF, UK
- ² Department of Veterinary Medical Sciences, University of Bologna, 50 Via Tolara di Sopra, Ozzano dell'Emilia, 40064 Bologna, BO, Italy
- ³ Department Adaptation du Vivant, UMR 7179 C.N.R.S./M.N.H.N, 55 Rue Buffon, 75005 Paris, France
- ⁴ Wildlife Research Unit, Agrarian Department, University of Naples Federico II, 100 Via Università, 80055 Portici, NA, Italy
- ⁵ School of Biological Sciences, University of Bristol, Life Sciences Building, 24 Tyndall Avenue, Bristol BS8 1TQ, UK

Published online: 22 May 2019

Springer

Appendix E

The table reports skull total length (mm, [TL]) of the 19 specimens from the MNHN reconstructed in *Chapter Three* with photogrammetry, μ CT and laser scans. Average skull length = 15.62; minimum = 10.41; maximum = 22.44.

Inventory Number	Family	Species	TL
MNHN-ZM-MO-1996-447	Molossidae	<i>Tadarida teniotis</i>	19.82
MNHN-ZM-MO-2007-81	Noctilionidae	<i>Noctilio albiventris</i>	20.48
MNHN-ZM-MO-1998-667	Phyllostomidae	<i>Carollia perspicillata</i>	20.44
MNHN-ZM-MO-2007-90	Phyllostomidae	<i>Desmodus rotundus</i>	22.44
MNHN-ZM-MO-1977-527	Phyllostomidae	<i>Glossophaga soricina</i>	18.42
MNHN-ZM-MO-1977-58	Rhinolophidae	<i>Rhinolophus ferrumequinum</i>	18.78
MNHN-ZM-MO-1932-4107	Rhinolophidae	<i>Rhinolophus hipposideros</i>	13.17
MNHN-ZM-MO-2003-222	Vespertilionidae	<i>Eptesicus serotinus</i>	17.00
MNHN-ZM-MO-1932-4270	Vespertilionidae	<i>Hypsugo savii</i>	11.70
MNHN-ZM-MO-2004-460	Vespertilionidae	<i>Miniopterus schreibersi</i>	13.20
MNHN-ZM-MO-1955-671	Vespertilionidae	<i>Myotis capaccinii</i>	15.15
MNHN-ZM-MO-1983-506	Vespertilionidae	<i>Myotis dasycneme</i>	15.30
MNHN-ZM-MO-1997-322	Vespertilionidae	<i>Myotis daubentoni</i>	13.61
MNHN-ZM-MO-2004-1308	Vespertilionidae	<i>Myotis emarginatus</i>	13.73
MNHN-ZM-MO-2003-316	Vespertilionidae	<i>Myotis nigricans</i>	11.61
MNHN-ZM-MO-1932-4158	Vespertilionidae	<i>Nyctalus noctula</i>	14.55
MNHN-ZM-MO-1932-4267	Vespertilionidae	<i>Pipistrellus nathusii</i>	11.73
MNHN-ZM-MO-2003-283	Vespertilionidae	<i>Pipistrellus pipistrellus</i>	10.41
MNHN-ZM-MO-1932-4160	Vespertilionidae	<i>Plecotus austriacus</i>	15.24

CHAPTER FOUR: Skull Shape of Insectivorous Bats: Evolutionary Trade-off between Feeding and Echolocation?

Statement on content presentation and publication

This chapter is currently in preparation for submission to the *Journal of Evolutionary Biology*.

Abstract

Morphological, functional and behavioural adaptations of bats are among the most diverse within mammals. A strong association between bat skull morphology and feeding behaviour has been suggested previously. However, morphological variation related to other drivers of adaptation (in particular echolocation) remains understudied. It is assumed that adaptations to echolocate are associated with soft tissue rather than bony structures, although some recent studies have started to challenge this assumption.

I assessed variation in skull morphology with respect to ecological group (*i.e.*, diet and emission type) and functional measures (*i.e.*, bite force, masticatory muscles and echolocation characteristics) using geometric morphometrics and comparative methods. This represents the first quantitative analysis of the relationship between skull form (particularly shape) and sound parameters within a broad taxonomic context.

This study suggested that variation in skull shape of 10 bat families is the result of adaptations to broad diet categories and sound emission types (*i.e.*, oral or nasal).

Nevertheless, I found that skull shape is adapted to echolocation parameters in insectivorous species, possibly because they (almost) entirely rely on this sensory system for locating and capturing prey. Finally, I identified a possible evolutionary trade-off in skull shape of insectivorous bats between feeding function (described by bite force and muscles mass) and sensory function (described by echolocation characteristics). Species with long rostra emit low frequency sounds able to travel long distances but have weaker bite forces.

The study advances our understanding of the relationship between skull morphology and specific features of echolocation and suggests that evolutionary constraints due to echolocation may differ between different groups within the Chiroptera.

Introduction

Morphological changes in the mammalian skull are driven by a variety of functional demands such as feeding ecology (Janis, 1990), environmental context (*e.g.* habitat productivity: Cardini *et al.*, 2007) and broad morphological drivers (*e.g.* allometric rule: Cardini, 2019). Flying mammals of the order Chiroptera face the additional challenge of effective echolocation, and so their skulls also have to behave as acoustic horns for efficient sound emission (Pedersen, 1998).

Multiple studies support a strong association between bat skull morphology and feeding function. In particular, diet preferences, bite force and masticatory muscles have been widely associated with skull size and shape variation in bats (Freeman, 1998; Aguirre *et al.*, 2002; Nogueira *et al.*, 2009; Santana *et al.*, 2010, 2012, amongst others).

Nevertheless, the majority of these studies have focused on one family only – the Phyllostomidae- (but see Senawi *et al.*, 2015; Hedrick & Dumont, 2018). Although this family is the most diverse in terms of diet and skull morphology (Wilson & Reeder, 2005), comparisons within a broader taxonomic context are required to detect more general patterns.

Laryngeal echolocating bats use acoustic emissions not only to locate prey and navigate the environment but also to communicate (Jones & Siemers, 2011). Divergence in acoustic emissions plays a role in bat speciation and diversification (Jones, 1997). Different degrees of head rotation are associated with emission type in bats: the head in nasal emitters is folded towards the chest while in oral emitters it rotates dorsally during ontogenesis (Pedersen, 1998). Besides this well-described dichotomy between oral and nasal emitters (Pedersen, 1998; Arbour *et al.*, 2019), our understanding of the influence of echolocation adaptation on the size and shape of bat skulls remains limited. Adaptations for echolocation are generally thought to be associated with soft tissue rather than bony

structures (Elemans *et al.*, 2011). It is therefore argued that cranial adaptations arise through selective forces acting on the larynx and associated muscles rather than direct selection on cranial shape (Pedersen, 2000). Evidence that bat skull size and shape are associated with echolocation parameters (in particular peak frequency) has been detected in some bat families (Jacobs *et al.*, 2014; Thiagavel *et al.*, 2017), but there is a significant gap in our understanding of how echolocation relates to morphology and whether or not a general pattern is present across families (particularly with respect to skull shape). Indeed, different selective pressures can result in different evolutionary trade-offs driving related taxa towards different evolutionary optima (Dumont *et al.*, 2014; Arbour *et al.*, 2019). Insectivorous bats are known to rely mainly on echolocation to detect and pursue their prey, in contrast with other bats (*e.g.* carnivorous species) that rely also on vision and olfaction (Bahlman & Kelt, 2007; Surlykke *et al.*, 2013; Ripperger *et al.*, 2019).

Thus, I set out to test the prediction that insectivorous species display an association between skull shape and echolocation characteristics due to a less flexible (but more specialised) sensory system. More specifically, I used geometric morphometrics and phylogenetic comparative methods to test the following main predictions:

- i. the association between feeding descriptors (*i.e.*, diet, bite force, and masticatory muscles) and morphology follows a general pattern within Chiroptera because similar biomechanical constraints apply to all taxa;
- ii. insectivorous bats display an association between skull morphology (*i.e.*, size and shape) and echolocation call parameters because they almost exclusively rely on sound emission to detect and pursue their prey;
- iii. insectivorous bats show a trade-off in skull shape between feeding and sensory function due to dual skull functions: processing hard food and optimising sound emission.

Methods

Sample

I performed statistical analyses on 185 bat skulls belonging to 67 species, from 10 different bat families. Data on skull morphology, diet, emission type, echolocation parameters and bite force were available for all species (see below). Additionally, for a subsample of 32 species (96 specimens; 5 bat families) masticatory muscle data were available and included in the analyses. Details on origins of specimens (museum collections) are reported in **Appendix F**.

Functional, ecological and morphological data

The full list of traits studied and parameter abbreviations used hereafter are reported in **Table 1**. Feeding (*i.e.*, bite force and muscles mass) and sensory (*i.e.*, echolocation parameters) data were acquired from the literature or collected in the field. Details on collection techniques and criterion for data selection are provided in the methodological chapter of this thesis (*Chapter Two*). The selected literature and raw data used in this study are provided in **Appendix A** for sensory parameters and **B** for feeding parameters.

To assess the relationship between morphology and ecological groups, I classified species by broad diet categories, ability for laryngeal echolocation, and emission type (the latter only within laryngeal echolocating species).

Table 1. Functional traits used as covariates in the present study. Traits in italics were available for only a subsample of data (n = 32).

Feeding parameters	Sensory parameters	Diet category	Echolocation	Emission type
Bite force	Peak frequency	Insectivorous	Non echolocation	Nasal
<i>Digastric muscle</i>	Start frequency	Frugivorous	Laryngeal echolocation	Oral
<i>Masseter muscle</i>	End frequency	Hematophagous		Both oral and nasal
<i>Temporalis muscle</i>	Bandwidth	Vertebrate eater		
<i>Pterygoid muscle</i>	Duration	Nectarivorous		
	Sweep rate	Omnivorous		
		Frugi/insectivorous		
		Necta/fruigivorous		
		Insect-vertebrate eater		

Diet was categorised by traditional groups inferred from Wilson and Reeder (2005) and is reported in **Table 1**. I followed Thiagavel *et al.* (2018) to categorise species according to whether they are capable of laryngeal echolocation or not. Echolocating bats were further categorised according to emission type, as species that use mouth emission, nasal emission, or emission from both nose and mouth, following references in **Appendix A** and additional references (Pedersen, 1998; Goudy-Trainor & Freeman, 2002; Surlykke *et al.*, 2013; Seibert *et al.*, 2015; Jakobsen *et al.*, 2018).

Morphological data were collected by geometric morphometric methods applied to 3D digital models of bat crania. An established photogrammetric protocol (Giacomini *et al.*, 2019, *Chapter Three*) and μ CT scans were employed to digitally reconstruct the models (**Appendix F**). The combination of 3D reconstruction techniques (*i.e.*, photogrammetry and μ CT scan) has been demonstrated to provide robust biological results in macroevolutionary analyses when appropriate preliminary tests are performed on a subsample of the data (Shearer *et al.*, 2017; Giacomini *et al.*, 2019). Details on the geometric morphometrics approach are reported in the methodological chapter of this thesis (*Chapter Two*).

Statistical analyses

All statistical analyses in this study were firstly performed under a classic approach (*i.e.*, OLS: ordinary least squares; PLS: partial least squares) and then repeated under a phylogenetic comparative approach (*i.e.*, PGLS: phylogenetic generalised least squares; phylogenetic PLS). In OLS and PGLS analyses, morphological traits (*i.e.*, univariate skull size and multivariate shape) were input as dependent variables and the functional traits (*i.e.*, feeding and sensory parameters, **Table 1**) as independents. I employed a series of pruned trees extracted from the calibrated and ultrametric phylogenetic tree built by Shi and Rabosky (2015), with tips corresponding to the species of my dataset (and sub

datasets). The trees were used to compute the phylogenetic variance-covariance matrices of each dataset employed in PGLS and phylogenetic PLS (Rohlf, 2006, 2007; Adams & Felice, 2014). The analyses were performed using the R packages “geomorph” (Adams & Otárola-Castillo, 2013) and “phytools” (Revell, 2012).

Morphological variation, phylogenetic signal and evolutionary allometry in bat skulls.

PCA was performed on Procrustes shape coordinates in order to visualise the morphological variation in the sample. The 3D model of *Artibeus jamaicensis* was warped on the consensus (*i.e.*, mean shape of the dataset), and the result was subsequently warped on the maximum and minimum shape of the first two PC axes to indicate major morphological variation in the dataset (Klingenberg, 2013). The warped model on the consensus was used as the reference mesh in all the subsequent shape visualizations to facilitate comparisons between the different analyses (see below).

The K statistic of Blomberg *et al.* (2003) was used to test for the presence of a phylogenetic signal in the morphological and functional parameters. The K statistic reflects the degree of congruence between the trait and the phylogeny (Blomberg *et al.*, 2003). Statistical significance of K and its multivariate extension K_{multiv} were assessed using randomization (Adams, 2014). The presence of a significant phylogenetic signal in morphological data confirms the need for phylogenetic comparative methods.

Evolutionary allometry was computed using Procrustes shape coordinates as dependent variables and the \log_{10} transformed centroid size as the independent variable (Cardini & Polly, 2013). The allometry was computed on the complete dataset in order to include most of the size variation and obtain a stable estimate of allometry (Klingenberg, 2016). PGLS analyses were performed to test for the presence of evolutionary allometry after taking the phylogenetic variance-covariance matrix into account (Rohlf, 2007; Adams & Collyer, 2015). Significant allometry (*i.e.*, correlation between shape and size), together with a significant correlation between size and functional traits, dictated the need to take size into

account when testing for relationships between shape and functional traits (Loy *et al.*, 1996). I computed OLS and PGLS models with shape as the dependent variable and each functional trait from **Table 1** as the independent (*i.e.*, shape~trait). I then recomputed the OLS and PGLS models introducing size (*i.e.*, log₁₀ centroid size) and its interaction with the functional trait as additional effects (*i.e.*, shape~size+trait+size:trait). This approach allowed me to control for allometric effect when assessing the relationship between shape and traits (Freckleton, 2009; Adams & Collyer, 2018).

Bat skull morphological variation by ecological groups. OLS and PGLS models were performed to assess the relationship between skull morphology (*i.e.*, size and shape) and ecological groups in bats (*i.e.*, diet category, ability to echolocate, and emission type). The allometric effect was taken into account by adding size and its interaction with the ecological variable as fixed effects. When the main effect of an ecological variable in PGLS was significant, a pairwise post hoc test was performed to assess which ecological groups differed from one another (applicable for ≥ 3 levels only). A Bonferroni-corrected post-hoc test was performed on the first PC of shape under the PGLS model. The reference mesh was warped onto the mean shape of each group (mean shape by group computed from PGLS predicted values of shape regressed on the ecological variable). An UPGMA cluster analysis on the distances between mean shape of groups was used to visualise and better identify differences and similarities in skull shape between ecological groups (see Meloro & O'Higgins, 2011). The UPGMA approach allowed to reconstruct a dendrogram from a pairwise similarity matrix and to show how the ecological groups cluster together.

Drivers of skull evolution in echolocating bats. OLS and PGLS models were performed with centroid size and Procrustes shape coordinates as dependent variables and functional parameters (*i.e.*, bite force, echolocation characteristics and muscle mass; **Table 1**) as the independent. Additionally, I recomputed OLS and PGLS for shape, accounting for evolutionary allometry. This required the introduction of size and its interaction with the

functional trait as main effects, as described above. Furthermore, as different groups can be exposed to different evolutionary pressures, the analyses testing for sensory constraints (*i.e.*, echolocation) were repeated within diet categories (*i.e.*, insectivorous versus other diets).

Shape variation associated to a sensory or feeding trait was visualised by plotting the regression score against the trait. The trait was previously size-corrected and \log_{10} transformed ($\log_{10}\text{corr.Trait}$) in order to remove the shape variation explained by the allometric effect (Blomberg *et al.*, 2003). 3D shape deformation was visualised by applying the Thin-Plate-Spline (TPS) algorithm on the reference mesh (*i.e.*, *A. jamaicensis* 3D model warped on the consensus). The shape predicted values (extracted from the PGLS model: $\text{shape} \sim \log_{10}\text{corr.Trait}$) were used as targets in the TPS algorithm. Specifically, the predicted shapes that showed the minimum and maximum scores for the trait were plotted to visualise shape deformation associated with that trait. (see *Chapter Two* for details).

Functional trade-off in skull shape of insectivorous bats. PLS was used to assess whether evolution of size and shape is influenced by feeding traits (*i.e.*, bite force and skull muscles) and sensory traits (*i.e.*, echolocation parameters) in insectivorous bats ($n = 19$). Functional traits were used in the PLS analyses only after confirming correlation with morphological variables under PGLS models (as computed in the previous section). PLS analysis finds the vector for each block of variables (*e.g.* shape variables and echolocation variables) that maximises block covariation. It does not assume any directionality (*i.e.*, does not assume a block as a dependent variable) and cannot account for interactions. For this reason, functional traits correlating with size were corrected for the centroid size before testing for covariation with shape in PLS analyses (in order to remove allometric effect). Size corrections for each trait were performed using the approach introduced by Blomberg *et al.* (2003) and described in *Chapter Two*. Covariation between variables blocks was quantified using the RV coefficient (Escoufier, 1973). Correction for shared

evolutionary history was applied using the phylogenetic variance-covariance matrix approach implemented in phylogenetic PLS (Adams & Felice, 2014). In addition, I tested for differences in strength of association between morphological-feeding blocks and morphological-sensorial blocks using z-scores (Adams & Collyer, 2016). The reference mesh was warped on the maximum and minimum shapes for the two phylo-PLS (*i.e.*, shape-feeding and shape-echolocation) to visualise shape covariation with feeding and echolocation. The comparison of shape changes that were related to echolocation and feeding provided insights into possible functional trade-offs.

Results

Phylogenetic signal and evolutionary allometry in bat skulls

Most of the morphological variation between the 67 bat species was described by principal components 1 (PC1) and 2 (PC2) (33.35% and 27.02%, respectively) (**Figure 1**). PC1 displayed shape variation related to rostrum length, zygomatic arch length and braincase height (all relative to centroid size), and separated non echolocating species (*i.e.*, Pteropodidae family) from echolocating species. PC2 showed variation mainly related to palatal length (*i.e.*, maxillary and palatine bones) and braincase length, with mouth emitting species displaying a longer palatal length but a shorter braincase with respect to nasal and nasal/mouth emitting species (**Figure 1**).

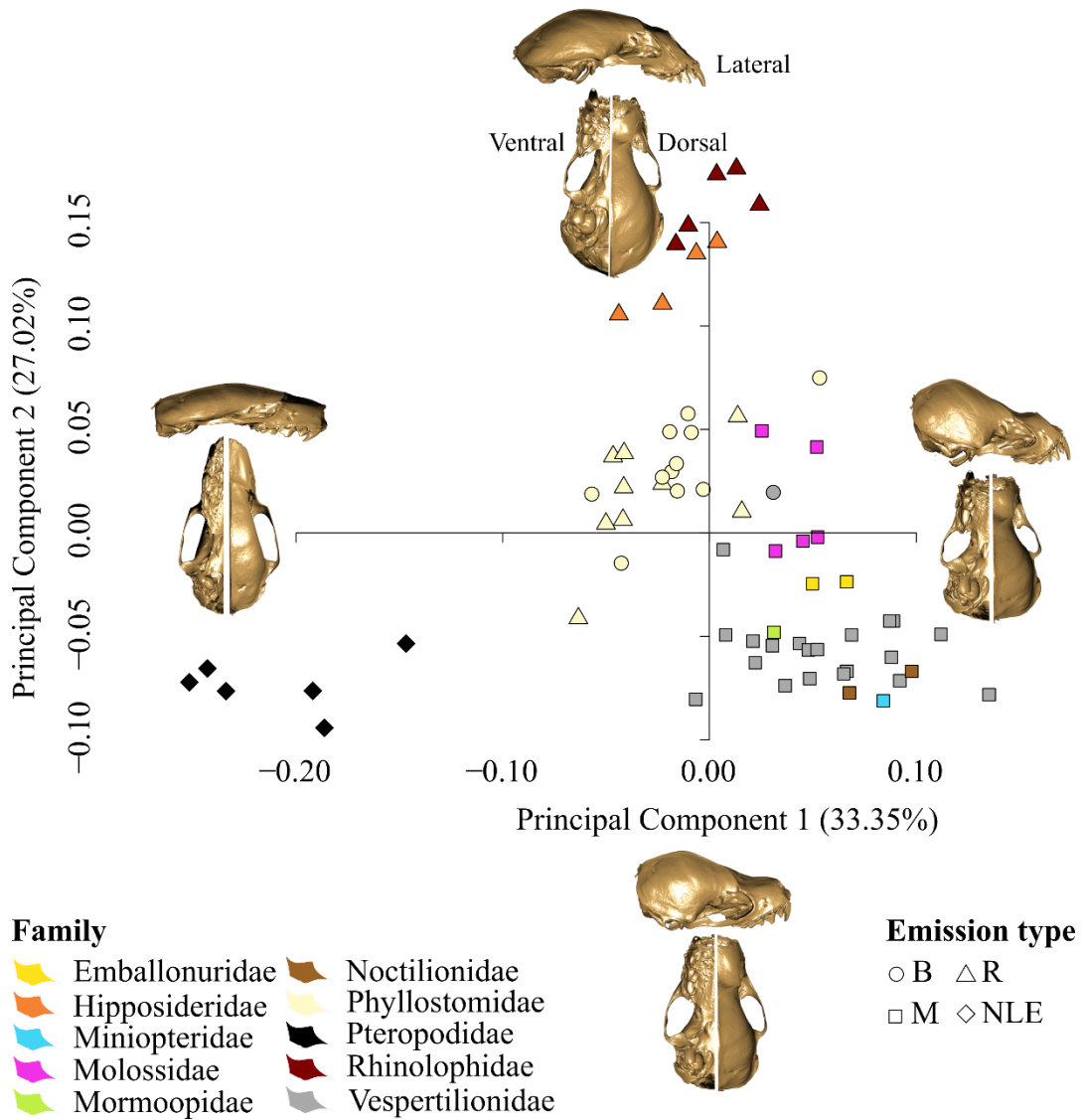


Figure 1. Plot of principal component analysis scores for all species of the complete dataset ($n = 67$), displayed by family and emission type (laryngeal echolocators: both mouth and nasal [B], nasal [R], mouth [M]; non echolocating species, [NLE]). Shape variation was reported on dorsal, ventral and lateral views by warping maximum and minimum PC variation of each axes on the *Artibeus jamaicensis* 3D model.

All morphological and functional parameters showed a significant phylogenetic signal except for the digastric and masseter muscles (**Table 2**). Variables describing feeding function showed a low K value, suggesting that these traits are less similar than would be predicted from their phylogenetic history. In contrast, K and K_{multiv} were high for sensory and morphological variables. A significant phylogenetic signal for morphological variables confirmed that phylogenetic comparative methods were necessary. Evolutionary allometry

was significant under the OLS model ($R^2 = 0.233$, $p = 0.001$). This result was supported by phylogenetic GLS where evolutionary allometry accounted for 10.31% of shape variance ($R^2 = 0.103$, $p = 0.001$).

Table 2. Phylogenetic signal for the morphological and functional traits (*i.e.*, bite force, digastric muscle, masseter muscle, temporalis muscle, pterygoid muscle, start frequency, end frequency, bandwidth, peak frequency, duration, sweep rate). The number of species in each analyses is reported in the first column (n = 67: full dataset; n = 61: laryngeal echolocating species; n = 32: species with muscle data). Significant p-values are in bold.

	n	K	p
Size	67	1.733	0.001
Shape	67	1.255	0.001
Bite force	61	0.865	0.001
Start frequency	61	1.179	0.001
End frequency	61	1.093	0.001
Bandwidth	61	1.217	0.001
Peak frequency	61	1.289	0.001
Duration	61	2.407	0.001
Sweep rate	61	2.042	0.001
Digastric muscle	32	0.396	0.455
Masseter muscle	32	0.585	0.054
Temporalis muscle	32	0.718	0.008
Pterygoid muscle	32	0.665	0.023

Bat skull morphological variation by ecological groups

Bat skull size and shape differed between echolocating and non echolocating groups also after phylogenetic correction (PGLS: for size $R^2 = 0.262$, $p = 0.001$; for shape: $R^2 = 0.110$, $p = 0.001$). When the allometric effect was taken into account, the amount of shape

explained by the ability to echolocate was smaller but still significant ($R^2 = 0.060$, $p = 0.001$; **Table 3** and **S1**). Echolocating species showed smaller skulls than non-echolocating ones. Furthermore, echolocating bats scored high, on PC1 presenting wider but shorter rostra, a taller braincase (*i.e.*, greater distance between basicranium and sagittal crest) and bigger cochlea and tympanic bulla (**Figure 1**).

Size variation explained by diet category was not significant after phylogenetic correction ($p = 0.123$). Nevertheless, diet category explained a major and significant proportion of the overall shape variance under the PGLS model ($R^2 = 0.210$, $p = 0.002$; this proportion was lower when accounting for the interaction with size, $R^2 = 0.181$, $p = 0.001$; **Table 3** and **S1**). This relationship was confirmed even after the exclusion of Pteropodidae from the analyses (PGLS accounting for allometric effect: $n = 61$, $R^2 = 0.204$, $p = 0.004$).

Three main shape nodes resulted from the cluster analyses on the mean shapes of each diet category (mean shapes extracted from PGLS predicted values): insectivorous/vertebrate eater, frugivorous and nectarivorous/hematophagous (**Figure 2**).

Table 3. Size (**A**) and shape (**B**) variance explained by each variable (R^2) and significance (p) for OLS and PGLS models. Sample size (*i.e.*, number of species) is reported in the first column ($n = 67$: full dataset; $n = 61$: echolocating bat only; $n = 32$: echolocating species with muscle data available). Significance of the PGLS models is in bold. The * indicates results for shape variance explained were computed by accounting for evolutionary allometry (\log_{10} centroid size as fixed factor in the model) and for interaction between trait and size (\log_{10} centroid size:trait).

A)	n	Size			
		R ² - OLS	p	R ² - PGLS	p
Echolocation (E)	67	0.539	0.001	0.217	0.001
Diet Category (DC)	67	0.489	0.001	0.193	0.123
Echolocation type (ET)	61	0.167	0.007	0.069	0.117
Bite force (BF)	61	0.673	0.001	0.474	0.001
Start frequency (SF)	61	0.020	0.296	0.145	0.005
End frequency (EF)	61	0.004	0.594	0.207	0.001
Bandwidth (BW)	61	0.004	0.610	0.020	0.278
Peak frequency (FP)	61	0.001	0.793	0.207	0.001
Duration (D)	61	0.016	0.329	0.091	0.017
Sweep rate (SR)	61	0.002	0.753	0.066	0.044
Digastric muscle (DIG)	32	0.594	0.001	0.022	0.423
Masseter muscle (MAS)	32	0.582	0.001	0.380	0.001
Temporalis muscle (TEM)	32	0.721	0.001	0.375	0.001
Pterygoid muscle (PTE)	32	0.602	0.001	0.328	0.001

B)	n	Shape				Shape*			
		R ² -OLS	p	R ² -PGLS	p	R ² -OLS	p	R ² -PGLS	p
E	67	0.2617	0.0010	0.1096	0.001	0.0901	0.001	0.0601	0.001
DC	67	0.3017	0.0010	0.2100	0.002	0.1524	0.001	0.1813	0.001
ET	61	0.3325	0.0010	0.1224	0.001	0.3006	0.001	0.1201	0.001
BF	61	0.0827	0.0010	0.0529	0.001	0.0250	0.086	0.0460	0.002
SF	61	0.0589	0.0030	0.0195	0.267	0.0685	0.002	0.0219	0.113
EF	61	0.1384	0.0010	0.0192	0.311	0.1476	0.001	0.0230	0.103
BW	61	0.0863	0.0010	0.0177	0.359	0.0840	0.001	0.0167	0.308
FP	61	0.1248	0.0010	0.0238	0.135	0.1293	0.001	0.0243	0.085
D	61	0.0910	0.0010	0.0164	0.415	0.0865	0.001	0.0188	0.208
SR	61	0.0947	0.0010	0.0160	0.458	0.0946	0.001	0.0158	0.343
DIG	32	0.0535	0.0790	0.0768	0.016	0.0787	0.016	0.0809	0.008
MAS	32	0.0525	0.1130	0.0648	0.029	0.0787	0.024	0.0750	0.010
TEM	32	0.0692	0.0340	0.0679	0.016	0.1197	0.002	0.0808	0.005
PTE	32	0.0574	0.0680	0.0672	0.014	0.1011	0.002	0.0822	0.005

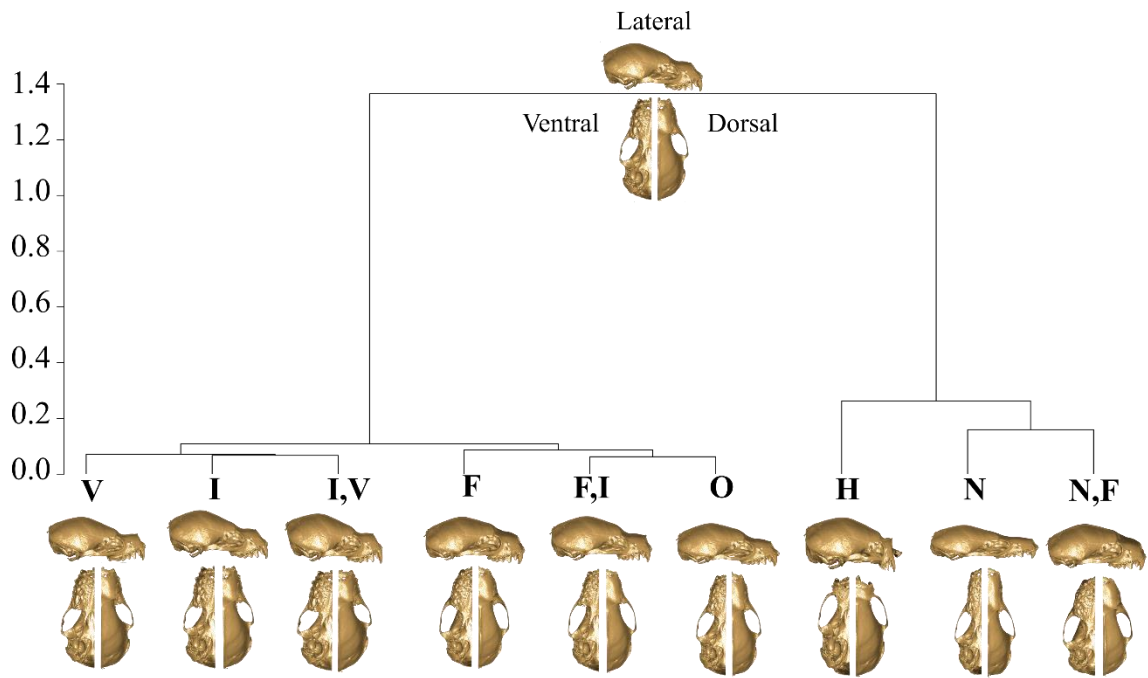


Figure 2. Cluster analysis of mean shape distances for each diet category using PGLS predicted values ($n = 67$). Warpings on the reference mesh showed the differences in shape between diet categories and mean shape (on the top) on lateral, ventral and dorsal view. Diet categories: V = vertebrate eater; I = insectivorous; I,V = insect and vertebrate eater; F = frugivorous; F,I = frugi/insectivorous; O = omnivorous; H = hematophagous; N = Nectarivorous; N,F = necta/fruigivorous.

Nectarivorous and hematophagous species displayed the most divergent skull shapes, with a long and narrow rostrum for the former and a short and wide rostrum for the latter.

Insectivorous/vertebrate eaters presented wider skulls, a taller occipital bone and a shorter rostrum compared to the frugivorous group (**Figure 2**). Almost 30% of shape variation of the 67 species along PC1 was represented by diet category ($R^2 = 0.288$, $p = 0.016$).

Pairwise post-hoc tests were performed on PC1, excluding diet categories with less than two observations (*i.e.*, hematophagous, nectarivorous, necta/frugivorous). Frugivorous species significantly differed in shape from vertebrates eaters ($p = 0.045$), insectivores ($p = 0.015$) and insect/vertebrate eaters ($p = 0.030$) but not from omnivores ($p = 0.999$) or fruit/insect eaters ($p = 0.705$).

The size variation among echolocating species that was explained by emission type was not significant after phylogenetic correction ($p = 0.117$). Nevertheless, emission type significantly explained shape variation in echolocating bats (PGLS accounting for allometric effect: $n = 61$, $R^2 = 0.120$, $p = 0.001$; **Table 3** and **S1**). In particular, mouth emitters showed a wider skull, shorter but taller braincase, and wider and longer palate compared to other emitting types. Furthermore, nasal emitters differed from nasal/mouth emitters presenting a relatively smaller tympanic bulla, longer rostrum and lower occipital bone (**Figure 3**). Over 50% of shape variation in the echolocating species ($n = 61$) along PC1 was represented by emission type ($R^2 = 0.539$, $p = 0.001$). The post-hoc test for emission type showed that only mouth emitters significantly differed from nasal and nasal/mouth emitters ($p = 0.003$ and $p = 0.012$; respectively).

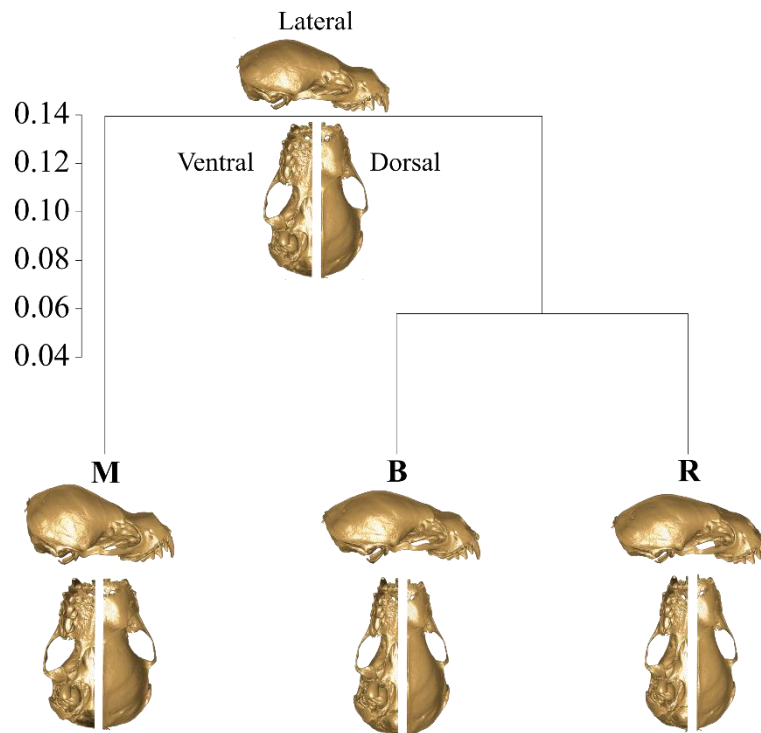


Figure 3. Cluster analyses of mean shape distances for each echolocation type (mouth, [M]; mouth and nose, [B]; nose, [R]) using predicted values from PGLS ($n = 61$). Warpings showed the differences in shape between echolocation types and mean shape (on the top) on lateral, ventral and dorsal view.

Drivers of skull evolution in echolocating bats

Skull size of echolocating bats was strongly and significantly associated with both feeding and sensory traits even after phylogenetic correction (**Table 3**). Variance explained by bite force and muscles (except for the digastric muscle) ranged from 32.8% to 47.7% of total size variance under the PGLS model. Species with bigger heads presented stronger bite forces (PGLS β coefficient = 0.380) and heavier masticatory muscles (PGLS β coefficient for masseter = 0.390, temporalis = 0.380, pterygoid = 0.422).

Less strong, but still significant, was the association between echolocation parameters (except for bandwidth) and skull size: variance explained by echolocation characteristics under PGLS models ranged from 6.6% to 20.7% of the overall size variance. Species with bigger heads had lower start frequency, end frequency, peak frequencies and shorter sweep rate (PGLS β coefficient = -0.540, -0.681, -0.716, -0.105; respectively) but longer call duration (PGLS β coefficient = 0.221).

After accounting for allometric effects and phylogenetic relatedness, shape correlated significantly with feeding parameters only (with variance explained ranging from 8.2% to 4.6% of total shape variation in PGLS models). In particular, species with a more powerful bite force showed a relatively longer and taller braincase, a lower occipital bone, and a shorter rostrum (warping on PGLS predicted values for minimum and maximum size-corrected bite force in **Figure 4A**). Similarly, species with heavier muscles showed wider skull, a shorter braincase and longer and wider zygomatic arch (**Figure 4B** for temporalis muscle; similar behaviour was displayed by the other muscles).

Sensory traits did not significantly correlate with shape after accounting for phylogenetic relatedness. Nevertheless, when the analyses were repeated within insectivorous bats ($n = 43$), the sensory parameters peak frequency, end frequency and start frequency were found to significantly correlate with shape (explaining from 4.4% to 5.8% of shape variance

under PGLS models accounting for allometric effects, **Table S1**). Insectivorous species emitting high frequencies showed a longer braincase and a narrower and shorter palate and rostrum (**Figure 4C** for peak frequency, a similar pattern was identified for end frequency and start frequency).

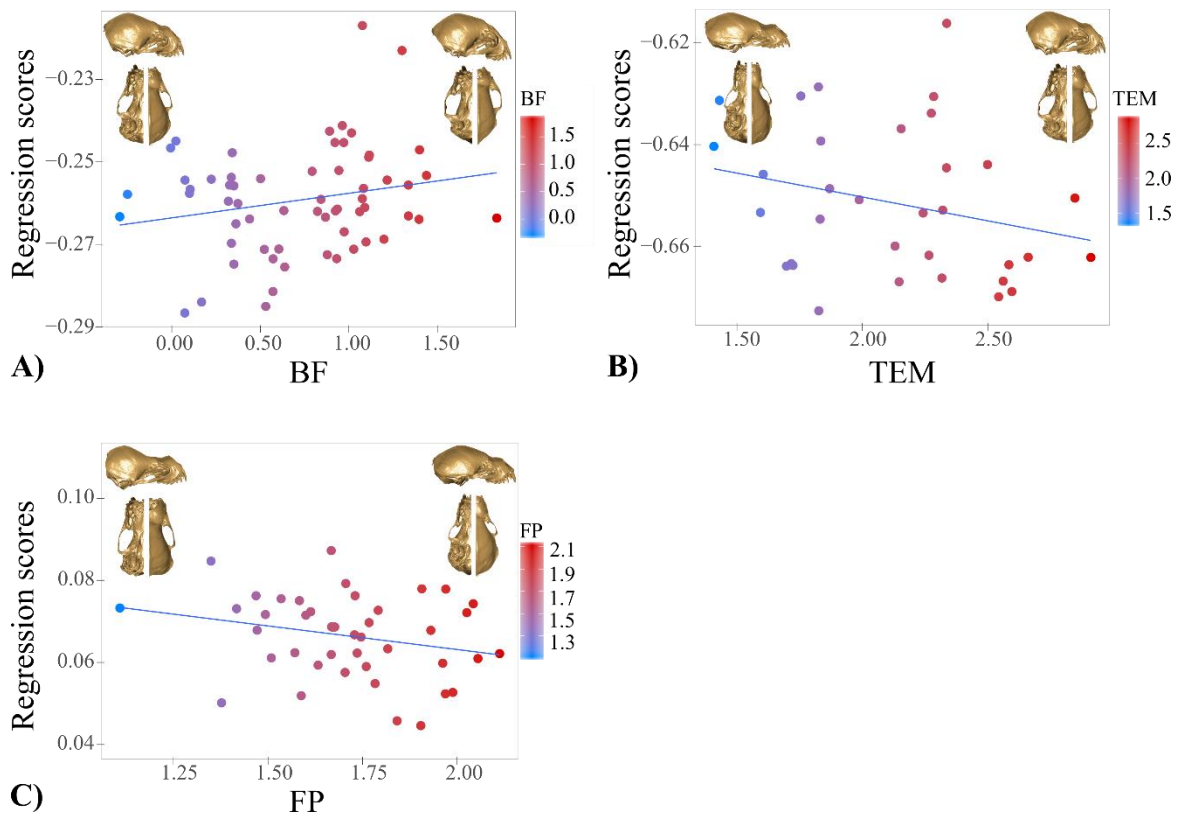


Figure 4. Plot of shape (as regression scores) and functional traits (as size-corrected and \log_{10} transformed; Blomberg *et al.*, 2003). **A:** bite force ($n = 61$, [BF]), **B:** temporalis muscle - as a muscle example ($n = 32$, [TEM]), **C:** peak frequency - as an example for echolocation characteristics ($n = 43$, [FP]). The colour gradient from blue to red defines increasing values of the trait. Skull warpings show the shape variation related to the minimum (left) and maximum (right) values for the functional parameters. 3D differences were magnified three times for bite force warpings, and two times for peak frequency and temporalis muscle warpings in order to facilitate interpretation of shape deformations.

Functional trade-off in skull shape of insectivorous bats

In accordance with the PGLS results for size, a phylogenetic PLS of functional parameters for insectivorous bats ($n = 19$) showed a strong covariation between size and both feeding (*i.e.*, bite force and muscles; digastric muscle excluded) and sensory (*i.e.*, echolocation; bandwidth excluded) groups of variables (R-PLS = 0.809, $p = 0.001$; R-PLS = 0.744, $p = 0.004$; respectively). Similarly, the phylo-PLS for shape of insectivorous bats showed strong correlation with all size-corrected feeding variables (R-PLS = 0.868, $p = 0.002$), but only size-corrected sensory variables start frequency, end frequency and peak frequency were correlated with shape (R-PLS = 0.741, $p = 0.022$).

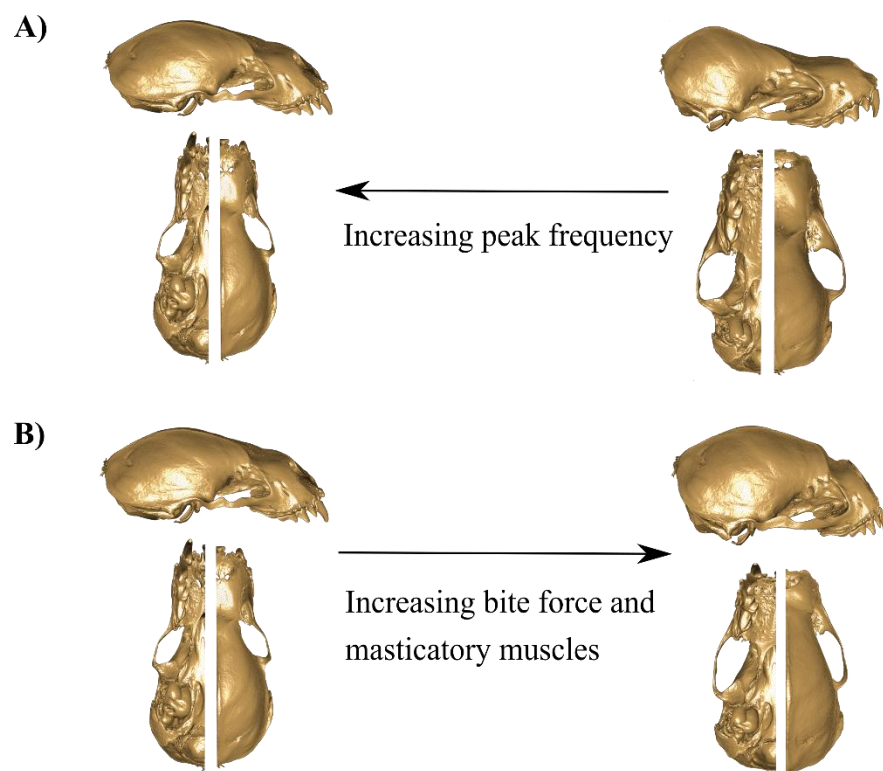


Figure 5. Skull warping representing phylo-PLS maximum and minimum deformation for shape related to functional traits (size-corrected and \log_{10} transformed). **A)** Shape deformation related to covariation with sensory variables (*i.e.*, frequency, end frequency and peak frequency); **B)** shape deformation related to covariation with feeding variables (*i.e.*, bite force and muscles). No magnification of shape differences was applied.

When assessing association strengths between phylo-PLSs (*i.e.*, two for size and two for shape, separately), associations of size with the feeding variables were stronger than those for sensory variables (effect-size: 3.688, 2.731; respectively). Nevertheless, this difference in magnitude was not statistically significant ($p = 0.221$). Similar results were found for the strength of associations between shape and functional variables (effect-size of feeding variables: 3.006; sensory variables: 2.027; $p = 0.210$).

The model warping on the phylo-PLS extreme for shape axis showed a congruent pattern to PGLS results presented in the previous section with a larger sample size (**Figure 5**). In particular, bats emitting high frequencies displayed a short rostrum, a short and narrow palate, and an increase in the length and a decrease in the height of the braincase (**Figure 5A**). Furthermore, species with higher muscle and bite force scores displayed a shorter and wider rostrum, and a taller skull (in particular brain case) (**Figure 5B**).

Discussion

In this study, I identified an association between skull shape and echolocation call parameters in insectivorous bats. Echolocation and feeding functions appear to constrain the same skull shape characteristics (*i.e.*, rostrum length) in insect-eating species indicating a possible functional trade-off. Interestingly, there was no evidence of skull shape adaptation to echolocation call parameters in species that echolocate but do not use echolocation for detection and pursuit of rapidly moving prey.

Skull morphology and bat ecological groups

This study shows that echolocating species have smaller skulls, suggesting an evolutionary constraint may be linked to laryngeal echolocation. Both flight and laryngeal echolocation

are considered energetically demanding activities, although echolocation represents a small proportion of this cost as sound emission is coupled to the wing stroke cycle (Voigt & Lewanzik, 2012). Thus, echolocation is unlikely to represent a limit *per se* on skull size in bats. On the contrary, laryngeal echolocation could have developed as a solution to small body size (and not *vice versa*). Thiagavel *et al.* (2018) recently suggested that eye size in small skulls is spatially constrained. Consequently, vision as a primary sensory strategy might not be a suitable evolutionary strategy for nocturnal predation. The general advantages that drive species towards reduced body size remain rather unclear (Blanckenhorn, 2000).

The results showed that bigger cochlea and tympanic bulla are common morphological traits found in all echolocating bats, supporting the idea that the cochlea hypertrophy is linked to laryngeal echolocation ability (Simmons *et al.*, 2008). In fact, cochlea size is known to scale with the vestibular system and to correlate with canal morphologies, which differentiate echolocating from non echolocating bats (Davies *et al.*, 2013a). I also found that echolocating bats show taller braincases, which might represent the need to accommodate a brain with different spatial constraints from non echolocating bats. For example, echolocating bats display larger auditory nuclei than non echolocating (Hutcheon *et al.*, 2002), even though their relative brain size is smaller (Jones & MacLarnon, 2004; Thiagavel *et al.*, 2018).

Within echolocating bats, mouth emitters significantly differed in shape from nasal and nasal/mouth emitters. Nasal emission is an innovation in bat skull morphology and implies deep cranial rearrangements (Pedersen, 2000). The shorter and narrower palate, together with the increased length and decreased height of the braincase seems to be connected to shape rearrangements due to the nasal emission (and nasal/mouth emission). Cochlear features (*i.e.*, basilar membrane length and number of cochlea turns) correlate with species-specific hearing limits (*i.e.*, maximum KHz audible by a bat species) and echolocation characteristics (Davies *et al.*, 2013b). Therefore, the differences in cochlea and tympanic

bullae relative size between oral and nasal emitters might indicate hearing specialization to a certain acoustic range.

Skull morphology and functional parameters in echolocating bats

Shape differences between diet categories confirmed what has been previously suggested in the literature: diet is an important driver of skull shape diversification in bats (Freeman, 1998; Nogueira *et al.*, 2005; Herrel *et al.*, 2008; Santana *et al.*, 2010, 2012, among others). Dumont *et al.* (2014) identified three cranial optima in the New World leaf-nosed bats (Phyllostomidae family) linked to different mechanical advantages: 1) nectarivorous, 2) insectivores, omnivores and some frugivorous, 3) bats specialised on hard fruits. In this dataset, I did not include species specialised on hard fruits such as *Ametrida centurio* (Gray, 1847), *Centurio senex* (Gray, 1842), or *Sphaeronycteris toxophyllum* (Peters, 1882), which show a much shorter and wider rostrum compared to other fruit eating species. Nevertheless, I identified two main clusters of diets: 1) carnivorous and frugivorous bats, and 2) nectarivorous/hematophagous bats. Nectarivorous species are known to display a highly specialised skull with long rostra and palates to support long tongue (Freeman, 1995; Nogueira *et al.*, 2009). Insectivorous/vertebrate eaters showed a shorter rostrum and taller braincase, providing higher resistance to torsion and wider area for muscle attachment compared to nectarivorous species. Vertebrate eaters are known to generally possess a long rostrum to generate wider gape angles (*i.e.*, so that bigger prey can be taken) and faster jaw closing (Santana & Cheung, 2016). In accordance with previous studies, frugivorous species presented moderately longer rostra due to diet flexibility (Freeman, 1998): many of the species we believed to be fruit eaters occasionally feed on nectar too (Lobova *et al.*, 2009). The hematophagous species *Desmodus rotundus* (Geoffroy, 1810) represents an exception to the general “form to function” relationship in bats. This species has a weak bite force, despite presenting a short rostrum and high braincase. *D. rotundus*

feeds on liquid material: sharp teeth allow for cutting the skin while the highly moveable tongue licks the blood (Greenhall, 1972). A shorter rostrum, together with a compact skull, might allow for greater movement coordination during feeding on active and live prey.

Insectivorous species showed an increase in braincase height, thereby providing a bigger area for muscle attachment and allowing generation of greater bite force. This may be less important for insectivorous species that feed on soft prey such as moths. In this case, it is likely that skull shape is also influenced by other non-dietary factors. Safi & Dechmann (2005) showed that the relative size of brain regions associated with hearing and spatial memory are correlated with habitat complexity in echolocating bats. As skull shape and brain accommodate to one another other during developmental stages (Richtsmeier & Flaherty, 2013), shape of the braincase might be indirectly adapted to habitat complexity.

Despite some exceptions (Jacobs *et al.*, 2007), allometry of peak frequency is an established pattern in some families of insectivorous bats (Jones, 1999; Thiagavel *et al.*, 2017; Jacobs & Bastian, 2018). Species with bigger body size and, hence, longer vocal folds produce lower frequencies. This is the first study that analysed the relationship between skull size and echolocation call parameters in a wide taxonomic context under phylogenetic comparative methods. In this study, I obtained new evidence for allometric scaling of phylogenetic independent echolocation characteristics in all sensory parameters (except bandwidth) across 10 families of bats. I also found that functional parameters describing both feeding (*i.e.*, bite force and muscles) and sensory traits (*i.e.*, echolocation parameters) evolutionarily correlate with skull shape in insectivorous bats (even if predicting only a relatively small portion of the overall shape variance). This suggests that insect eaters were exposed to selective pressures linked not only to feeding function but also to echolocation.

My results also support Thiagavel *et al.*'s (2018) hypothesis on the retention of a trade-off between vision and echolocation in extant species. Nectar, fruit, blood and vertebrate

eating species use vision and smell in combination with echolocation to detect and locate food items (Bahlman & Kelt, 2007; Surlykke *et al.*, 2013; Ripperger *et al.*, 2019). These species share a similar hunting ecology: they hunt static food items in cluttered environments through a passive or active gleaning mode (Denzinger & Schnitzler, 2013). In contrast, insectivorous bats have evolved the use of echolocation as their main sensory system for prey detection and pursuit of rapidly-moving prey. This might explain why only insectivorous bats display a significant association between skull shape and echolocation. The taxonomic coverage within this study did not allow me to treat nectarivorous, frugivorous, hematophagous and vertebrate-eating species as independent groups; instead, they were treated as one group (*i.e.*, non-insectivorous species). In future studies, these diet categories should be analysed independently to fully investigate the hypothesis that skull shape of insectivorous species underwent a stronger selective pressure linked to echolocation compared to non-insect eating bats.

My results also suggest that bat skull shape may play a role in sound propagation not only in Rhinolophidae and Hipposideridae bats (where the nasal chambers behave as a resonance structure) but in other insectivorous species too. It is unlikely, however, that the oral cavity of mouth-emitting species behaves as a resonance chamber: the size of the aperture is too large for sound to be retained inside the cavity to create a resonance effect. Echolocation call structure underwent strong selection due to ecological constraints. In other words, different call types define specialization to different environments (*i.e.*, open, edge, clutter habitats) (Jones, 1999; Schnitzler & Kalko, 2001). The sample size in this study did not allow testing for morphological differences related to call structures (*i.e.*, different combinations of frequency modulation and constant frequency, Jones & Teeling, 2006) within insectivorous species. However, I hypothesise that species with different call structures may present different slopes of association between echolocation parameters (in particular peak frequency) and shape. This is supported by the fact that multiharmonic

frequency modulated calls are believed to be more rudimentary, and species producing this type of call display improved visual ability, possibly even within insectivorous bats (*e.g. Micronycteris* genus) (Thiagavel *et al.*, 2018). Furthermore, species emitting constant frequencies (mainly from the nose) may present a stronger relationship between skull shape and peak frequency given that their nasal chamber has a resonance function (Armstrong & Coles, 2007; Jacobs *et al.*, 2014).

Evolutionary trade-off in insectivorous bats

The strength of the associations in the phylo-PLS suggested that feeding and sensory functions are equally important in driving skull evolution in insectivorous bats (for both size and shape). In contrast, Jacobs *et al.* (2014) found that the resting frequency explains a greater proportion of shape variance compared to bite force suggesting that the pattern might differ between bat families.

My results also suggest that insectivorous bats present a possible trade-off between feeding and sensory functions with respect to the length of the rostrum. Species with a shorter rostrum tend to display relatively larger muscles and bite forces but higher echolocation frequencies. Higher bite forces and larger muscles are functionally advantageous as they allow for the possible consumption of a wider range of prey (Aguirre *et al.*, 2003). On the other hand, whether high frequencies are disadvantageous is debatable, questioning the idea of a trade-off between biting and echolocation. A known disadvantage of high frequencies is the range of their effectiveness: atmospheric attenuation is severe, allowing detectability in the short-field only (Lawrence & Simmons, 1982). Species emitting low frequencies have a long-field resolution, but their bite force is weaker and their long rostrum is less resistant to torsion. Higher frequencies might promote niche specialization allowing for the detection of smaller prey: the wavelength of the sound emitted has to be shorter than the circumference of the object in order to produce strong echoes (Pye, 1993;

Jones, 1999). Species emitting very low frequency calls are potentially unable to detect small prey (Barclay, 1986; Barclay & Brigham, 1991; Safi & Siemers, 2010). It is argued, however, that most bats use frequencies three or more times higher than necessary to detect the smallest prey in their diet (Jakobsen *et al.*, 2013). Furthermore, higher frequencies allow for higher beam directionality, which maximises the effectiveness of the echoes in the focal area and “isolates” echoes from the periphery (Surlykke *et al.*, 2009). Thus, while beam directionality and detectability of smaller prey appear to be potential advantages in niche exploitation, the potential disadvantage is atmospheric attenuation. Studies aiming to understand why high frequencies evolved and the associated advantages and disadvantages are likely to provide further insights on the existence of a trade-off between biting and echolocation in insectivorous bats.

The results presented in this study are based on a relatively small sample (19 species) and should be intended as the first preliminary attempt to study the relationship between skull shape and echolocation. Studies on taxonomically more diverse sample are needed to confirm the general pattern (*i.e.*, short rostrum for high frequencies) and to assess potentially different associations between families or ecological groups (*e.g.* nasal and oral emitters). Further investigation on a functional trade-off between feeding and echolocation will be possible only when additional datasets on bite force and masticatory muscles become available.

In conclusion, skull diversification among bat families is mainly driven by sound emission type and broad diet preferences. Echolocation parameters are associated with skull shape in insectivorous species only, suggesting that insectivores underwent a stronger selection due to the preferential use of echolocation as sensory system. Both emitted frequency and bite force influence the rostrum length, suggesting a possible trade-off between echolocation and feeding functions.

References

- Adams, D.C. 2014. A Generalized K Statistic for Estimating Phylogenetic Signal from Shape and Other High-Dimensional Multivariate Data. *Syst. Biol.* **63**: 685–697.
- Adams, D.C. & Collyer, M.L. 2016. On the comparison of the strength of morphological integration across morphometric datasets. *Evolution (N. Y.)*. **70**: 2623–2631.
- Adams, D.C. & Collyer, M.L. 2015. Permutation tests for phylogenetic comparative analyses of high-dimensional shape data: What you shuffle matters. *Evolution (N. Y.)*. **69**: 823–829.
- Adams, D.C. & Collyer, M.L. 2018. Phylogenetic ANOVA: Group-clade aggregation, biological challenges, and a refined permutation procedure. *Evolution (N. Y.)*. **72**: 1204–1215.
- Adams, D.C. & Felice, R.N. 2014. Assessing Trait Covariation and Morphological Integration on Phylogenies Using Evolutionary Covariance Matrices. *PLoS One* **9**: e94335.
- Adams, D.C. & Otárola-Castillo, E. 2013. geomorph: an r package for the collection and analysis of geometric morphometric shape data. *Methods Ecol. Evol.* **4**: 393–399.
- Aguirre, L.F., Herrel, A., van Damme, R. & Matthysen, E. 2002. Ecomorphological analysis of trophic niche partitioning in a tropical savannah bat community. *Proc. R. Soc. London. Ser. B Biol. Sci.* **269**: 1271–1278.
- Aguirre, L.F., Herrel, A., Van Damme, R. & MatThysen, E. 2003. The implications of food hardness for diet in bats. *Funct. Ecol.* **17**: 201–212.
- Arbour, J.H., Curtis, A.A. & Santana, S.E. 2019. Signatures of echolocation and dietary ecology in the adaptive evolution of skull shape in bats. *Nat. Commun.* **10**: 2036.
- Armstrong, K.N. & Coles, R.B. 2007. Echolocation Call Frequency Differences Between Geographic Isolates of *Rhinonicteris Aurantia* (Chiroptera: Hipposideridae): Implications of Nasal Chamber Size. *J. Mammal.* **88**: 94–104.
- Bahlman, J.W. & Kelt, D.A. 2007. Use of Olfaction During Prey Location by the Common Vampire Bat (*Desmodus rotundus*)1. *Biotropica* **39**: 147–149.
- Barclay, R.M.R. 1986. The echolocation calls of hoary (*Lasiurus cinereus*) and silver-haired (*Lasionycteris noctivagans*) bats as adaptations for long- versus short-range foraging strategies and the consequences for prey selection. *Can. J. Zool.* **64**: 2700–2705.
- Barclay, R.M.R. & Brigham, R.M. 1991. Prey detection, dietary niche breadth, and body size in bats: why are aerial insectivorous bats so small? *Am. Soc. Nat.* **137**: 693–703.
- Blanckenhorn, W.U. 2000. The Evolution of Body Size: What Keeps Organisms Small? *Q. Rev. Biol.* **75**: 385–407.
- Blomberg, S.P., Garland, T. & Ives, A.R. 2003. Testing for phylogenetic signal in comparative data: behavioral traits are more labile. *Evolution (N. Y.)*. **57**: 717–745.
- Blomberg, S.P., Lefevre, J.G., Wells, J.A. & Waterhouse, M. 2012. Independent Contrasts and PGLS Regression Estimators Are Equivalent. *Syst. Biol.* **61**: 382–391.
- Cardini, A. 2019. Craniofacial allometry is a rule in evolutionary radiations of placentals. *bioRxiv* 513754.

- Cardini, A., Jansson, A.-U. & Elton, S. 2007. A geometric morphometric approach to the study of ecogeographical and clinal variation in vervet monkeys. *J. Biogeogr.* **34**: 1663–1678.
- Cardini, A. & Polly, P.D. 2013. Larger mammals have longer faces because of size-related constraints on skull form. *Nat. Commun.* **4**: 2458.
- Davies, K.T.J., Bates, P.J.J., Maryanto, I., Cotton, J.A. & Rossiter, S.J. 2013a. The Evolution of Bat Vestibular Systems in the Face of Potential Antagonistic Selection Pressures for Flight and Echolocation. *PLoS One* **8**: 8–10.
- Davies, K.T.J., Maryanto, I. & Rossiter, S.J. 2013b. Evolutionary origins of ultrasonic hearing and laryngeal echolocation in bats inferred from morphological analyses of the inner ear. *Front. Zool.* **10**: 2.
- Denzinger, A. & Schnitzler, H. 2013. Bat guilds , a concept to classify the highly diverse foraging and echolocation behaviors of microchiropteran bats. *Front. Zool.* **4**: 1–15.
- Dumont, E.R., Samadevam, K., Grosse, I., Warsi, O.M., Baird, B. & Davalos, L.M. 2014. Selection for mechanical advantage underlines multiple cranial optima in the new world leaf-nosed bat. *Evolution (N. Y.)* **68**: 1436–1449.
- Elemans, C.P.H., Mead, A.F., Jakobsen, L. & Ratcliffe, J.M. 2011. Superfast Muscles Set Maximum Call Rate in Echolocating Bats. *Science* **333**: 1885 LP – 1888.
- Escoufier, Y. 1973. Le Traitement des Variables Vectorielles. *Biometrics* **29**: 751:760.
- Freckleton, R.P. 2009. The seven deadly sins of comparative analysis. *J. Evol. Biol.* **22**: 1367–1375.
- Freeman, P.W. 1998. Form, function, and evolution in skulls and teeth of bats. In: *Bat Biology and Conservation* (T. H. Kunz & P. A. Racey, eds), pp. 140–156. Smithsonian Institution Press, Washington.
- Freeman, P.W. 1995. Nectarivorous feeding mechanisms in bats. *Biol. J. Linn. Soc.* **56**: 439–463.
- Giacomini, G., Scaravelli, D., Herrel, A., Veneziano, A., Russo, D. & Brown, R.P. 2019. 3D photogrammetry of bat skulls: perspectives for macro-evolutionary analyses. *J. Evol. Biol.* **in press**.
- Goudy-Trainor, A. & Freeman, P.W. 2002. Call Parameters and Facial Features in Bats: A Surprising Failure of form Following Function. *Acta Chiropterologica* **4**: 1–16.
- Greenhall, A.M. 1972. The biting and feeding habits of the Vampire bat, *Desmodus rotundus*. *J. Zool.* **168**: 451–461.
- Hedrick, B.P. & Dumont, E.R. 2018. Putting the leaf-nosed bats in context: a geometric morphometric analysis of three of the largest families of bats. *J. Mammal.* **99**: 1042–1054.
- Herrel, A., De Smet, A., Aguirre, L.F. & Aerts, P. 2008. Morphological and mechanical determinants of bite force in bats: do muscles matter? *J. Exp. Biol.* **211**: 86–91.
- Hutcheon, J.M., Kirsch, J.A.W. & Garland Jr, T. 2002. A Comparative Analysis of Brain Size in Relation to Foraging Ecology and Phylogeny in the Chiroptera. *Brain. Behav. Evol.* **60**: 165–180.
- Jacobs, D.S., Barclay, R.M.R. & Walker, M.H. 2007. The allometry of echolocation call frequencies of insectivorous bats: why do some species deviate from the pattern? *Oecologia* **152**: 583–594.

- Jacobs, D.S. & Bastian, A. 2018. High Duty Cycle Echolocation May Constrain the Evolution of Diversity within Horseshoe Bats (Family: Rhinolophidae). *Diversity* 10: 85.
- Jacobs, D.S., Bastian, A. & Bam, L. 2014. The influence of feeding on the evolution of sensory signals: A comparative test of an evolutionary trade-off between masticatory and sensory functions of skulls in southern African Horseshoe bats (Rhinolophidae). *J. Evol. Biol.* **27**: 2829–2840.
- Jakobsen, L., Brinkløv, S. & Surlykke, A. 2013. Intensity and directionality of bat echolocation signals. *Front. Physiol.* **4**: 89.
- Jakobsen, L., Hallam, J., Moss, C.F. & Hedenström, A. 2018. Directionality of nose-emitted echolocation calls from bats without a nose leaf (*Plecotus auritus*). *J. Exp. Biol.* **221**.
- Jakobsen, L., Ratcliffe, J.M. & Surlykke, A. 2012. Convergent acoustic field of view in echolocating bats. *Nature* **493**: 93.
- Janis, C.M. 1990. Correlation of Cranial and Dental Variables with Dietary Preferences in Mammals: A Comparison of Macropodoids and Ungulates. *Mem. Queensl. Museum.* **28**: 349–366.
- Jones, G. 1997. Acoustic signals and speciation: the roles of natural and sexual selection in the evolution of cryptic species. *Adv. Study Behav.* **26**: 317:354.
- Jones, G. 1999. Scaling of echolocation call parameters in bats. *J. Exp. Biol.* **202**: 3359–3367.
- Jones, G. & Siemers, B.M. 2011. The communicative potential of bat echolocation pulses. *J. Comp. Physiol. A* **197**: 447–457.
- Jones, G. & Teeling, E. 2006. The evolution of echolocation in bats. *Trends Ecol. Evol.* **21**: 149–156.
- Jones, K.E. & MacLarnon, A.M. 2004. Affording Larger Brains: Testing Hypotheses of Mammalian Brain Evolution on Bats. *Am. Nat.* **164**: E20–E31.
- Klingenberg, C.P. 2016. Size, shape, and form: concepts of allometry in geometric morphometrics. *Dev. Genes Evol.* **226**: 113–137.
- Klingenberg, C.P. 2013. Visualizations in geometric morphometrics: how to read and how to make graphs showing shape changes. *Hystrix, Ital. J. Mammal.* **24**: 15–24.
- Lawrence, B.D. & Simmons, J.A. 1982. Measurements of atmospheric attenuation at ultrasonic frequencies and the significance for echolocation by bats. *J. Acoust. Soc. Am.* **71**: 585–590.
- Lobova, T.A., Geiselman, C.K. & Mori, S.A. 2009. Seed Dispersal by Bats in the Neotropics, 1st ed. New York Botanical Garden, New York.
- Loy, A., Cataudella, S. & Corti, M. 1996. Shape Changes during the Growth of the Sea Bass, *Dicentrarchus labrax* (Teleostea: Perciformes), in Relation to Different Rearing Conditions BT - Advances in Morphometrics. In: (L. F. Marcus, M. Corti, A. Loy, G. J. P. Naylor, & D. E. Slice, eds), pp. 399–405. Springer US, Boston, MA.
- Meloro, C. & O’Higgins, P. 2011. Ecological Adaptations of Mandibular Form in Fissiped Carnivora. *J. Mamm. Evol.* **18**: 185–200.
- Nogueira, M.R., Monteiro, L.R., Peracchi, A.L. & de Araújo, A.F.B. 2005. Ecomorphological analysis of the masticatory apparatus in the seed-eating bats, genus *Chiroderma* (Chiroptera: Phyllostomidae). *J. Zool.* **266**: 355–364.

- Nogueira, M.R., Peracchi, A.L. & Monteiro, L.R. 2009. Morphological correlates of bite force and diet in the skull and mandible of phyllostomid bats. *Funct. Ecol.* **23**: 715–723.
- Pedersen, S.C. 1998. Morphometric Analysis of the Chiropteran Skull with Regard to Mode of Echolocation. *J. Mammal.* **79**: 91–103.
- Pedersen, S.C. 2000. Skull growth and the acoustical axis of the head in bats. In: *Ontogeny, functional ecology, and evolution of bats* (R. A. Adams & S. C. Pedersen, eds), p. 174:213. Cambridge University Press, New York.
- Pye, J.D. 1993. Is fidelity futile? The “true” signal is illusory, especially with ultrasound. *Bioacoustics* **4**: 271–286.
- Revell, L.J. 2012. phytools: an R package for phylogenetic comparative biology (and other things). *Methods Ecol. Evol.* **3**: 217–223.
- Richtsmeier, J.T. & Flaherty, K. 2013. Hand in glove: brain and skull in development and dysmorphogenesis. *Acta Neuropathol.* **125**: 469–489.
- Ripperger, S.P., Rehse, S., Wacker, S., Kalko, E., Schulz, S., Rodriguez-Herrera, B., *et al.* 2019. Nocturnal scent in a “bird-fig”: a cue to attract bats as additional dispersers? *bioRxiv* 418970.
- Rohlf, F.J. 2006. A Comment on Phylogenetic Correction. *Evolution (N. Y.)* **60**: 1509–1515.
- Rohlf, F.J. 2007. Comparative methods for the analysis of continuous variables: geometric interpretations. *Evolution (N. Y.)* **55**: 2143–2160.
- Safi, K. & Dechmann, D.K.N. 2005. Adaptation of brain regions to habitat complexity: a comparative analysis in bats (Chiroptera). *Proc. R. Soc. B Biol. Sci.* **272**: 179–186.
- Safi, K. & Siemers, B.M. 2010. Implications of sensory ecology for species coexistence: biased perception links predator diversity to prey size distribution. *Evol. Ecol.* **24**: 703–713.
- Santana, S.E. & Cheung, E. 2016. Go big or go fish: morphological specializations in carnivorous bats. *Proc. R. Soc. B Biol. Sci.* **283**: 20160615.
- Santana, S.E., Dumont, E.R. & Davis, J.L. 2010. Mechanics of bite force production and its relationship to diet in bats. *Funct. Ecol.* **24**: 776–784.
- Santana, S.E., Grosse, I.R. & Dumont, E.R. 2012. Dietary hardness, loading behavior, and the evolution of skull form in bats. *Evolution (N. Y.)* **66**: 2587–2598.
- Schnitzler, H.-U. & Kalko, E.K. V. 2001. Echolocation by Insect-Eating Bats. *Bioscience* **51**: 557–569.
- Seibert, A.-M., Koblitz, J.C., Denzinger, A. & Schnitzler, H.-U. 2015. Bidirectional Echolocation in the Bat *Barbastella barbastellus*: Different Signals of Low Source Level Are Emitted Upward through the Nose and Downward through the Mouth. *PLoS One* **10**: e0135590.
- Senawi, J., Schmieder, D., Siemers, B. & Kingston, T. 2015. Beyond size – morphological predictors of bite force in a diverse insectivorous bat assemblage from Malaysia. *Funct. Ecol.* **29**: 1411–1420.
- Shearer, B.M., Cooke, S.B., Halenar, L.B., Reber, S.L., Plummer, J.E., Delson, E., *et al.* 2017. Evaluating causes of error in landmark-based data collection using scanners. *PLoS One* **12**: e0187452.

- Shi, J.J. & Rabosky, D.L. 2015. Speciation dynamics during the global radiation of extant bats. *Evolution (N. Y.)* **69**: 1528–1545.
- Simmons, N.B., Seymour, K.L., Habersetzer, J. & Gunnell, G.F. 2008. Primitive Early Eocene bat from Wyoming and the evolution of flight and echolocation. *Nature* **451**: 818.
- Surlykke, A., Jakobsen, L., Kalko, E. & Page, R. 2013. Echolocation intensity and directionality of perching and flying fringe-lipped bats, *Trachops cirrhosus* (Phyllostomidae). *Front. Physiol.* **4**: 1–9.
- Surlykke, A., Pedersen, S.B. & Jakobsen, L. 2009. Echolocating bats emit a highly directional sonar sound beam in the field. *Proc. R. Soc. B Biol. Sci.* **276**: 853–860.
- Thiagavel, J., Cechetto, C., Santana, S.E., Jakobsen, L., Warrant, E.J. & Ratcliffe, J.M. 2018. Auditory opportunity and visual constraint enabled the evolution of echolocation in bats. *Nat. Commun.* **9**: 98.
- Thiagavel, J., Santana, S.E. & Ratcliffe, J.M. 2017. Body Size Predicts Echolocation Call Peak Frequency Better than Gape Height in Vespertilionid Bats. *Sci. Rep.* **7**: 828.
- Voigt, C.C. & Lewanzik, D. 2012. ‘No cost of echolocation for flying bats’ revisited. *J. Comp. Physiol. B* **182**: 831–840.
- Wilson, D.E. & Reeder, D.M. 2005. *Mammal Species of the World: A Taxonomic and Geographic Reference*, 3rd ed. (D. E. Wilson & D. M. Reeder, eds). The John Hopkins University Press, Baltimore.

Supplementary Information

Supplementary Tables

Table S1. Procrustes ANOVA tables for allometry (logCS), ecological groups (*i.e.*, echolocation and diet categories) and functional parameters (*i.e.*, bite force, muscles mass, echolocation parameters). Analyses by ability to laryngeal echolocate (E) and diet category (DC) are presented for the complete dataset (n = 67). Analyses for emission type (ET), bite force (BF) and muscles (digastric-DIG, masseter- MAS, temporalis- TEM and pterygoid- PTE) were computed for laryngeal echolocating bats only (n = 61; n = 32 for muscles). Analyses for echolocation parameters (start frequency- SF, end frequency- EF, peak frequency-FP, bandwidth- BW, duration- D and) are presented for insectivorous bats only (n = 43). **[Continued on next pages]**

	OLS							PGLS						
	Df	SS	MS	Rsq	F	Z	Pr(>F)	Df	SS	MS	Rsq	F	Z	Pr(>F)
logCS	1	0.2968	0.2968	0.2325	22.0775	5.8030	0.001	1	0.0020	0.0020	0.1031	7.9012	5.3044	0.001
E	1	0.1150	0.1150	0.0901	8.5565	4.8167	0.001	1	0.0012	0.0012	0.0601	4.6024	4.2329	0.001
logCS:E	1	0.0178	0.0178	0.0139	1.3206	1.5337	0.060	1	0.0003	0.0003	0.0145	1.1110	0.8484	0.188
Residuals	63	0.8470	0.0134	0.6635				63	0.0161	0.0003	0.8223			
Total	66	1.2766						66	0.0195					

	OLS							PGLS						
	Df	SS	MS	Rsq	F	Z	Pr(>F)	Df	SS	MS	Rsq	F	Z	Pr(>F)
logCS	1	0.2968	0.2968	0.2325	23.5687	5.9021	0.001	1	0.0020	0.0020	0.1031	8.6243	5.5153	0.001
DC	8	0.1945	0.0243	0.1524	1.9308	4.3993	0.001	8	0.0035	0.0004	0.1813	1.8953	3.3532	0.001
logCS:DC	5	0.1304	0.0261	0.1021	2.0706	4.2300	0.001	5	0.0018	0.0004	0.0937	1.5679	3.0945	0.002
Residuals	52	0.6549	0.0126	0.5130				52	0.0121	0.0002	0.6218			
Total	66	1.2766						66	0.0195					
	Df	SS	MS	Rsq	F	Z	Pr(>F)	Df	SS	MS	Rsq	F	Z	Pr(>F)
logCS	1	0.0818	0.0818	0.0897	8.9834	4.2398	0.001	1	0.0010	0.0010	0.0620	4.3659	4.1145	0.001
ET	2	0.2740	0.1370	0.3006	15.0546	6.9549	0.001	2	0.0020	0.0010	0.1201	4.2267	5.3341	0.001
logCS:ET	2	0.0551	0.0276	0.0605	3.0291	4.8633	0.001	2	0.0006	0.0003	0.0362	1.2749	1.6171	0.057
Residuals	55	0.5005	0.0091	0.5492				55	0.0130	0.0002	0.7816			
Total	60	0.9114						60	0.0166					
	Df	SS	MS	Rsq	F	Z	Pr(>F)	Df	SS	MS	Rsq	F	Z	Pr(>F)
logCS	1	0.0818	0.0818	0.0897	5.8575	3.4756	0.001	1	0.0010	0.0010	0.0620	4.0153	3.8922	0.001
BF	1	0.0228	0.0228	0.0250	1.6326	1.4346	0.086	1	0.0008	0.0008	0.0460	2.9744	3.1219	0.002
logCS:BF	1	0.0113	0.0113	0.0124	0.8124	0.1079	0.435	1	0.0002	0.0002	0.0113	0.7288	-0.2933	0.594
Residuals	57	0.7956	0.0140	0.8729				57	0.0146	0.0003	0.8807			
Total	60	0.911447						60	0.0166					
	Df	SS	MS	Rsq	F	Z	Pr(>F)	Df	SS	MS	Rsq	F	Z	Pr(>F)
logCS	1	0.0414	0.0414	0.0820	3.0703	2.1328	0.019	1	0.0008	0.0008	0.0775	2.6384	2.4664	0.008
DIG	1	0.0820	0.0820	0.1624	6.0840	3.2528	0.002	1	0.0008	0.0008	0.0829	2.8220	2.5993	0.004
logCS:DIG	1	0.0041	0.0041	0.0082	0.3068	-1.2281	0.9	1	0.0002	0.0002	0.0171	0.5834	-0.5377	0.702
Residuals	28	0.3773	0.0135	0.7474				28	0.0081	0.0003	0.8225			
Total	31	0.5048						31	0.0098					

	OLS							PGLS						
	Df	SS	MS	Rsq	F	Z	Pr(>F)	Df	SS	MS	Rsq	F	Z	Pr(>F)
logCS	1	0.0414	0.0414	0.0820	2.7803	1.9628	0.027	1	0.0008	0.0008	0.0775	2.5757	2.4068	0.009
MAS	1	0.0433	0.0433	0.0858	2.9097	2.0377	0.024	1	0.0005	0.0005	0.0552	1.8346	1.6426	0.051
logCS:MAS	1	0.0035	0.0035	0.0069	0.2330	-1.6475	0.955	1	0.0002	0.0002	0.0248	0.8240	0.1227	0.449
Residuals	28	0.4166	0.0149	0.8254				28	0.0083	0.0003	0.8425			
Total	31	0.5048						31	0.0098					
	Df	SS	MS	Rsq	F	Z	Pr(>F)	Df	SS	MS	Rsq	F	Z	Pr(>F)
logCS	1	0.0414	0.0414	0.0820	2.9818	2.0822	0.02	1	0.0008	0.0008	0.0775	2.5909	2.4247	0.009
TEM	1	0.0698	0.0698	0.1382	5.0286	2.9196	0.001	1	0.0006	0.0006	0.0653	2.1823	1.9826	0.022
logCS:TEM	1	0.0051	0.0051	0.0102	0.3703	-0.9644	0.828	1	0.0002	0.0002	0.0197	0.6575	-0.3205	0.617
Residuals	28	0.3885	0.0139	0.7696				28	0.0082	0.0003	0.8376			
Total	31	0.5048						31	0.0098					
	Df	SS	MS	Rsq	F	Z	Pr(>F)	Df	SS	MS	Rsq	F	Z	Pr(>F)
logCS	1	0.0414	0.0414	0.0820	2.9958	2.0902	0.021	1	0.0008	0.0008	0.0775	2.6207	2.4536	0.008
PTE	1	0.0623	0.0623	0.1235	4.5128	2.8631	0.001	1	0.0006	0.0006	0.0609	2.0583	1.9456	0.027
logCS:PTE	1	0.0144	0.0144	0.0286	1.0439	0.7181	0.239	1	0.0003	0.0003	0.0336	1.1364	0.7939	0.220
Residuals	28	0.3867	0.0138	0.7660				28	0.0081	0.0003	0.8280			
Total	31	0.5048						31	0.0098					
	Df	SS	MS	Rsq	F	Z	Pr(>F)	Df	SS	MS	Rsq	F	Z	Pr(>F)
logCS	1	0.0541	0.0541	0.0852	4.0439	2.4403	0.0150	1	0.0010	0.0010	0.0926	4.3462	3.5998	0.001
SF	1	0.0490	0.0490	0.0770	3.6573	2.5244	0.0090	1	0.0005	0.0005	0.0441	2.0695	2.1435	0.020
logCS:Sf	1	0.0103	0.0103	0.0162	0.7713	0.1099	0.4380	1	0.0003	0.0003	0.0327	1.5375	1.5677	0.072
Residuals	39	0.5222	0.0134	0.8215				39	0.0088	0.0002	0.8306			
Total	42	0.6356						42	0.0106					

	OLS							PGLS						
	Df	SS	MS	Rsq	F	Z	Pr(>F)	Df	SS	MS	Rsq	F	Z	Pr(>F)
logCS	1	0.0541	0.0541	0.0852	5.1596	2.8277	0.003	1	0.0010	0.0010	0.0926	4.3158	3.5914	0.001
EF	1	0.1631	0.1631	0.2566	15.5428	4.9420	0.001	1	0.0006	0.0006	0.0523	2.4384	2.5694	0.006
logCS:EF	1	0.0091	0.0091	0.0143	0.8672	0.8200	0.214	1	0.0002	0.0002	0.0187	0.8712	0.2726	0.392
Residuals	39	0.4093	0.0105	0.6439				39	0.0089	0.0002	0.8365			
Total	42	0.6356						42	0.0106					
	Df	SS	MS	Rsq	F	Z	Pr(>F)	Df	SS	MS	Rsq	F	Z	Pr(>F)
logCS	1	0.0541	0.0541	0.0852	4.2832	2.5354	0.009	1	0.0010	0.0010	0.0926	4.2982	3.5651	0.001
BW	1	0.0813	0.0813	0.1279	6.4291	3.4086	0.001	1	0.0004	0.0004	0.0338	1.5688	1.4248	0.082
logCS:BW	1	0.0072	0.0072	0.0113	0.5692	-0.2876	0.587	1	0.0004	0.0004	0.0338	1.5675	1.5558	0.061
Residuals	39	0.4930	0.0126	0.7756				39	0.0089	0.0002	0.8399			
Total	42	0.6356						42	0.0106					
	Df	SS	MS	Rsq	F	Z	Pr(>F)	Df	SS	MS	Rsq	F	Z	Pr(>F)
logCS	1	0.0541	0.0541	0.0852	4.8486	2.7274	0.003	1	0.0010	0.0010	0.0926	4.3541	3.6126	0.001
FP	1	0.1382	0.1382	0.2174	12.3755	4.6034	0.001	1	0.0006	0.0006	0.0580	2.7295	2.7991	0.003
logCS:FP	1	0.0078	0.0078	0.0122	0.6952	0.2508	0.383	1	0.0002	0.0002	0.0203	0.9548	0.4806	0.303
Residuals	39	0.4355	0.0112	0.6852				39	0.0088	0.0002	0.8291			
Total	42	0.6356						42	0.0106					
	Df	SS	MS	Rsq	F	Z	Pr(>F)	Df	SS	MS	Rsq	F	Z	Pr(>F)
logCS	1	0.0541	0.0541	0.0852	4.4256	2.5843	0.007	1	0.0010	0.0010	0.0926	4.1846	3.5196	0.001
D	1	0.0752	0.0752	0.1184	6.1487	3.3451	0.001	1	0.0003	0.0003	0.0328	1.4813	1.3288	0.100
logCS:D	1	0.0291	0.0291	0.0458	2.3785	1.9277	0.036	1	0.0001	0.0001	0.0120	0.5412	-0.8471	0.790
Residuals	39	0.4771	0.0122	0.7507				39	0.0092	0.0002	0.8627			
Total	42	0.6356						42	0.0106					

	OLS							PGLS						
	Df	SS	MS	Rsq	F	Z	Pr(>F)	Df	SS	MS	Rsq	F	Z	Pr(>F)
logCS	1	0.0541	0.0541	0.0852	4.4304	2.5882	0.007	1	0.0010	0.0010	0.0926	4.2436	3.5416	0.001
SR	1	0.0912	0.0912	0.1434	7.4595	3.6733	0.001	1	0.0004	0.0004	0.0334	1.5330	1.3998	0.090
logCS:SR	1	0.0137	0.0137	0.0215	1.1196	0.8427	0.216	1	0.0002	0.0002	0.0233	1.0682	0.6741	0.248
Residuals	39	0.4766	0.0122	0.7499				39	0.0090	0.0002	0.8507			
Total	42	0.6356						42	0.0106					

Appendix F

Specimen information and 3D reconstruction techniques used in *Chapter Four*. Inventory number (IN). Reconstruction technique (Rec.): PHO = photogrammetry (n = 160); μ CT = micro CT scan (n = 25). Museums acronyms: NHMUK = Natural History Museum London; MNHN = Muséum national d'Histoire naturelle (Paris); IRSNB = Royal Belgian Institute of Natural Science (Brussels); MNSB = Magyar Természettudományi Múzeum (Budapest); ZMUC = Statens Naturhistoriske Museum (Copenhagen); WML = World Museum (Liverpool); NMW = Naturhistorisches Museum (Vienna); Morphosource = samples from Morphosource repository made available by Shi *et al.* (2018).

Family	Species	IN	Museum	Rec.
Emballonuridae	<i>Emballonura monticola</i>	9.1.5.474	NHMUK	PHO
Emballonuridae	<i>Taphozous melanopogon</i>	550	ZMUC	PHO
Emballonuridae	<i>Taphozous melanopogon</i>	11.12.21.4	NHMUK	PHO
Hipposideridae	<i>Hipposideros cervinus</i>	41240	IRSNB	PHO
Hipposideridae	<i>Hipposideros cervinus</i>	41239	IRSNB	PHO
Hipposideridae	<i>Hipposideros cervinus</i>	2379	ZMUC	PHO
Hipposideridae	<i>Hipposideros cervinus</i>	2380	ZMUC	PHO
Hipposideridae	<i>Hipposideros diadema</i>	41233	IRSNB	PHO
Hipposideridae	<i>Hipposideros diadema</i>	82	ZMUC	PHO
Hipposideridae	<i>Hipposideros diadema</i>	2875	ZMUC	PHO
Hipposideridae	<i>Hipposideros diadema</i>	MO-1878-1922	MNHN	μ CT
Hipposideridae	<i>Hipposideros larvatus</i>	41236	IRSNB	PHO
Hipposideridae	<i>Hipposideros larvatus</i>	1884	ZMUC	PHO
Hipposideridae	<i>Hipposideros ridleyi</i>	83.422	NHMUK	PHO
Miniopteridae	<i>Miniopterus schreibersi</i>	MO-2004-460	MNHN	PHO
Miniopteridae	<i>Miniopterus schreibersi</i>	509	ZMUC	PHO

Family	Species	IN	Museum	Rec.
Miniopteridae	<i>Miniopterus schreibersi</i>	MO-1984-1095	MNHN	μCT
Molossidae	<i>Cheiromeles torquatus</i>	44.10.17.7	NHMUK	PHO
Molossidae	<i>Cheiromeles torquatus</i>	23.10.7.10	NHMUK	PHO
Molossidae	<i>Molossus molossus</i>	920	ZMUC	PHO
Molossidae	<i>Molossus molossus</i>	598	ZMUC	PHO
Molossidae	<i>Molossus rufus</i>	587	ZMUC	PHO
Molossidae	<i>Molossus rufus</i>	674	ZMUC	PHO
Molossidae	<i>Nyctinomops laticaudatus</i>	3.4.7.5	NHMUK	PHO
Molossidae	<i>Tadarida teniotis</i>	MO-1996-447	MNHN	PHO
Molossidae	<i>Tadarida teniotis</i>	1043	ZMUC	PHO
Mormoopidae	<i>Mormoops megalophylla</i>	27.11.19.17	NHMUK	PHO
Mormoopidae	<i>Mormoops megalophylla</i>	27.11.19.19	NHMUK	PHO
Mormoopidae	<i>Mormoops megalophylla</i>	71.2254	NHMUK	PHO
Mormoopidae	<i>Pteronotus parnellii</i>	75.592	NHMUK	PHO
Mormoopidae	<i>Pteronotus parnellii</i>	65.604	NHMUK	PHO
Mormoopidae	<i>Pteronotus parnellii</i>	11.5.25.34	NHMUK	PHO
Mormoopidae	<i>Pteronotus parnellii</i>	96.307	NHMUK	PHO
Mormoopidae	<i>Pteronotus parnellii</i>	MO-1995-867	MNHN	μCT
Mormoopidae	<i>Pteronotus parnellii</i>	709	ZMUC	PHO
Noctilionidae	<i>Noctilio albiventris</i>	2007-81	MNHN	PHO
Noctilionidae	<i>Noctilio leporinus</i>	940	ZMUC	PHO
Noctilionidae	<i>Noctilio leporinus</i>	MO-2015-1576	MNHN	μCT
Phyllostomidae	<i>Anoura geoffroyi</i>	14.5.21.1	NHMUK	PHO
Phyllostomidae	<i>Anoura geoffroyi</i>	71.2266	NHMUK	PHO
Phyllostomidae	<i>Artibeus jamaicensis</i>	MO-1957-158A	MNHN	μCT
Phyllostomidae	<i>Artibeus lituratus</i>	21670	IRSNB	PHO
Phyllostomidae	<i>Artibeus lituratus</i>	21703	IRSNB	PHO
Phyllostomidae	<i>Artibeus lituratus</i>	21672	IRSNB	PHO
Phyllostomidae	<i>Artibeus lituratus</i>	L.20	ZMUC	PHO
Phyllostomidae	<i>Artibeus lituratus</i>	232C	IRSNB	PHO
Phyllostomidae	<i>Carollia brevicauda</i>	21729	IRSNB	PHO

Family	Species	IN	Museum	Rec.
Phyllostomidae	<i>Carollia brevicauda</i>	21720	IRSNB	PHO
Phyllostomidae	<i>Carollia brevicauda</i>	1403	ZMUC	PHO
Phyllostomidae	<i>Carollia castanea</i>	21691	IRSNB	PHO
Phyllostomidae	<i>Carollia castanea</i>	13.10.2.2	NHMUK	PHO
Phyllostomidae	<i>Carollia castanea</i>	13.10.2.6	NHMUK	PHO
Phyllostomidae	<i>Carollia perspicillata</i>	MO-1998-667	MNHN	PHO
Phyllostomidae	<i>Chiroderma villosum</i>	871	ZMUC	PHO
Phyllostomidae	<i>Chiroderma villosum</i>	872	ZMUC	PHO
Phyllostomidae	<i>Desmodus rotundus</i>	2007-90	MNHN	PHO
Phyllostomidae	<i>Desmodus rotundus</i>	I.G.:25855	IRSNB	PHO
Phyllostomidae	<i>Desmodus rotundus</i>	L.46	ZMUC	PHO
Phyllostomidae	<i>Desmodus rotundus</i>	L.45	ZMUC	PHO
Phyllostomidae	<i>Glossophaga soricina</i>	MO-1977-527	MNHN	PHO
Phyllostomidae	<i>Glossophaga soricina</i>	21687	IRSNB	PHO
Phyllostomidae	<i>Glossophaga soricina</i>	21694	IRSNB	PHO
Phyllostomidae	<i>Glossophaga soricina</i>	781	ZMUC	PHO
Phyllostomidae	<i>Lophostoma silvicolum</i>	MO-1986-154	MNHN	μCT
Phyllostomidae	<i>Lophostoma silvicolum</i>	MO-2016-198	MNHN	μCT
Phyllostomidae	<i>Lophostoma silvicolum</i>	MO-2016-197	MNHN	μCT
Phyllostomidae	<i>Micronycteris hirsuta</i>	98.10.9.13	NHMUK	PHO
Phyllostomidae	<i>Micronycteris hirsuta</i>	1937.8.30.14	NHMUK	PHO
Phyllostomidae	<i>Micronycteris megalotis</i>	721	ZMUC	PHO
Phyllostomidae	<i>Micronycteris megalotis</i>	27.11.1.57	NHMUK	PHO
Phyllostomidae	<i>Micronycteris minuta</i>	2016-97	MNHN	μCT
Phyllostomidae	<i>Micronycteris minuta</i>	1.7.11.17	NHMUK	PHO
Phyllostomidae	<i>Mimon crenulatum</i>	AMNH-64541	Morphosource	μCT
Phyllostomidae	<i>Mimon crenulatum</i>	AMNH-236001	Morphosource	μCT
Phyllostomidae	<i>Phyllostomus discolor</i>	11.5.25.67	NHMUK	PHO
Phyllostomidae	<i>Phyllostomus discolor</i>	MO-2016-146	MNHN	μCT
Phyllostomidae	<i>Phyllostomus hastatus</i>	744	ZMUC	PHO
Phyllostomidae	<i>Phyllostomus hastatus</i>	34.9.2.15	NHMUK	PHO

Family	Species	IN	Museum	Rec.
Phyllostomidae	<i>Phyllostomus hastatus</i>	MO-1988-82	MNHN	μCT
Phyllostomidae	<i>Platyrrhinus helleri</i>	2016-842	MNHN	μCT
Phyllostomidae	<i>Platyrrhinus helleri</i>	2016-847	MNHN	μCT
Phyllostomidae	<i>Sturnira lilium</i>	900	ZMUC	PHO
Phyllostomidae	<i>Sturnira lilium</i>	1.6.6.21	NHMUK	PHO
Phyllostomidae	<i>Sturnira lilium</i>	2016-882	MNHN	μCT
Phyllostomidae	<i>Trachops cirrhosus</i>	24.1.3.32	NHMUK	PHO
Phyllostomidae	<i>Trachops cirrhosus</i>	20.7.14.34	NHMUK	PHO
Phyllostomidae	<i>Uroderma bilobatum</i>	MO-1976-295	MNHN	μCT
Phyllostomidae	<i>Uroderma bilobatum</i>	21713	IRSNB	PHO
Pteropodidae	<i>Cynopterus brachyotis</i>	41089	IRSNB	PHO
Pteropodidae	<i>Cynopterus brachyotis</i>	41091	IRSNB	PHO
Pteropodidae	<i>Cynopterus brachyotis</i>	1146	ZMUC	PHO
Pteropodidae	<i>Eidolon helvum</i>	17295	IRSNB	PHO
Pteropodidae	<i>Eidolon helvum</i>	181B	IRSNB	PHO
Pteropodidae	<i>Epomophorus wahlbergi</i>	AMNH-187275	Morphosource	μCT
Pteropodidae	<i>Pteropus poliocephalus</i>	32.6.1.3	NHMUK	PHO
Pteropodidae	<i>Pteropus poliocephalus</i>	32.6.1.1	NHMUK	PHO
Pteropodidae	<i>Pteropus vampyrus</i>	2368	ZMUC	PHO
Pteropodidae	<i>Rousettus aegyptiacus</i>	M6257	ZMUC	PHO
Rhinolophidae	<i>Rhinolophus affinis</i>	8.1.30.7	NHMUK	PHO
Rhinolophidae	<i>Rhinolophus affinis</i>	9.1.5.152	NHMUK	PHO
Rhinolophidae	<i>Rhinolophus blasii</i>	1035	ZMUC	PHO
Rhinolophidae	<i>Rhinolophus ferrumequinum</i>	MO-1977-58	MNHN	PHO
Rhinolophidae	<i>Rhinolophus ferrumequinum</i>	1980.789	WML	PHO
Rhinolophidae	<i>Rhinolophus ferrumequinum</i>	9156	NMW	PHO
Rhinolophidae	<i>Rhinolophus ferrumequinum</i>	10421	NMW	PHO
Rhinolophidae	<i>Rhinolophus ferrumequinum</i>	8907	NMW	PHO
Rhinolophidae	<i>Rhinolophus ferrumequinum</i>	45847	NMW	PHO
Rhinolophidae	<i>Rhinolophus ferrumequinum</i>	28021	NMW	PHO
Rhinolophidae	<i>Rhinolophus ferrumequinum</i>	MO-1977-56	MNHN	μCT

Family	Species	IN	Museum	Rec.
Rhinolophidae	<i>Rhinolophus hipposideros</i>	MO-1932-4107	MNHN	PHO
Rhinolophidae	<i>Rhinolophus hipposideros</i>	39.226	NHMUK	PHO
Rhinolophidae	<i>Rhinolophus mehelyi</i>	no number	NHMUK	PHO
Rhinolophidae	<i>Rhinolophus mehelyi</i>	62.238	NHMUK	PHO
Vespertilionidae	<i>Eptesicus furinalis</i>	AMNH-124387	Morphosource	μCT
Vespertilionidae	<i>Eptesicus serotinus</i>	MO-2003-222	MNHN	PHO
Vespertilionidae	<i>Eptesicus serotinus</i>	158	ZMUC	PHO
Vespertilionidae	<i>Eptesicus serotinus</i>	1040	ZMUC	PHO
Vespertilionidae	<i>Eptesicus serotinus</i>	4080	ZMUC	PHO
Vespertilionidae	<i>Eptesicus serotinus</i>	3044	ZMUC	PHO
Vespertilionidae	<i>Hypsugo savii</i>	2420.6	MNSB	PHO
Vespertilionidae	<i>Hypsugo savii</i>	4581.1	MNSB	PHO
Vespertilionidae	<i>Hypsugo savii</i>	MO-1932-4270	MNHN	PHO
Vespertilionidae	<i>Hypsugo savii</i>	1042	ZMUC	PHO
Vespertilionidae	<i>Kerivoula papillosa</i>	93.4.1.30	NHMUK	PHO
Vespertilionidae	<i>Murina cyclotis</i>	78.1543	NHMUK	PHO
Vespertilionidae	<i>Myotis albescens</i>	MO-1949-118	MNHN	μCT
Vespertilionidae	<i>Myotis bechsteinii</i>	15717	IRSNB	PHO
Vespertilionidae	<i>Myotis bechsteinii</i>	3865	ZMUC	PHO
Vespertilionidae	<i>Myotis bechsteinii</i>	57.37.1.	MNSB	PHO
Vespertilionidae	<i>Myotis bechsteinii</i>	73.110.1.	MNSB	PHO
Vespertilionidae	<i>Myotis blythii</i>	5.12.2.7.	NHMUK	PHO
Vespertilionidae	<i>Myotis brandtii</i>	58.3.1.	MNSB	PHO
Vespertilionidae	<i>Myotis brandtii</i>	68.529.5.	MNSB	PHO
Vespertilionidae	<i>Myotis brandtii</i>	8094B	IRSNB	PHO
Vespertilionidae	<i>Myotis brandtii</i>	5085	IRSNB	PHO
Vespertilionidae	<i>Myotis brandtii</i>	15725	IRSNB	PHO
Vespertilionidae	<i>Myotis brandtii</i>	1104	ZMUC	PHO
Vespertilionidae	<i>Myotis capaccinii</i>	2004-1316	MNHN	μCT
Vespertilionidae	<i>Myotis capaccinii</i>	MO-1955-671	MNHN	PHO
Vespertilionidae	<i>Myotis dasycneme</i>	18892	NMW	PHO

Family	Species	IN	Museum	Rec.
Vespertilionidae	<i>Myotis dasycneme</i>	MO-1983-506	MNHN	PHO
Vespertilionidae	<i>Myotis dasycneme</i>	1117	ZMUC	PHO
Vespertilionidae	<i>Myotis dasycneme</i>	374	ZMUC	PHO
Vespertilionidae	<i>Myotis dasycneme</i>	5099	IRSNB	PHO
Vespertilionidae	<i>Myotis dasycneme</i>	5096	IRSNB	PHO
Vespertilionidae	<i>Myotis daubentonii</i>	MO-1997-322	MNHN	PHO
Vespertilionidae	<i>Myotis daubentonii</i>	54.86.1	MNSB	PHO
Vespertilionidae	<i>Myotis daubentonii</i>	55.16.1	MNSB	PHO
Vespertilionidae	<i>Myotis daubentonii</i>	57.61.3	MNSB	PHO
Vespertilionidae	<i>Myotis daubentonii</i>	4546.2	MNSB	PHO
Vespertilionidae	<i>Myotis daubentonii</i>	51428	NMW	PHO
Vespertilionidae	<i>Myotis daubentonii</i>	51596	NMW	PHO
Vespertilionidae	<i>Myotis emarginatus</i>	2004-1308	MNHN	PHO
Vespertilionidae	<i>Myotis emarginatus</i>	1036	ZMUC	PHO
Vespertilionidae	<i>Myotis myotis</i>	5063	IRSNB	PHO
Vespertilionidae	<i>Myotis mystacinus</i>	MO-2000-384	MNHN	μCT
Vespertilionidae	<i>Myotis mystacinus</i>	1988.215	WML	PHO
Vespertilionidae	<i>Myotis mystacinus</i>	35431-9	IRSNB	PHO
Vespertilionidae	<i>Myotis mystacinus</i>	15742	IRSNB	PHO
Vespertilionidae	<i>Myotis nattereri</i>	1981.92.2	WML	PHO
Vespertilionidae	<i>Myotis nattereri</i>	2633	ZMUC	PHO
Vespertilionidae	<i>Myotis nattereri</i>	2782	ZMUC	PHO
Vespertilionidae	<i>Myotis nigricans</i>	2016-976	MNHN	μCT
Vespertilionidae	<i>Myotis nigricans</i>	MO-2003-316	MNHN	PHO
Vespertilionidae	<i>Myotis nigricans</i>	17093	IRSNB	PHO
Vespertilionidae	<i>Myotis nigricans</i>	L.62	ZMUC	PHO
Vespertilionidae	<i>Nyctalus noctula</i>	MO-1932-4158	MNHN	PHO
Vespertilionidae	<i>Nyctalus noctula</i>	MO-1932-4157	MNHN	PHO
Vespertilionidae	<i>Nyctalus noctula</i>	42235	NMW	PHO
Vespertilionidae	<i>Nyctalus noctula</i>	56.91.2.	MNSB	PHO
Vespertilionidae	<i>Nyctalus noctula</i>	56.91.5.	MNSB	PHO

Family	Species	IN	Museum	Rec.
Vespertilionidae	<i>Nyctalus noctula</i>	65.54.1.	MNSB	PHO
Vespertilionidae	<i>Pipistrellus pipistrellus</i>	2004-1365	MNHN	μCT
Vespertilionidae	<i>Pipistrellus pipistrellus</i>	69279	NMW	PHO
Vespertilionidae	<i>Pipistrellus pipistrellus</i>	MO-2003-283	MNHN	PHO
Vespertilionidae	<i>Pipistrellus pipistrellus</i>	1981.91.3	WML	PHO
Vespertilionidae	<i>Pipistrellus pipistrellus</i>	39507	IRSNB	PHO
Vespertilionidae	<i>Pipistrellus pipistrellus</i>	5407	IRSNB	PHO
Vespertilionidae	<i>Pipistrellus pipistrellus</i>	65244	NMW	PHO
Vespertilionidae	<i>Plecotus austriacus</i>	MO-1932-4160	MNHN	PHO
Vespertilionidae	<i>Plecotus austriacus</i>	54.80.1	MNSB	PHO
Vespertilionidae	<i>Plecotus austriacus</i>	57.31.1	MNSB	PHO
Vespertilionidae	<i>Plecotus austriacus</i>	37262	NMW	PHO
Vespertilionidae	<i>Plecotus austriacus</i>	52845	NMW	PHO
Vespertilionidae	<i>Scotophilus kuhlii</i>	2849	ZMUC	PHO

References Appendix F

Shi, J.J., Westeen, E.P. & Rabosky, D.L. 2018. Digitizing extant bat diversity: An open-access repository of 3D μCT-scanned skulls for research and education. *PLoS One* **13**: e0203022.

CHAPTER FIVE: Skull Morphological Adaptations to Acoustic Emissions: Peak Frequency in Bats

Statement on content presentation and publication

This chapter is currently in preparation for submission to *Zoological Journal of Linnean Society*.

Abstract

Head morphology of echolocating species (*i.e.*, toothed whales and bats) faces functional demands due to ultrasound emission and reception. Other than the scaling of echolocation call parameters (in particular peak frequency) on skull size, little is known on the evolutionary pressures of echolocation on the skull form of echolocating species. Given the wide diversity of sounds emitted by bats, they represent an ideal model to study the role of peak frequency in skull morphological diversification.

I tested for the relationship between skull morphology (*i.e.*, size and shape) and peak frequency in a taxonomically diverse dataset (*i.e.*, ~65% of bat genera covering all laryngeally echolocating families). The combination of multiple sensory strategies used by non-insectivorous species (*e.g.* frugivorous) might “relax” the pressure exerted by peak frequency on their skull morphology. Therefore, I tested different dietary groups separately. 3D reconstructions of bat skulls were used to quantify morphological variation using geometric morphometrics. Phylogenetic Generalised Least Squares were employed to assess associations between skull morphological variation and peak frequency.

Skull shape of all insectivorous families correlated with peak frequency. In contrast to my prediction, I found that one group of non-insectivorous bats (*i.e.*, frugivorous species) also presented significant skull shape (but not size) adaptations to frequency emitted. In both insectivorous and frugivorous species, high frequencies were associated with a short rostrum. This study also indicated that peak frequency more intensively constrains skull shape of nasal emitters compared to mouth emitters even though the skulls of both showed an association with peak frequency. These results suggest that peak frequency plays an important role in bat skull evolution and not only in insectivorous bats. Echolocation adaptations appears to be evolutionary conservative within frugivorous species even if they use combined sensory strategies to locate food.

Introduction

A variety of functional drivers can simultaneously influence the same phenotypic trait, often resulting in complex adaptive systems or functional trade-offs (Majid & Kruspe, 2018; Wu *et al.*, 2018, see also *Chapter Four*). The diverse designs of mammalian skulls are an example of adaptation to different functional demands imposed by sensorial and feeding functions (Dumont *et al.*, 2009; Figueirido *et al.*, 2013). Echolocating mammals use sounds as the main sensory system to both navigate and detect prey and so face physical acoustic demands on head morphology (*e.g.* toothed whales' mandibles: Barroso *et al.*, 2012). Other than the allometric scaling of frequencies emitted by toothed whales and bats, *i.e.*, the negative correlation between skull size and frequencies emitted (Jones, 1999; May-Collado *et al.*, 2007), little is known of how cranial morphological adaptation evolved under echolocation pressures.

Chiroptera evolved echolocation as an additional sensory system to perceive the environment and locate food items in the dark (Griffin, 1958), with at least 1,060 bat species known to use ultrasound emission to navigate and forage (IUCN, 2019). Despite a likely single origin of echolocation (Veselka *et al.*, 2010; Fenton & Ratcliffe, 2017; Wang *et al.*, 2017), different strategies and morphological adaptations have evolved within the order to efficiently project sound in open space. Specifically, bats can echolocate through either the mouth or nostrils, leading to different head rotations that straighten the phonal channel (Pedersen, 1998). A further morphological difference is shown within the nasal emitters: New World nasal emitters (Phyllostomidae family) present simple nasal passages, while some Old World nasal emitters have complex nasal chambers in their nostrils. These morphological adaptations to echolocation are not the only ones known to be related to the optimization of sound emission. At a finer scale, the size of nasal chambers in Rhinolophidae and Hipposideridae species (Old World nasal emitters) probably evolved in

tandem with the frequency emitted, as the latter is enhanced through resonance effect of the nasal structure (Armstrong & Coles, 2007; Jacobs *et al.*, 2014).

I investigated the relationship between cranial shape and the most studied echolocation call parameter (*i.e.*, peak frequency). The aim of this study was to identify which morphological features covary with peak frequency and, therefore, appear to be under evolutionary pressures associated with echolocation. In *Chapter Four*, I showed that the skull shape of insectivorous bats correlated with echolocation call parameters. In the present chapter, I first tested if this pattern was confirmed within a more taxonomically and ecologically diverse sample (~65% of echolocating bat genera). Species were analysed by emission type as differences between nasal and oral emission represent the main morphological dichotomy in bat skulls associated to echolocation (Pedersen, 2000; Arbour *et al.*, 2019). Other ecological variables (*i.e.*, echolocation call design and diet) were used to identify possible different evolutionary paths due to ecological specialization. Specifically, cranial morphology of species combining multiple sensory strategies (*e.g.* some frugivorous species, Ripperger *et al.*, 2019) may be subject to a weaker selection pressure due to echolocation compared to insectivorous species that (almost) exclusively rely on echolocation to locate food. Echolocation call designs (*i.e.*, temporal and frequency structure of the sound) have evolved multiple times in distant lineages (Jones & Teeling, 2006), and are considered good proxies for preferred hunting habitat as they evolved to face the environmental challenges specific to each habitat types (*i.e.*, open, edge, clutter habitats) (Siemers *et al.*, 2001; Denzinger & Schnitzler, 2013). Different acoustic constraints may apply to the cranial morphology of species emitting different call designs. Geometric morphometrics and phylogenetic comparative methods were used to test the following predictions:

- (i) Skull shape and size of non-insectivorous species are not constrained by echolocation characteristics (*i.e.*, peak frequency) as they use an integrated sensory system to locate and pursue the prey;
- (ii) Call design plays a role in shaping the relationship between peak frequency and skull morphology of insectivorous species as different acoustic constraints may apply;
- (iii) Peak frequency strongly influences rostrum shape of constant frequency nasal emitters because of the resonance effect within the nasal chambers.

Methods

Sample

I performed statistical analyses on 443 specimens belonging to 219 species covering all nineteen families of laryngeal echolocating bats. This dataset represents about 65% of genera within the order Chiroptera. Specimen details (*i.e.*, museum collections and inventory number) are reported in **Appendix G**.

Functional, ecological and morphological data

Functional and ecological data were collected as described in *Chapter Two*. The peak frequency for each species was acquired from the literature or collected in the field. Details on selected literature and raw data are provided in **Appendix C**.

To assess the relationship between morphology and ecological groups I classified the species by broad diet categories, emission type and call design. As for *Chapter Four*, diet was assigned to the traditional categories inferred from Wilson and Reeder (2005) and is reported in **Table 1**.

Table 1. Ecological categories for each group that were used as independent variables. Categorisation of call designs from Jones and Teeling (2006).

Emission Type	Call Design	Diet
Old World nasal emitters	Narrowband, dominated by fundamental harmonic (c)	Insectivorous
New World nasal emitters (Phyllostomidae)	Narrowband, multiharmonic (d)	Frugivorous
Oral emitters	Short, broadband, dominated by fundamental harmonic (e)	Hematophagous
	Short, broadband, multiharmonic (f)	Vertebrate eater
	Long, broadband, multiharmonic (g)	Nectarivorous
	Constant frequency (h)	Omnivorous
		Frugi/insectivorous
		Necta/fruigivorous
		Insect-vertebrate eater

Some species that were believed to emit sounds exclusively from the nose have been recently reported to also emit from the mouth (*e.g.* Surlykke *et al.*, 2013). However, as relatively few studies have focused on the topic, I could not categorise all species in this extensive dataset into the emission categories used in *Chapter Four* (*i.e.*, oral, nasal, and both). Therefore, emission type was categorised as oral emission or nasal emission, the latter subcategorised into New World (*i.e.*, Phyllostomidae species) and Old World species (for references see **Appendix C**). Nasal emission implies considerable rearrangements of skull morphology (Pedersen, 2000), but different selective pressures might apply to these two groups as nasal chambers in some Old World nasal-emitters are known to behave as resonance structures (Armstrong & Coles, 2007; Jacobs *et al.*, 2014). Species were grouped by call designs following Jones & Teeling (2006). Specifically the presence of harmonics, the magnitude of broadband portions and the duration of the call were assessed. I used geometric morphometric methods to collect morphological data on 3D models of bat skulls. The models were reconstructed in 3D through an established photogrammetric

protocol (Giacomini *et al.*, 2019) and using a μ CT scanner (**Appendix G**). The full geometric morphometrics protocol is reported in *Chapter Two*.

Statistical analyses

Allometry (*i.e.*, correlation between shape and size) and phylogenetic non-independence can lead to incorrect evolutionary inferences about morphological variation, unless accounted for in the analyses (phylogenetic non-independence: Felsenstein, 1985; allometry: Loy *et al.*, 1996). In order to assess if phylogenetic comparative methods were necessary, I tested for the presence of a significant phylogenetic signal in morphological traits (*i.e.*, \log_{10} centroid size and Procrustes shape coordinates) and in peak frequency. Blomberg *et al.*'s K statistic and its multivariate extension for shape (K_{multiv}) were used to assess the presence and significance of a phylogenetic signal (Blomberg *et al.*, 2003; Adams, 2014). To evaluate the presence and significance of allometry I performed an ordinary least squares regression (OLS) with shape (*i.e.*, Procrustes shape coordinates) as the dependent variable and size (*i.e.*, \log_{10} centroid size) as the independent (Cardini & Polly, 2013). I repeated the analysis using phylogenetic generalised least squares regression (PGLS) in order to take phylogenetic relatedness into account (Rohlf, 2007; Adams & Collyer, 2015).

Correlations between morphological traits and functional traits (*i.e.*, categorical variables: diet, emission type, call design; continuous variable: peak frequency) were first tested under a traditional approach (*i.e.*, OLS). Because evolutionary allometry was significant (see Results), size was always included in the OLS (and in the PGLS, see below) as a fixed effect and as an interaction with peak frequency when testing for shape variance. Hence, I controlled for the allometric effect when assessing shape adaptation to peak frequency (Freckleton, 2009; Adams & Collyer, 2018). Furthermore, as morphological traits and peak frequency showed a significant phylogenetic signal (see Results), I controlled for species

phylogenetic non-independence by repeating all the analyses using PGLS models. I used a recently published ultrametric and calibrated tree (Shi & Rabosky, 2015) to compute the variance-covariance matrix employed in the PGLS (Adams & Felice, 2014). The tree was pruned with the tips corresponding to the species of the dataset and subdatasets. OLS and PGLS analyses were first performed on the complete dataset and subsequently repeated by emission type, call design and family in order to further explore potentially diverse evolutionary patterns due to ecological adaptations. Furthermore, OLS and PGLS models were used to test whether the angle between the basicranium (*i.e.*, distance between landmarks 5 and 6) and the palatal plane (*i.e.*, distance between landmarks 6 and 7) was different between oral and nasal emitters (both Old and New world). The sine transformed angles of the 219 species were input as the dependent variable and the emission type as the independent variable. Shape variation in the 219 bat species was analysed using principal component analysis (PCA) of Procrustes shape coordinates for each species (the species' average shape was used when more than one specimen was available per species). The 3D model of *Cheiromeles torquatus* was the closest fit to the dataset mean shape and so the model was warped on the consensus (*i.e.*, mean shape) by applying the Thin-Plate-Spline (TPS) algorithm (Bookstein, 1989). This reference mesh was subsequently warped on the maximum and minimum shape of the first two PC axes to show major morphological variation in the dataset (Klingenberg, 2013).

Shape variation associated to peak frequency was visualised by plotting the regression score against the size-corrected and \log_{10} transformed peak frequency ($\log_{10}\text{corr.FP}$). This approach removed the shape variation explained by the allometric effect (Blomberg *et al.*, 2003). The TPS algorithm was applied on the reference mesh used above to visualise 3D shape changes correlated with peak frequency. The predicted values of shape that were computed under a PGLS model ($\text{shape} \sim \log_{10}\text{corr.FP}$) were used to visualise bat skull shape associated with minimum and maximum peak frequency (see *Chapter Two* for details).

I performed all the analyses in R software (R Core Team, 2019) using “geomorph” (Adams

& Otárola-Castillo, 2013), “phytools” (Revell, 2012), “RRPP” (Collyer & Adams, 2018) and “geiger” (Pennell *et al.*, 2014) packages.

Results

Both morphological variables (*i.e.*, size and shape) and peak frequency showed significant phylogenetic signals confirming that phylogenetic comparative methods were necessary for subsequent analyses. Morphological variables showed relatively low values for K (and K_{multiv}), suggesting that these traits are less similar than predicted from their phylogenetic history (size: $K = 0.766$, $p = 0.001$; shape: $K_{multiv} = 0.900$, $p = 0.001$). In contrast, K was high for peak frequency ($K = 1.306$, $p = 0.001$).

Evolutionary allometry accounted for a relatively small but still significant proportion of shape variance after phylogenetic correction ($R^2 = 0.067$, $p = 0.001$), confirming the need to control for size when testing for association between peak frequency and shape under OLS and PGLS models.

Size and shape by ecological groups

Size (*i.e.*, \log_{10} transformed centroid size) of the 219 species did not differ between echolocation types and call designs after phylogenetic correction (PGLS: $p = 0.175$; $p = 0.076$; respectively; **Table 2A**). Nevertheless, diet category explained a significant proportion of size variance (PGLS: $R^2 = 0.117$, $p = 0.002$; **Table 2A**).

Table 2. Size (**A**) and shape (as PC1 and PC2; [**B**]) variance explained by each categorical variable (R^2) and statistic significance (p) for 219 echolocating bat species. Significance of the PGLS models reported in bold.

A)	Size			
	R ² -OLS	p	R ² -PGLS	p
Emission type	0.209	0.001	0.015	0.175
Call design	0.201	0.001	0.044	0.076
Diet	0.271	0.001	0.117	0.002

B)	Shape- PC1				Shape- PC2			
	R ² -OLS	p	R ² -PGLS	p	R ² -OLS	p	R ² -PGLS	p
Emission type	0.761	0.001	0.304	0.001	0.135	0.001	0.014	0.209
Call design	0.666	0.001	0.121	0.002	0.164	0.001	0.095	0.017
Diet	0.113	0.002	0.016	0.876	0.319	0.001	0.18	0.002

Shape variation between the 219 bat species explained by the first two principal components (PCs) was 35.92% (PC1) and 16.34% (PC2). PC1 separated species according to emission type, with oral emitting species scoring lower than the nasal emitters (**Figure 1**). Emission type and call design were good predictors of shape variance along PC1, explaining 30% and 12%, respectively, of variance under PGLS models (**Table 2B**). PC1 represented variation in height and width of braincases and length of palate. Over 30% of PC1 variation was described by differences in the angle between the basicranium and palatal planes (PGLS: $R^2 = 0.326$, $p = 0.001$; **Table 2B**). Specifically, oral emitters displayed a significantly greater angle between the basicranium and palate planes compared to nasal emitters (PGLS: $R^2 = 0.033$ $p = 0.01$; **Figure 1**). The oral emitters of the genus *Mormoops* showed the greatest angle between the palate plane and the basicranium (~231°).

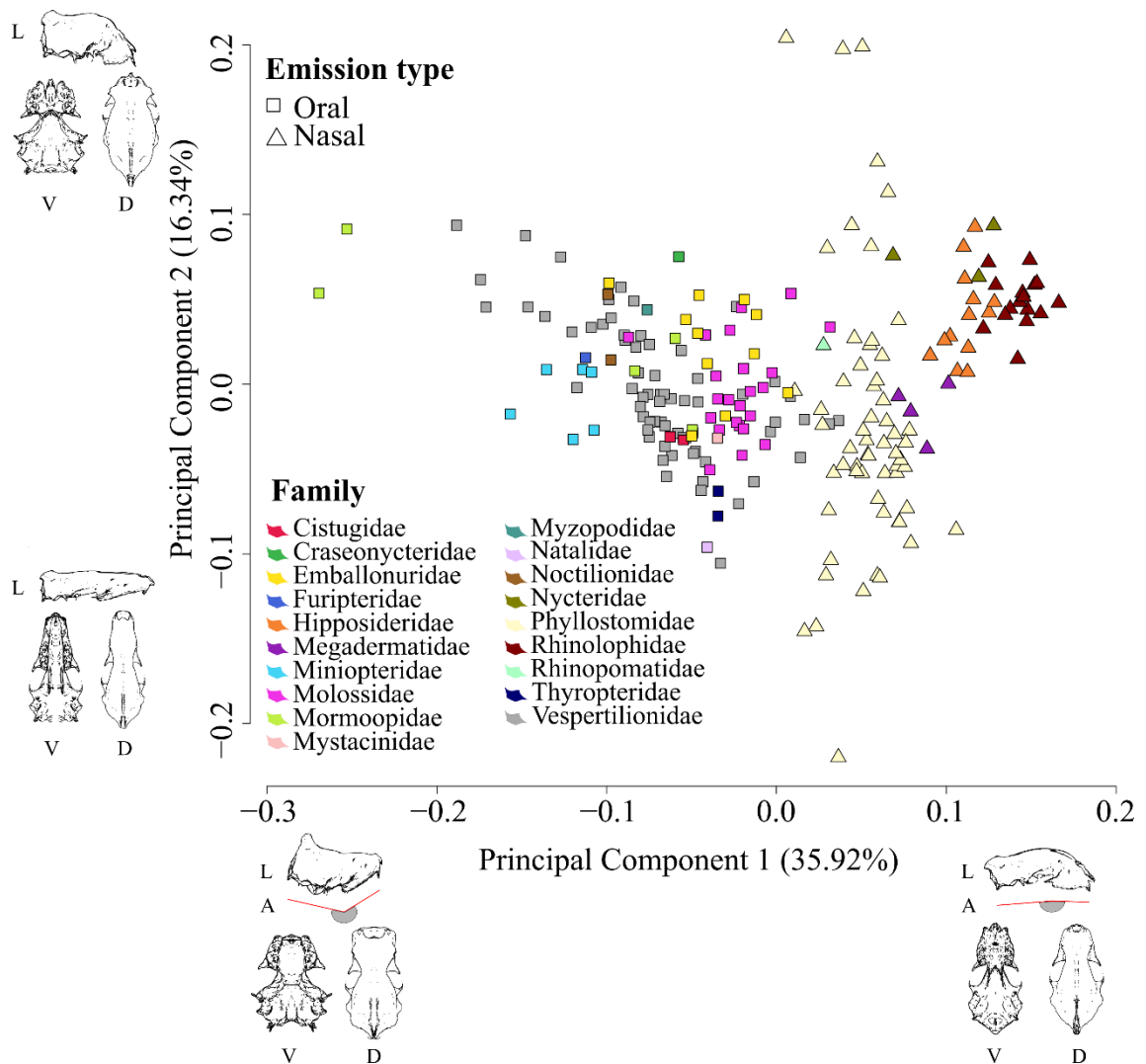


Figure 1. Principal component analysis of 219 species of echolocating bats displayed by family and emission type (O = oral, N = nasal). Shape variation was reported on dorsal (D), ventral (V) and lateral (L) views by warping maximum and minimum PC variation of each axes onto the reference mesh. Differences in angles between the basicranium and palate planes (A) were associate to emission type.

PC2 separated species according to their diet category and food hardness, with nectar eaters (*i.e.*, soft food) scoring low and hard fruit eaters scoring high. Diet and call design explained 18% and 9%, respectively, of shape variance along PC2 under PGLS models (**Table 2B**). Shape differences in PC2 were represented by variation in skull height and rostrum length. Species feeding on nectar (*e.g.* *Choeronycteris mexicana*) displayed long rostra and decreased braincase height. In contrast, hard fruit eaters, such as the highly

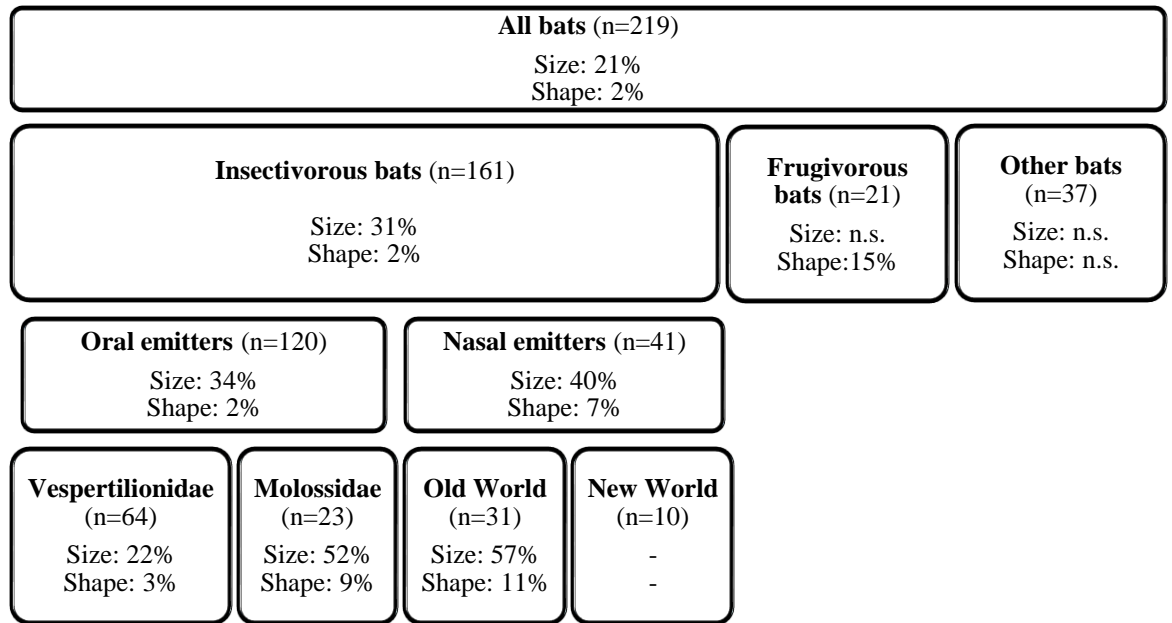
specialised *Ametrida centurio*, *Centurio senex* and *Sphaeronycteris toxophyllum*, presented brachycephalic skulls. Comparable results were obtained when all shape coordinates were used in the analyses instead of the single PCs (**Table S1**).

Both size and shape were heavily influenced by family, which accounted for over 30% of size variance and 51% of skull shape (*i.e.*, all shape coordinates) ($R^2 = 0.373$, $p = 0.001$; $R^2 = 0.514$, $p = 0.001$, respectively). Such a strong phylogenetic signal explained the differences in R^2 and p values between OLS and PGLS of **Table 2**.

Size and peak frequency

The allometric effect of peak frequency was strong for all species and within all ecological groups (*i.e.*, diet, emission type and call design) with the exception of non-insectivorous species, where no allometric effect was detected (**Figure 2**).

A)



B)

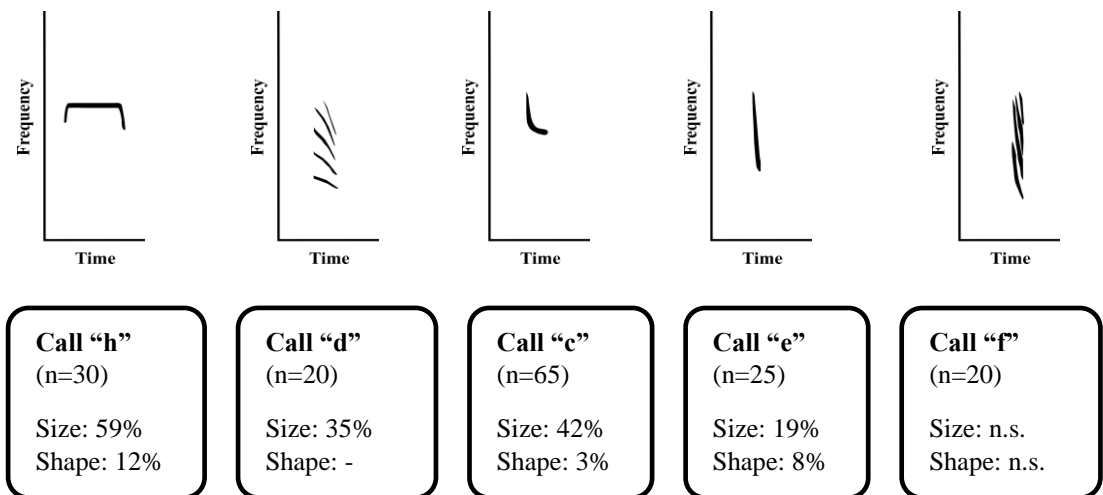


Figure 2. Size and shape correlation with peak frequency by emission type (A) and by call design for insectivorous bats (B) under PGLS models. Variation explained by each PGLS model is reported as a percentage when statistically significant; n.s. stands for non-significant results. The analysis was not performed for New World nasal emitters because of a small sample size (n = 10). Spectrograms of call designs not in scale. Call "h": Rhinolophidae (n = 16), Hipposideridae (n = 13), *P. parnellii*; call "d": Emballonuridae (n = 11), Mormoopidae (n = 5), Thyropteridae (n = 2), *Craseonycteris thonglongyai* and *Rhinopoma microphyllum*; call "c": Cistugidae (n = 2), Miniopteridae (n = 6), Molossidae (n = 23), Vespertilionidae (n = 34); call "e": Vespertilionidae (n = 24) and *Furipterus horrens*; call "f": Phyllostomidae (n = 10), Vespertilionidae (n = 6), *Megaderma spasma*, *Mystacina tuberculata*, *Natalus tumidirostris* and *Nycteris hispida*.

The overall size of all 219 bat species was significantly correlated with peak frequency even after phylogenetic correction (OLS: $R^2 = 0.024$, $p = 0.021$; PGLS: $R^2 = 0.214$, $p = 0.001$). Specifically, species with bigger heads showed a lower peak frequency (PGLS β coefficient = -0.287).

Skull size of insectivorous bats presented high correlation with peak frequency (PGLS: $n = 161$, $R^2 = 0.307$, $p = 0.001$); however, no allometric effect was detected in peak frequency among either frugivorous or other bat species (PGLS: $n = 21$, $R^2 = 0.051$, $p = 0.317$; $n = 37$, $R^2 = 0.053$, $p = 0.176$; respectively).

Within the insectivorous bat dataset, I repeated the test separately by emission type. Oral emitters showed a slightly weaker correlation compared to nasal emitters (PGLS: $n = 120$, $R^2 = 0.341$, $p = 0.001$; $n = 41$, $R^2 = 0.397$, $p = 0.001$, respectively). Within the nasal emitters, some species shifted from the allometric pattern. Specifically, *Macrophyllum macrophyllum* was smaller in head size than predicted by their peak frequency while *Hipposideros diadema* was bigger than expected (**Figure 3A**). Furthermore, Old World nasal emitters (*i.e.*, Rhinolophidae, Megadermatidae, Nycteridae) showed the strongest allometric relationship (PGLS: $n = 31$, $R^2 = 0.572$, $p = 0.001$; **Figure S1**). The sample size for insectivorous nasal emitters from the New World was too small for this group to be tested separately ($n = 10$).

Within the oral emitters, two of the most diverse families (*i.e.*, Vespertilionidae and Molossidae) showed different allometric effects (**Figure 3B**). Skull size of Vespertilionidae species showed the lowest allometric effect on peak frequency (PGLS: $n = 64$, $R^2 = 0.224$, $p = 0.001$) while Molossidae showed the greatest (PGLS: $n = 23$, $R^2 = 0.520$, $p = 0.001$). Only *Cheiromeles torquatus* deviated from the association pattern of size and peak frequency within the Molossidae family (**Figure S2**), while the pattern of Vespertilionidae family was more complex (**Figure S3**).

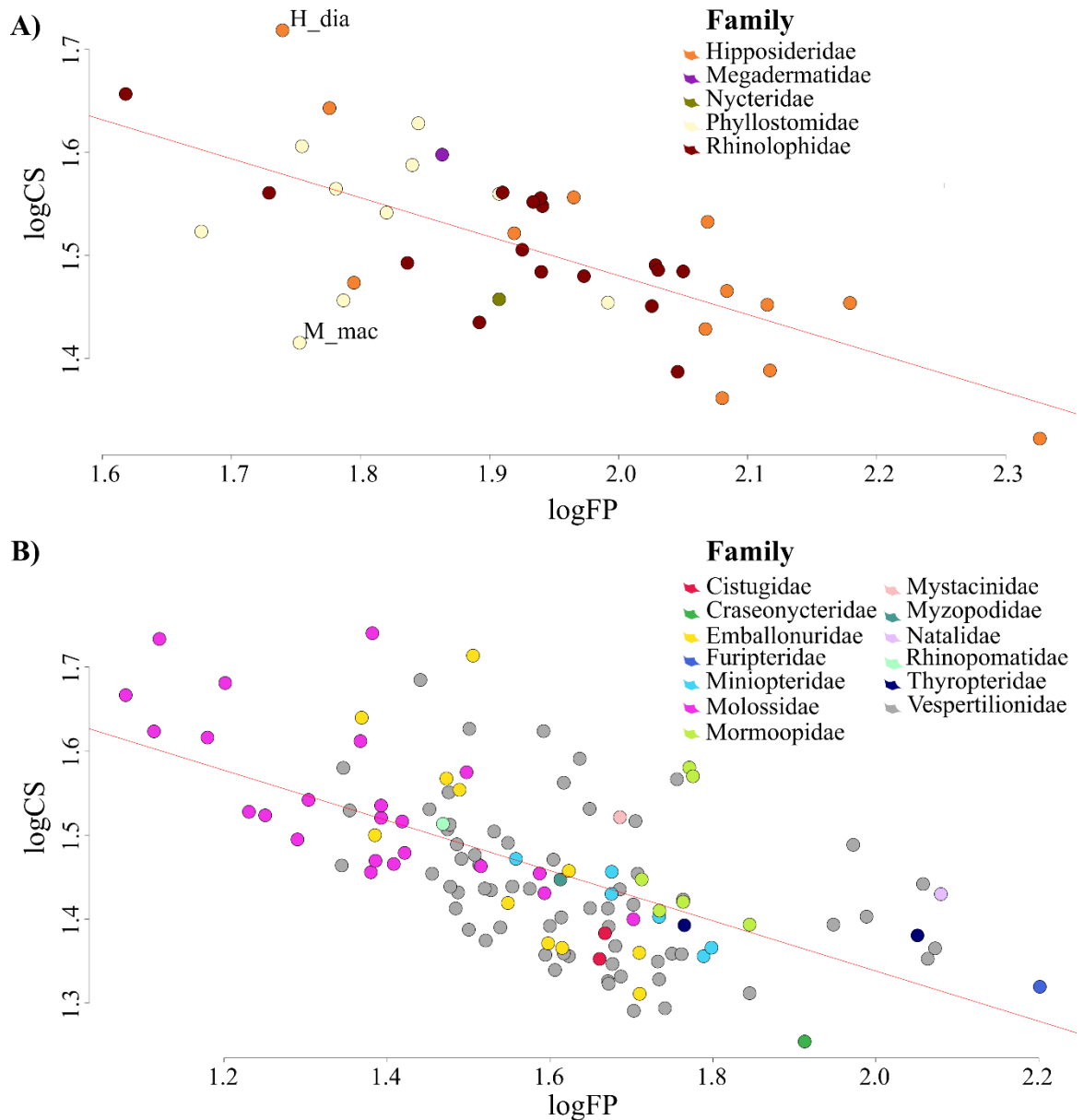


Figure 3. Allometric effect on peak frequency for insectivorous bats: nasal emitting species (**A**) and oral emitting species (**B**). The graphs represent the correlations under PGLS models of \log_{10} transformed centroid size ($\log_{10}CS$) and \log_{10} transformed peak frequency ($\log_{10}FP$). Text labels indicate the outliers (*H_dia*: *Hipposideros diadema*, *M_mac*: *Macrophyllum macrophyllum*).

Furthermore, species emitting different types of calls displayed different strengths of association between peak frequency and skull size (**Figure 2B** and **Table 3**). Bats emitting components of constant frequency sounds (“h”: *i.e.*, Rhinolophidae, Hipposideridae and *Pteronotus parnellii*) showed the highest allometric effect (PGLS: $n = 30$, $R^2 = 0.586$, $p =$

0.001; **Figure S4**). Skull size of narrowband multiharmonic (“d”) and monoharmonic (“c”) emitting species showed a lower, but still strong, correlation with peak frequency (PGLS: $n = 20$, $R^2 = 0.350$, $p = 0.006$; $n = 65$, $R^2 = 0.421$, $p = 0.001$, respectively; **Figure S5 & S6**). Species emitting broadband monoharmonic calls (“e”) presented the weakest allometric effect (PGLS: $n = 25$, $R^2 = 0.191$, $p = 0.024$; **Figure S7**). Only skull size of bats emitting broadband multiharmonic signals (“f”) did not show an allometric effect for peak frequency (PGLS: $n = 20$, $R^2 = 0.002$, $p = 0.867$). Only one species emits call type “g” (*i.e.*, *Myzopoda aurita*), and therefore, no statistical test was applied within this category.

Table 3. Size and shape (as Procrustes coordinates) variance explained by each call design (R^2) and statistical significance (p). Significance of the PGLS models reported in bold.

	n	Size		Shape	
		R ² -PGLS	p	R ² -PGLS	p
Narrowband, monoharmonic (c)	65	0.421	0.001	0.030	0.049
Narrowband, multiharmonic (d)	20	0.350	0.006	0.035	0.770
Short, broadband, monoharmonic (e)	25	0.191	0.024	0.071	0.033
Short, broadband, multiharmonic (f)	20	0.002	0.867	0.076	0.114
Constant frequency (h)	30	0.586	0.001	0.115	0.001

Shape and peak frequency

Peak frequency explained a small proportion of skull shape variance under the PGLS models. Peak frequency was significantly associated with skull shape within the complete dataset and within most ecological group’s sub-datasets (*i.e.*, diet, emission type and call design) (**Figure 2**).

Shapes of all 219 species significantly correlated with peak frequency under the OLS

model after accounting for size ($R^2 = 0.095$, $p = 0.001$). This correlation was less strong but still significant after phylogenetic correction ($R^2 = 0.015$, $p = 0.002$). The overall shape deformation suggested that species with higher peak frequencies had narrower rostra and shorter maxilla (*i.e.*, shorter nasal chamber area) and decreasing relative size of tympanic bullae (**Figure 4**).

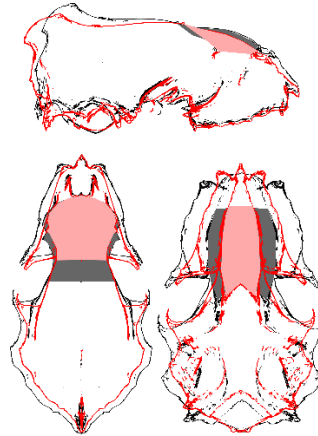


Figure 4. Shape deformations for all insectivorous bats computed on the predicted values extracted from PGLS models of shape predicted by peak frequency (as \log_{10} and size-corrected). The black and red outlines describe the species with lowest and highest peak frequency, respectively. Hard palate and rostrum highlighted in grey and pink, respectively.

When this association was explored by diet, skull shape of frugivorous bats presented the highest correlation with peak frequency (PGLS: $n = 21$, $R^2 = 0.154$, $p = 0.001$), while insectivorous species followed the overall pattern described above (PGLS: $n = 161$, $R^2 = 0.017$, $p = 0.002$). Other bats did not present a significant correlation with peak frequency (PGLS: $n = 37$, $R^2 = 0.028$, $p = 0.336$).

Frugivorous species emitting high peak frequency presented a shorter and narrower maxilla and a taller skull. The palate was shorter and wider, and the relative size of the tympanic bullae decreased for higher frequencies (**Figure 5**). This pattern was followed also by the highly specialised hard-fruit eaters *Ametrida centurio*, *Centurio senex* and *Sphaeronycteris toxophyllum*.

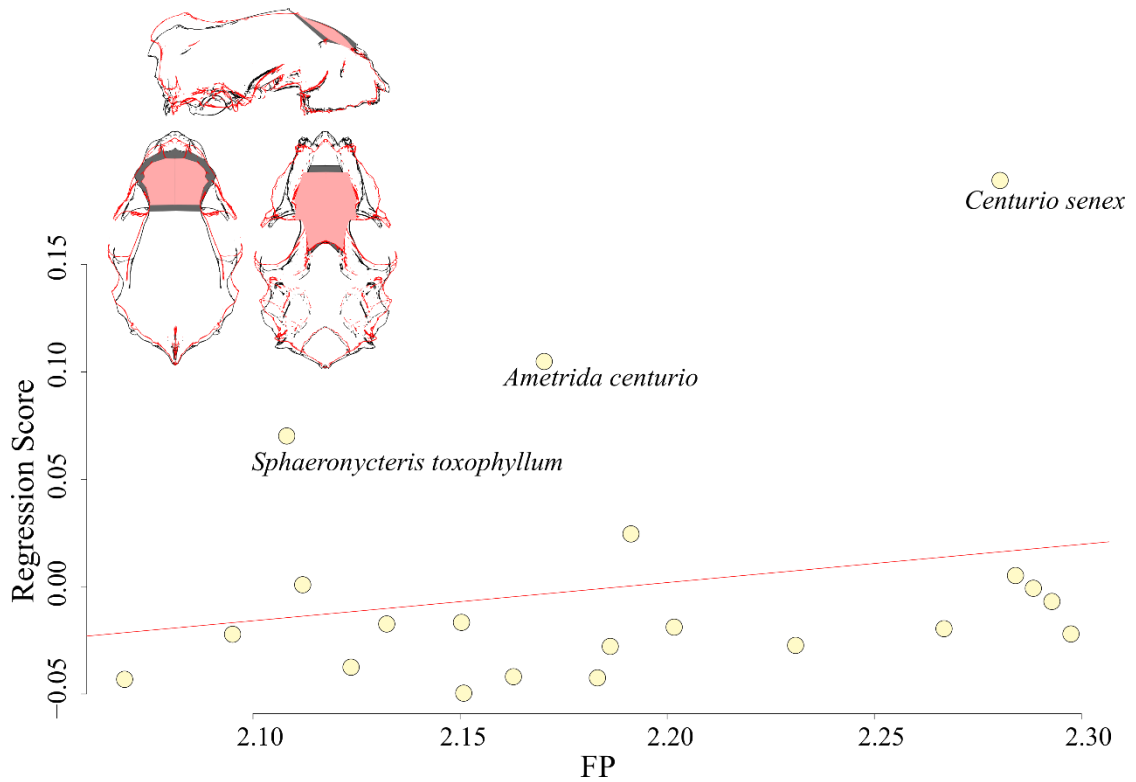


Figure 5. Plot of shape (as regression score) and peak frequency for frugivorous bats. Shape deformations or frugivorous bats ($n = 21$, Phyllostomidae) were computed on the predicted values extracted from the PGLS model of shape predicted by peak frequency (as \log_{10} and size-corrected, [FP]). The black and red outlines describe the species with the lowest and highest peak frequencies, respectively. Hard palate and rostrum highlighted in grey and pink, respectively.

I repeated the analyses within insectivorous bats after dividing species by emission type (*i.e.*, nasal or oral). As for size, oral emitters presented a weaker correlation between shape and peak frequency compared to nasal emitters (PGLS: $n = 120$, $R^2 = 0.020$, $p = 0.012$; $n = 41$, $R^2 = 0.067$, $p = 0.002$, respectively). In both groups of nasal emitters (*i.e.*, New and Old World), high frequencies were associated with narrower and shorter nasal chambers (**Figure 6A**).

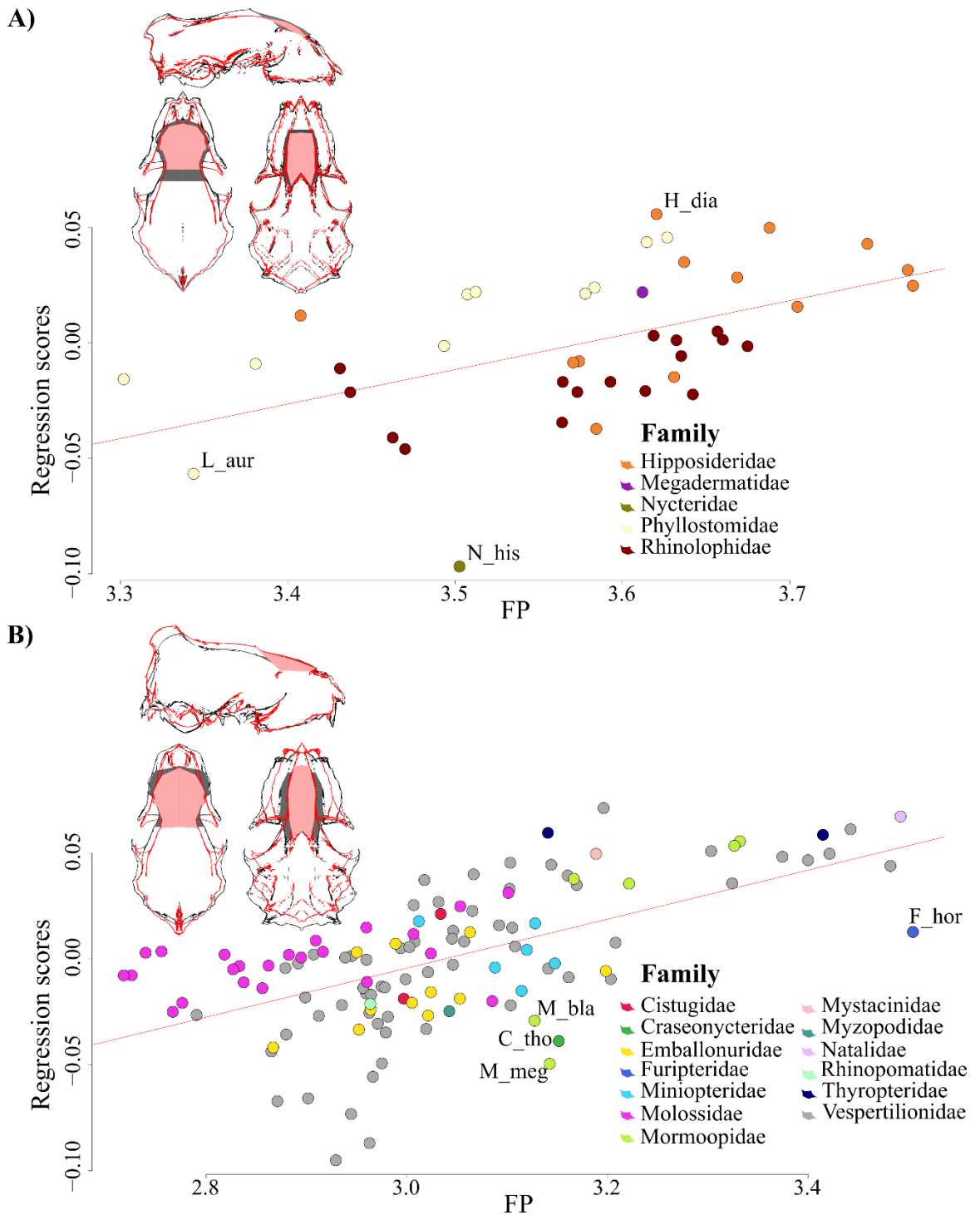


Figure 6. Plot of shape (as regression score) and peak frequency (\log_{10} transformed and size-corrected, [FP]) for insectivorous bats: nasal emitting species (**A**) and oral emitting species (**B**). Shape deformations were computed on the predicted values extracted from the PGLS models of shape predicted by peak frequency (as \log_{10} and size-corrected). The black and red outlines describe the species with the lowest and highest peak frequencies, respectively. Hard palate and rostrum highlighted in grey and pink, respectively. Labels indicate the outliers (nasal emitters: H_dia: *Hipposideros diadema*, N_his: *Nycteris hispida*, L_aur: *Lonchorhina aurita*; oral emitters: C_tho: *Craseonycteris thonglongyai*, F_hor: *Furipterus horrens*, M_meg: *Mormoops megalophylla*, M_bla: *Mormoops blainvillei*).

High frequencies were also associated with narrow palates in oral emitters, but the whole skull was elongated (palate and rostrum included; **Figure 6B**). Relative size of tympanic bullae decreased for higher frequencies in both nasal and oral emitters.

In Old World nasal emitters, peak frequency explained over 10% of skull shape variance under the PGLS model (PGLS: $n = 31$, $R^2 = 0.109$, $p = 0.001$; **Figure S8**). No separate test was conducted for the New World insectivorous species due to a small sample size ($n = 10$).

As for the size of mouth emitters, the relationship between shape and peak frequency varied in slope within families under the PGLS model (**Table S2**). Moreover, *Mormoops* species, *Furipterus horrens* and *Craseonycteris thonglongyai* largely deviated from the overall pattern of oral emitters (**Figure 6B**). Molossids showed a higher correlation between shape variables and peak frequency (PGLS: $n = 23$, $R^2 = 0.087$, $p = 0.011$) compared to the vespertilionids (PGLS: $n = 66$, $R^2 = 0.033$, $p = 0.021$). Family of Molossidae displayed a shorter but wider rostrum and a longer braincase for higher frequencies (**Figure S9**). In accordance with the deformation pattern of the oral emitters, Vespertilionidae species presented longer braincases and shorter rostra (but slightly longer palates), and smaller tympanic bullae (**Figure S10**).

Insectivorous species emitting echolocation calls with different structure showed differences in the patterns of association between skull shape and peak frequency (**Figure 2B** and **Table 3**). Specifically, nasal emitting bats producing constant frequency calls presented the highest correlation between shape and peak frequency (PGLS: $n = 30$, $R^2 = 0.115$, $p = 0.001$). Species emitting “c” signals showed a weaker but still significant correlation (PGLS: $n = 65$, $R^2 = 0.030$, $p = 0.049$). Skulls of species emitting “h” or “c” calls presented short rostrum for high peak frequency (**Figure S11** and **S12**, respectively). Species relying on broadband monoharmonic calls (“e”) showed a significant relationship between shape and peak frequency (PGLS: $n = 25$, $R^2 = 0.071$, $p = 0.033$). These species

presented narrow rostra (the length remained unvaried) and long palates for high frequencies (**Figure S13**). Finally, species emitting broadband and narrowband multiharmonic signals (*i.e.*, “f” and “d” calls) did not show a correlation between skull shape and peak frequency (PGLS: $n = 20$, $R^2 = 0.076$, $p = 0.114$; $n = 20$, $R^2 = 0.035$, $p = 0.770$; respectively).

Discussion

In this study, I obtained the first evidence that skull shape adaptations of insectivorous species to peak frequency are maintained across most of the ecological groups analyzed (except species with call design “e”: short, broadband, monoharmonic calls). Specifically, emission of high frequencies are associated with rostrum shortening and tympanic bulla shrinking. Skull morphology of constant frequency nasal emitters showed the strongest correlation with peak frequency, suggesting that a resonance effect is achieved with nasal chamber adjustment in both size and shape. Contrary to my prediction, functional demands linked to echolocation appear to strongly influence skull shape in frugivorous species despite their use of multiple sensory systems to locate food. As fruit-eaters evolved from an insectivore ancestor, the association between shape and frequencies might be evolutionary conservative. Conversely, echolocation parameters may still behave as an active evolutionary pressure on the skull shape of these species.

Palate orientation and head position

This study shows that oral emitters present wide palatal-basicranium angles (*i.e.*, palate elevated respect to the basicranium) suggesting that an upward tilted skull might promote effective sound projection throughout the mouth. In oral emitters, the projection of the sound is also probably facilitated by the upward position of the head during flight due to the sound pathway being perpendicular to the transverse axis of the mouth (Vanderelst *et*

al., 2015). I suggest that this configuration imposes different constraints on head muscles and bones of oral emitters with respect to nasal emitters, and can help explain the nature of the relationship between skull shape and peak frequency in this group (see below).

Ontogenetic studies have revealed that the orofacial complex of nasal emitting bats goes through different developmental stages compared to other mammals (Pedersen, 1998). In oral emitters, the orofacial complex rotates dorsally on the basicranium in a way that the head unfolds from the chest during pre-natal growth, similar to other non-echolocating mammals (Pedersen, 2000). Conversely, nasal emitting species do not rotate the palate dorsally: this anatomical configuration optimises the alignment of the nasal passage with the larynx (Pedersen, 2000). Therefore, the combination of head rotation, palate orientation, and head position during flight likely contributes to efficient sound projection from the mouth or the nose of echolocating species (**Figure 7**).

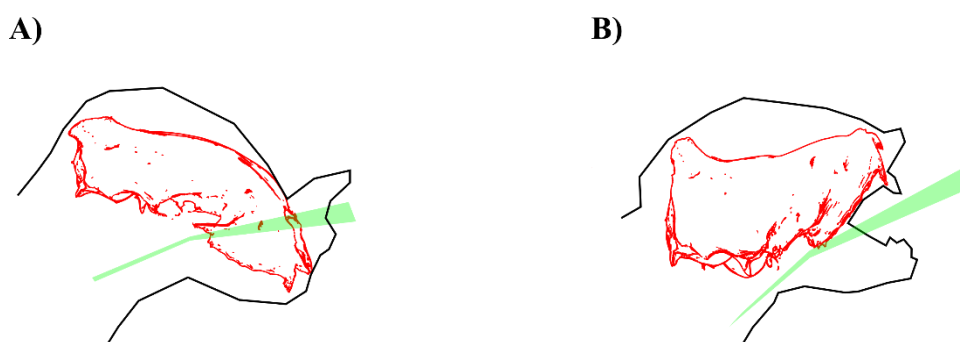


Figure 7. Head axis rotation (information obtained from Pedersen, 2000) and positioning during echolocation (information obtained from Vanderelst *et al.*, 2015) in nasal emitting species (**A**) and oral emitting species (**B**). In oral emitters, the basicranium-palatal plane is “tilted”.

Size and peak frequency

Peak frequency scales with body size in insectivorous species (Jones, 1999). Insectivorous species with small bodies produce high frequencies because of a physical acoustic

principle. In other words, short/thinner acoustic folds and smaller resonance structures produce higher frequencies. Furthermore, small body sizes increases manoeuvrability of flying animals and, as a consequence, hunting success in a cluttered environment (Norberg, 1986; Norberg & Rayner, 1987). High frequency sounds are advantageous in a cluttered environment as they reduce scatter echoes from the background (Denzinger & Schnitzler, 2013). Therefore, ecology and physical acoustics regulate the relationship between peak frequency and skull size.

In this study, even when non-insectivorous species were excluded from this sample, some species still deviated from the allometric pattern typical of their ecological category.

Deviation from the allometric relationship can be explained by different non-mutually exclusive hypotheses (Jacobs *et al.*, 2007). Species that deviate from the pattern either (i) exhibit specialised hunting strategies where larger skulls, and hence heavier bodies, are not disadvantageous (*i.e.*, gleaning and perch-hunting); (ii) adjust their frequencies range in relation to prey size (valid only for bats emitting low frequencies; *e.g.* Barclay, 1986); (iii) exhibit a sound emission that diverges from the acoustic detectability range of eared moths in order to increase their hunting success; or (iv) exhibit frequencies that show acoustic displacement to facilitate intraspecific communication success.

Within the nasal emitters in this study, *Macrophyllum macrophyllum* displayed smaller centroid size than predicted by its peak frequency. This species hunts on water and displays a very flexible hunting strategy: it can shift from aerial hawking to trawling (Weinbeer *et al.*, 2013). This flexibility in hunting behaviour potentially allowed for the evolution of low peak frequency, promoting niche specialization in order to avoid competition. Conversely, *H. diadema* showed a larger size than predicted by the peak frequency. This species has been previously indicated as a “partial carnivore” based on its morphological similarities to the other vertebrate eater species, even if no vertebrate material was found in faeces or stomach content (Pavey & Burwell, 1997). The species

typically hunts in bouts by perching to detect prey movement and then feeding on slow-moving preys captured in flight (Pavey & Burwell, 2000). The increment in the body size of *H. diadema* is likely to be the result of hunting specialization on slow prey (such as Coleoptera), which require less manoeuvrability during flight.

Different allometric slopes were identified within oral emitters. This suggests that even after removing the variance explained by the phylogenetic relatedness, species within the same family retain similar patterns. Molossidae presented the strongest allometric effect with only the greater naked bat (*C. torquatus*) deviating from the pattern (*i.e.*, larger skull size than predicted by the peak frequency). It has been proposed that morphological divergence in Molossidae bats is related to dietary specialization, specifically to prey hardness (Giménez & Giannini, 2016). *C. torquatus* is the largest aerial hawking insectivorous bats (~160 gr), and based on its skull morphology, it probably feeds on hard food (Heller, 1995). It is considered to be a fast flying species (Barclay & Brigham, 1991). Detection of small insects might be limited by a low frequency call (~24 KHz) as the wavelength might not be long enough to produce informative echoes (Pye, 1993). Therefore, *C. torquatus* might have evolved a higher frequency to detect prey that would otherwise not be detectable at a predicted frequency of 7 KHz (*i.e.*, predicted by its body size; Heller, 1995).

When all phyllostomids were analysed together, no significant relationship between skull size and peak frequency was detected (**Table S3**) in accordance with a previous study (Jones, 1999). The echolocation call structures of most of the phyllostomids suggest that they are gleaners (Schnitzler & Kalko, 2001) and they use additional sensorial cues to locate their food (*e.g.* vision, olfaction, and prey-generated acoustic cues; Surlykke *et al.*, 2013; Ripperger *et al.*, 2019). This would “relax” the allometric pressure of peak frequency since larger bodies would not be disadvantageous (Jacobs *et al.*, 2007). However, recent studies found that some insectivorous phyllostomids show aerial hawking behaviour,

suggesting that an exception for this family might exist (*e.g.* *M. macrophyllm* and *Lonchorhina aurita*; Weinbeer *et al.*, 2013; Gessinger *et al.*, 2019). A dataset with a larger sample of insectivorous phyllostomids should be analysed in order to confirm the allometric effect for this ecological group. Also, it has been hypothesized that noseleaf size might scale with peak frequency instead of skull size (Jakobsen *et al.*, 2012). This is particularly plausible for nasal emitting species considering that the sound diffracts from the nostrils and its acoustic properties (*e.g.* directionality) are influenced by the geometry of the channels and the “baffle” (effect produced by the noseleaf) (Zhuang & Müller, 2006; Feng *et al.*, 2012). Despite the valid theoretical framework, no correlation between noseleaf morphology and peak frequency has been detected yet in this family (Goudy-Trainor & Freeman, 2002).

In this study, I showed that the allometric effect of peak frequency differs in insectivorous species with different emission types and call designs. Specifically, adaptation of skull size to peak frequency was stronger for species producing constant frequency calls (call type “h”) and call type “c”, particularly within the Molossidae. These two groups of echolocators use the extreme range of frequencies: high frequencies within constant frequency species and low frequencies within the Molossidae. All species producing call type “h” are nasal emitters, except for *P. parnellii*. These species experience a resonance effect when the sound travels inside their nasal chambers: therefore, size adjustments are fundamental to “tune” the cavity and enhance the correct frequency (Armstrong & Coles, 2007; Jacobs *et al.*, 2014). The resonance effect is not relevant for mouth emitters. Hence, it seems likely that peak frequency coevolved with size to increase niche partitioning between ecologically similar species within the Molossidae.

Insectivorous species emitting call type “e” (*i.e.*, Vespertilionidae and *Furipterus horrens*) showed the lowest correlation between size and peak frequency. These species emit in the medium-high frequency range (from ~32 KHz of *Scotomanes ornatus* to ~160 KHz of *F.*

horrens, in this sample) and they display different hunting strategies (Denzinger & Schnitzler, 2013). It is worth noting that “e” calls are characterised by a long sweep of frequencies and the energy of the call is more equally distributed along this sweep than in other call types. Therefore, the size of the echolocator system (*i.e.*, skull and echolocating muscles) might be less influenced by one specific frequency within this group. Conversely, in the skull shape of these species I found a relatively strong correlation with peak frequency (see next section).

Shape and peak frequency

The relative strength of association between shape and echolocation followed a similar pattern as identified in the correlation between size and peak frequency (with exception for frugivorous and call type “e” insectivorous species).

In the current study, I confirmed that skull shape of insectivorous species is influenced by peak frequency in a taxonomically diverse sample ($n = 161$). A shorter rostrum (*i.e.*, maxilla) was associated with high frequencies in all ecological groups. The only exception was for species emitting call type “e”; here, peak frequency variation was not associated with relative rostrum length but with rostrum width. Furthermore, in this study, the tympanic bulla was proportionally bigger for species emitting lower peak frequency across all taxa when size was removed. Large tympanic cavities are believed to be an adaptation towards improving low-frequency hearing in terrestrial mammals (Webster, 1966). In bats, almost all components of the middle ear (*i.e.*, tympanic membrane, pars flaccida and stapes) are smaller for species emitting higher frequencies (Henson 1961). Proportionally smaller bullae for species emitting higher frequencies might indicate further adaptation towards acuity in certain frequency ranges.

I suggest that two mechanisms can lead to the rostrum adaptation to peak frequency and therefore two hypotheses can be formulated: (i) a physical acoustic principle, such as

resonance effect or harmonic filtering, drives the direct co-evolution between skull shape and frequency emitted (physical acoustic hypothesis) or (ii) skull shape adaptations to peak frequency are the indirect outcome of selection forces exerted by echolocating muscles (mechanical hypothesis). Short rostrum for high frequency indicates that nasal chamber shape might influence the resonance effect in nasal emitters (New and Old World). Therefore, acoustic dynamics explain the nasal emitting species' (particularly in call "h" species) adaptation of nasal chamber shape to peak frequency. However, rostrum adaptation to echolocating muscles, and thus indirectly to peak frequency, might be a more appropriate explanation in the mouth emitters' case. In this case, echolocation parameters (*e.g.* peak frequency) are adapted to skull morphology within an integrated and complex system where other functional demands are also involved. Position and size of laryngeal muscles might have strong consequences on the shape of the skull. For example, Plotsky *et al.* (2016) showed that larynx repositioning is associated with cranio-facial variation in dogs. Insectivorous bats evolved big and fast laryngeal muscles, in particular cricothyroid muscle, to control tension and oscillation of the vocal folds during generation of ultrasonic sounds (Elemans *et al.*, 2011). It is possible that differences in the muscles of the larynx, which are under direct evolutionary pressure due to echolocation, lead to rearrangements of skull shape features. A comparative morphological study of the bat phonetic system and an assessment of its covariation with skull anatomy has the potential to elucidate such hypotheses.

Similar to size, results suggest that the functional demands of echolocation in nasal emitting species might be greater than oral emitters. As predicted, call type "h" emitting species showed the highest association between peak frequency and shape indicating that relative size of the rostrum (and therefore nasal chamber) is adapted to further increase the resonance effect.

Skull shape of molossids showed the highest association between morphology and echolocation within the oral emitters. These species emit a mixture of frequency modulated and quasi-constant frequency calls (*i.e.*, call type “c”), and, with the exception of *Molossops temminckii*, they are all aerial hawking hunters in open space (Schnitzler & Kalko, 2001). There are some parallelisms with the case of rhinolophids where all the species present similar diet, call design (*i.e.*, call type “h”) and hunting strategy (*i.e.*, narrow space flutter detecting forager) within the family (Denzinger & Schnitzler, 2013). Therefore, the relationship between peak frequency and skull shape can be easily detected in these families rather than in vespertilionids that evolved different hunting strategies (therefore the relationship between shape and peak frequency potentially has different patterns relative to hunting strategy). This is supported by the fact that echolocation parameters correlates with wing morphology in Vespertilionidae species (Thiagavel *et al.*, 2017) but not in Rhinolophidae as they have similar wing design (Jacobs & Bastian, 2018). Contrary to my expectations, skull shape of monoharmonic frequency modulation emitting species (call type “e”; some Vespertilionidae and *F. horrens*) were evolutionarily associated to peak frequency. This is particularly surprising given that frequency modulation calls are characterised by a long frequency sweep that makes parameterisation challenging and potentially less stable. Within this pattern, *Myotis* species showed different skull shapes for similar emitted frequencies suggesting that peak frequency might not have co-evolved with skull shape in these species. Different hunting strategies have evolved in this genus in order to avoid food competition (*e.g.* Arlettaz, 1999; Siemers & Schnitzler, 2004). Therefore environmental and prey specialization might exert a stronger evolutionary pressure on skull morphology than peak frequency.

My prediction that frugivorous bats would not present a correlation between skull shape and echolocation was rejected. In this species, I found that cranial shape, in particular rostrum relative size and braincase height, is evolutionarily associated to peak frequency.

Most frugivorous bats, similar to blood, nectar and vertebrate eaters, rely on both active echolocation and other sensory strategies, but it is still unclear to what extent the shift between strategies is flexible and if there are species that rely on one sensory system only. Even if a trade-off between vision and echolocation has been hypothesised for phyllostomids (Thiagavel *et al.*, 2018), there is currently no evidence of nasal chamber morphological adaptations to olfactory ability (Eiting *et al.*, 2014). Whether morphological adaptations of nasal passages to echolocation demands is stronger, or simply more evolutionarily resilient, than olfactory ones still need to be investigated. Both insectivorous and frugivorous nasal emitters (including call “h” emitters) presented short rostra for high frequencies suggesting that decreased relative volume of nasal passages is an adaptation to high frequency emission, regardless of the diet or phylogenetic history. Nevertheless, it is unlikely that skull adaptations to peak frequency in frugivorous species allow for the same magnitude of the resonance effect as in call “h” emitting species. Indeed, most Phyllostomidae species shift energy between different harmonics of the broadband call (call “f”; *e.g.* Murray *et al.*, 2001) challenging the acoustical tuning of the nasal passages. Expanding the “mechanical hypothesis”, the association of peak frequency to skull shape in frugivorous species might result from the direct adaptation of peak frequency to noseleaf shape (that behaves as an acoustic baffle), and as a consequence, to the bony support of the noseleaf (*i.e.*, maxilla). Studies focusing on comparative anatomies of vocal muscles, larynx position and noseleaf shape can provide valuable insights into the topic.

In conclusion, these analyses have provided an improved understanding of the factors influencing bat skull evolution. Skull size is influenced by diet, and a strong allometric effect exists on the peak frequency of insectivorous bats. Different magnitudes in the allometric effect were found between families and emission types (*i.e.*, oral or nasal). Diet and emission type significantly correlated with skull shape variation. Skull shape is optimised to emit peak frequency in insectivorous and frugivorous bats, but different

ecological groups (*i.e.*, emission type and call design) showed different magnitudes of association. The overall patterns of association between shape and peak frequency seem consistent: species emitting high peak frequency displayed shorter rostra and small tympanic bullae relative to their skull size. A detailed quantification of foraging guilds and habitat complexity might further clarify the evolutionary patterns of skull morphology and echolocation within some bat families (*e.g.* Vespertilionidae).

References

- Adams, D.C. 2014. A Generalized K Statistic for Estimating Phylogenetic Signal from Shape and Other High-Dimensional Multivariate Data. *Syst. Biol.* **63**: 685–697.
- Adams, D.C. & Collyer, M.L. 2015. Permutation tests for phylogenetic comparative analyses of high-dimensional shape data: What you shuffle matters. *Evolution (N. Y.)* **69**: 823–829.
- Adams, D.C. & Collyer, M.L. 2018. Phylogenetic ANOVA: Group-clade aggregation, biological challenges, and a refined permutation procedure. *Evolution (N. Y.)* **72**: 1204–1215.
- Adams, D.C. & Felice, R.N. 2014. Assessing Trait Covariation and Morphological Integration on Phylogenies Using Evolutionary Covariance Matrices. *PLoS One* **9**: e94335.
- Adams, D.C. & Otárola-Castillo, E. 2013. geomorph: an r package for the collection and analysis of geometric morphometric shape data. *Methods Ecol. Evol.* **4**: 393–399.
- Arbour, J.H., Curtis, A.A. & Santana, S.E. 2019. Signatures of echolocation and dietary ecology in the adaptive evolution of skull shape in bats. *Nat. Commun.* **10**: 2036.
- Arlettaz, R. 1999. Habitat selection as a major resource partitioning mechanism between the two sympatric sibling bat species *Myotis myotis* and *Myotis blythii*. *J. Anim. Ecol.* **68**: 460–471.
- Armstrong, K.N. & Coles, R.B. 2007. Echolocation Call Frequency Differences Between Geographic Isolates of *Rhinonicteris Aurantia* (Chiroptera: Hipposideridae): Implications of Nasal Chamber Size. *J. Mammal.* **88**: 94–104.
- Barclay, R.M.R. 1986. The echolocation calls of hoary (*Lasiurus cinereus*) and silver-haired (*Lasionycteris noctivagans*) bats as adaptations for long- versus short-range foraging strategies and the consequences for prey selection. *Can. J. Zool.* **64**: 2700–2705.
- Barclay, R.M.R. & Brigham, R.M. 1991. Prey detection, dietary niche breadth, and body size in bats: why are aerial insectivorous bats so small? *Am. Soc. Nat.* **137**: 693–703.
- Barroso, C., Cranford, T.W. & Berta, A. 2012. Shape analysis of odontocete mandibles: Functional and evolutionary implications. *J. Morphol.* **273**: 1021–1030.
- Blomberg, S.P., Garland, T. & Ives, A.R. 2003. Testing for phylogenetic signal in comparative data: behavioral traits are more labile. *Evolution (N. Y.)* **57**: 717–745.

- Bookstein, F.L. 1989. "Size and Shape": A Comment on Semantics. *Syst. Zool.* **38**: 173–180.
- Cardini, A. & Polly, P.D. 2013. Larger mammals have longer faces because of size-related constraints on skull form. *Nat. Commun.* **4**: 2458.
- Collyer, M.L. & Adams, D.C. 2018. RRPP: An r package for fitting linear models to high-dimensional data using residual randomization. *Methods Ecol. Evol.* **9**: 1772–1779.
- Denzinger, A. & Schnitzler, H. 2013. Bat guilds , a concept to classify the highly diverse foraging and echolocation behaviors of microchiropteran bats. *Front. Zool.* **4**: 1–15.
- Dumont, E.R., Herrel, A., Medellín, R.A., Vargas-Contreras, J.A. & Santana, S.E. 2009. Built to bite: cranial design and function in the wrinkle-faced bat. *J. Zool.* **279**: 329–337.
- Eiting, T.P., Perot, J.B. & Dumont, E.R. 2014. How much does nasal cavity morphology matter? Patterns and rates of olfactory airflow in phyllostomid bats. *Proc. R. Soc. B Biol. Sci.* **282**: 20142161–20142161.
- Elemans, C.P.H., Mead, A.F., Jakobsen, L. & Ratcliffe, J.M. 2011. Superfast Muscles Set Maximum Call Rate in Echolocating Bats. *Science* **333**: 1885–1888.
- Felsenstein, J. 1985. Phylogenies and the Comparative Method. *Am. Nat.* **125**: 1–15.
- Feng, L., Gao, L., Lu, H. & Müller, R. 2012. Noseleaf Dynamics during Pulse Emission in Horseshoe Bats. *PLoS One* **7**: e34685.
- Fenton, M.B. & Ratcliffe, J.M. 2017. Sensory biology: Bats united by cochlear development. *Nat. Ecol. Evol.* **1**: 46.
- Figuerido, B., Tseng, Z.J. & Martín-Serra, A. 2013. Skull shape evolution in durophagous carnivorans. *Evolution (N. Y.)* **67**: 1975–1993.
- Freckleton, R.P. 2009. The seven deadly sins of comparative analysis. *J. Evol. Biol.* **22**: 1367–1375.
- Gessinger, G., Gonzalez-Terrazas, T.P., Page, R.A., Jung, K. & Tschapka, M. 2019. Unusual echolocation behaviour of the common sword-nosed bat *Lonchorhina aurita*: an adaptation to aerial insectivory in a phyllostomid bat? *R. Soc. Open Sci.* **6**: 182165.
- Giacomini, G., Scaravelli, D., Herrel, A., Veneziano, A., Russo, D. & Brown, R.P. 2019. 3D photogrammetry of bat skulls: perspectives for macro-evolutionary analyses. *J. Evol. Biol.* **in press**.
- Giménez, A.L. & Giannini, N.P. 2016. Morphofunctional segregation in Molossid bats (Chiroptera: Molossidae) from the South American southern cone. *Hystrix, Ital. J. Mammal.* **27**.
- Goudy-Trainor, A. & Freeman, P.W. 2002. Call Parameters and Facial Features in Bats: A Surprising Failure of form Following Function. *Acta Chiropterologica* **4**: 1–16.
- Griffin, D.R. 1958. *Listening in the dark: The acoustic orientation of bats and men*. Yale Univer. Press, Oxford, England.
- Heller, K.G. 1995. Echolocation and body size in insectivorous bats: the case of the giant naked bat *Cheiromeles torquatus* (Molossidae). *Le Rhinolophe* **11**: 27–38.
- IUCN. 2019. The IUCN Red List of Threatened Species. Version 2019-2. <http://www.iucnredlist.org>. Downloaded on 30 July 2019.
- Jacobs, D.S., Barclay, R.M.R. & Walker, M.H. 2007. The allometry of echolocation call frequencies of insectivorous bats: why do some species deviate from the pattern?

Oecologia **152**: 583–594.

- Jacobs, D.S. & Bastian, A. 2018. High Duty Cycle Echolocation May Constrain the Evolution of Diversity within Horseshoe Bats (Family: Rhinolophidae). *Diversity* **10**: 85.
- Jacobs, D.S., Bastian, A. & Bam, L. 2014. The influence of feeding on the evolution of sensory signals: A comparative test of an evolutionary trade-off between masticatory and sensory functions of skulls in southern African Horseshoe bats (Rhinolophidae). *J. Evol. Biol.* **27**: 2829–2840.
- Jakobsen, L., Ratcliffe, J.M. & Surlykke, A. 2012. Convergent acoustic field of view in echolocating bats. *Nature* **493**: 93.
- Jones, G. 1999. Scaling of echolocation call parameters in bats. *J. Exp. Biol.* **202**: 3359–3367.
- Jones, G. & Teeling, E. 2006. The evolution of echolocation in bats. *Trends Ecol. Evol.* **21**: 149–156.
- Loy, A., Cataudella, S. & Corti, M. 1996. Shape Changes during the Growth of the Sea Bass, *Dicentrarchus labrax* (Teleostea: Perciformes), in Relation to Different Rearing Conditions BT - Advances in Morphometrics. In: (L. F. Marcus, M. Corti, A. Loy, G. J. P. Naylor, & D. E. Slice, eds), pp. 399–405. Springer US, Boston, MA.
- Majid, A. & Kruspe, N. 2018. Hunter-Gatherer Olfaction Is Special. *Curr. Biol.* **28**: 409–413.e2.
- May-Collado, L.J., Agnarsson, I. & Wartzok, D. 2007. Reexamining the relationship between body size and tonal signals frequency in whales: a comparative approach using a novel phylogeny. *Mar. Mammal Sci.* **23**: 524–552.
- Murray, K.L., Robbins, L.W. & Britzke, E.R. 2001. Variation in Search-Phase Calls of Bats. *J. Mammal.* **82**: 728–737.
- Norberg, U.M. 1986. Evolutionary Convergence in Foraging Niche and Flight Morphology in Insectivorous Aerial-Hawking Birds and Bats. *Ornis Scand. (Scandinavian J. Ornithol.)* **17**: 253–260.
- Norberg, U.M. & Rayner, J.M.V. 1987. Ecological Morphology and Flight in Bats (Mammalia; Chiroptera): Wing Adaptations, Flight Performance, Foraging Strategy and Echolocation. *Philos. Trans. R. Soc. Lond. B. Biol. Sci.* **316**: 335–427.
- Pavey, C.R. & Burwell, C.J. 2000. Foraging ecology of three species of hipposiderid bats in tropical rainforest in north-east Australia. *Wildl. Res.* **27**: 283–287.
- Pavey, C.R. & Burwell, C.J. 1997. The diet of the diadem leaf-nosed bat *Hipposideros diadema*: confirmation of a morphologically-based prediction of carnivory. *J. Zool.* **243**: 295–303.
- Pedersen, S.C. 1998. Morphometric Analysis of the Chiropteran Skull with Regard to Mode of Echolocation. *J. Mammal.* **79**: 91–103.
- Pedersen, S.C. 2000. Skull growth and the acoustical axis of the head in bats. In: *Ontogeny, functional ecology, and evolution of bats* (R. A. Adams & S. C. Pedersen, eds), p. 174:213. Cambridge University Press, New York.
- Pennell, M.W., Eastman, J.M., Slater, G.J., Brown, J.W., Uyeda, J.C., FitzJohn, R.G., *et al.* 2014. geiger v2.0: an expanded suite of methods for fitting macroevolutionary models to phylogenetic trees. *Bioinformatics* **30**: 2216–2218.
- Plotsky, K., Rendall, D., Chase, K. & Riede, T. 2016. Cranio-facial remodeling in

- Pye, J.D. 1993. Is fidelity futile? The “true” signal is illusory, especially with ultrasound. *Bioacoustics* **4**: 271–286.
- domestic dogs is associated with changes in larynx position. *J. Anat.* **228**: 975–983.
- R Core Team 2019. R: A language and environment for statistical computing. R Foundation for Statistical Computing, Vienna, Austria. URL <https://www.R-project.org/>.
- Revell, L.J. 2012. phytools: an R package for phylogenetic comparative biology (and other things). *Methods Ecol. Evol.* **3**: 217–223.
- Ripperger, S.P., Rehse, S., Wacker, S., Kalko, E.K.V., Schulz, S., Rodriguez-Herrera, B., *et al.* 2019. Nocturnal scent in a “bird-fig”: a cue to attract bats as additional dispersers? *bioRxiv* 418970.
- Rohlf, F.J. 2007. Comparative methods for the analysis of continuous variables: geometric interpretations. *Evolution (N. Y.)* **55**: 2143–2160.
- Schnitzler, H.-U. & Kalko, E.K.V. 2001. Echolocation by Insect-Eating Bats. *Bioscience* **51**: 557–569.
- Shi, J.J. & Rabosky, D.L. 2015. Speciation dynamics during the global radiation of extant bats. *Evolution (N. Y.)* **69**: 1528–1545.
- Siemers, B.M., Kalko, E.K.V. & Schnitzler, H.U. 2001. Echolocation behavior and signal plasticity in the Neotropical bat *Myotis nigricans* (Schinz, 1821) (Vespertilionidae): A convergent case with European species of *Pipistrellus*? *Behav. Ecol. Sociobiol.* **50**: 317–328.
- Siemers, B.M. & Schnitzler, H.-U. 2004. Echolocation signals reflect niche differentiation in five sympatric congeneric bat species. *Lett. to Nat.* **429**: 657–661.
- Surlykke, A., Jakobsen, L., Kalko, E.K.V. & Page, R. 2013. Echolocation intensity and directionality of perching and flying fringe-lipped bats, *Trachops cirrhosus* (Phyllostomidae). *Front. Physiol.* **4**: 1–9.
- Thiagavel, J., Cechetto, C., Santana, S.E., Jakobsen, L., Warrant, E.J. & Ratcliffe, J.M. 2018. Auditory opportunity and visual constraint enabled the evolution of echolocation in bats. *Nat. Commun.* **9**: 98.
- Thiagavel, J., Santana, S.E. & Ratcliffe, J.M. 2017. Body Size Predicts Echolocation Call Peak Frequency Better than Gape Height in Vespertilionid Bats. *Sci. Rep.* **7**: 828.
- Vanderelst, D., Peremans, H., Razak, N.A., Verstraelen, E. & Dimitriadis, G. 2015. The Aerodynamic Cost of Head Morphology in Bats: Maybe Not as Bad as It Seems. *PLoS One* **10**: e0118545.
- Veselka, N., McErlain, D.D., Holdsworth, D.W., Eger, J.L., Chhem, R.K., Mason, M.J., *et al.* 2010. A bony connection signals laryngeal echolocation in bats. *Nature* **463**: 939–942.
- Wang, Z., Zhu, T., Xue, H., Fang, N., Zhang, J., Zhang, L., *et al.* 2017. Prenatal development supports a single origin of laryngeal echolocation in bats. *Nat. Ecol. & Evol.* **1**: 21.
- Webster, D.B. 1966. Ear Structure and Function in Modern Mammals. *Am. Zool.* **6**: 451–466. Oxford University Press.
- Weinbeer, M., Kalko, E.K.V. & Jung, K. 2013. Behavioral flexibility of the trawling long-legged bat, *Macrophyllum macrophyllum* (Phyllostomidae). *Front. Physiol.* **4**: 342.
- Wilson, D.E. & Reeder, D.M. 2005. *Mammal Species of the World: A Taxonomic and*

Geographic Reference, 3rd ed. (D. E. Wilson & D. M. Reeder, eds). The John Hopkins University Press, Baltimore.

Wu, J., Jiao, H., Simmons, N.B., Lu, Q. & Zhao, H. 2018. Testing the sensory trade-off hypothesis in New World bats. *Proc. R. Soc. B Biol. Sci.* **285**: 20181523.

Zhuang, Q. & Müller, R. 2006. Noseleaf Furrows in a Horseshoe Bat Act as Resonance Cavities Shaping the Biosonar Beam. *Phys. Rev. Lett.* **97**: 218701.

Supplementary Information

Supplementary Tables

Table S1. Shape (as Procrustes Coordinates) variance explained by each categorical variable (R^2) and statistic significance (p) for 219 echolocating bat species. Significance of the PGLS models reported in bold.

	R ² -OLS	p	R ² -PGLS	p
Emission type	0.337	0.001	0.042	0.001
Call design	0.325	0.001	0.065	0.014
Diet category	0.165	0.002	0.069	0.018
Angle	0.218	0.001	0.070	0.001

Table S2. Procrustes Anova table with phylogenetic correction (PGLS) on shape of oral emitters (n = 120). Peak frequency was size-corrected (corr.FP) in order to remove the allometric effect of size (Blomberg *et al.*, 2003). Note the high interaction between size-corrected peak frequency and family.

	Df	SS	MS	Rsq	F	Z	Pr(>F)
corr.FP	1	0.0007	0.0007	0.0167	2.4948	2.3808	0.013
Family	12	0.0038	0.0003	0.0931	1.1571	0.6708	0.208
corr.FP:Family	6	0.0089	0.0015	0.2199	5.4689	5.0147	0.001
Residuals	100	0.0272	0.0003	0.6703			
Total	119	0.0406					

Table S3. Anova for skull size of phyllostomids (n = 59). No correlation was found with peak frequency (FP) when accounting for phylogeny (PGLS).

	Df	SS	MS	Rsq	F	Z	Pr(>F)
FP	1	0.0005	0.0005	0.0201	1.1676	0.6328	0.29
Residuals	57	0.0227	0.0004	0.9799			
Total	58	0.0232					

Supplementary Figures

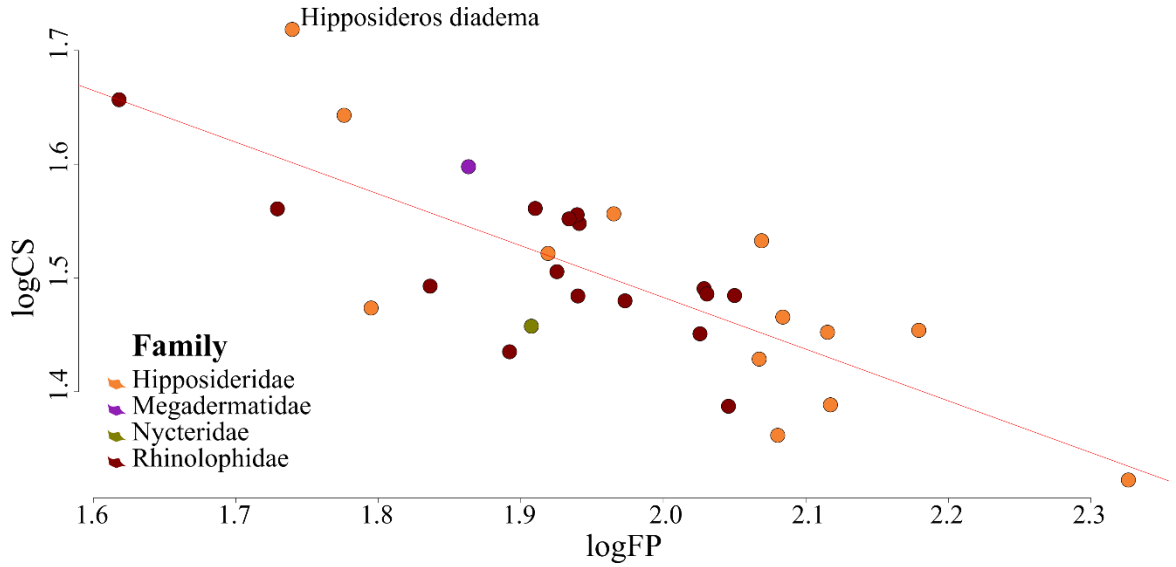


Figure S1. Allometric effect on peak frequency for Old World nasal emitting species. The graph represents the correlation under PGLS model of log₁₀ transformed centroid size (logCS) and log₁₀ transformed peak frequency (logFP).

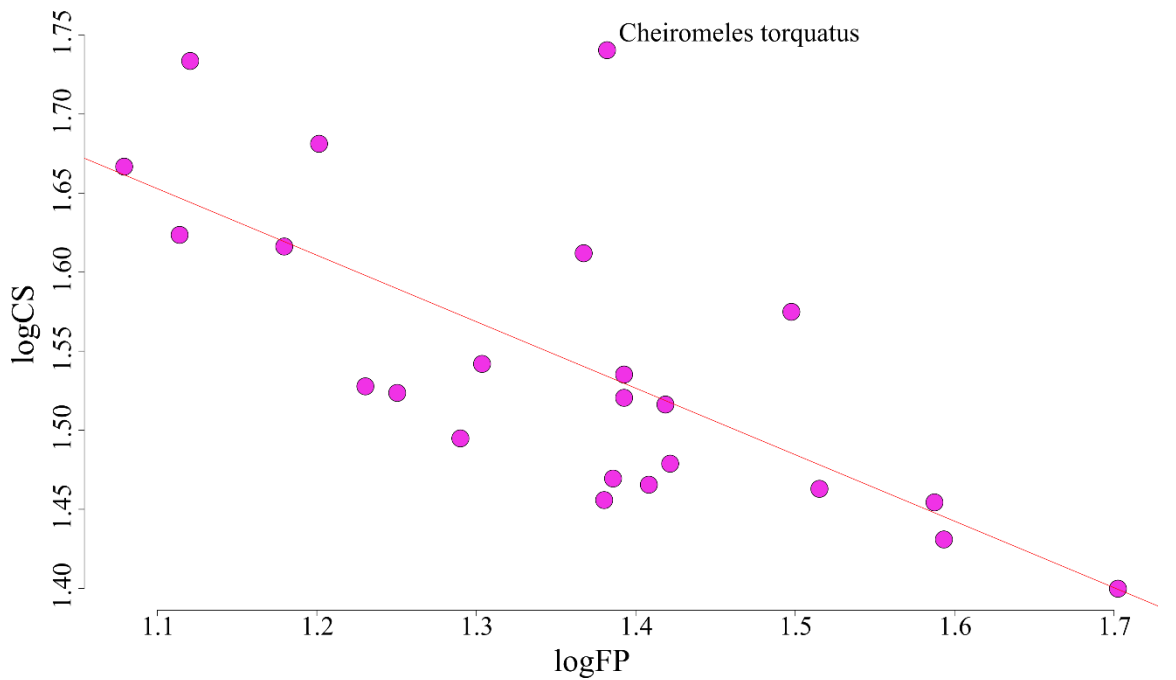


Figure S2. Allometric effect on peak frequency for species from the Molossidae family. The graph represents the correlation under PGLS model of log₁₀ transformed centroid size (logCS) and log₁₀ transformed peak frequency (logFP).

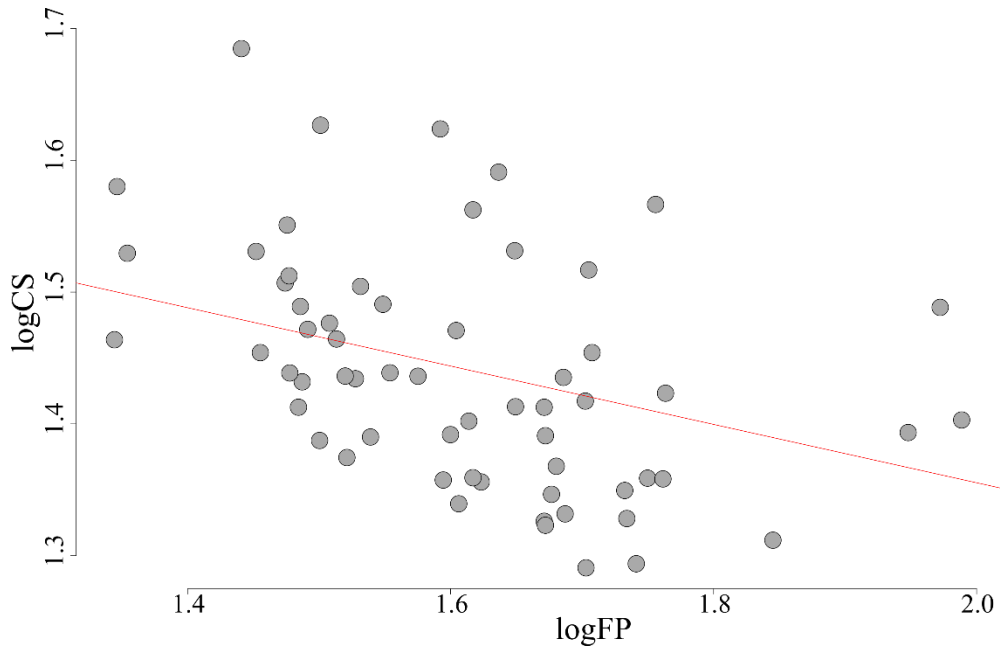


Figure S3. Allometric effect on peak frequency for species from the Vespertilionidae family. The graph represents the correlation under PGLS model of log₁₀ transformed centroid size (logCS) and log₁₀ transformed peak frequency (logFP).

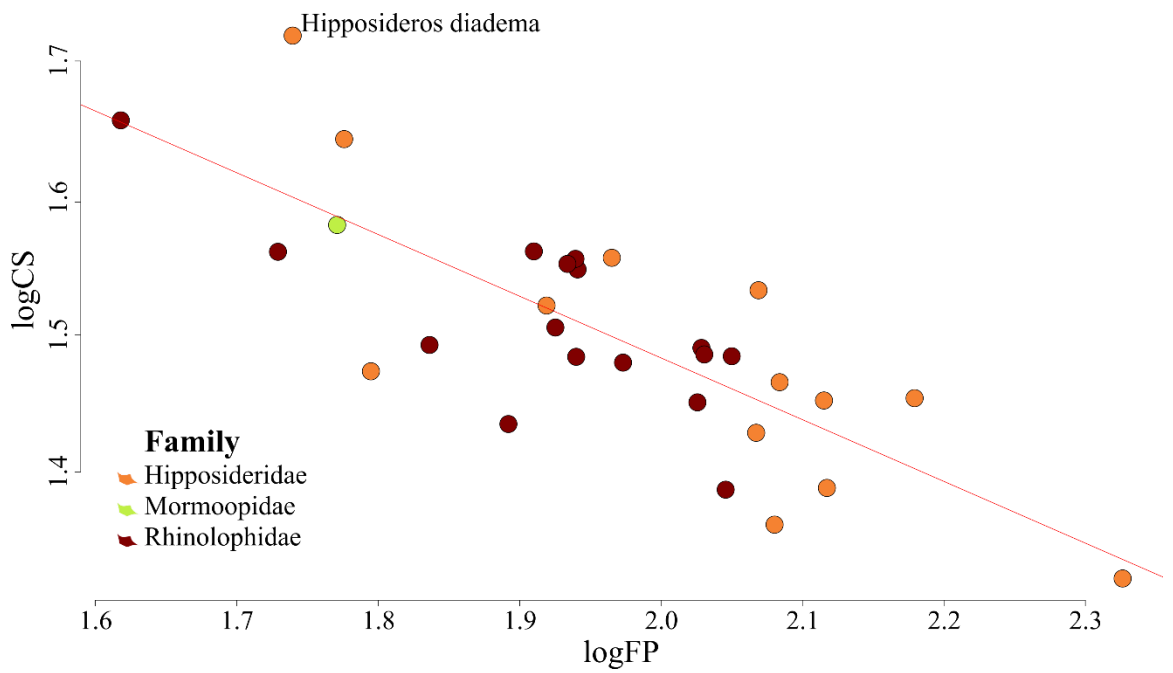


Figure S4. Allometric effect on peak frequency for bat species emitting call type "h" (*i.e.*, constant frequency calls). The graph represents the correlation under PGLS model of log₁₀ transformed centroid size (logCS) and log₁₀ transformed peak frequency (logFP).

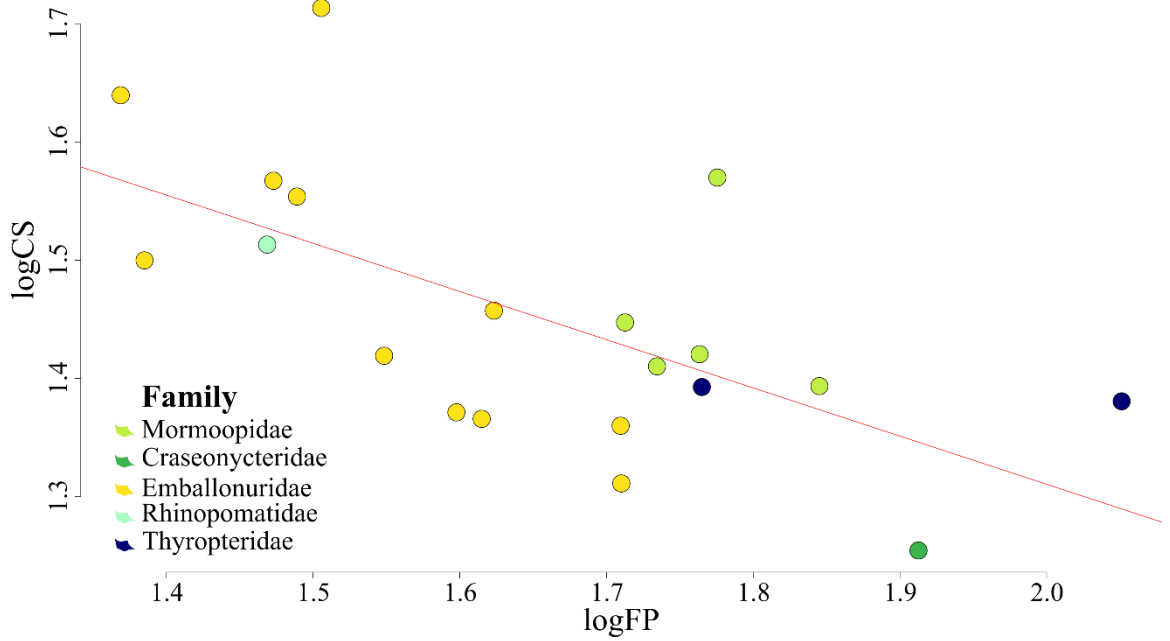


Figure S5. Allometric effect on peak frequency for bat species emitting call type “d” (*i.e.*, narrowband, multiharmonic calls). The graph represents the correlation under PGLS model of \log_{10} transformed centroid size (logCS) and \log_{10} transformed peak frequency (logFP).

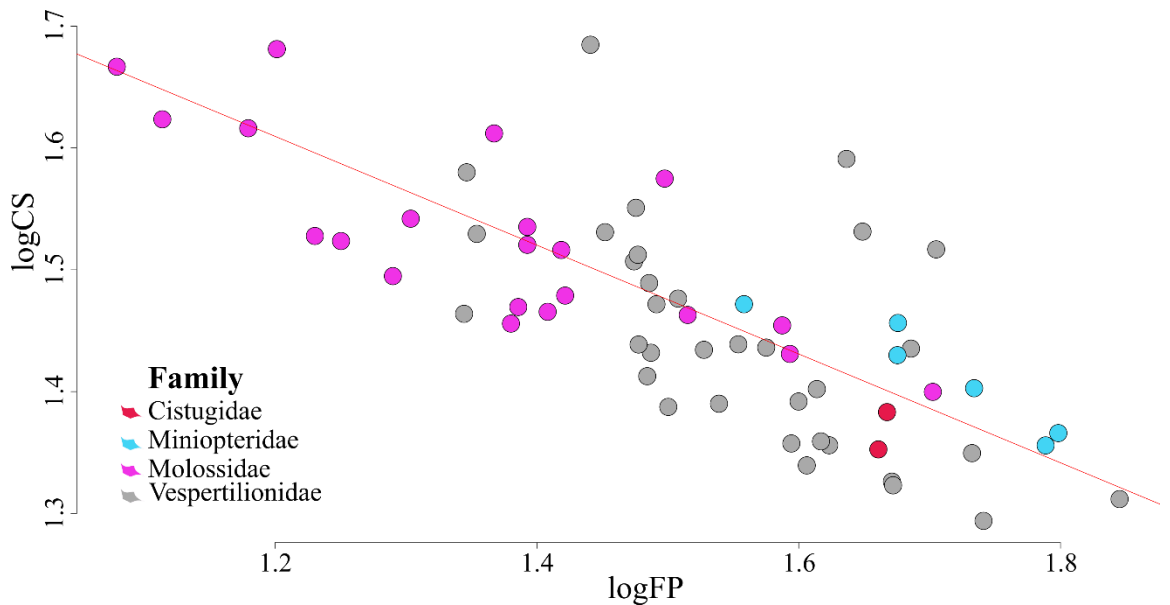


Figure S6. Allometric effect on peak frequency for bat species emitting call type “c” (*i.e.*, narrowband, monoharmonic calls). The graph represents the correlation under PGLS model of \log_{10} transformed centroid size (logCS) and \log_{10} transformed peak frequency (logFP).

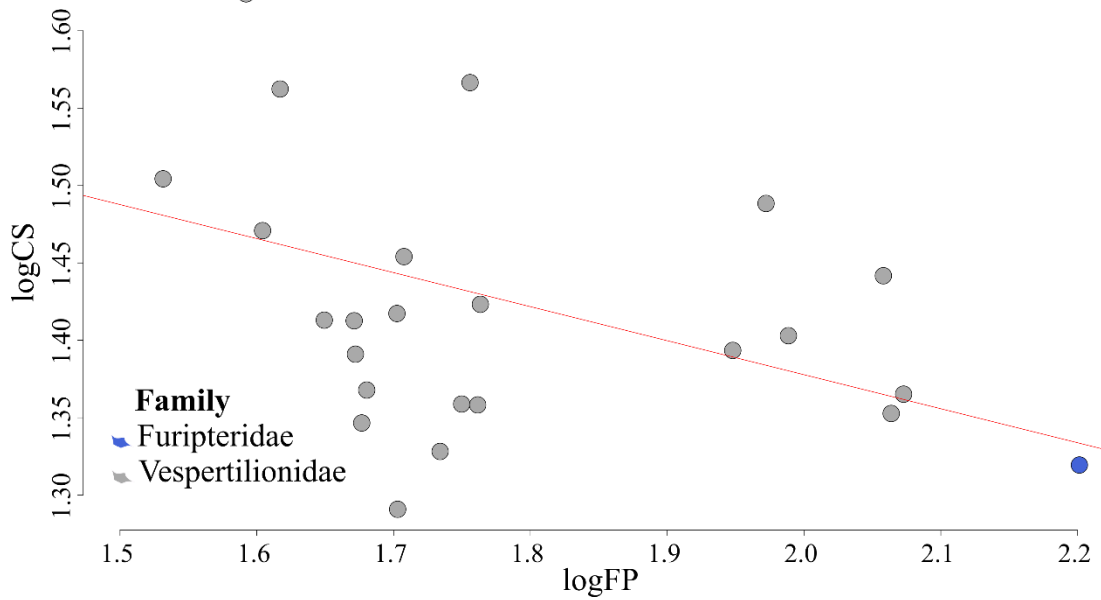


Figure S7. Allometric effect on peak frequency for bat species emitting call type “e” (*i.e.*, broadband, monoharmonic calls). The graph represents the correlation under PGLS model of \log_{10} transformed centroid size (logCS) and \log_{10} transformed peak frequency (logFP).

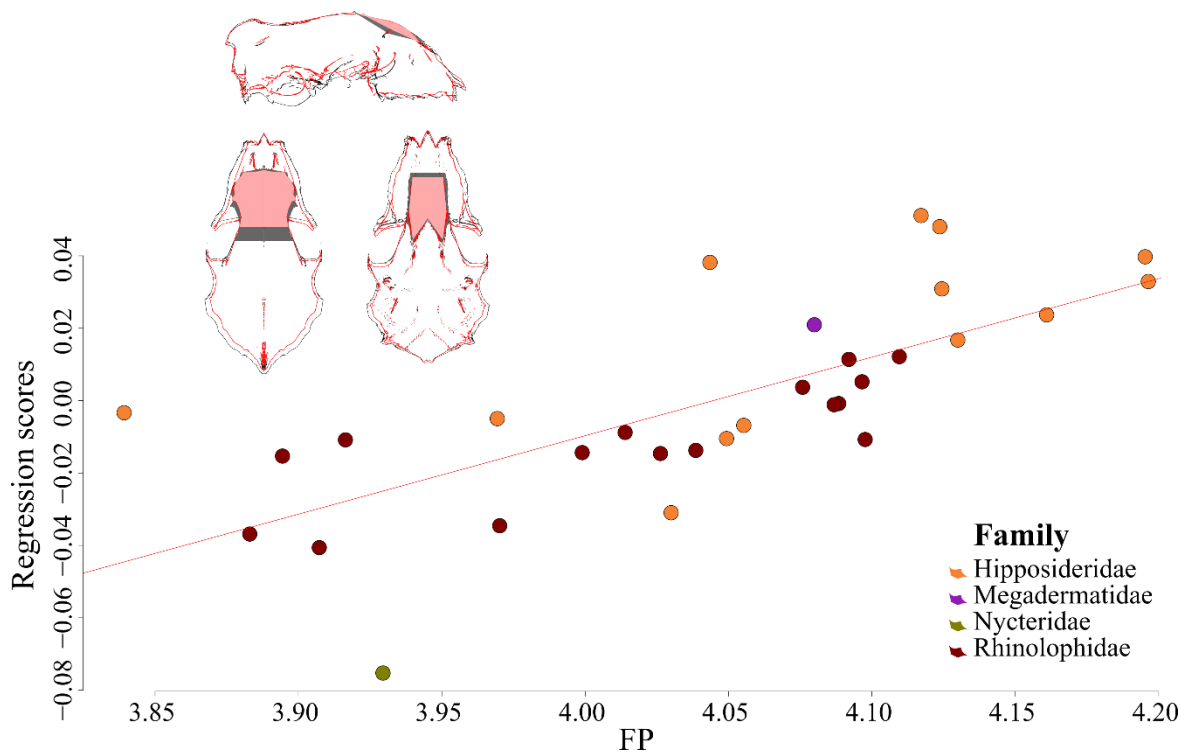


Figure S8. Plot of shape (as regression score) and peak frequency (as \log_{10} transformed and size-corrected, [FP]) for insectivorous Old World nasal emitting species. Shape deformations represent species with lowest (black outline) and highest (red outline) peak frequency. Hard palate and rostrum highlighted in grey and pink, respectively.

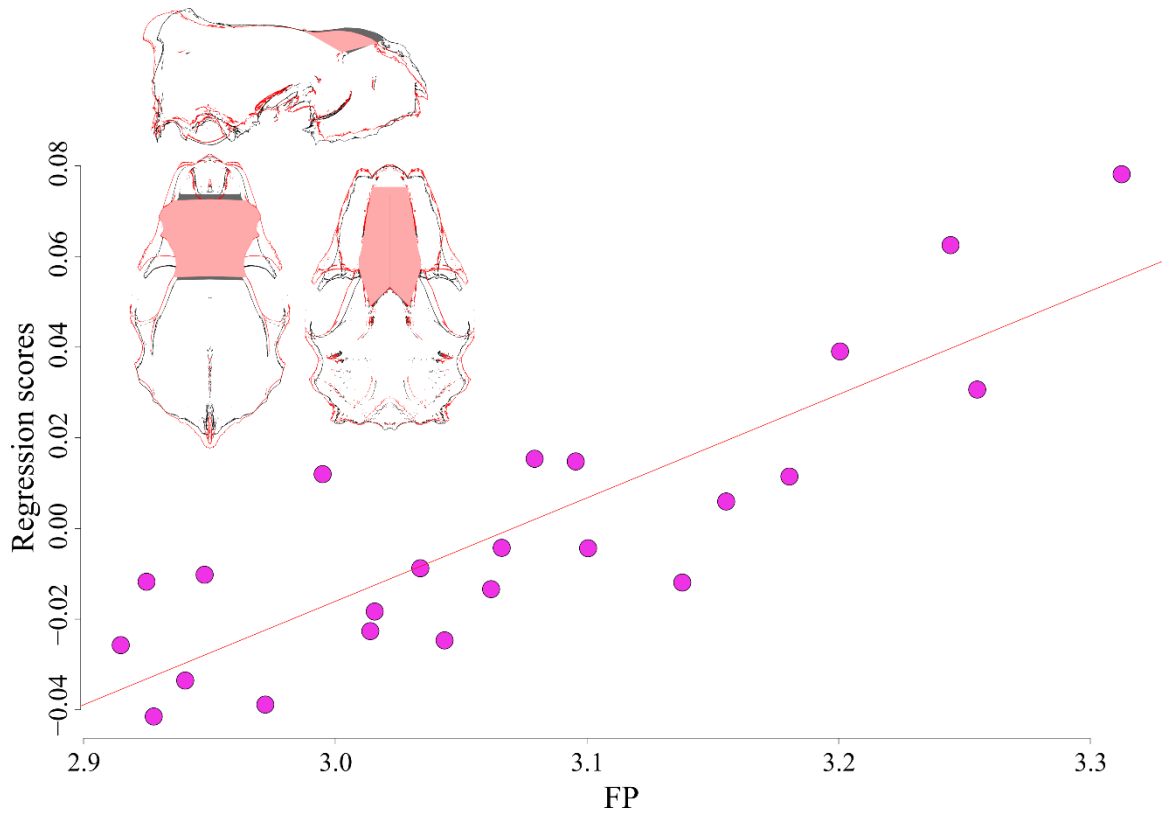


Figure S9. Plot of shape (as regression score) and peak frequency (as \log_{10} transformed and size-corrected, [FP]) for species from the Molossidae family. Shape deformations represent species with lowest (black outline) and highest (red outline) peak frequency. Hard palate and rostrum highlighted in grey and pink, respectively.

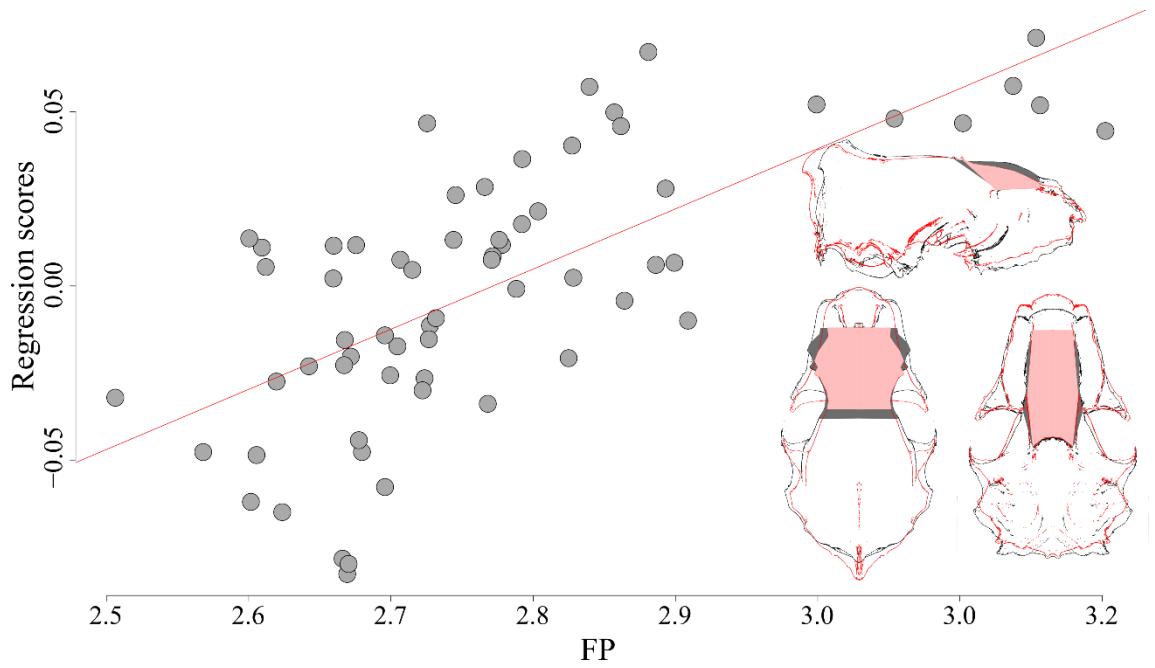


Figure S10. Plot of shape (as regression score) and peak frequency (as \log_{10} transformed and size-corrected, [FP]) for species from the Vespertilionidae family. Shape deformations represent species with lowest (black outline) and highest (red outline) peak frequency. Hard palate and rostrum highlighted in grey and pink, respectively.

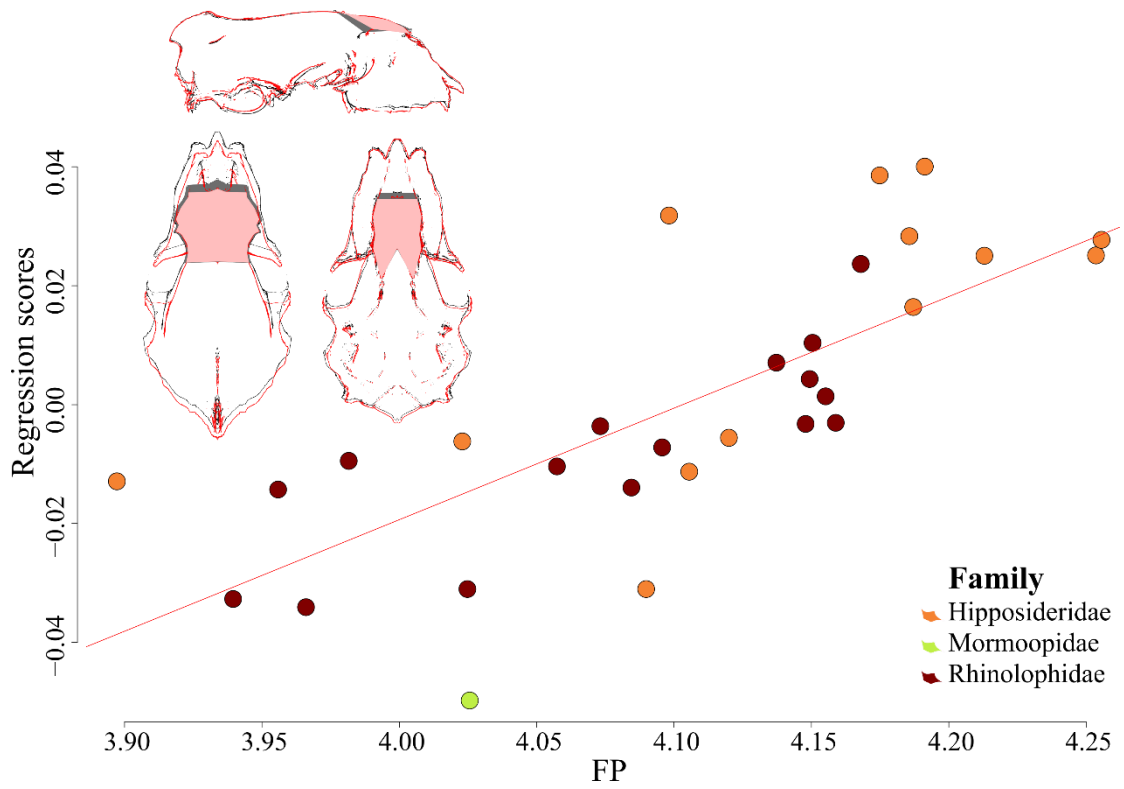


Figure S11. Plot of shape (as regression score) and peak frequency (as \log_{10} transformed and size-corrected [FP]) for species emitting call type “h” (*i.e.*, constant frequency calls). Shape deformations represent species with lowest (black outline) and highest (red outline) peak frequency. Hard palate and rostrum highlighted in grey and pink, respectively.

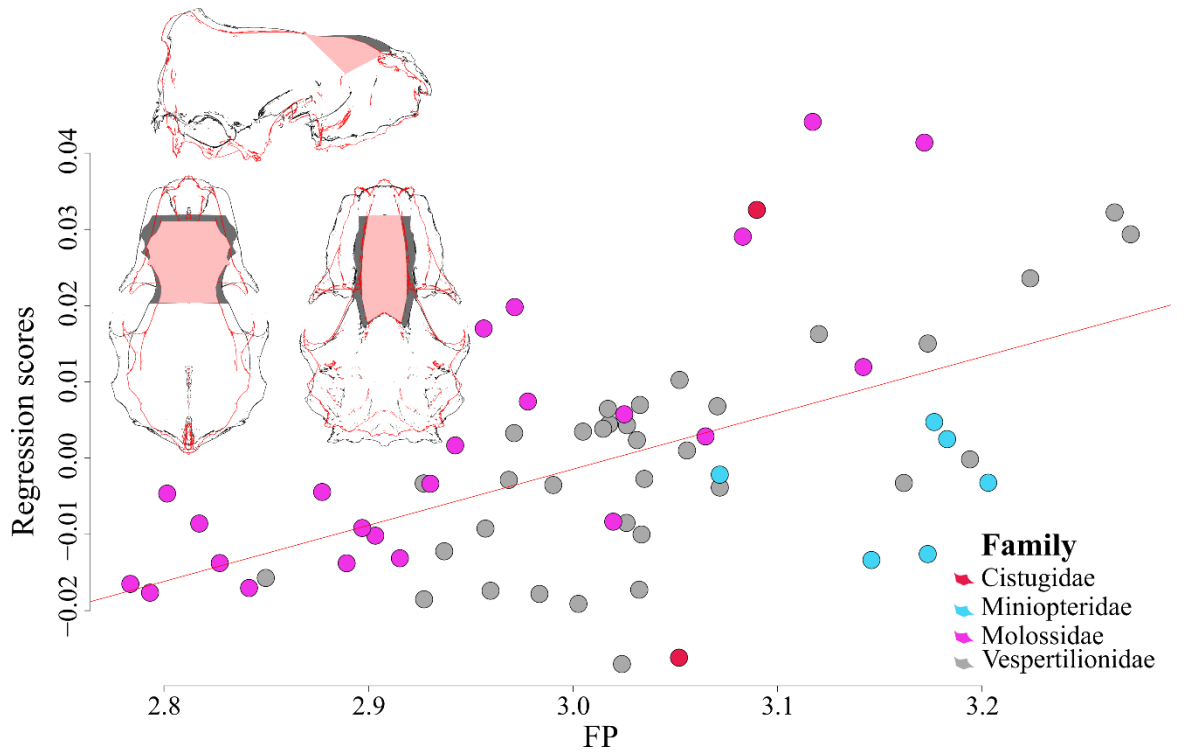


Figure S12. Plot of shape (as regression score) and peak frequency (as \log_{10} transformed and size-corrected, [FP]) for species emitting call type “c” (*i.e.*, narrowband, monoharmonic calls). Shape deformations represent species with lowest (black outline) and highest (red outline) peak frequency. Hard palate and rostrum highlighted in grey and pink, respectively.

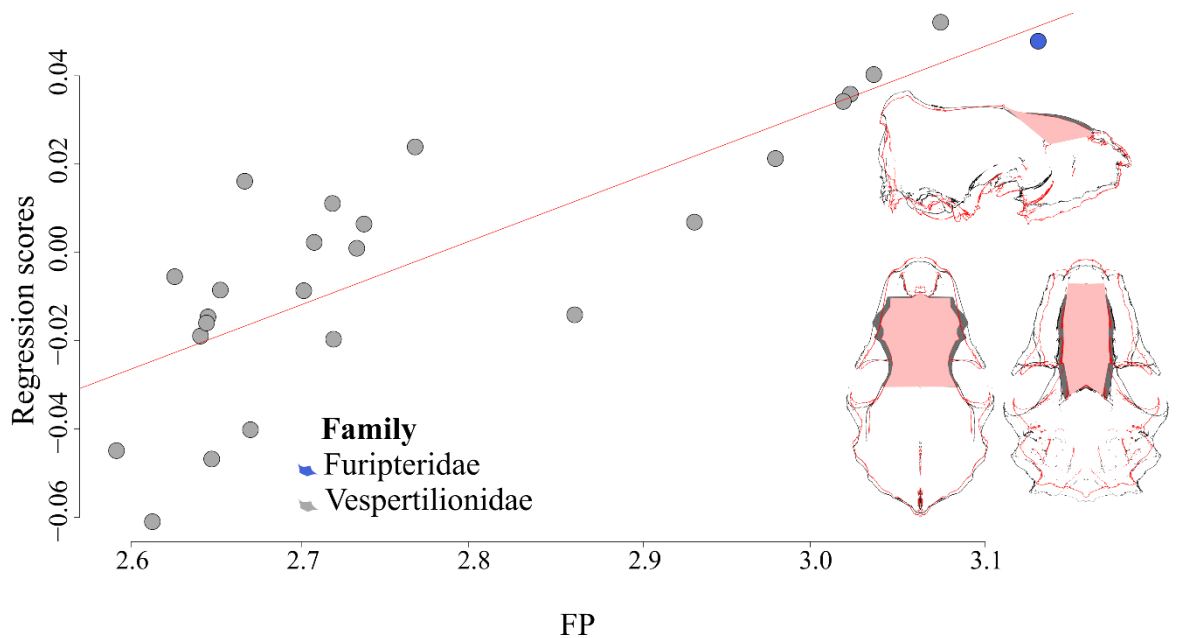


Figure S13. Plot of shape (as regression score) and peak frequency (as \log_{10} transformed and size-corrected), [FP] for species emitting call type “e” (*i.e.*, broadband, monoharmonic calls). Shape deformations represent species with lowest (black outline) and highest (red outline) peak frequency. Hard palate and rostrum highlighted in grey and pink, respectively.

Appendix G

Specimen information and 3D reconstruction techniques used in *Chapter Five*. Inventory number (IN). Reconstruction technique (Rec.): PHO = photogrammetry (n =381); μ CT = micro CT scan (n =62). Museums acronyms: NHMUK = Natural History Musuem London; MNHN = Muséum national d'Histoire naturelle (Paris); IRSNB = Royal Belgian Institute of Natural Science (Brussels); MNSB = Magyar Természettudományi Múzeum (Budapest); ZMUC = Statens Naturhistoriske Museum (Copenhagen); WML = World Museum (Liverpool); NMW = Naturhistorisches Museum (Vienna); Morphosource = samples from Morphosource repository made available by Shi *et al.* (2018).

Family	Species	IN	Museum	Rec.
Cistugidae	<i>Cistugo lesueuri</i>	27.4.1.3	NHMUK	PHO
Cistugidae	<i>Cistugo seabrae</i>	25.1.2.7	NHMUK	PHO
Craseonycteridae	<i>Craseonycteris thonglongyai</i>	77.2996	NHMUK	PHO
Emballonuridae	<i>Balantiopteryx plicata</i>	98.3.1.28	NHMUK	PHO
Emballonuridae	<i>Diclidurus virgo</i>	95.8.17.4	NHMUK	PHO
Emballonuridae	<i>Emballonura diana</i>	2878	ZMUC	PHO
Emballonuridae	<i>Emballonura diana</i>	2879	ZMUC	PHO
Emballonuridae	<i>Emballonura monticola</i>	9.1.5.474	NHMUK	PHO
Emballonuridae	<i>Peropteryx macrotis</i>	546o547	ZMUC	PHO
Emballonuridae	<i>Peropteryx macrotis</i>	L.54	ZMUC	PHO
Emballonuridae	<i>Rhynchonycteris naso</i>	1948-408	MNHN	μ CT
Emballonuridae	<i>Rhynchonycteris naso</i>	MO-1932-2970	MNHN	μ CT
Emballonuridae	<i>Saccolaimus saccolaimus</i>	98.10.7.4	NHMUK	PHO
Emballonuridae	<i>Saccolaimus saccolaimus</i>	98.10.7.5	NHMUK	PHO
Emballonuridae	<i>Saccopterix bilineata</i>	MO-1932-2861	MNHN	μ CT
Emballonuridae	<i>Saccopterix bilineata</i>	MO-1952-844	MNHN	μ CT
Emballonuridae	<i>Saccopterix bilineata</i>	MO-1957-174	MNHN	μ CT
Emballonuridae	<i>Taphozous longimanus</i>	12.11.29.67	NHMUK	PHO
Emballonuridae	<i>Taphozous melanopogon</i>	550	ZMUC	PHO

Family	Species	IN	Museum	Rec.
Emballonuridae	<i>Taphozous melanopogon</i>	11.12.21.4	NHMUK	PHO
Emballonuridae	<i>Taphozous nudiventris</i>	1475	ZMUC	PHO
Furipteridae	<i>Furipterus horrens</i>	2016-925	MNHN	μCT
Furipteridae	<i>Furipterus horrens</i>	71.6.20.1	NHMUK	PHO
Hipposideridae	<i>Asellia tridens</i>	17.259	IRSNB	PHO
Hipposideridae	<i>Asellia tridens</i>	17259	IRSNB	PHO
Hipposideridae	<i>Asellia tridens</i>	17260	IRSNB	PHO
Hipposideridae	<i>Asellia tridens</i>	MO-1995-1837	MNHN	μCT
Hipposideridae	<i>Aselliscus stoliczkanus</i>	MO-1948-359B	MNHN	μCT
Hipposideridae	<i>Cloeotis percivali</i>	66.5456	NHMUK	PHO
Hipposideridae	<i>Hipposideros bicolor</i>	71	ZMUC	PHO
Hipposideridae	<i>Hipposideros calcaratus</i>	2863	ZMUC	PHO
Hipposideridae	<i>Hipposideros calcaratus</i>	2868	ZMUC	PHO
Hipposideridae	<i>Hipposideros cervinus</i>	2379	ZMUC	PHO
Hipposideridae	<i>Hipposideros cervinus</i>	2380	ZMUC	PHO
Hipposideridae	<i>Hipposideros cervinus</i>	41239	IRSNB	PHO
Hipposideridae	<i>Hipposideros cervinus</i>	41240	IRSNB	PHO
Hipposideridae	<i>Hipposideros cyclops</i>	13332	IRSNB	PHO
Hipposideridae	<i>Hipposideros diadema</i>	82	ZMUC	PHO
Hipposideridae	<i>Hipposideros diadema</i>	2875	ZMUC	PHO
Hipposideridae	<i>Hipposideros diadema</i>	41233	IRSNB	PHO
Hipposideridae	<i>Hipposideros diadema</i>	MO-1878-1922	MNHN	μCT
Hipposideridae	<i>Hipposideros fulvus</i>	21.1.17.124	NHMUK	PHO
Hipposideridae	<i>Hipposideros fulvus</i>	21.1.17.128	NHMUK	PHO
Hipposideridae	<i>Hipposideros larvatus</i>	1884	ZMUC	PHO
Hipposideridae	<i>Hipposideros larvatus</i>	41236	IRSNB	PHO
Hipposideridae	<i>Hipposideros ridleyi</i>	83.422	NHMUK	PHO
Hipposideridae	<i>Rhinonictoris aurantia</i>	57.10.24.10	NHMUK	PHO
Hipposideridae	<i>Triaenops persicus</i>	75.2546	NHMUK	PHO
Megadermatidae	<i>Cardioderma cor</i>	10.6.225	NHMUK	PHO
Megadermatidae	<i>Cardioderma cor</i>	MO-1972-484A	MNHN	μCT

Family	Species	IN	Museum	Rec.
Megadermatidae	<i>Macroderma gigas</i>	92.5.20.2	NHMUK	PHO
Megadermatidae	<i>Megaderma lyra</i>	MO-1985-1413	MNHN	μCT
Megadermatidae	<i>Megaderma spasma</i>	54.3.21.5	NHMUK	PHO
Miniopteridae	<i>Miniopterus australis</i>	54.900	NHMUK	PHO
Miniopteridae	<i>Miniopterus inflatus</i>	75.895	NHMUK	PHO
Miniopteridae	<i>Miniopterus inflatus</i>	75.897	NHMUK	PHO
Miniopteridae	<i>Miniopterus magnater</i>	41251	IRSNB	PHO
Miniopteridae	<i>Miniopterus pusillus</i>	1222	ZMUC	PHO
Miniopteridae	<i>Miniopterus pusillus</i>	1223	ZMUC	PHO
Miniopteridae	<i>Miniopterus pusillus</i>	41085	IRSNB	PHO
Miniopteridae	<i>Miniopterus pusillus</i>	41088	IRSNB	PHO
Miniopteridae	<i>Miniopterus schreibersi</i>	509	ZMUC	PHO
Miniopteridae	<i>Miniopterus schreibersi</i>	MO-1984-1095	MNHN	μCT
Miniopteridae	<i>Miniopterus schreibersi</i>	MO-2004-460	MNHN	PHO
Miniopteridae	<i>Miniopterus tristis</i>	2896	ZMUC	PHO
Miniopteridae	<i>Miniopterus tristis</i>	2897	ZMUC	PHO
Miniopteridae	<i>Miniopterus tristis</i>	2899	ZMUC	PHO
Miniopteridae	<i>Miniopterus tristis</i>	2900	ZMUC	PHO
Molossidae	<i>Chaerephon ansorgei</i>	4907	IRSNB	PHO
Molossidae	<i>Chaerephon nigeriae</i>	12949	IRSNB	PHO
Molossidae	<i>Chaerephon plicatus</i>	696	ZMUC	PHO
Molossidae	<i>Chaerephon plicatus</i>	41266	IRSNB	PHO
Molossidae	<i>Chaerephon plicatus</i>	41277	IRSNB	PHO
Molossidae	<i>Chaerephon pumilus</i>	2322	ZMUC	PHO
Molossidae	<i>Chaerephon pumilus</i>	2323	ZMUC	PHO
Molossidae	<i>Chaerephon pumilus</i>	2324	ZMUC	PHO
Molossidae	<i>Cheiromeles torquatus</i>	23.10.7.10	NHMUK	PHO
Molossidae	<i>Cheiromeles torquatus</i>	44.10.17.7	NHMUK	PHO
Molossidae	<i>Eumops auripendulus</i>	687	ZMUC	PHO
Molossidae	<i>Eumops auripendulus</i>	23.8.9.2	NHMUK	PHO
Molossidae	<i>Eumops bonariensis</i>	2.11.7.2	NHMUK	PHO

Family	Species	IN	Museum	Rec.
Molossidae	<i>Eumops bonariensis</i>	98.3.4.35	NHMUK	PHO
Molossidae	<i>Eumops perotis</i>	682	ZMUC	PHO
Molossidae	<i>Eumops perotis</i>	MO-1939-1117	MNHN	PHO
Molossidae	<i>Eumops underwoodi</i>	61.1625	NHMUK	PHO
Molossidae	<i>Molossops temminckii</i>	580	ZMUC	PHO
Molossidae	<i>Molossops temminckii</i>	98.3.4.13	NHMUK	PHO
Molossidae	<i>Molossus molossus</i>	598	ZMUC	PHO
Molossidae	<i>Molossus molossus</i>	920	ZMUC	PHO
Molossidae	<i>Molossus molossus</i>	MO-1983-2259	MNHN	μCT
Molossidae	<i>Molossus rufus</i>	587	ZMUC	PHO
Molossidae	<i>Molossus rufus</i>	674	ZMUC	PHO
Molossidae	<i>Mops condylurus</i>	1507	ZMUC	PHO
Molossidae	<i>Mops condylurus</i>	16007	IRSNB	PHO
Molossidae	<i>Mops condylurus</i>	16017	IRSNB	PHO
Molossidae	<i>Mormopterus jugularis</i>	47.9.1.51	NHMUK	PHO
Molossidae	<i>Mormopterus planiceps</i>	6.8.1.52	NHMUK	PHO
Molossidae	<i>Nyctinomops laticaudatus</i>	3.4.7.5	NHMUK	PHO
Molossidae	<i>Otomops martiensseni</i>	10704	IRSNB	PHO
Molossidae	<i>Otomops martiensseni</i>	65.364	NHMUK	PHO
Molossidae	<i>Otomops wroughtoni</i>	13.4.9.3	NHMUK	PHO
Molossidae	<i>Promops centralis</i>	MO-1995-983	MNHN	μCT
Molossidae	<i>Sauromys petrophilus</i>	73.522	NHMUK	PHO
Molossidae	<i>Tadarida aegyptiaca</i>	75.2667	NHMUK	PHO
Molossidae	<i>Tadarida brasiliensis</i>	16.10.3.101	NHMUK	PHO
Molossidae	<i>Tadarida brasiliensis</i>	MO-1983-2266	MNHN	μCT
Molossidae	<i>Tadarida teniotis</i>	1043	ZMUC	PHO
Molossidae	<i>Tadarida teniotis</i>	MO-1996-447	MNHN	PHO
Mormoopidae	<i>Mormoops blainvillei</i>	7.1.1.722	NHMUK	PHO
Mormoopidae	<i>Mormoops blainvillei</i>	75.593	NHMUK	PHO
Mormoopidae	<i>Mormoops megalophylla</i>	27.11.19.17	NHMUK	PHO
Mormoopidae	<i>Mormoops megalophylla</i>	27.11.19.19	NHMUK	PHO

Family	Species	IN	Museum	Rec.
Mormoopidae	<i>Mormoops megalophylla</i>	71.2254	NHMUK	PHO
Mormoopidae	<i>Pteronotus davyi</i>	69.1262	NHMUK	PHO
Mormoopidae	<i>Pteronotus davyi</i>	88.8.4.7	NHMUK	PHO
Mormoopidae	<i>Pteronotus parnellii</i>	11.5.25.34	NHMUK	PHO
Mormoopidae	<i>Pteronotus parnellii</i>	65.604	NHMUK	PHO
Mormoopidae	<i>Pteronotus parnellii</i>	75.592	NHMUK	PHO
Mormoopidae	<i>Pteronotus parnellii</i>	96.307	NHMUK	PHO
Mormoopidae	<i>Pteronotus parnellii</i>	MO-1995-867	MNHN	μCT
Mormoopidae	<i>Pteronotus personatus</i>	69.1261	NHMUK	PHO
Mormoopidae	<i>Pteronotus rubiginosus</i>	709	ZMUC	PHO
Mormoopidae	<i>Pteronotus rubiginosus</i>	21.11.1.44	NHMUK	PHO
Mystacinidae	<i>Mystacina tuberculata</i>	62.2116	NHMUK	PHO
Myzopodidae	<i>Myzopoda aurita</i>	99.11.3.5	NHMUK	PHO
Myzopodidae	<i>Myzopoda aurita</i>	MO-1907-618	MNHN	μCT
Natalidae	<i>Natalus tumidirostris</i>	71.2302	NHMUK	PHO
Natalidae	<i>Natalus tumidirostris</i>	94.9.25.22	NHMUK	PHO
Noctilionidae	<i>Noctilio albiventris</i>	2007-81	MNHN	PHO
Noctilionidae	<i>Noctilio leporinus</i>	940	ZMUC	PHO
Noctilionidae	<i>Noctilio leporinus</i>	MO-2015-1576	MNHN	μCT
Nycteridae	<i>Nycteris grandis</i>	16784	IRSNB	PHO
Nycteridae	<i>Nycteris hispida</i>	3157	ZMUC	PHO
Nycteridae	<i>Nycteris thebaica</i>	3172	ZMUC	PHO
Phyllostomidae	<i>Ametrida centurio</i>	97.2.28.1	NHMUK	PHO
Phyllostomidae	<i>Anoura caudifer</i>	791	ZMUC	PHO
Phyllostomidae	<i>Anoura caudifer</i>	L.17	ZMUC	PHO
Phyllostomidae	<i>Anoura geoffroyi</i>	14.5.21.1	NHMUK	PHO
Phyllostomidae	<i>Anoura geoffroyi</i>	71.2266	NHMUK	PHO
Phyllostomidae	<i>Ariteus flavescens</i>	862	ZMUC	PHO
Phyllostomidae	<i>Artibeus fuliginosus</i>	21675	IRSNB	PHO
Phyllostomidae	<i>Artibeus fuliginosus</i>	21702	IRSNB	PHO
Phyllostomidae	<i>Artibeus jamaicensis</i>	MO-1957-158A	MNHN	μCT

Family	Species	IN	Museum	Rec.
Phyllostomidae	<i>Artibeus lituratus</i>	21670	IRSNB	PHO
Phyllostomidae	<i>Artibeus lituratus</i>	21672	IRSNB	PHO
Phyllostomidae	<i>Artibeus lituratus</i>	21703	IRSNB	PHO
Phyllostomidae	<i>Artibeus lituratus</i>	232C	IRSNB	PHO
Phyllostomidae	<i>Artibeus lituratus</i>	L.20	ZMUC	PHO
Phyllostomidae	<i>Artibeus planirostris</i>	21671	IRSNB	PHO
Phyllostomidae	<i>Artibeus planirostris</i>	21704	IRSNB	PHO
Phyllostomidae	<i>Artibeus planirostris</i>	21731	IRSNB	PHO
Phyllostomidae	<i>Brachyphylla cavernarum</i>	18.4.1.11	NHMUK	PHO
Phyllostomidae	<i>Brachyphylla cavernarum</i>	MO-2001-2245	MNHN	μCT
Phyllostomidae	<i>Carollia brevicauda</i>	1403	ZMUC	PHO
Phyllostomidae	<i>Carollia brevicauda</i>	21720	IRSNB	PHO
Phyllostomidae	<i>Carollia brevicauda</i>	21729	IRSNB	PHO
Phyllostomidae	<i>Carollia castanea</i>	13.10.2.2	NHMUK	PHO
Phyllostomidae	<i>Carollia castanea</i>	13.10.2.6	NHMUK	PHO
Phyllostomidae	<i>Carollia castanea</i>	21691	IRSNB	PHO
Phyllostomidae	<i>Carollia perspicillata</i>	MO-1998-667	MNHN	PHO
Phyllostomidae	<i>Centurio senex</i>	MO-1962-2639	MNHN	μCT
Phyllostomidae	<i>Chiroderma trinitatum</i>	80.751	NHMUK	PHO
Phyllostomidae	<i>Chiroderma trinitatum</i>	80.752	NHMUK	PHO
Phyllostomidae	<i>Chiroderma villosum</i>	871	ZMUC	PHO
Phyllostomidae	<i>Chiroderma villosum</i>	872	ZMUC	PHO
Phyllostomidae	<i>Choeronycteris mexicana</i>	27.11.19.35	NHMUK	PHO
Phyllostomidae	<i>Chrotopterus auritus</i>	719	ZMUC	PHO
Phyllostomidae	<i>Chrotopterus auritus</i>	4.1.5.4	NHMUK	PHO
Phyllostomidae	<i>Chrotopterus auritus</i>	5.8.1.3	NHMUK	PHO
Phyllostomidae	<i>Dermanura phaeotis</i>	2003.180	NHMUK	PHO
Phyllostomidae	<i>Dermanura phaeotis</i>	61.1617	NHMUK	PHO
Phyllostomidae	<i>Desmodus rotundus</i>	2007-90	MNHN	PHO
Phyllostomidae	<i>Desmodus rotundus</i>	I.G.25855	IRSNB	PHO
Phyllostomidae	<i>Desmodus rotundus</i>	L.45	ZMUC	PHO

Family	Species	IN	Museum	Rec.
Phyllostomidae	<i>Desmodus rotundus</i>	L.46	ZMUC	PHO
Phyllostomidae	<i>Diaemus youngi</i>	3.7.1.7	NHMUK	PHO
Phyllostomidae	<i>Diaemus youngi</i>	3.7.1.8	NHMUK	PHO
Phyllostomidae	<i>Diphylla eucaudata</i>	15.7.11.8	NHMUK	PHO
Phyllostomidae	<i>Diphylla eucaudata</i>	24.3.1.80	NHMUK	PHO
Phyllostomidae	<i>Erophylla sezekorni</i>	UMMZ-68205	Morphosource	μCT
Phyllostomidae	<i>Glossophaga longirostris</i>	11.5.25.83	NHMUK	PHO
Phyllostomidae	<i>Glossophaga soricina</i>	781	ZMUC	PHO
Phyllostomidae	<i>Glossophaga soricina</i>	21687	IRSNB	PHO
Phyllostomidae	<i>Glossophaga soricina</i>	21694	IRSNB	PHO
Phyllostomidae	<i>Glossophaga soricina</i>	MO-1977-527	MNHN	PHO
Phyllostomidae	<i>Lionycteris spurrelli</i>	1980.712	NHMUK	PHO
Phyllostomidae	<i>Lonchorhina aurita</i>	11.5.25.37	NHMUK	PHO
Phyllostomidae	<i>Lonchorhina aurita</i>	14.4.4.1	NHMUK	PHO
Phyllostomidae	<i>Lophostoma silvicolum</i>	MO-1986-154	MNHN	μCT
Phyllostomidae	<i>Lophostoma silvicolum</i>	MO-2016-197	MNHN	μCT
Phyllostomidae	<i>Lophostoma silvicolum</i>	MO-2016-198	MNHN	μCT
Phyllostomidae	<i>Macrophyllum macrophyllum</i>	65.613	NHMUK	PHO
Phyllostomidae	<i>Macrotus californicus</i>	61.1611	NHMUK	PHO
Phyllostomidae	<i>Macrotus californicus</i>	98.3.1.39	NHMUK	PHO
Phyllostomidae	<i>Macrotus waterhousii</i>	29.3.17.6	NHMUK	PHO
Phyllostomidae	<i>Macrotus waterhousii</i>	39.150	NHMUK	PHO
Phyllostomidae	<i>Mesophylla macconnelli</i>	15.10.5.3	NHMUK	PHO
Phyllostomidae	<i>Micronycteris hirsuta</i>	1937.8.30.14	NHMUK	PHO
Phyllostomidae	<i>Micronycteris hirsuta</i>	98.10.9.13	NHMUK	PHO
Phyllostomidae	<i>Micronycteris megalotis</i>	721	ZMUC	PHO
Phyllostomidae	<i>Micronycteris megalotis</i>	27.11.1.57	NHMUK	PHO
Phyllostomidae	<i>Micronycteris microtis</i>	2016-90	MNHN	μCT
Phyllostomidae	<i>Micronycteris minuta</i>	1.7.11.17	NHMUK	PHO
Phyllostomidae	<i>Micronycteris minuta</i>	2016-97	MNHN	μCT
Phyllostomidae	<i>Mimon bennetti</i>	3.7.1.153	NHMUK	PHO

Family	Species	IN	Museum	Rec.
Phyllostomidae	<i>Mimon bennetti</i>	65.618	NHMUK	PHO
Phyllostomidae	<i>Mimon crenulatum</i>	AMNH-64541	Morphosource	μCT
Phyllostomidae	<i>Mimon crenulatum</i>	AMNH-236001	Morphosource	μCT
Phyllostomidae	<i>Monophyllus luciae</i>	32.4.1.11	NHMUK	PHO
Phyllostomidae	<i>Monophyllus redmani</i>	75.594	NHMUK	PHO
Phyllostomidae	<i>Phylloderma stenops</i>	4.7.4.39	NHMUK	PHO
Phyllostomidae	<i>Phylloderma stenops</i>	65.626	NHMUK	PHO
Phyllostomidae	<i>Phyllonycteris poeyi</i>	4.5.4.12	NHMUK	PHO
Phyllostomidae	<i>Phyllostomus discolor</i>	11.5.25.67	NHMUK	PHO
Phyllostomidae	<i>Phyllostomus discolor</i>	MO-2016-146	MNHN	μCT
Phyllostomidae	<i>Phyllostomus elongatus</i>	17083	IRSNB	PHO
Phyllostomidae	<i>Phyllostomus elongatus</i>	RBINS-17082	IRSNB	μCT
Phyllostomidae	<i>Phyllostomus hastatus</i>	744	ZMUC	PHO
Phyllostomidae	<i>Phyllostomus hastatus</i>	34.9.2.15	NHMUK	PHO
Phyllostomidae	<i>Phyllostomus hastatus</i>	MO-1988-82	MNHN	μCT
Phyllostomidae	<i>Phyllostomus latifolius</i>	1.6.4.42	NHMUK	PHO
Phyllostomidae	<i>Phyllostomus latifolius</i>	1.6.4.45	NHMUK	PHO
Phyllostomidae	<i>Platyrrhinus brachycephalus</i>	2016-834	MNHN	μCT
Phyllostomidae	<i>Platyrrhinus brachycephalus</i>	2016-836	MNHN	μCT
Phyllostomidae	<i>Platyrrhinus brachycephalus</i>	24.3.1.55	NHMUK	PHO
Phyllostomidae	<i>Platyrrhinus brachycephalus</i>	96.6.2.8	NHMUK	PHO
Phyllostomidae	<i>Platyrrhinus helleri</i>	2016-842	MNHN	μCT
Phyllostomidae	<i>Platyrrhinus helleri</i>	2016-847	MNHN	μCT
Phyllostomidae	<i>Platyrrhinus lineatus</i>	861	ZMUC	PHO
Phyllostomidae	<i>Platyrrhinus lineatus</i>	22.3.1.10	NHMUK	PHO
Phyllostomidae	<i>Platyrrhinus lineatus</i>	3.7.7.34	NHMUK	PHO
Phyllostomidae	<i>Platyrrhinus lineatus</i>	L.25	ZMUC	PHO
Phyllostomidae	<i>Pygoderma bilabiatum</i>	874	ZMUC	PHO
Phyllostomidae	<i>Pygoderma bilabiatum</i>	2.11.7.5	NHMUK	PHO
Phyllostomidae	<i>Rhinophylla pumilio</i>	776	ZMUC	PHO
Phyllostomidae	<i>Rhinophylla pumilio</i>	27.1.1.49	NHMUK	PHO

Family	Species	IN	Museum	Rec.
Phyllostomidae	<i>Sphaeronycteris toxophyllum</i>	1287	ZMUC	PHO
Phyllostomidae	<i>Sphaeronycteris toxophyllum</i>	17097	IRSNB	PHO
Phyllostomidae	<i>Sphaeronycteris toxophyllum</i>	5.2.5.4	NHMUK	PHO
Phyllostomidae	<i>Sturnira lilium</i>	900	ZMUC	PHO
Phyllostomidae	<i>Sturnira lilium</i>	1.6.6.21	NHMUK	PHO
Phyllostomidae	<i>Sturnira lilium</i>	2016-882	MNHN	μCT
Phyllostomidae	<i>Sturnira ludovici</i>	11.5.25.119	NHMUK	PHO
Phyllostomidae	<i>Sturnira ludovici</i>	11.5.25.122	NHMUK	PHO
Phyllostomidae	<i>Sturnira tildae</i>	65.639	NHMUK	PHO
Phyllostomidae	<i>Trachops cirrhosus</i>	20.7.14.34	NHMUK	PHO
Phyllostomidae	<i>Trachops cirrhosus</i>	24.1.3.32	NHMUK	PHO
Phyllostomidae	<i>Uroderma bilobatum</i>	21713	IRSNB	PHO
Phyllostomidae	<i>Uroderma bilobatum</i>	MO-1976-295	MNHN	μCT
Phyllostomidae	<i>Vampyriscus brocki</i>	2016-917	MNHN	μCT
Phyllostomidae	<i>Vampyriscus brocki</i>	2016-918	MNHN	μCT
Phyllostomidae	<i>Vampyrodes caraccioli</i>	21732	IRSNB	PHO
Phyllostomidae	<i>Vampyrum spectrum</i>	73.a	NHMUK	PHO
Phyllostomidae	<i>Vampyrum spectrum</i>	MO-1889-907	MNHN	PHO
Rhinolophidae	<i>Rhinolophus affinis</i>	8.1.30.7	NHMUK	PHO
Rhinolophidae	<i>Rhinolophus affinis</i>	9.1.5.152	NHMUK	PHO
Rhinolophidae	<i>Rhinolophus alcyone</i>	13667	IRSNB	PHO
Rhinolophidae	<i>Rhinolophus blasii</i>	1035	ZMUC	PHO
Rhinolophidae	<i>Rhinolophus capensis</i>	75.8.9.10	NHMUK	PHO
Rhinolophidae	<i>Rhinolophus clivosus</i>	1846B	IRSNB	PHO
Rhinolophidae	<i>Rhinolophus darlingi</i>	6.8.2.32	NHMUK	PHO
Rhinolophidae	<i>Rhinolophus ferrumequinum</i>	1980.789	WML	PHO
Rhinolophidae	<i>Rhinolophus ferrumequinum</i>	8907	NMW	PHO
Rhinolophidae	<i>Rhinolophus ferrumequinum</i>	9156	NMW	PHO
Rhinolophidae	<i>Rhinolophus ferrumequinum</i>	10421	NMW	PHO
Rhinolophidae	<i>Rhinolophus ferrumequinum</i>	28021	NMW	PHO
Rhinolophidae	<i>Rhinolophus ferrumequinum</i>	45847	NMW	PHO

Family	Species	IN	Museum	Rec.
Rhinolophidae	<i>Rhinolophus ferrumequinum</i>	MO-1977-56	MNHN	μCT
Rhinolophidae	<i>Rhinolophus ferrumequinum</i>	MO-1977-58	MNHN	PHO
Rhinolophidae	<i>Rhinolophus fumigatus</i>	13660	IRSNB	PHO
Rhinolophidae	<i>Rhinolophus fumigatus</i>	13662	IRSNB	μCT
Rhinolophidae	<i>Rhinolophus hildebrandtii</i>	59.354	NHMUK	PHO
Rhinolophidae	<i>Rhinolophus hipposideros</i>	39.226	NHMUK	PHO
Rhinolophidae	<i>Rhinolophus hipposideros</i>	MO-1932-4107	MNHN	PHO
Rhinolophidae	<i>Rhinolophus landeri</i>	13663	IRSNB	PHO
Rhinolophidae	<i>Rhinolophus megaphyllus</i>	23.1.5.2	NHMUK	PHO
Rhinolophidae	<i>Rhinolophus megaphyllus</i>	3.8.3.4	NHMUK	PHO
Rhinolophidae	<i>Rhinolophus mehelyi</i>	62.238	NHMUK	PHO
Rhinolophidae	<i>Rhinolophus mehelyi</i>	no number	NHMUK	PHO
Rhinolophidae	<i>Rhinolophus pusillus</i>	6121	IRSNB	PHO
Rhinolophidae	<i>Rhinolophus simulator</i>	71.2449	NHMUK	PHO
Rhinolophidae	<i>Rhinolophus swinnyi</i>	14481	IRSNB	PHO
Rhinopomatidae	<i>Rhinopoma microphyllum</i>	573	ZMUC	PHO
Rhinopomatidae	<i>Rhinopoma microphyllum</i>	2845	ZMUC	PHO
Rhinopomatidae	<i>Rhinopoma microphyllum</i>	2847	ZMUC	PHO
Thyropteridae	<i>Thyroptera discifera</i>	28.5.2.101	NHMUK	PHO
Thyropteridae	<i>Thyroptera discifera</i>	28.7.21.20	NHMUK	PHO
Thyropteridae	<i>Thyroptera tricolor</i>	505	ZMUC	PHO
Thyropteridae	<i>Thyroptera tricolor</i>	2016-940	MNHN	μCT
Vespertilionidae	<i>Antrozous pallidus</i>	21.9.3.4	NHMUK	PHO
Vespertilionidae	<i>Antrozous pallidus</i>	61.468	NHMUK	PHO
Vespertilionidae	<i>Barbastella barbastellus</i>	2640	ZMUC	PHO
Vespertilionidae	<i>Barbastella barbastellus</i>	2642	ZMUC	PHO
Vespertilionidae	<i>Barbastella barbastellus</i>	MO-1962-1754	MNHN	μCT
Vespertilionidae	<i>Barbastella barbastellus</i>	MO-2003-225	MNHN	μCT
Vespertilionidae	<i>Chalinolobus gouldii</i>	24.3.7.2	NHMUK	PHO
Vespertilionidae	<i>Chalinolobus gouldii</i>	66.3476	NHMUK	PHO
Vespertilionidae	<i>Eptesicus brasiliensis</i>	L.64	ZMUC	PHO

Family	Species	IN	Museum	Rec.
Vespertilionidae	<i>Eptesicus furinalis</i>	AMNH-124387	Morphosource	μCT
Vespertilionidae	<i>Eptesicus fuscus</i>	162	ZMUC	PHO
Vespertilionidae	<i>Eptesicus fuscus</i>	163	ZMUC	PHO
Vespertilionidae	<i>Eptesicus fuscus</i>	14971	IRSNB	PHO
Vespertilionidae	<i>Eptesicus hottentotus</i>	M6248	ZMUC	PHO
Vespertilionidae	<i>Eptesicus nilssonii</i>	2628	ZMUC	PHO
Vespertilionidae	<i>Eptesicus serotinus</i>	158	ZMUC	PHO
Vespertilionidae	<i>Eptesicus serotinus</i>	1040	ZMUC	PHO
Vespertilionidae	<i>Eptesicus serotinus</i>	3044	ZMUC	PHO
Vespertilionidae	<i>Eptesicus serotinus</i>	4080	ZMUC	PHO
Vespertilionidae	<i>Eptesicus serotinus</i>	MO-2003-222	MNHN	PHO
Vespertilionidae	<i>Glauconycteris argentata</i>	22.7.17.60	NHMUK	PHO
Vespertilionidae	<i>Glauconycteris argentata</i>	24.1.1.64	NHMUK	PHO
Vespertilionidae	<i>Glischropus tylopus</i>	10.4.568	NHMUK	PHO
Vespertilionidae	<i>Harpiocephalus harpia</i>	79.11.15.18	NHMUK	PHO
Vespertilionidae	<i>Harpiocephalus harpia</i>	9.1.5.357	NHMUK	PHO
Vespertilionidae	<i>Hesperoptenus tickelli</i>	98.9.2.2	NHMUK	PHO
Vespertilionidae	<i>Histiotus montanus</i>	59.4.7	MNSB	PHO
Vespertilionidae	<i>Histiotus montanus</i>	68.97.1	MNSB	PHO
Vespertilionidae	<i>Hypsugo savii</i>	1042	ZMUC	PHO
Vespertilionidae	<i>Hypsugo savii</i>	2420.6	MNSB	PHO
Vespertilionidae	<i>Hypsugo savii</i>	4581.1	MNSB	PHO
Vespertilionidae	<i>Hypsugo savii</i>	MO-1932-4270	MNHN	PHO
Vespertilionidae	<i>Ia io</i>	98.22.20.	MNSB	PHO
Vespertilionidae	<i>Kerivoula hardwickei</i>	9.1.5.417	NHMUK	PHO
Vespertilionidae	<i>Kerivoula papillosa</i>	93.4.1.30	NHMUK	PHO
Vespertilionidae	<i>Kerivoula picta</i>	910	ZMUC	PHO
Vespertilionidae	<i>Laephotis wintoni</i>	72.4399	NHMUK	PHO
Vespertilionidae	<i>Lasionycteris noctivagans</i>	334	ZMUC	PHO
Vespertilionidae	<i>Lasionycteris noctivagans</i>	7.7.7.2316	NHMUK	PHO
Vespertilionidae	<i>Lasiurus borealis</i>	363	ZMUC	PHO

Family	Species	IN	Museum	Rec.
Vespertilionidae	<i>Lasiurus borealis</i>	14981	IRSNB	PHO
Vespertilionidae	<i>Lasiurus borealis</i>	14984	IRSNB	PHO
Vespertilionidae	<i>Lasiurus cinereus</i>	367	ZMUC	PHO
Vespertilionidae	<i>Lasiurus cinereus</i>	MO-1939-1096	MNHN	μCT
Vespertilionidae	<i>Lasiurus ega</i>	364	ZMUC	PHO
Vespertilionidae	<i>Lasiurus ega</i>	365	ZMUC	PHO
Vespertilionidae	<i>Murina cyclotis</i>	78.1543	NHMUK	PHO
Vespertilionidae	<i>Murina tubinaris</i>	16.3.26.8	NHMUK	PHO
Vespertilionidae	<i>Myotis albescens</i>	MO-1949-118	MNHN	μCT
Vespertilionidae	<i>Myotis bechsteinii</i>	3865	ZMUC	PHO
Vespertilionidae	<i>Myotis bechsteinii</i>	15717	IRSNB	PHO
Vespertilionidae	<i>Myotis bechsteinii</i>	57.37.1.	MNSB	PHO
Vespertilionidae	<i>Myotis bechsteinii</i>	73.110.1.	MNSB	PHO
Vespertilionidae	<i>Myotis blythii</i>	5.12.2.7.	NHMUK	PHO
Vespertilionidae	<i>Myotis bocagii</i>	10723	IRSNB	PHO
Vespertilionidae	<i>Myotis brandtii</i>	1104	ZMUC	PHO
Vespertilionidae	<i>Myotis brandtii</i>	15725	IRSNB	PHO
Vespertilionidae	<i>Myotis brandtii</i>	5085	IRSNB	PHO
Vespertilionidae	<i>Myotis brandtii</i>	58.3.1.	MNSB	PHO
Vespertilionidae	<i>Myotis brandtii</i>	68.529.5.	MNSB	PHO
Vespertilionidae	<i>Myotis brandtii</i>	8094B	IRSNB	PHO
Vespertilionidae	<i>Myotis capaccinii</i>	2004-1316	MNHN	μCT
Vespertilionidae	<i>Myotis capaccinii</i>	MO-1955-671	MNHN	PHO
Vespertilionidae	<i>Myotis dasycneme</i>	374	ZMUC	PHO
Vespertilionidae	<i>Myotis dasycneme</i>	1117	ZMUC	PHO
Vespertilionidae	<i>Myotis dasycneme</i>	18892	NMW	PHO
Vespertilionidae	<i>Myotis dasycneme</i>	MO-1983-506	MNHN	PHO
Vespertilionidae	<i>Myotis dasycneme</i>	5096	IRSNB	PHO
Vespertilionidae	<i>Myotis dasycneme</i>	5099	IRSNB	PHO
Vespertilionidae	<i>Myotis daubentonii</i>	4546.2	MNSB	PHO
Vespertilionidae	<i>Myotis daubentonii</i>	51428	NMW	PHO

Family	Species	IN	Museum	Rec.
Vespertilionidae	<i>Myotis daubentonii</i>	51596	NMW	PHO
Vespertilionidae	<i>Myotis daubentonii</i>	54.86.1	MNSB	PHO
Vespertilionidae	<i>Myotis daubentonii</i>	55.16.1	MNSB	PHO
Vespertilionidae	<i>Myotis daubentonii</i>	57.61.3	MNSB	PHO
Vespertilionidae	<i>Myotis daubentonii</i>	MO-1997-322	MNHN	PHO
Vespertilionidae	<i>Myotis emarginatus</i>	1036	ZMUC	PHO
Vespertilionidae	<i>Myotis emarginatus</i>	2004-1308	MNHN	PHO
Vespertilionidae	<i>Myotis keenii</i>	14987	IRSNB	PHO
Vespertilionidae	<i>Myotis keenii</i>	14988	IRSNB	PHO
Vespertilionidae	<i>Myotis myotis</i>	5063	IRSNB	PHO
Vespertilionidae	<i>Myotis mystacinus</i>	1988.215	WML	PHO
Vespertilionidae	<i>Myotis mystacinus</i>	15742	IRSNB	PHO
Vespertilionidae	<i>Myotis mystacinus</i>	35431-9	IRSNB	PHO
Vespertilionidae	<i>Myotis mystacinus</i>	MO-2000-384	MNHN	μCT
Vespertilionidae	<i>Myotis nattereri</i>	2633	ZMUC	PHO
Vespertilionidae	<i>Myotis nattereri</i>	2782	ZMUC	PHO
Vespertilionidae	<i>Myotis nattereri</i>	1981.92.2	WML	PHO
Vespertilionidae	<i>Myotis nattereri</i>	2004-1299	MNHN	μCT
Vespertilionidae	<i>Myotis nigricans</i>	17093	IRSNB	PHO
Vespertilionidae	<i>Myotis nigricans</i>	2016-976	MNHN	μCT
Vespertilionidae	<i>Myotis nigricans</i>	L.62	ZMUC	PHO
Vespertilionidae	<i>Myotis nigricans</i>	MO-2003-316	MNHN	PHO
Vespertilionidae	<i>Myotis simus</i>	21727	IRSNB	μCT
Vespertilionidae	<i>Myotis welwitschii</i>	RBINS-4789	IRSNB	μCT
Vespertilionidae	<i>Neoromicia capensis</i>	10707	IRSNB	PHO
Vespertilionidae	<i>Neoromicia nana</i>	10710	IRSNB	PHO
Vespertilionidae	<i>Neoromicia nana</i>	13861	IRSNB	PHO
Vespertilionidae	<i>Nyctalus lasiopterus</i>	19390	NMW	PHO
Vespertilionidae	<i>Nyctalus lasiopterus</i>	MO-1921-68A	MNHN	μCT
Vespertilionidae	<i>Nyctalus leisleri</i>	1041	ZMUC	PHO
Vespertilionidae	<i>Nyctalus leisleri</i>	MO-1959-171	MNHN	μCT

Family	Species	IN	Museum	Rec.
Vespertilionidae	<i>Nyctalus noctula</i>	42235	NMW	PHO
Vespertilionidae	<i>Nyctalus noctula</i>	56.91.2.	MNSB	PHO
Vespertilionidae	<i>Nyctalus noctula</i>	56.91.5.	MNSB	PHO
Vespertilionidae	<i>Nyctalus noctula</i>	65.54.1.	MNSB	PHO
Vespertilionidae	<i>Nyctalus noctula</i>	MO-1932-4157	MNHN	PHO
Vespertilionidae	<i>Nyctalus noctula</i>	MO-1932-4158	MNHN	PHO
Vespertilionidae	<i>Nycticeinops schlieffeni</i>	1492	ZMUC	PHO
Vespertilionidae	<i>Nycticeinops schlieffeni</i>	10715	IRSNB	PHO
Vespertilionidae	<i>Nyctophilus geoffroyi</i>	15.3.13.10	NHMUK	PHO
Vespertilionidae	<i>Nyctophilus geoffroyi</i>	77.12.10.8	NHMUK	PHO
Vespertilionidae	<i>Otonycteris hemprechi</i>	19.7.7.12.13	NHMUK	PHO
Vespertilionidae	<i>Pipistrellus kuhlii</i>	12.328	IRSNB	PHO
Vespertilionidae	<i>Pipistrellus kuhlii</i>	MO-1983-1498	MNHN	μCT
Vespertilionidae	<i>Pipistrellus nathusii</i>	CN2700	ZMUC	PHO
Vespertilionidae	<i>Pipistrellus nathusii</i>	MO-1932-4218	MNHN	μCT
Vespertilionidae	<i>Pipistrellus nathusii</i>	MO-1932-4267	MNHN	PHO
Vespertilionidae	<i>Pipistrellus pipistrellus</i>	69279	NMW	PHO
Vespertilionidae	<i>Pipistrellus pipistrellus</i>	1981.91.3	WML	PHO
Vespertilionidae	<i>Pipistrellus pipistrellus</i>	2004-1365	MNHN	μCT
Vespertilionidae	<i>Pipistrellus pipistrellus</i>	39507	IRSNB	PHO
Vespertilionidae	<i>Pipistrellus pipistrellus</i>	5407	IRSNB	PHO
Vespertilionidae	<i>Pipistrellus pipistrellus</i>	MO-2003-283	MNHN	PHO
Vespertilionidae	<i>Pipistrellus pygmaeus</i>	61734	NMW	PHO
Vespertilionidae	<i>Pipistrellus pygmaeus</i>	69285	NMW	PHO
Vespertilionidae	<i>Plecotus auritus</i>	1975.513	WML	PHO
Vespertilionidae	<i>Plecotus auritus</i>	2004-1440	MNHN	μCT
Vespertilionidae	<i>Plecotus auritus</i>	5101	IRSNB	PHO
Vespertilionidae	<i>Plecotus auritus</i>	5102	IRSNB	PHO
Vespertilionidae	<i>Plecotus auritus</i>	MO-2003-270	MNHN	μCT
Vespertilionidae	<i>Plecotus auritus</i>	MO-2004-1428	MNHN	PHO
Vespertilionidae	<i>Plecotus austriacus</i>	37262	NMW	PHO

Family	Species	IN	Museum	Rec.
Vespertilionidae	<i>Plecotus austriacus</i>	52845	NMW	PHO
Vespertilionidae	<i>Plecotus austriacus</i>	54.80.1	MNSB	PHO
Vespertilionidae	<i>Plecotus austriacus</i>	57.31.1	MNSB	PHO
Vespertilionidae	<i>Plecotus austriacus</i>	MO-1932-4160	MNHN	PHO
Vespertilionidae	<i>Plecotus macrobullaris</i>	33344	NMW	PHO
Vespertilionidae	<i>Plecotus macrobullaris</i>	2009.46.3.	MNSB	PHO
Vespertilionidae	<i>Rhogeessa tumida</i>	3.2.1.1	NHMUK	PHO
Vespertilionidae	<i>Rhogeessa parvula</i>	333b	ZMUC	PHO
Vespertilionidae	<i>Scotomanes ornatus</i>	15.9.1.31	NHMUK	PHO
Vespertilionidae	<i>Scotomanes ornatus</i>	15.9.1.36	NHMUK	PHO
Vespertilionidae	<i>Scotophilus kuhlii</i>	2849	ZMUC	PHO
Vespertilionidae	<i>Scotophilus leucogaster</i>	19901	IRSNB	PHO
Vespertilionidae	<i>Scotophilus leucogaster</i>	19927.A	IRSNB	PHO
Vespertilionidae	<i>Scotophilus nigrita</i>	39509	IRSNB	PHO
Vespertilionidae	<i>Scotophilus nux</i>	7041	IRSNB	PHO
Vespertilionidae	<i>Scotophilus nux</i>	7043	IRSNB	PHO
Vespertilionidae	<i>Tylonycteris pachypus</i>	16.3.25.13	NHMUK	PHO
Vespertilionidae	<i>Vespertilio murinus</i>	3081	ZMUC	PHO
Vespertilionidae	<i>Vespertilio murinus</i>	3083	ZMUC	PHO
Vespertilionidae	<i>Vespertilio murinus</i>	3268	ZMUC	PHO
Vespertilionidae	<i>Vespertilio murinus</i>	RBINS-38279	IRSNB	μCT

References Appendix G

Shi, J.J., Westeen, E.P. & Rabosky, D.L. 2018. Digitizing extant bat diversity: An open-access repository of 3D μCT-scanned skulls for research and education. *PLoS One* **13**: e0203022.

CHAPTER SIX: General Conclusion

This thesis was able to validate the use of the photogrammetry technique for the reconstruction and analyses of small and complex 3D objects such as bat skulls. I found that the photogrammetry technique generated comparable raw information (*i.e.*, 3D models) to μ CT and laser scan approaches. 3D models of bat skulls obtained with photogrammetry were then validated for macroevolutionary analyses. This provided the methodological basis for my subsequent analyses of bat skull evolution.

Both of the macroevolutionary studies in this thesis clarified the impact of functional demands on interspecific bat skull variation. No previous studies had addressed the evolutionary relationship between echolocation parameters and skull shape variation. I found that species-specific echolocation parameters correlated with cranial morphology in insectivorous and frugivorous species. This correlation was stronger for nasal emitting species (both insectivorous and frugivorous) than oral emitters. Nevertheless, morphological adaptations of skull shape to peak frequency followed a similar pattern within the order, regardless of the mode of echolocation (*i.e.*, oral/nasal) and diet (*i.e.*, insectivorous/frugivorous). Specifically, species emitting low frequencies tended to show longer rostra that were also associated with reduced bite force. This indicates a possible trade-off between the sensory system and feeding functions. Specifically, elongation of the rostrum is associated with the emission of low frequencies, which favour the long-distance detection of prey, but it is also associated with a weaker bite force and poor resistance to mechanical bending forces.

Photogrammetry for small and complex skulls

Photogrammetry has been widely used to provide raw material (as 3D digital models) for evolutionary analyses and its accuracy for large specimens (>150 mm length) has proven

similar to other more expensive techniques (Fahlke & Autenrieth, 2016; Fruciano *et al.*, 2017). However, technique comparison on the accuracy of 3D reconstruction has received little attention for small and complex objects (*e.g.* small mammal skulls). In *Chapter Three*, I showed that 3D models reconstructed through photogrammetry, μ CT scan and laser scan deliver similar biological conclusions when macroevolutionary analyses are performed on small mammal skulls (~15 mm average length). Similarly, I provided evidence that datasets built with combined-techniques can be used in macroevolutionary studies when a preliminary sensitivity analysis is performed (see also Robinson & Terhune, 2017). These findings allowed the application of such an approach in the subsequent studies of this thesis.

Functional correlates of bat skull evolution

A correlation between cranial shape and feeding ecology has been detected across different lineages of mammals (*e.g.* marsupials and carnivore, Wroe & Milne, 2007; Goswami *et al.*, 2011), some reptiles (*e.g.* lizards, Herrel & Holanova, 2008) and birds (*e.g.* finches, Herrel *et al.*, 2005). Skull morphology of some bat families seems to follow the same pattern showing an association with feeding function described by diet category, bite force and masticatory muscles (Aguirre *et al.*, 2002; Herrel *et al.*, 2008; Santana *et al.*, 2010).

Chapter Four provided additional evidence of the correlation between skull shape morphology and feeding function across 10 bat families: a long rostrum was associated with lower bite force and smaller masticatory muscles (relative to body size). Previous studies of mammal vocalization have focused on the mechanism of sound production and resonance effect induced by soft tissue rearrangement (*e.g.* Frey *et al.*, 2012). *Chapters Four* and *Five* represent the first study focusing on the relationship between sound characteristics (*i.e.*, peak frequency) and skull shape in mammals. Based on the results of *Chapter Four*, only the skull shape of insectivorous species was evolutionarily correlated

with echolocation parameters (*i.e.*, peak frequency, start frequency and end frequency). This supports the prediction that the skulls of insectivorous bats might be under stronger selection due to echolocation compared to bats relying on a multiple-sensory system (*i.e.*, echolocation, vision and olfaction). However, in this chapter, non-insectivorous species were analysed together as the sample size did not allow for a more indepth exploration of each diet category. Shape deformation analyses showed that insectivorous bats with longer rostra and bigger tympanic bullae (relative to their body size) tended to emit lower peak frequencies (advantageous as they travel long distances). This, and the poor bite performance associated with longer rostra, indicates a possible trade-off between echolocation and feeding function, at least in insectivorous bats.

Skull shape adaptations to peak frequency

The negative scaling of frequencies on body size of birds, frogs and mammals is well reported in the literature (e.g. Riede & Fitch, 1999; Martin *et al.*, 2011; Gingras *et al.*, 2013). The 219 bat species analysed in *Chapter Five* followed the same acoustic allometric rule, with exception for the phyllostomids and vertebrate eaters. Studies on mammal vocalization have previously noticed that some species do not follow the acoustic allometric rule showing either positive (some felids; Peters *et al.*, 2008) or not significant correlation between frequency and body size (e.g. harbor seal pups; Khan *et al.*, 2006). The reasons behind the failure of the acoustic allometric rule in these species are still unknown but the acoustic characteristics of the environment might play a role in shaping this relationship (Hauser, 1993). Furthermore, Garcia *et al.* (2017) suggested that vocal fold length potentially decouples from body mass in primates. If this mechanism is relevant for bats too, it could explain why echolocation frequencies of phyllostomids and vertebrate eaters do not correlate with skull size (this thesis) or body size (Jones, 1999). *Chapter Five* further suggested that different emission types and call designs play a role in the

association pattern between peak frequency and skull morphology in this ecological group. Nasal emitting species were more constrained by adaptation to different peak frequencies, in both size and shape, with respect to mouth emitters. Species belonging to different families showed different slopes. For example, the skull shape of species emitting constant-frequency calls (*i.e.*, Rhinolophidae and Hipposideridae) showed the highest correlation to peak frequency because of the resonance effect of the nasal chambers. Ecologically diverse families, such as the Vespertilionidae family, presented a weaker correlation between skull shape and peak frequency. This family displays different call designs (Jones and Teeling 2006) and hunting strategies (Denzinger and Schnitzler 2013) that might imply within-family patterns that require a finer-scale investigation.

A wide taxa coverage (~65% of bat genera) also showed that the skull shape of frugivorous phyllostomids equally correlated with peak frequency. This is against the hypothesis that skull shape of non-insectivorous species is under a weaker evolutionary pressure due to echolocation because they combine different sensory systems to locate and pursue their food (*e.g.* Ripperger *et al.*, 2019). Conversely, it suggests that peak frequency is still constraining skull shape of phyllostomid bats, or as phyllostomids probably evolved from an insectivorous ancestor (Freeman, 2000), that adaptations to echolocation are evolutionarily conservative. Although beyond the scope of this study, a deeper investigation on the association between skull shape and echolocation within other non-insectivorous bats is deserved. Nectarivorous species are extremely specialised: the rostrum is elongated to reach the nectar and to accommodate the long tongue (Winter & von Helversen, 2003). Therefore, the rostrum of these species is likely to be less influenced by peak frequency. On the other hand, carnivory is the extreme of a continuous gradient describing animalivory (*i.e.*, carnivorous and insectivorous species), suggesting that carnivorous species might retain specializations due to echolocation (Giannini & Kalko, 2005).

In agreement with *Chapter Four*, long rostra and big tympanic bullae (relative to the skull size) were associated with the emission of low frequency sounds within most of the investigated ecological groups. This suggests that if an evolutionary trade-off exists in insectivorous species (see *Chapter Four*), it might also be present in frugivorous species. As traits are influenced by both sources of direct and indirect selection, two non-mutually exclusive hypothesis can be formulated to explain the evolutionary correlation between skull shape and peak frequency in insectivorous species. The physical acoustic hypothesis argues that a physical acoustic principle, such as a resonance effect or harmonic filtering, drives the direct correlation between shape and frequency emitted (as in Rhinolophidae and Hipposideridae species). The mechanical hypothesis considers the spatial and mechanical demands of echolocating muscles as moulding forces on the skull shape. Therefore, the correlation between peak frequency and shape is an indirect effect. This latter hypothesis might explain the correlation of peak frequency with skull shape of oral emitting species.

Thesis limitations and future directions

Photogrammetry of bat skulls

Even if photogrammetry provides an easy-to-use and affordable framework for 3D reconstruction of small specimens, it is worth mentioning that a detailed reconstruction of thin and/or shiny structures (such as the zygomatic arch and teeth) is problematic (Mitchell & Chadwick, 2008; Mallison & Wings, 2014). Therefore, this prevents the study of such challenging morphological structures on small skulls by means of photogrammetry. In future studies, the use of focus stacking techniques might be considered if more details on small structures are needed (Brecko *et al.*, 2014; Nguyen *et al.*, 2014; Santella & Milner, 2017). The number of photographs and acquisition time increase enormously with the focus stacking technique (1,300 - 4,400 pictures for each sample). However, the

implementation of custom-made automatized systems represents a possible solution (with time per sample ranging from 20 to 210 mins, Nguyen *et al.*, 2014).

Semi-landmarks placed on curves or surfaces can provide additional valuable information as many morphological structures cannot be quantified by using only traditional landmarks (Gunz & Mitteroecker, 2013). The effect of possible surface irregularities resulting from photogrammetric reconstruction should be assessed when a semi-landmark approach is used to quantify size and shape of small 3D objects.

Future studies should also explore whether the photogrammetry technique is suitable to investigate questions on microevolutionary processes. The morphological variation within microevolutionary studies is much smaller than macroevolutionary ones. Therefore, an assessment of whether the technique error is greater than the variation between individuals is necessary (*e.g.* for laser scan: Marcy *et al.*, 2018).

Functional correlates of bat skull evolution

Sampling error, due to low taxa representation, can arise during macroevolutionary analyses when the data collected do not cover the diversity of an entire clade (Klingenberg, 2013). Bats represent the second most specious mammal order on Earth and the remarkable morphological diversity is the result of their evolutionary history and adaptations to different sensory strategies, diets, hunting strategies and roosting ecology (Altringham, 2011). Thus, exploring the morphological variation within this order under a macroevolutionary framework is challenging. *Chapter Four* represents the first attempt to evaluate the relative influence of feeding and echolocation functions on skull morphological variation. Nevertheless, taxa coverage in this study is limited by the difficulties of gathering bite force and muscles data in the field (and as a result in the literature). Future studies that report bite force and masticatory muscle data from other echolocating species will allow greater understanding of the relative strengths of functional

drivers of bat skull evolution. This, together with investigations on the advantages and disadvantages of high frequencies, will allow evaluation of whether the functional trade-off between feeding and sensory systems is present in the skull shape of non-insectivorous bats (*e.g.* nectarivorous and vertebrate eaters).

Skull shape adaptation to peak frequency

Even if a correlation between skull shape and echolocation parameters is evident within insectivorous species, further studies are needed to uncover the mechanisms responsible for such a relationship. Analyses of larynx muscle diversity and the performance of acoustic simulations can provide a greater understanding of the physical and acoustical mechanisms responsible for the phenomenon. Assessing the covariation between morphology of species phonetic apparatus (*i.e.*, larynx and echolocating muscle diversity) and skull morphology might reveal if skull shape of oral emitters correlates with peak frequency because of the “mechanical hypothesis”. Acoustic simulations, through finite-element method (FEM), have already proven useful for investigating the acoustic function of the nasal chambers in two rhinolophid species (Li & Ma, 2013; Ma *et al.*, 2016). Application of FEM and boundary-element method to sound emission and propagation in frugivorous phyllostomids would be necessary to confirm the lack of a resonance effect in the nasal passages of these species.

Other bony structures of the head might be correlated with peak frequency. Mandibular shape in echolocating odontocetes is believed to play a role in sound reception (Barroso *et al.*, 2012). Even if bat mandible evolution appears to have been more driven by diet than by echolocation (Arbour *et al.*, 2019), it would be valuable to investigate the relationship between mandibular shape and echolocation parameters in bats.

The Brownian motion model used in this thesis assumes that both ancestors and descendants evolve towards the same evolutionary optimum. This theoretical model leads

to the concept of “inherited maladaptation” formulated by Hansen and Orzack (2005): the descendant species will evolve towards the ancestral optimum even if the environmental conditions have changed. Therefore, this fixed “optimum” does not necessarily maximise the optimal state of the descendant. Being able to account for a shift in evolutionary optima allows separation of adaptive processes from white noise (*i.e.*, evolutionary conservative values for a specific trait) and to model potential evolutionary “jumps” due to environmental changes and niche specializations (Hansen, 2014). Several authors, however, have warned against the use of such models given the statistical knowledge and tools currently available. Many of the algorithms available to select the best evolutionary model incorrectly favour multi peak models over simpler models (Cooper *et al.*, 2016; Adams & Collyer, 2017). Moreover, the computational requirements to assess the best evolutionary model is prohibitive when complex models are involved. Therefore, many authors reduce data dimensionality by selecting some PCs only (*e.g.* Arbour *et al.*, 2019). This approach can be misleading as PCA (and phylogenetic PCA) transformation sorts the variables into PC axes by which evolutionary model they follow (*e.g.* Brownian, Ornstein–Uhlenbeck, Early Bursts) (Uyeda *et al.*, 2015). Using only a few PCs may lead to misinterpretation of evolutionary processes as a biased subsample is selected from a pool of multivariate variables (Mitteroecker *et al.*, 2004; Uyeda *et al.*, 2015). These and other reasons have fuelled the ongoing scientific debate on the application of complex phylogenetic multivariate methods in evolutionary studies (for a summary see Cooper & Matschiner, 2019). Future statistical and theoretical advances in the field of phylogenetic comparative methods, that test for and choose the best evolutionary model without biases (Adams & Collyer, 2017), will allow further exploration of the impact of echolocation call parameters on bat skull evolution.

References

- Adams, D.C. & Collyer, M.L. 2017. Multivariate Phylogenetic Comparative Methods: Evaluations, Comparisons, and Recommendations. *Syst. Biol.* **67**: 14–31.
- Aguirre, L.F., Herrel, A., van Damme, R. & Matthysen, E. 2002. Ecomorphological analysis of trophic niche partitioning in a tropical savannah bat community. *Proc. R. Soc. London. Ser. B Biol. Sci.* **269**: 1271–1278.
- Altringham, J.D. 2011. Bats: From Evolution to Conservation, 2nd ed. Oxford University Press, Oxford.
- Arbour, J.H., Curtis, A.A. & Santana, S.E. 2019. Signatures of echolocation and dietary ecology in the adaptive evolution of skull shape in bats. *Nat. Commun.* **10**: 2036.
- Barroso, C., Cranford, T.W. & Berta, A. 2012. Shape analysis of odontocete mandibles: Functional and evolutionary implications. *J. Morphol.* **273**: 1021–1030.
- Brecko, J., Mathys, A., Dekoninck, W., Leponce, M., VandenSpiegel, D. & Semal, P. 2014. Focus stacking: Comparing commercial top-end set-ups with a semi-automatic low budget approach. A possible solution for mass digitization of type specimens. *Zookeys* **464**: 1–23.
- Cooper, N. & Matschiner, M. 2019. Phylogenetics and Comparative Methods: The Bright and Dark Sides. *Methods Ecol. Evol.*
- Cooper, N., Thomas, G.H., Venditti, C., Meade, A. & Freckleton, R.P. 2016. A cautionary note on the use of Ornstein Uhlenbeck models in macroevolutionary studies. *Biol. J. Linn. Soc.* **118**: 64–77.
- Denzinger, A. & Schnitzler, H. 2013. Bat guilds, a concept to classify the highly diverse foraging and echolocation behaviors of microchiropteran bats. *Front. Zool.* **4**: 1–15.
- Fahlke, J. & Autenrieth, M. 2016. Photogrammetry VS. Micro-CT scanning for 3D surface generation of typical vertebrate fossil – a case study. *J. Paleontol. Tech.* **14**: 1–18.
- Freeman, P.W. 2000. Macroevolution in Microchiroptera : Recoupling morphology and ecology with phylogeny. *Evol. Ecol. Res.* **2**: 317–335.
- Frey, R., Volodin, I., Volodina, E., Carranza, J. & Torres-Porras, J. 2012. Vocal anatomy, tongue protrusion behaviour and the acoustics of rutting roars in free-ranging Iberian red deer stags (*Cervus elaphus hispanicus*). *J. Anat.* **220**: 271–292. John Wiley & Sons, Ltd (10.1111).
- Fruciano, C., Celik, M.A., Butler, K., Dooley, T., Weisbecker, V. & Phillips, M.J. 2017. Sharing is caring? Measurement error and the issues arising from combining 3D morphometric datasets. *Ecol. Evol.* **7**: 7034–7046.
- Garcia, M., Herbst, C.T., Bowling, D.L., Dunn, J.C. & Fitch, W.T. 2017. Acoustic allometry revisited: morphological determinants of fundamental frequency in primate vocal production. *Sci. Rep.* **7**: 10450.
- Giannini, N.P. & Kalko, E.K.V. 2005. The guild structure of animalivorous leaf-nosed bats of Barro Colorado Island, Panama, revisited. *Acta Chiropterologica* **7**: 131–146.
- Gingras, B., Boeckle, M., Herbst, C.T. & Fitch, W.T. 2013. Call acoustics reflect body size across four clades of anurans. *J. Zool.* **289**: 143–150. John Wiley & Sons, Ltd (10.1111).
- Goswami, A., Milne, N. & Wroe, S. 2011. Biting through constraints: cranial morphology, disparity and convergence across living and fossil carnivorous mammals. *Proc. R.*

- Soc. B Biol. Sci.* **278**: 1831–1839. Royal Society.
- Gunz, P. & Mitteroecker, P. 2013. Semilandmarks: a method for quantifying curves and surfaces. *Hystrix, Ital. J. Mammal.* **24**: 103–109.
- Hansen, T.F. 2014. Use and Misuse of Comparative Methods in the Study of Adaptation BT - Modern Phylogenetic Comparative Methods and Their Application in Evolutionary Biology: Concepts and Practice. In: (L. Z. Garamszegi, ed), pp. 351–379. Springer Berlin Heidelberg, Berlin, Heidelberg.
- Hansen, T.F. & Orzack, S.H. 2005. Assessing current adaptation and phylogenetic inertia as explanations of trait evolution: the need for controlled comparisons. *Evolution (N. Y.)*. **59**: 2063–2072.
- Hauser, M.D. 1993. The Evolution of Nonhuman Primate Vocalizations: Effects of Phylogeny, Body Weight, and Social Context. *Am. Nat.* **142**: 528–542. The University of Chicago Press.
- Hedrick, B.P. & Dumont, E.R. 2018. Putting the leaf-nosed bats in context: a geometric morphometric analysis of three of the largest families of bats. *J. Mammal.* **99**: 1042–1054.
- Herrel, A., De Smet, A., Aguirre, L.F. & Aerts, P. 2008. Morphological and mechanical determinants of bite force in bats: do muscles matter? *J. Exp. Biol.* **211**: 86–91.
- Herrel, A. & Holanova, V. 2008. Cranial morphology and bite force in Chamaeleolis lizards – Adaptations to molluscivory? *Zoology* **111**: 467–475.
- Herrel, A., Podos, J., Huber, S.K. & Hendry, A.P. 2005. Evolution of bite force in Darwin’s finches: a key role for head width. *J. Evol. Biol.* **18**: 669–675. John Wiley & Sons, Ltd (10.1111).
- Jones, G. 1999. Scaling of echolocation call parameters in bats. *J. Exp. Biol.* **202**: 3359 LP – 3367.
- Jones, G. & Teeling, E. 2006. The evolution of echolocation in bats. *Trends Ecol. Evol.* **21**: 149–156.
- Khan, C.B., Markowitz, H. & McCowan, B. 2006. Vocal development in captive harbor seal pups, *Phoca vitulina richardii*: Age, sex, and individual differences. *J. Acoust. Soc. Am.* **120**: 1684–1694. Acoustical Society of America.
- Klingenberg, C.P. 2013. Cranial integration and modularity: insights into evolution and development from morphometric data. *Hystrix, Ital. J. Mammal.* **24**: 43–58.
- Li, T. & Ma, X. 2013. Numerical Research on the Acoustic Features of the Vocal Tract in a Horseshoe Bat, *Rhinolophus Hipposideros*. In: Proceedings of the 2013 International Conference on Computer Sciences and Applications, pp. 549–553. IEEE Computer Society, Washington, DC, USA.
- Ma, X., Li, T. & Lu, H. 2016. The acoustical role of vocal tract in the horseshoe bat, *Rhinolophus pusillus*. *J. Acoust. Soc. Am.* **139**: 1264–1271.
- Mallison, H. & Wings, O. 2014. Photogrammetry in paleontology- A practical guide. *J. Paleontol. Tech.* **12**: 1–31.
- Marcy, A.E., Fruciano, C., Phillips, M.J., Mardon, K. & Weisbecker, V. 2018. Low resolution scans can provide a sufficiently accurate, cost- and time-effective alternative to high resolution scans for 3D shape analyses. *PeerJ* **6**: e5032.
- Martin, J.P., Doucet, S.M., Knox, R.C. & Mennill, D.J. 2011. Body size correlates negatively with the frequency of distress calls and songs of Neotropical birds. *J. F.*

- Ornithol.* **82**: 259–268. John Wiley & Sons, Ltd (10.1111).
- Mitchell, H.L. & Chadwick, R.G. 2008. Challenges of photogrammetric intra-oral tooth measurement. *Arch. Photogramm. Remote Sens. Spat. Inf. Sci.* Vol. XXXVII. Part B5. Beijing 2008.
- Mitteroecker, P., Gunz, P., Bernhard, M., Schaefer, K. & Bookstein, F.L. 2004. Comparison of cranial ontogenetic trajectories among great apes and humans. *J. Hum. Evol.* **46**: 679–698.
- Nguyen, C.V, Lovell, D.R., Adcock, M. & La Salle, J. 2014. Capturing Natural-Colour 3D Models of Insects for Species Discovery and Diagnostics. *PLoS One* **9**: e94346.
- Peters, G., Baum, L., Peters, M.K. & Tonkin-Leyhausen, B. 2008. Spectral characteristics of intense mew calls in cat species of the genus *Felis* (Mammalia: Carnivora: Felidae). *J. Ethol.* **27**: 221.
- Riede, T. & Fitch, T. 1999. Vocal tract length and acoustics of vocalization in the domestic dog (*Canis familiaris*). *J. Exp. Biol.* **202**: 2859 LP – 2867.
- Ripperger, S.P., Rehse, S., Wacker, S., Kalko, E., Schulz, S., Rodriguez-Herrera, B., *et al.* 2019. Nocturnal scent in a “bird-fig”: a cue to attract bats as additional dispersers? bioRxiv 418970.
- Robinson, C. & Terhune, C.E. 2017. Error in geometric morphometric data collection: Combining data from multiple sources. *Am. J. Phys. Anthropol.* **164**: 62–75.
- Santana, S.E., Dumont, E.R. & Davis, J.L. 2010. Mechanics of bite force production and its relationship to diet in bats. *Funct. Ecol.* **24**: 776–784.
- Santella, M. & Milner, A.R. 2017. Coupling focus stacking with photogrammetry to illustrate small fossil teeth. *J. Paleontol. Tech.* **18**: 1–17.
- Uyeda, J.C., Caetano, D.S. & Pennell, M.W. 2015. Comparative Analysis of Principal Components Can be Misleading. *Syst. Biol.* **64**: 677–689.
- Winter, Y. & von Helversen, O. 2003. Operational Tongue Length in Phyllostomid Nectar-Feeding Bats. *J. Mammal.* **84**: 886–896.
- Wroe, S. & Milne, N. 2007. Convergence and remarkably consistent constraint in the evolution of carnivore skull shape. *Evolution (N. Y.)*. **61**: 1251–1260. John Wiley & Sons, Ltd (10.1111).